UNIVERSITY OF MINNESOTA
ST. ANTHONY FALLS HYDRAULIC LABORATORY

Project Report No. 253

GRAVITY CURRENTS IN LAKES, RESERVOIRS AND COASTAL REGIONS: TWO-LAYER STRATIFIED FLOW ANALYSIS

by

Juchiro Akiyama

and

Heinz G. Stefan

Prepared with Support from

MINNESOTA SEA GRANT PROGRAM, NOAA, DEPARTMENT OF COMMERCE;
NATIONAL SCIENCE FOUNDATION;
and LEGISLATIVE COMMISSION ON MINNESOTA RESOURCES

March, 1987
Minneapolis, Minnesota

St. Anthony Falls Hydraulic Laboratory
University of Minnesota

Project Report No. 253

GRAVITY CURRENTS IN LAKES, RESERVOIRS AND COASTAL REGIONS: TWO-LAYER STRATIFIED FLOW ANALYSIS

by

Juchiro Akiyama

and

Heinz G. Stefan

Prepared with Support from

Minnesota Sea Grant Program, NOAA, Department of Commerce;
National Science Foundation;
and Legislative Commission on Minnesota Resources

March, 1987
Minneapolis, Minnesota

ABSTRACT

Suspension gravity currents (turbidity currents) occurring in lakes, reservoirs, and the ocean are investigated theoretically. When the turbid water, a mixture of suspended particles and clear water, is introduced in a quiescent body of clear water, the turbid mixture flows downslope due to its larger density. Turbidity currents derive this driving force from the sediment in suspension. Such turbidity currents are essentially non-uniform and in disequilibrium because of water entrainment across the upper boundary of the flowing layer. Therefore, turbidity currents can be erosive or depositive, accelerating or decelerating as they travel over the sloping bed, exchanging sediment between the bed and the flow. The governing equations which describe the movement of gradually varied steady-state turbidity currents occuring in sloping channels with constant as well as variable widths are developed. In order to incorporate the mechanism of sediment exchange into the model, the sediment entrainment function is derived by utilizing data for suspended sediment transport in free-surface open channel flows and is applied to the analysis. The model is also applied to actual field sites. Such turbidity currents can be originated by various processes when large amounts of sediment are put into suspension. One mechanism investigated both theoretically and experimentally is the direct inflow of dense river water into a reservoir. This phenomenon is sometimes referred to as "plunging flow."

The results obtained herein are expected to be useful for applications by geologists, oceanographers, and hydraulic engineers, who are concerned with understanding the impact of turbidity currents on

natural environments, for example, the redistribution of sands in the ocean, subsurface morphology, and with modeling of water quality and transport of dissolved solids, suspended matter in lakes and reservoirs.

ACKNOWLEDGEMENTS

The authors acknowledge with appreciation partial financial assistance by the following sponsors of the research reported herein.

The National Science Foundation sponsored research in the area of plunging flow under Contract No. NSF CEE-8308471.

The Legislative Commission on Minnesota Resources sponsored work connected with Minnesota lake processes.

The Minnesota Sea Grant Program, supported by the NOAA Office of Sea Grant, Department of Commerce, contributed partial support for the turbidity current model under Grant No. NA83-AA-D-00056.[1]

[1]Minnesota Sea Grant Program Research Contribution No. 25. The U. S. Government is authorized to reproduce and distribute reprints for government purposes, not withstanding any copyright notation that may appear hereon.

CONTENTS

LIST OF FIGURES

LIST OF TABLES

LIST OF SYMBOLS IN TEXT

A = Aspect ratio (b/h) (Chap. 2)

A = channel aspect ratio (W/H) [Chap. 5 and 6]

a = reference level (= 0.05H)

B = layer averaged buoyancy force

B_f buoyancy flux (= UBH)

b = flow (channel) half width [Chap. 2]

b = local buoyancy force [Chap. 4, 5, and 6]

b_H = buoyancy force at y = H

C = vertically averaged volumetric concentration of suspended sediment

C_b = total shear stress coefficient at the bed ($C_{bo} + C_{b1} + C_{b2}$)

C_{bo} = friction coefficient due to skin friction

C_{b1} = drag coefficient due to bed forms

C_{b2} = additional friction coefficient due to the presence of suspended sediment

C_{wo} = friction coefficient at the wall

c = local mean value of volumetric concentration of suspended sediment

c_a = local mean values of reference volumetric concentration at y = 0.05H

c_{ai} = value of c_i at y = a

c_{ae} = equilibrium value of c_a

c_{aei} = equilibrium value of c_{ai}

c_i = value of c for material in the ith grain size range

D = volumetric entrainment flux from bed [Chap. 3]

D = layer total energy dissipation [Chap. 4]

D_i = geometric mean grain size of the ith size range of bed material

D_s = diameter of sediment particle

D_{50} = median grain size of bed material

D_* = non-dimensional sediment particle size

E = volumetric entrainment flux from bed [Chap. 3]

E = turbulent energy dissipation rate due to viscosity [Chap. 4]

E_s = sediment entrainment function at y = 0.05H

E_{si} = sediment entrainment function at y = 0.05H for the ith grain size range, per fraction of bed material content in that range

E_s^* = sediment entrainment coefficient for buoyancy force

E_w = water entrainment function

F = densimetric Froude number [Chap. 2]

F_i = densimetric Froude number [Chap. 4]

F_d = densimetric Froude number downstream of plunge region

F_{dn} = F_d value for mild slope

F_{ds} = F_d value for steep slope

F_f = flow force

F_x inter. = x-component of friction force along the interface

$F_{x\ sur.}$ = x-component of friction on the water surface

F_y = mean vertical volumetric flux of suspended sediment

f_b = bed friction coefficient

f_i = interfacial friction coefficient [Chap. 2]

$f_{i=1\sim3}$ = shape factor [chap. 4, 5, 6]

f_t = total friction coefficient ($= f_b + f_i$)

f_w = wall friction coefficient

G = weight correction factor for C. V. II

g = acceleration of gravity

H = flow depth (open channel flow) and flow thickness (gravity current)

H_1 = distance from the channel bed to the point of maximum velocity

H_2 = distance from the point of maximum velocity to the point of zero velocity

h = flow depth [Chap. 2]

Δh = rise of water level ($= \eta + \Delta$)

h_c = internal critical depth

h_d = flow depth downstream of plunge region

h_{dm} = flow depth downstream of the plunge region for mild slope

h_{ds} = flow depth downstream of the plunge region for steep slope

h_l = flow depth of lower layer downstream of plunge region

h_m = flow depth of mixing layer downstream of plunge region

h_p = plunge depth

h_u = flow depth of upper layer downstream of plunge region

I = layer integrated work done against buoyancy force

J = Δ/H

K = D_s/H

k = fractional depth ($=h_d/h_p$) [Chap. 2]

k = turbulent kinetic energy [Chap. 4]

k_s = skin roughness

L = length of plunge region

m = fractional width

m_1, m_2 = correction factor

n = normalized length of plunge region ($= L/h_o$) [Chap. 2]

n = exponent of entrainment function (= - 1.0) [Chap. 4, 5]

P = pressure force per unit wall length [Chap. 2]

P = layer integrated turbulent energy production [Chap. 4]

P_i = fraction of bed material in the ith grain size range

p = local pressure

Q = volumetric flow rate [Chap. 2]

Q_f = volume flux [Chap. 4]

R = overall Richardson number

R_f = overall Richardson number at $\hat{x} = 4000$

R_{fl} = flux Richardson number

R_p = particle Reynolds number

$R_{x\ wall}$ = x-component of pressure force from the side wall

r_o = c_{ae}/C

S = channel bed slope

$S_{i=1\sim2}$ = shape factors for velocity and buoyancy profiles

$\bar{T}$ = vertically average temperature

t = time

Δt_s = time interval for occurences of a continuous turbidity current

U = layered averaged flow velocity

u = x-component of local velocity

u_* = bed shear velocity

V_f = settling velocity of sediment particle

V_{fi} = settling velocity associated with size D_i

v = y-component of local velocity

v_e = entrainment velocity

W = channel full width [Chap. 5]

W_* = non-dimensional settling velocity of sediment particle

w = z-component of local velocity

x = downstream coordinate

x_p = distance from channel inlet to the plunge line

y = vertical coordinate

z = lateral coordinate

α = ratio of h_p to h_c

α_i = ratio of f_b to f_i

δ = divergence angle of the side wall (half-angle of the diffuser) (Chap. 2, 5, and 6)

δ = layer thickness defined by $u(\delta) = 1/2u_{max}$

δ_D = displacement thickness

β = $\tan \theta/(A_o F_o)$ [Chap. 2]

β = factor of proportionality [Chap. 3]

β = empirical constant for water entrainment function [Chap. 4]

γ = rate of initial mixing $(= Q_a/Q_o)$

Δ = small rise of water level due to stagnation effect [Chap. 2]

Δ = bed form height

δ = divergence angle of the side wall (half-angle of the diffuser)

δ_m = layer thickness defined by $u(\delta) = 1/2u_{max}$

δ_d = displacement thickness

ϵ = density difference relative to ambient density [Chap. 2]

ϵ = kinematic eddy diffusivity of suspended sediment [Chap. 3]

ζ = momentum correction factor

η = rise of water elevation due to channel expansion [Chap. 2]

η = non-dimensional length sale $(= y/\delta)$ [Chap. 4]

η_b = bed elevation

θ = channel bed slope

κ = von Karmon constant (= 0.41)

λ = bed porosity

μ = suspension parameter (= u_*/V_f)

μ_i = u_*/v_i

υ = kinematic viscosity of water

Π = similarity parameter for sediment entrainment function

Π_i = $R_{p50}^{0.5}(D_i/D_{50})^{1.4}$

Π_c = threshold value of Π, roughly equal to five

ρ = water density [Chap. 2]

ρ = density of sediment-water mixture [Chap. 3, 4, 5, 6]

$\Delta\rho$ = excess density relative to ambient water density [Chap. 2]

ρ_s = density of suspended sediment

ρ_w = density of water [Chap. 3, 4, 5, 6]

σ = specific gravity of sediment

τ = shear stress

τ_b = shear stress at the channel bed

τ_w = shear stress at the wall

τ_* = Shield's parameter

ϕ = correction factor for reaction force

Ψ = stagnation index

χ = ratio of H_1 to H_2

Subscripts:

a	=	refers to ambient water [Chap. 2]
a	=	refers to a parameter at elevation y = a = 0.05H above the bed [Chap. 3, 4, 5, 6]
b	=	refers to property at the bed
c	=	refers to critical or threshold value
d	=	refers to downstream end of plunge region
H	=	refers to a parameter at elevation y = H abov the bed
o	=	refers to initial value of a parameter
p	=	refers to vertical section through plunge line
s	=	refers to sediment related parameter
w	=	refers to clear water
x	=	refers to x-component

Superscripts:

I	=	refers to control volume I
II	=	refers to control volume II
*	=	refers to non-dimensional depth [Chap. 2]
*	=	refers to a parameter related to buoyancy force [Chap. 4, 5, 6]
'	=	refers to fluctuating (turbulent) component of a parameter
^	=	refers to normalized value of a parameter (relative to initial value at x = 0)
~	=	refers to value of a parameter related to homogeneous wall jet
—	=	refers to value of an averaged property

1. INTRODUCTION

When water with density ($\rho_a + \Delta\rho_o$) flows into, over, or under ambient water with density (ρ_a), a density current is observed. The velocity and dimensions of the density current depend on the condition of the ambient water (well-mixed, stratified) and on the density difference between the ambient and inflow water (positive or negative).

The density difference in nature may be created by one or several of the following parameters:

1) Temperature difference.

2) Dissolved substances.

3) Suspended particles.

The stagnant receiving water can be homogeneous or stratified due to temperature and/or dissolved and suspended solids, and be classified as

1) Well-mixed, which is characterized by uniform water density of the ambient water, i.e., there is no stratification, or

2) Stratified, which is characterized by non-uniform water density of the ambient water, i.e., stratification and typically one or several thermoclines exist.

Dependent on the direction of the buoyancy force, density currents are, in general, classified as follows:

1) Positively Buoyant Flows ($\Delta\rho_o < 0$).

Flow of less-dense fluid flows over ambient fluid; a typical example of this family of flows is the surface buoyant jet.

2) Negatively Buoyant Flows ($\Delta\rho_o > 0$).

A denser fluid flows under ambient fluid; a typical example of this

family of flows is a dense bottom current, underflow, or turbidity current, which travel downslope.

Various kinds of density currents are generated dependent on the combination of the above mentioned three factors, namely, the cause of the density difference, condition of ambient water, and the direction of the buoyancy force.

This thesis is mainly concerned with turbulent negatively buoyant flows generated by dense inflows into stagnant, homogeneous (well-mixed) ambient water.

The density of inflow water is primarily determined by its temperature and/or solids content, whereas the density of the ambient fluid is primarily determined by the temperature provided that there is no production of turbulence by wind or wave action in the receiving water (calm periods). Turbulence is needed for sustaining a significant turbidity. Fig. 1-1 shows schematically the fate of dense inflows carrying suspended particles into such basins.

A dense inflow changes its form in downstream direction by entraining or depositing suspended particles, and by entraining ambient clear water: a plunge flow (formation of internal flow), supercritical gravity current (development or decay stage), internal hydraulic jump (transitional stage), and subcritical gravity current (decay stage). In a subcritical gravity current, the flow vanishes by settling of all suspended particles.

When the inflowing water is denser than the surface lake water, the inflow proceeds to the so-called plunge point (line), where it becomes submerged beneath the lake surface and forms an underflow. Usually, the

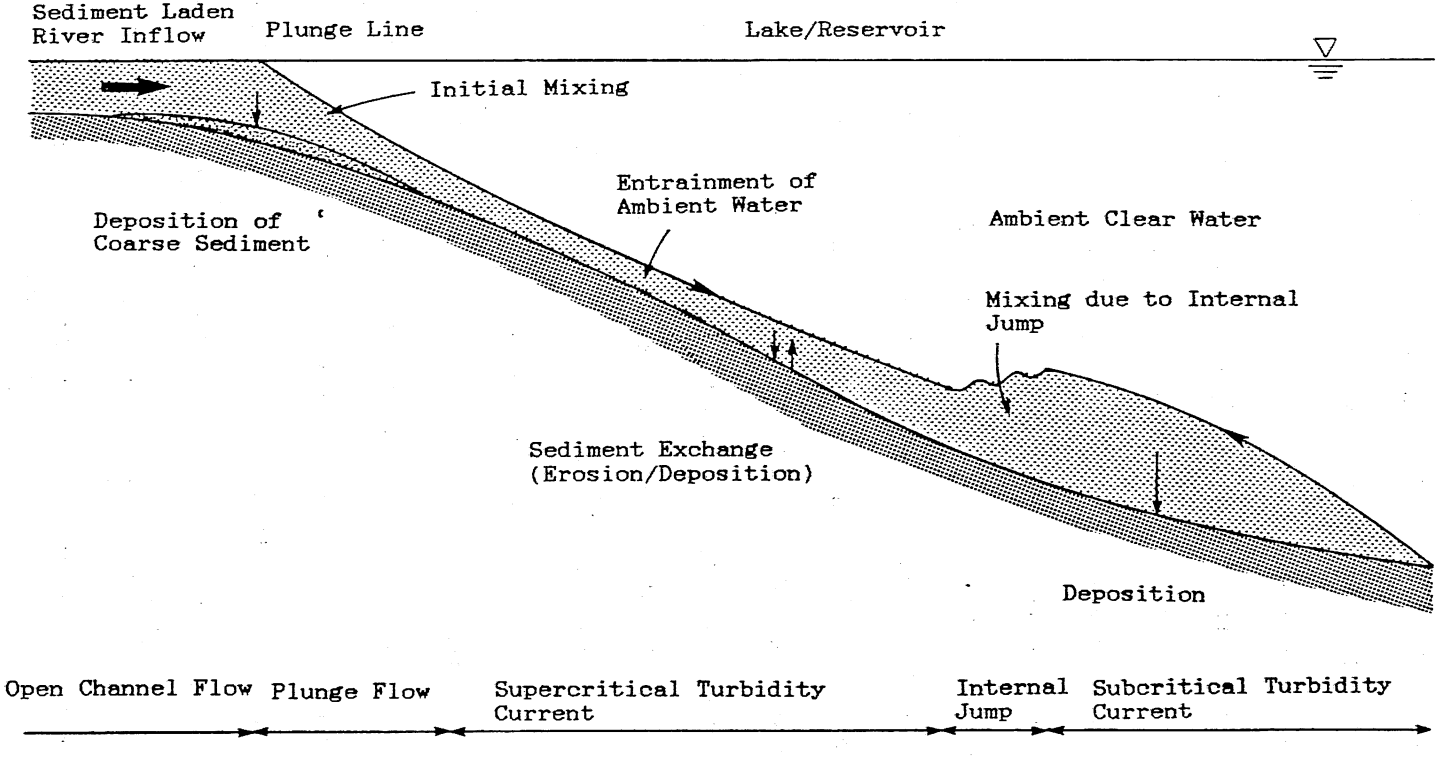

Fig. 1-1 Inflow of sediment laden river water into a lake (schematic).

density current becomes diluted due to local mixing at this point. The rapid reduction of velocities near the entrance is also responsible for the deposition of the larger sediment particles and the formation of delta deposits when the river water is transporting a mixture of different sizes of sediments. The behavior of a gravity current in terms of its velocity, density, and flow depth depends on the plunging phenomenon (the location, the amount of local dilution and sediment deposition in the plunge region). This plunging flow yields the initial conditions for the resulting gravity current.

When a dense inflow is carrying suspended sediment, the bottom geometry of a channel or basin around a plunge region is changed by suspended sediments settling onto the bed. Deposited sediments can be transported downstream as bed load. It is not certain whether suspension plunge flows are always depositive or erosive. Erosive plunge flows may be possible on steep slopes although subaqueous flows are generally slow. The flow velocity must be smallest near the plunge line and will increase in downstream direction on a steep slope.

Deposition is dominant for coarser sediments resulting in the formation of deltas, or fore-set beds with a steep slope, as studied by river investigators. It is often observed that the bed changes from a steep to a less steep slope in downstream direction as depicted in Fig. 1-1. A typical field example of the problem under consideration is given in Fig. 1-2a. Fig. 1-2b shows the velocity correlation between sediment laden river discharge and dense bottom current at point L-3 in Fig. 1-2a. Prior to studying the deposition of coarser sediment particles in the plunge region, it is necessary to investigate a

non-suspension plunge flow, because the plunging flow itself has not been well understood yet. The plunge phenomenon dealt with in this thesis is, therefore, a non-suspension flow which consists of a dense inflow caused by temperature difference or dissolved matter.

In a manner similar to open channel hydraulics, subaqueous flows (internal flows) have two flow regimes; supercritical and subcritical.

The flows are controlled from upstream to downstream in supercritical flow, or from downstream to upstream in subcritical flows as indicated by arrows in Fig. 1-1. The internal hydraulic jump is the mechanism by which a density current changes from the former to the latter regime.

A major difference between suspended sediment transport in open channel flows and subsurface gravity currents must also be noted. In open channl flow, the passive admixture assumption permits the velocity and sediment concentration profiles to be determined separately from the system of equations of motion. Suspended sediment does affect the turbulence structure to a certain extent, but does not influence much the hydraulic condition (mean flow properties) in open channel sediment transport. In gravity currents, on the contrary, suspended sediment is the essential agent which creates the density difference and thus produces internal flows. This fact makes prediction of the behavior of subcritical suspension gravity currents very difficult, especially since they are expected to vanish completely at some distance downstream of an internal hydraulic jump as described previously. There exists no hydraulic model to estimate the rate of subsurface sediment transport in a subcritical gravity currents. In particular, it appears to be

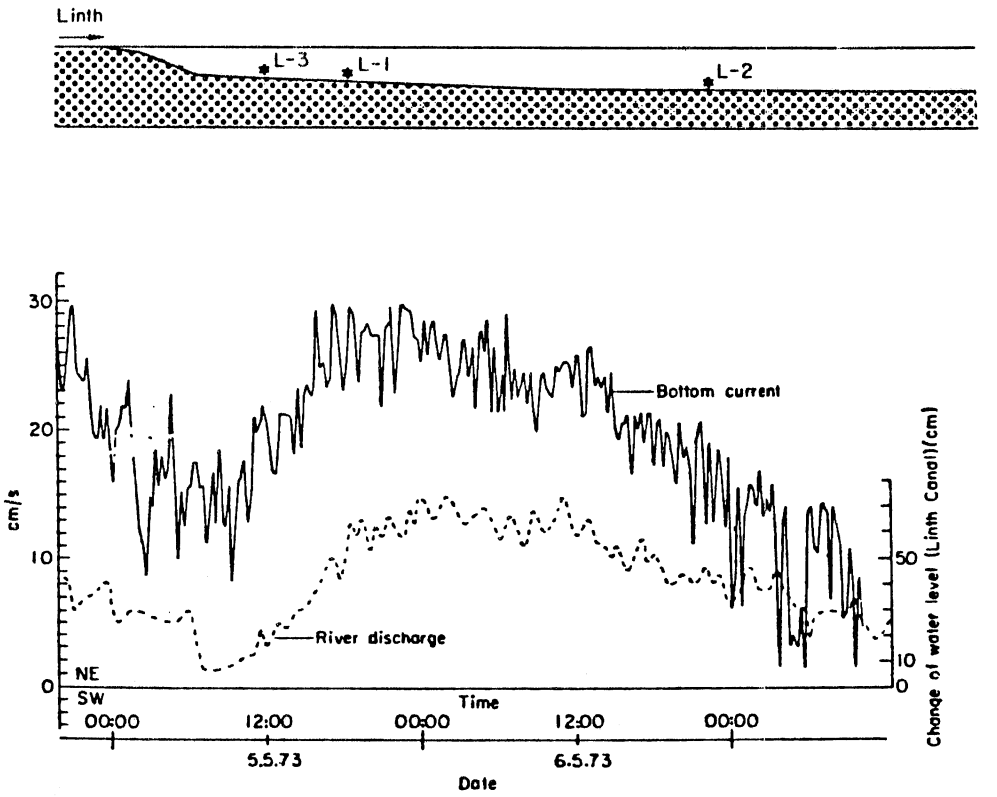

Fig. 1-2 Measurements of density underflows from Walensee, Switzerland at the station L-3 (after Lambert et al. [1976])

impossible to predict the behavior of internally subcritical suspension gravity currents till they completely vanish.

Suspension gravity currents considered herein are supercritical flows over steep slopes, but the model proposed in this thesis can also be used for internally subcritical flow.

The situation shown in Fig. 1-1 occurs frequently with turbid water. The introduction of turbid water and transport, erosion and deposition of sediment by turbidity currents are of significance for pollution in the marine environments, reservoir sedimentation, subaqueous geological and geographical features, and analysis of aquatic biological environments.

In chapter 2, the onset of underflow due to the direct inflow of denser water into well-mixed stagnant water (plunging phenomenon) is investigated. Horizontal inflow into two-dimensional sloping basins, which represent reservoirs, lakes, and estuaries is investigated theoretically. Two basin configurations are considered: a sloping constant width and a horizontal diverging channel. The former analysis is directed towards prediction of the depth at plunge line in terms of essential independent parameter governing the problem. These parameters include the inflow densimetric Froude number (F_o), the initial mixing rate (γ), the bed slope (S), and the friction coefficient (f_b) at the bed. The obtained equations for plunge depth are compared with available data. The latter analysis consists of experimental and analytical investigation. The effects of channel expansion on plunging phenomenon are mainly examined. Experiments were conducted in a horizontal laboratory channel with slightly diverging walls to simulate

this plunging flow. A temperature difference between inflow and ambient provided the necessary density differential. Temperature profiles and flow visualization were used to determine flow conditions in the plunging region. It was found that dilution rate (γ) of the inflow, densimetric Froude number at plunging (F_p), and other factors of the flow are related to divergence angle (δ) of the flume, inflow densimetric Froude number (F_o), initial aspect ratio at channel inlet (A_o), and other independent variables. Densimetric Froude numbers from 0.56 to 0.89 occured at the plunging line. Channel divergence angles (half-angle) from 1^o to 15^o were investigated. Volumetric flow rates in the sinking flow increased up to 45% during the plunging process. Maximum entrainment rates were related to divergence angle. Water depths downstream from the plunge line were from 0.65 to 0.9 times the depth at the plunge line, and channel widths downstream from plunge line were from 1.05 to 1.83 times the width at the plunge line.

In Chapter 3, experimental and field data for open channel suspension are used to establish a function predicting the rate of entrainment of non-cohesive sediment into suspension. Both uniform and non-uniform bed material are considered. Analysis is based on dimensional arguments and a similarity collapse method. It is found that the sediment entrainment function (E_s) has two independent parameters; suspension parameter (V_f/u_*) and particle Reynolds number (R_p), and has a very steep slope with suspension parameter, this reflects the explosive nature of the sediment entrainment mechanism. The entrainment function can be applied to sedimentation and erosion problems of slightly non-uniform, non-equilibrium flows in rivers,

lakes, and estuaries, and the coastal regions. The results are used for simulating turbidity currents with sediment exchange between the current and the bed.

In Chapter 4, the equations which govern the movement of two-dimensional gradually varied turbidity currents in reservoirs, lakes, and on the coastal shelf are derived and solved numerically. Turbidity currents are characterized as sediment-laden gravity currents that exchange sediment with the bed by erosion or deposition as the flow travels downslope. Turbidity currents derive this driving force from sediment in suspension. The sediment entrainment function obtained in Chapter 3 is applied in the model.

Turbidity currents can be eroding or depositing, accelerating or decelerating, dependent on the combination of initial conditions (H_o, B_o, R_o), bed slope (θ), kinematic viscosity of water (υ), channel bottom friction coefficient (C_{bo}), and submerged specific gravity (σ) and size (D_s) of sediment particles provided that the entrainment functions of water (E_w) and sediment (E_s) are properly given.

Gravity currents with and without erosion and deposition are examined qualitatively in order to understand the effects of suspended sediment exhange in the flow.

In Chapter 5, the equations which govern the movement of three-dimensional gradually varied turbidity currents in a slightly diverging and sloping channel are derived and solved numerically. There are similarities and differences between diverging and non-diverging cases. In diverging-sloping channels, the behavior of the flows is dependent on initial channel aspect ration (A_o), side wall slope (δ),

and frictional coefficient (C_{wo}) at the wall in addition to parameters for the non-diverging case.

Therefore, the effects of these three parameters on the physics of the flows are mainly investigated.

In Chapter 6, the model developed in Chapter 4 is applied to actual field cases. In order to demonstrate the validity of the model for turbidity currents, two cases are considered as examples; man-made tailings currents in Lake Superior, Minnesota near Silver Bay and natural turbidity currents in Scripps Submarine Canyon.

In Chapter 7, final comments and general conclusions of Chapter 2 through 6 are presented.

2. ONSET OF GRAVITY CURRENTS

2.1 Outline and Summary of Previous Work

A gravity current is often caused by the inflow of cold water, suspended sediment laden water or of polluted water into a lake, reservoir, or coastal region with a density smaller than that of the inflow. High concentrations of suspended sediments are observed in rivers during flood periods, while high concentrations of dissolved materials can be a consequence of pollution, and may occur during periods of low flow as well. When heavier water is introduced into lighter ambient water over a bottom slope, the inflow pushes the ambient water until it reaches a balance of forces, and at that point starts to sink beneath the ambient water as shown in Fig. 1-1. This phenomenon is sometimes referred to as a "plunging flow," and the location of the onset of submergence as a "plunge line" or "plunge point."

The onset of the submergence of the inflow can be associated with intense local mixing resulting in dilution due to the abrupt change of the flow depth The mixing in the plunge region is sometimes called "entrance mixing" or "initial dilution." Such local mixing is usually distinguished from the entrainment of ambient water across the interface of a more conventional stratified flow. Several investigators, including Ellison and Turner [1959], Ashida and Egashira [1975], and Tsubaki and Komatsu [1979] have investigated this entrainment across an interface. Entrainment and mixing may be less noticable or insignificant on a mild slope compared to a steep slope. Several analytical and experimental studies of underflows and overflows have

been carried out, but until very recently little attention has been given to the plunge phenomenon itself.

In the field, the location of the plunge line is sometimes visible because of the accumulation of debris and/or the difference in color between the relatively clear ambient water and turbid inflowing water. In particular, the accumulation of debris in the vicinity of the plunge line is indirect evidence that ambient water, induced by the shear stress generated by the plunging flow, is transported towards the plunge line. It is natural to expect that some of the induced flow is entrained into the inflowing water instead of just recirculating. The plunging phenomenon has been observed in the field by Bata and Knezevich [1958], Elder and Wunderlich [1975], Ford, Johnson and Monismith [1980], Ford and Johnson [1981], Hebbert, Imberger, Loh, and Peterson [1979], Howard [1953], Kennedy, Thornton and Carell [1981], Normark and Dickson [1976], Wunderlich and Elder [1975], and Lambert, Kelts, and Marshall [1976].

The study of plunging flows is of significance for water quality management, particularly for the modeling of transport of dissolved solids, suspended matter, and/or colder water by the resulting density current in reservoirs, lake, and coastal regions.

Several models for prediction of plunge depth have been proposed (Table 2-1). Some of these are founded on laboratory experimental work (Singh and Shah [1971], Itakura and Kishi [1981]) or on field studies (Elder and Wunderlich [1972], Ford, Johnson, and Monismith [1980], Ford and Johnson [1981], and Wunderlich and Elder [1973]), and others on theoretical studies (Akiyama and Stefan [1981], Akiyama and Stefan

[1984], Akiyama and Stefan [1987], Fukuoka, Fukushima, and Nakamura [1980], Hebbert, Imberg, Loh, and Peterson [1979], Jain [1980], Kan and Tamai [1981], Savage and Brimberg [1975] and Farrell and Stefan [1986]). Understanding the behavoir of the non-suspension plunging phenomenon is the first stage of investigating the more complex flow of a suspension type, where the density difference is due to solid particles in suspension. The density differences in the laboratory experiments are, therefore, created by either temperature or salinity.

Based on laboratory experiments, Singh and Shah [1971] proposed an empirical relation for the plunge depth. They presented their measurments of plunge depth (h_p) as a function of a critical depth ($h_c = (q/g')^{1/3}$), and they provided a linear least-square fit of their data (g' denotes reduced acceleration of gravity = $g\Delta\rho/\rho$). Experiments were conducted in a channel with relatively steep slope ranging from S = 1/47 to 1/179.

Elder and Wunderlich [1971] found that it is typical of all inflow types (i.e., overflow, underflow, and interflow) that the inflow deepens until a critical depth (h_c) is reached. They observed a critical Froude number of about 0.5 at the plunge point during field studies in Fontana Reservoir. A similar approach was taken by Itakura and Kishi [1979] who proposed $F_p = 1.0$.

Savage and Brimberg [1975] presented two analyses for the plunging phenomenon. One of the analyses was based on the assumption of no loss of energy in the vicinity of the plunge point. The flow was treated as inviscid and it was shown the $F_p = 0.5$. The other of their analyses was based on a gradually-varied two layer system. This second analysis

TABLE 2-1 Summary of Typical Equations for Plunge Depth.

Investigator	Plunge Depth (h_p)	f	S	Y
Jain 1981	$1.6 \left(\frac{\alpha_i}{1+\alpha_i}\right)^{0.126} \cdot \left(\frac{8S}{f_t}\right)^{0.008} \cdot \left(\frac{q^2}{\epsilon_o g}\right)^{1/3}$	o	o	x
Hebbert et al. 1979	$1.16 \left(\frac{q^2}{\epsilon_o g}\right)^{1/5}$ for Wellington Reservoir	o	o	x
Savage & Brimberg 1975	$\left\{\frac{2.05}{1+\alpha_i}\left(\frac{S}{f}\right)^{0.478}\right\}^{-2/3} \cdot \left(\frac{q^2}{\epsilon_o g}\right)^{1/3}$	o	o	x
Singh & Shah 1971	$1.85 + 1.3 \left(\frac{q^2}{\epsilon_o g}\right)^{1/3}$	x	x	x
Wunderlich & Elder 1973	$\left(\frac{1}{0.5}\right)^{2/3} \cdot \left(\frac{q^2}{\epsilon_o g}\right)^{1/3}$	x	x	x
Akiyama & Stefan (this study)				
(Mild Slope)	$\frac{1}{2}\left[\left(\frac{2+\gamma}{2} + \frac{S_2 S}{f_t} + \sqrt{\left(\frac{2+\gamma}{2} + \frac{S_2 S}{f_t}\right)^2 - \frac{4}{1+\gamma}\left(\frac{S_2 S}{f_t}\right)}\right)\right]\left(\frac{f_t}{S S_2}\right)^{1/3}\left(\frac{q_o^2}{\epsilon_o g}\right)^{1/3}$	o	o	o
(Steep Slope)	$\frac{1}{2}\left[\left(\frac{2+\gamma}{2} + S_1\right) + \sqrt{\left(\frac{2+\gamma}{2} + S_1\right)^2 - \frac{4}{1+\gamma} S_1}\right]\left(\frac{1}{S_1}\right)^{1/3}\left(\frac{q_o^2}{\epsilon_o g}\right)^{1/3}$	x	o	o

f = Bed friction coefficient
S = bed slope
Y = dilution coefficient

o = Parameters considered
x = Parameters not considered

f_t = total friction coefficient

$K = f_t/S_2$

S_1, S_2 = coefficients

α_i = ratio of interfacial to bed shear stress

considered the viscosity of water. They not only considered the existence of interfacial profiles similar to Bata [1953] after the plunge point, but also carried out calculations up to the water surface in order to predict the plunge depth in terms of the bed slope (θ), the bed friction coefficient (f_b), and the interfacial friction coefficient (f_i).

Jain [1980] critically examined the paper by Savage and Brimberg [1975]. He showed that the solution based on energy conserving flow is physically impossible. The energy dissipation near the plunge point is essential to the flow mechanism. He also examined Savage and Brimberg's second analysis, and concluded that the profile calculation is sensitive to the direction of numerical integration. The direction should be that in which the hydraulic control is acting. This is in agreement with an earlier analysis for non-suspension gravity currents by Stefan [1973].

Hebbert et al. [1979] applied conservation of mass, volume, and momentum to a cross-section upstream and downstream of the plunge point. They developed a semi-theoretical formula with the aid of field data from the Wellington Reservoir. The form of their result differs slightly from others, since they assumed a triangular instead of a rectangular cross-section.

Kan and Tamai [1981] conducted experiments in a sloping-diverging channel ($db/dx = 0.1$), and could not find much difference in F_p between diverging and non-diverging cases based on their data. They, therefore, proposed that the formula for a non-diverging channel could be applied approximately for a diverging case as well.

Fukuoka et al. [1980] applied Benjamin's [1968] analysis for the cavity flow in a closed conduit to plunging flow, and examined the predicted plunge depth with some laboratory experimental data (S = 1/10 and 1/60), for steep slope only, where initial mixing is not negligible. They proposed that plunge depth is strictly a local phenomenon, and concluded that Reynolds number and channel bed slope are insignificant for plunge depth. It must be noted that their analysis dealt with the plunging phenomenon of the non-initial mixing case, and that perhaps the results can be applied to steep slopes only.

Akiyama and Stefan [1984] considered that initial mixing and channel characteristics are essential in the plunging phenomen, and both effects are theoretically taken into account in the prediction of plunge depth by considering the plunging flow region as well as the resulting underflow region. They proposed that two flow regimes below the plunge point can be distinguished depending on whether the channel slope is mild or steep and each flow regime has a different plunge depth. Akiyama and Stefan [1981] extended the analysis from a well-mixed reservoir to plunging flow in a multi-layered (stratified) reservoir.

Akiyama and Stefan [1987] investigated the effect of channel divergence and found that it is of significance in the determination of the plunge depth and initial mixing rate. They also found theoretically and experimentally that for the plunging phenomenon in a diverging channel the initial conditions such as initial densimetric Froude number (F_o) and initial channel aspect ratio (A_o) are also important, (these parameters do not control plunging flow in a channel with parallel side walls) and proposed a model for which the energy dissipation near the

plunge line is taken into account. Energy dissipation appears to be of considerable importance in entraining plunging flow, and it is found experimentally that the rate of initial dilution depends systematically on the amount of energy dissipation.

Farrell and Stefan [1986] employed a numerical method to simulate the entire flow field, including plunging, underflow, and induced recirculating flow, by directly solving the unsteady equations of motion including a buoyancy modified k - ϵ - model for turbulence. The triangular two dimensional flow domain, which represents a reservoir cross-section and compared their results for plunge depth obtained from numerical experiments, with their experimental results (S = 1/21). A similar kind of analysis was also conducted by Harper and Waldrop [1981] using an eddy diffusion model.

In all of the cases described above the plunging flow occured in a laterally confined channel, and the flow remained attached to both side walls. If the flow separates, the flow behaves like jet flow instead of channel flow. According to Akiyama and Stefan [1987], the separation of the flow starts to be observed when the half divergence angle (δ) of the side wall is around 7^{o}, dependent on inflow Reynolds number. When δ = 15^{o}, the inflow separates at the end of the approach channel.

Very recently the plunging flow in a laterally unconfined basin has been studied (Kan and Tamai [1981], Hauenstein and Dracos [1984]), Johnson et al.[1986] conducted experiments of negatively buoyant inflows into diffusers (diverging channels) with several angles, and found experimentally typical flow regimes and patterns. They also found experimentally that the major portion of the dilution occurs in the

momentum dominated region if the flow is separated. The dilution in the process of plunging (buoyancy dominated region) is minor.

Hauenstein and Dracos [1984] considered the situation that a basin is totally unbounded (laterally and in flow direction). The bottom of the basin is a plane, of constant roughness and inclined at angle θ. They divide the flow region into two subregions, momentum and buoyancy dominated regions. and obtained a semi-theoretical formula to predict plunge depth in terms of initial depth, source Froude number, slope, and aspect ratio, applying jet flow analysis in the momentum dominated region and using regression analysis.

Prior to Hauenstein and Dracos [1984], Kan and Tamai [1981] independently obtained very similar results based on an almost identical approach.

Research approaches and experimental conditons used previously in analyses of plunging flow problems are summerized as follows.

(i) Experimental Conditions

Channels or tanks with sloping bottoms are used in laboratory experiments to represent reservoirs, lakes, and coastal regions.

Two-dimensional models are applied to the non-diverging sloping channel with a variable bed slope (e.g. Singh and Shah [1971], Kan and Tamai [1981], Fukuoka et al. [1980], and Itakura and Kishi [1979]), or the diverging horizontal channel (Akiyama and Stefan [1986] and Johnson et al. [1986]), or the sloping diverging channel (Kan and Tamai [1981]), or the laterally unbounded horizontal basin (Johnson et al. [1986]), and laterally unbounded sloping basin (Hauenstein and Dracos [1984]).

Channels used in experiments differ from each other. Besides differences of the receiving water, the most noticeable difference, which is considered critical, is the condition of the approach channel. Some measurements were made with an approach channel that has the same slope as the basin bed (e.g., Itakura and Kishi [1979], Kan and Tamai [1981]), others use a horizontal approach channel (e.g., Fukuoka et al. [1980], Hauenstein and Dracos [1984], Johnson et al. [1986]). None of the approach channel configurations reflect actual field situations. The latter is, however, more realistic than the former.

Since most rivers transport sediment as suspended and bed load, common features such as "Top-set beds," "Fore-set beds," "Bottom-set beds," and "Density current beds" are observed in reservoirs. Top-set beds have very mild slopes, and the bed slope suddenly increases at the "shoulder." The bed slopes become milder for Fore-set beds in downstream direction.

(ii) Analysis

1) Empirical analysis uses regression analysis for field or laboratory data (Singh and Shah [1971], Elder and Wunderlich [1972]).

2) Numerical analysis solves an entire flow domain (entire reservoir) including the induced movement of ambient water by plunging flow by a numerical method (Farell and Stefan [1986]).

3) Gradually varied flow analysis uses equations for the underflow up to the water surface and treats the plunging region as a part of the underflow (e.g., Savage and Brimberg [1975], Jain [1981]).

4) Integral type analysis applies a control volume to the plunge region, separating the flow domain into a homogeneous open channel, plunge, and underflow region (Hebbert et al. [1979], Akiyama and Stefan [1984], Akiyama and Stefan [1987], Kan and Tamai [1981], and Fukuoka et al. [1980]).

2.2 General Flow Model

Non-separating plunging flows, i.e., plunging flows which remain attached to laterally confining channel walls will be investigated herein (Fig.2-1).

If the plunge line is approximated by a line as shown in Fig. 2-1, ignoring the effects of side wall friction the equation of plunge depth can be expressed in the general form:

$$h_p = (1/F_p^2)(q_o/g')^{1/3} \qquad 2\text{-}1$$

where h_p = the plunge depth

F_p = the densimetric Froude number at plunge line

g' = the reduced acceleration of gravity (= $\epsilon_o g$)

q_o = the inflow flux per unit span (= $Q_o/2b_p$)

Q_o = the total inflow

b_p = one-half the plunge width

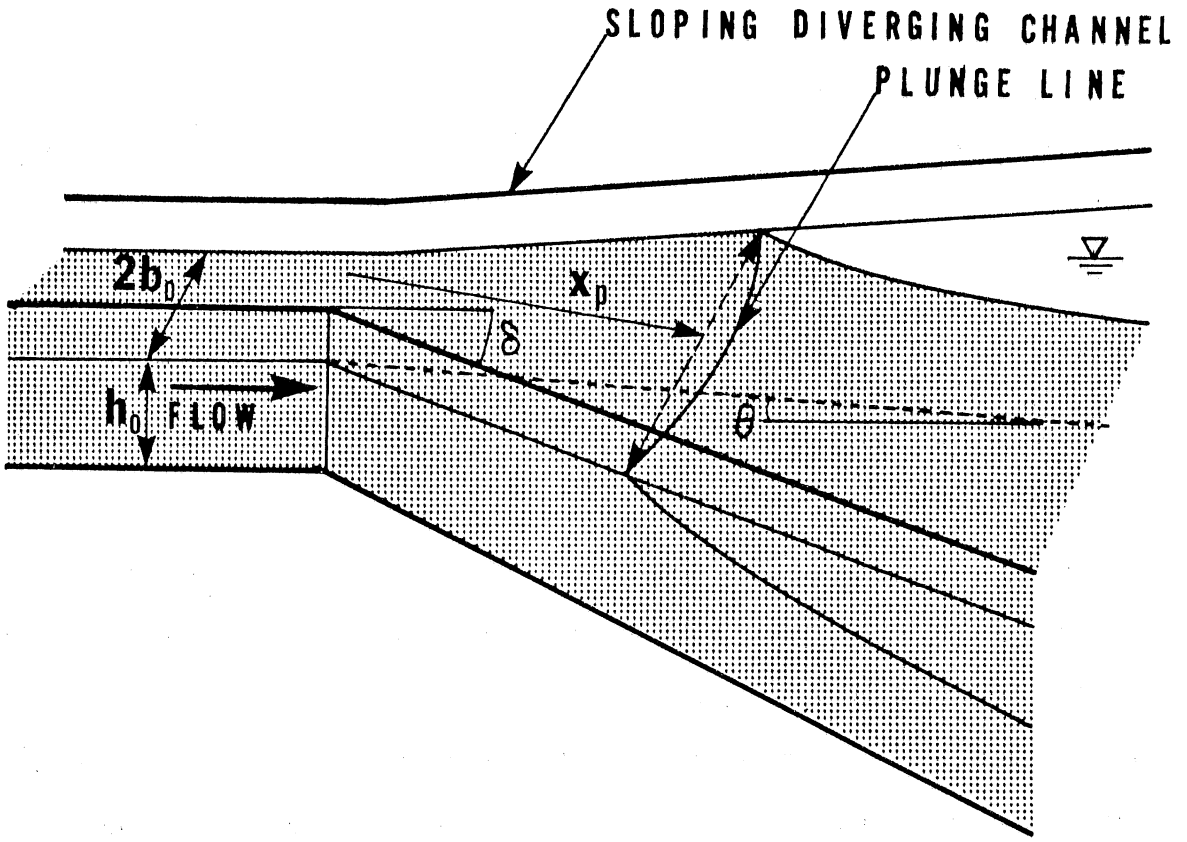

Fig. 2-1 Plunging flow in a sloping-diverging channel (schematic)

To find the location of the plunge line (h_p) is thus equivalent to determining the densimetric Froude number at the plunge line (F_p). It must be noted that plunging flows in a sloping diverging channel have two characteristic length scales; h_p and b_p. However, h_p and b_p are related to each other through the distance (x_p) from channel inlet to plunge line.

$$h_p - h_o = x_p \tan\theta \qquad 2\text{-}2$$

$$b_p - b_o = x_p \tan\delta \qquad 2\text{-}3$$

Hence,

$$\frac{h_p}{h_o} = A_o \frac{\tan\theta}{\tan\delta} \left(\frac{b_p}{b_o} - 1\right) + 1 \qquad 2\text{-}4$$

where A_o is the initial channel half-aspect ratio ($= b_o/h_o$). It is necessary to determine one of the characteristic length scales. Typical field and laboratory examples of the formation of the plunging phenomenon and the resulting underflow in a reservoir were given e.g., by Wunderlich and Elder [1973] and Hebbert et al. [1979], and Fukuoka et al. [1986] and Johnson et al. [1986] respectively. Typical examples of velocity and temperature profiles of non-diverging plunging flows and resulting density currents over steep bottom slopes are shown in Fig. 2-2 ~ 2-5. Measurements were conducted by Johnson et al. [1986].

Figure 2-2a is for the plunge flow bottom slope with S = 1/21, intial Froude number F_o = 2.0, Reynolds number at inlet Re_o = 4510, and

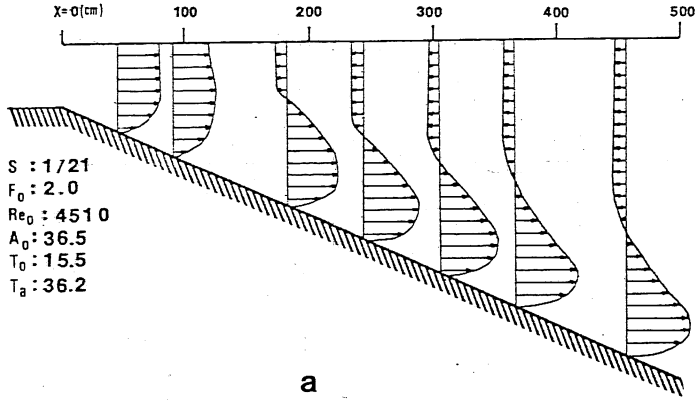

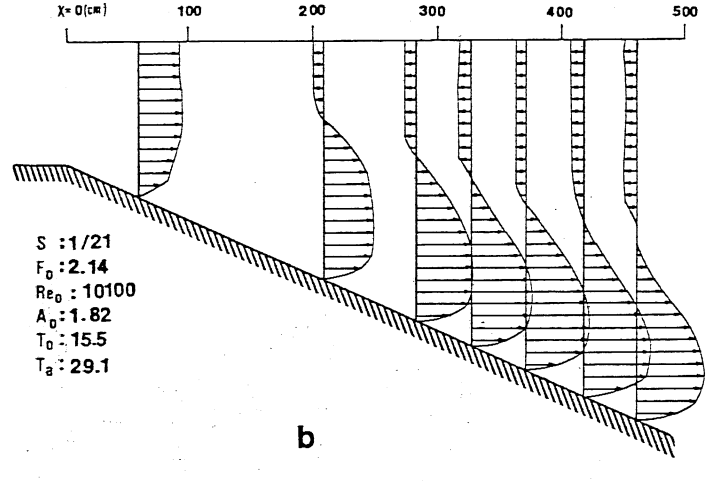

Fig. 2-2 Succesive velocity profiles of a plunging flow.

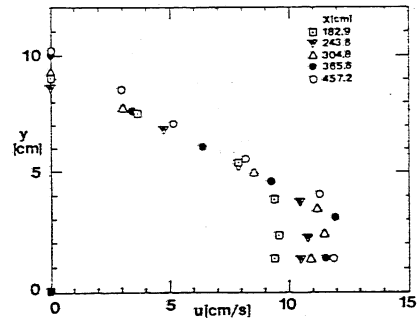

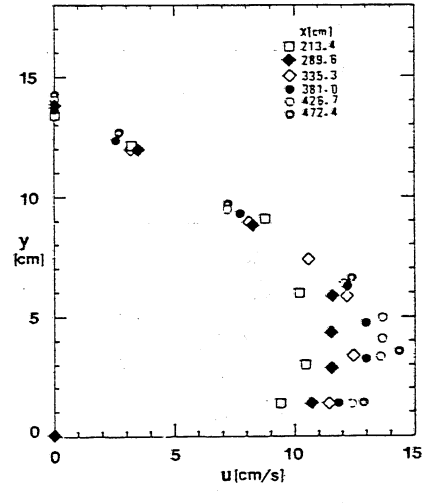

Fig. 2-3 Velocity profiles (from plunge to underflow region).

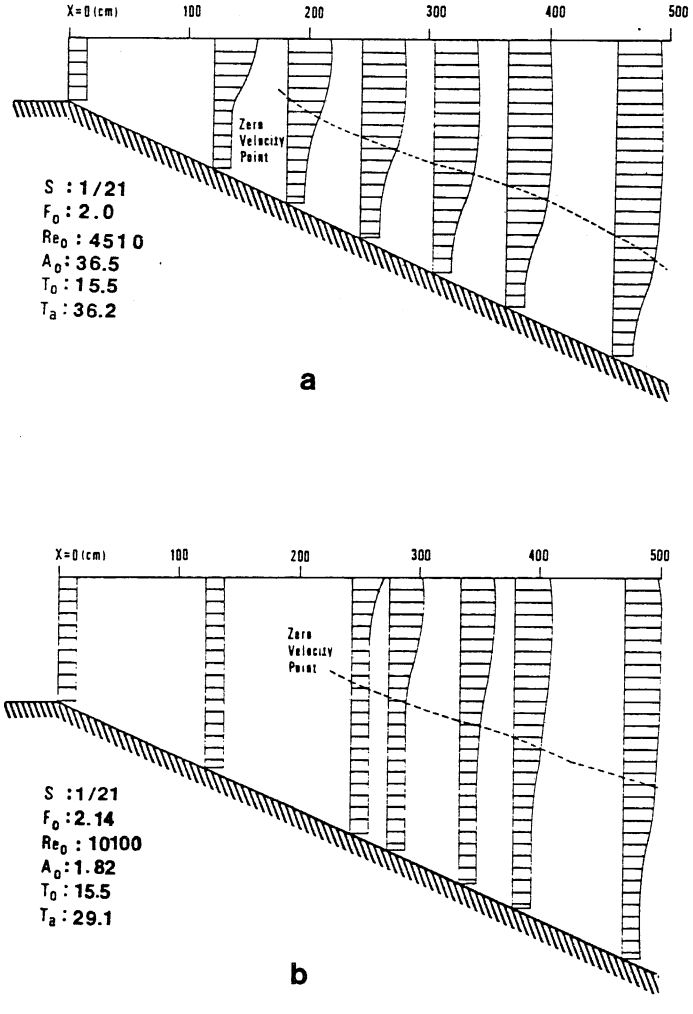

Fig. 2-4 Succesive temperature profiles of a plunging flow.

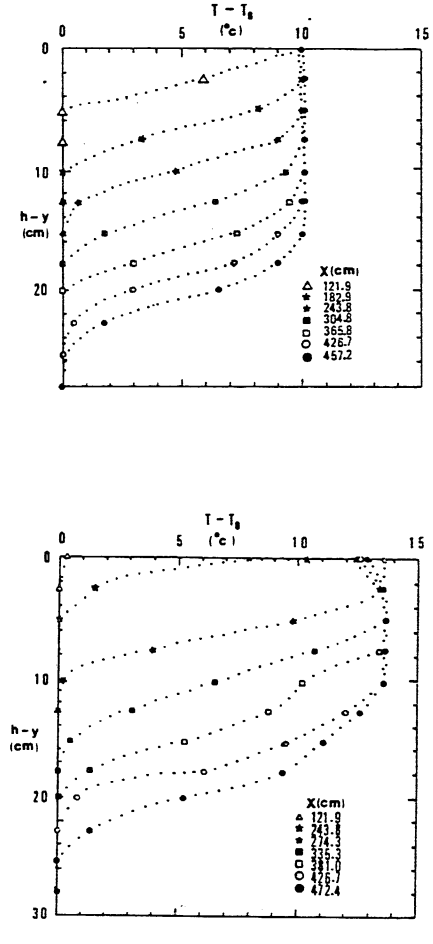

Fig. 2-5 Temperature profiles (from plunge to underflow region).

initial half-aspect ratio $A_o = 3.65$, and Fig. 2-2b for $S = 1/21$, $F_o = 2.14$, $Re_o = 10100$, and $A_o = 1.82$.

As can be seen in Fig. 2-2 velocity profiles of the ambient, induced flow are almost uniform at any section in the plunging region, while velocity profiles of the inflowing water change from homogeneous open channel flow to underflow within a relatively short distance. Similarity of velocity profiles does not appear to exist, and the flows are accelerated in the plunge region (Fig. 2-3). These observations are also confirmed by other investigators, for example, Fukuoka et al. [1980]. The velocity zero point is added to the temperature profiles (Fig. 2-4) in order to see the relationship between velocity and temperature distributions, as shown in Fig. 2-5. Similarity of temperature profiles does not exist either. The plunging occurs over a relatively short distance compared to the length of the underflow region. Herein, the plunge phenomenon can be defined as the transitional flow from homogeneous open channel flow to stratified, entraining underflow. The flow field, therefore, is divided into three fairly distinct regions, called "homogeneous," "plunge," and "underflow" regions as illustrated in Fig. 1-1. Consequently in the analysis, plunging flows are treated as transitional flows.

The role of the inflow is to push ahead the ambient water, while the underflow has to transport away the plunge pool water. When both rates are matched, the actual plunge point (line) has found it proper position. Inflow and underflow conditions are hence equally significant for the understanding of the dynamics of the plunging phenomenon.

Initial mixing between inflow and ambient water must be considered and taken into account in the analysis or model.

The plunge depth can be determined by the force balance with the aid of additional information about both underflow and mixing characteristics.

2.3 Analysis

2.3.1 Purpose

Consideration of the effects of the receiving basin characteristics and of initial mixing on F_p seems to be lacking in previous investigations. The noticeable scatter of F_p and γ values in Table 2-2 and 2-3 may be attributed partially to differences in these characteristics. Physical parameters controlling the plunge phenomenon are, therefore, considered to come from initial conditions as well as channel characteristics in the present analysis.

Channel divergence and channel bed slope provide two degrees of freedom to the mechanism of plunging flow. Although the divergence angle δ in impoundments is frequently larger than the bottom slope θ, the effect of channel divergence on the plunge phenomenon has not been theoretically studied by previous investigators.

Plunging flow considered theoretically herein is a non-separating (attached) flow. The primary objectives are:

a) the location of the "plunging point (line)" at which the inflow sinks beneath the ambient water; plunge depth (h_p) and half-width (b_p), or alternatively F_p.

b) the rate of "initial (entrance) mixing" (γ) during the

plunging, which is expressed by the ratio of total entrainment rate (Q_a) to inflow rate (Q_o): $\gamma = Q_a/Q_o$.

c) the understanding of the flow structure.

However, closure of the plunging flow analysis, when initial dilution γ is incorporated, appears to be theoretically impossible even in the simplest case (non-diverging sloping case). Therefore, the plunge phenomenon is investigated not only theoretically but also experimentally.

2.3.2 Governing Parameters of a Plunging Flow

Consider the plunging region in a sloping-diverging channel of rectangular cross-section as shown in Fig. 2-6. The inflowing water has a larger uniform density ($\rho_a + \Delta\rho_a$) than that of ambient water of a uniform density (ρ_a), and a discharge Q_o. The ambient water into which the plunging occurs has a uniform density (ρ_a), and is entrained at a rate Q_a. The discharge (Q_d) downstream of the plunge line has an average density ($\rho_a + \Delta\rho_d$). Plunge flow travels under the action of reduced acceleration of gravity ($g' = \Delta\rho_o/\rho_a$).

The characteristic dimensions at which plunging occurs are the plunge depth (h_p) and the half-width (b_p) instead of only the plunge depth (h_p) used in previous analyses. Other important dimensions are the depth (h_d) of underflow downstream of the plunge line, the corresponding half-width (b_d), the depth of ambient water downstream of the plunge line (h_a), and the initial outlet depth (h_o). The channel characteristics which are important include roughness of bottom (f_b) and side wall (f_w), bottom slope (θ), divergence angle (half-angle) of the

side wall (δ), and initial outlet half-width (b_o). Both bottom slope (θ) and divergence angle (δ) are constant. The independent variables are θ, δ, h_o, b_o, Q_o, $\Delta\rho_o$, ρ_a, and g. The dependent variables are h_d, b_d, Q_a and $\Delta\rho_d$. The latter describe the effluent from the plunging region. Symbols are defined in Fig. 2-6.

A densimetric Froude number is defined, in general, by

$$F_i = \frac{Q_i}{\sqrt{\epsilon_i g b_i^2 h_i^3}} \qquad 2\text{-}5$$

Where Q = total discharge, g = acceleration of gravity, h = characteristic flow depth, b = characteristic flow half-width, and $\epsilon = \Delta\rho_o/\rho_a$ = density difference relative to ambient density. The subscript i designates the location of the densimetric Froude number at the outlet (i = o), at the plunge line (i = p), and farther downstream (i = d).

The set of parameters will be reduced to the following dimensionless ones:

$(F_p, \theta, \delta, Q_a/Q_o, b_o/h_o, h_d/h_p, b_p/b_d, f_w, f_b)$.

2.3.3 Governing Equations of a Plunging Flow

In order to understand the role of each parameter, the governing equation of plunging flow in a slightly diverging sloping channel are considered.

A plunge flow is treated as a "rapidly varied" flow in the sense used in open channel flow, and thus an integral approach (control volume analysis) is adopted.

Non-uniformity of both velocity and density profiles (vertical and horizontal) are taken care of by shape factors introduced later.

Considering the plunge region (main control volume C.V.I) in Fig. 2-6, the relationship for total volumetric flow (incompressible flow) and mass flow (mass conserving flow) between "p" and "d" are, respectively:

a) Conservation of Volume

$$Q_p + Q_a = Q_d \qquad 2\text{-}6$$

b) Conservation of Mass

$$(\rho_a + \Delta\rho_o)\, Q_p + \rho_a Q_a = (\rho_a + \Delta\rho_d)\, Q_d \qquad 2\text{-}7$$

Defining the initial mixing rate γ by the fraction of ambient entrained total flow rate Q_a to total initial flow rate Q_o $(= Q_p)$, Eqs. 2-6 and 2-7 yield:

$$Q_d = (1 + \gamma)\, Q_p = (1 + \gamma)\, Q_o \qquad 2\text{-}8$$

and

$$\Delta\rho_d = \Delta\rho_o/(1 + \gamma) \qquad 2\text{-}9$$

The initial density difference $\Delta\rho_o$ and the density difference downstream of the plunge line $\Delta\rho_d$, both relative to ambient density ρ_a are therefore expressed as:

$$\Delta\rho_d/\rho_a = \epsilon_d = \epsilon_o/(1 + \gamma) \qquad 2\text{-}10$$

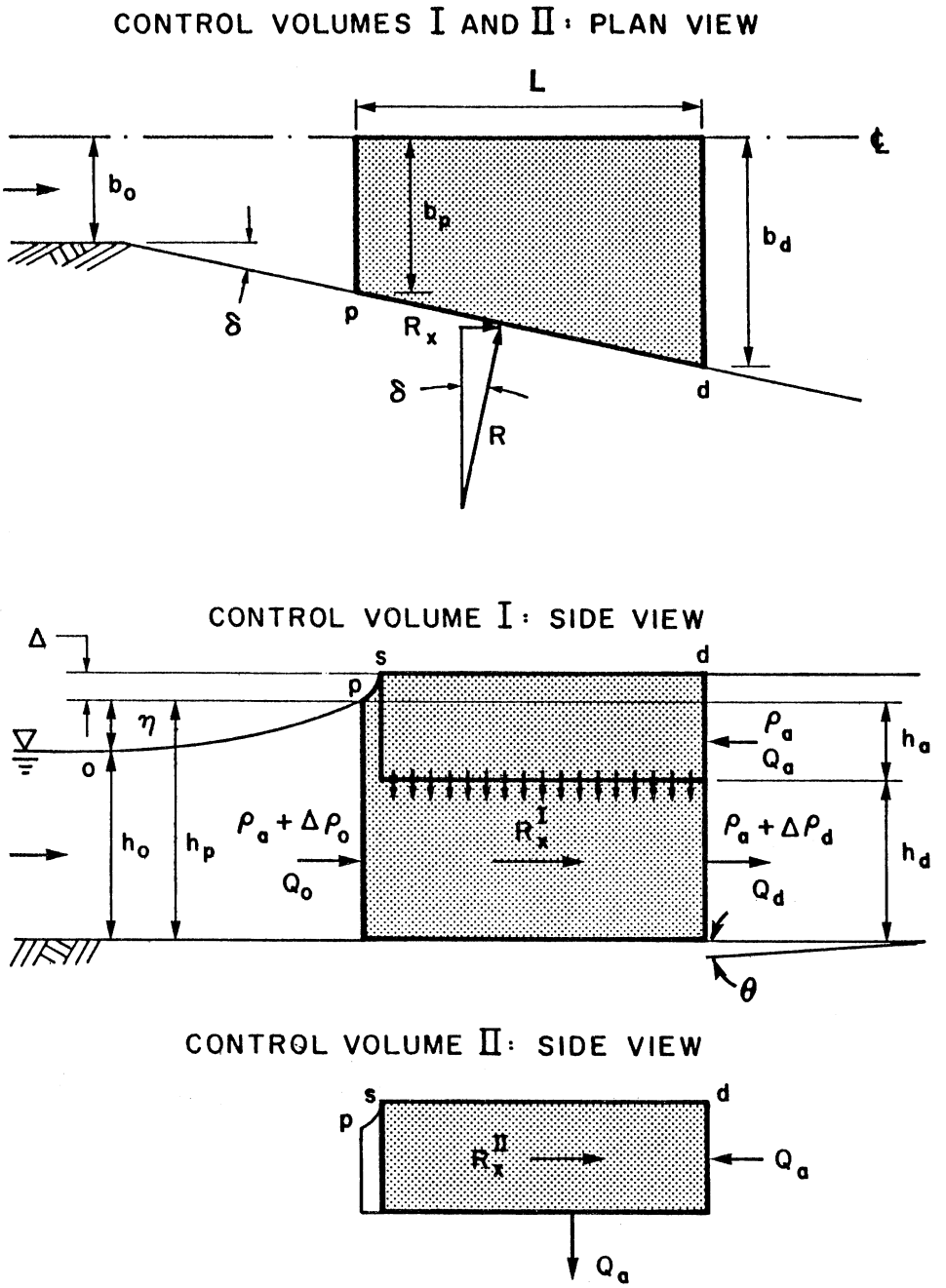

Fig. 2-6 Definition of control volumes I and II in plunge region

In this analysis the density differences are very small, such that $0[\epsilon_o]$ and $0[\epsilon_d] \ll 1$.

The difference of the water level Δh between the point "o" and the point "s" where the inflowing water with density $(\rho_a + \Delta\rho_o)$ will submerge beneath the ambient water with density ρ_a, is caused by the reduction of flow velocity towards the plunge line. Such a difference of water level is not only due to the gradual expansion of the cross-sectional area, but also the existence of a stagnation-like point "s," $\Delta h = \eta + \Delta$.

c) Energy Equation

Applying Bernoulli's equation along a free surface between an arbitrary point "p" in the vicinity of the plunge line and the point "s,"

$$\psi \frac{(\rho_a + \Delta\rho_o)U_p^2}{2} = (\rho_a + \Delta\rho_o)g\Delta \qquad 2\text{-}11$$

or

$$\frac{\Delta}{h_p} = \psi \frac{\epsilon_o F_p^2}{2} \qquad 2\text{-}12$$

where Δ is the difference in water surface levels between "p" and "s." The parameter ψ is introduced in the equation above in order to incorporate the effects of energy conversion and dissipation near the plungeline. $1 - \psi$ is the fraction of kinetic energy (potential) lost during the plunging process. The parameter ψ is called "stagnation index." The stagnation index can vary from 0 to 1.

No energy dissipation exists if $\psi = 1$, some energy dissipation if $0 < \psi < 1$, and complete energy dissipation for $\psi = 0$.

d) Momentum Equation (Main Control Volume C.V.I)

Considering the force balance between sections "p" and "d," the equation of x-momentum with respect to the main control volume C.V.I (Fig. 2-6) under Boussinesq's approximation is:

$$\zeta_p \rho_a Q_p U_p - \zeta_d \rho_a Q_d U_d - \zeta_a \rho_a Q_a U_a =$$

$$- \frac{g}{2} (\rho_a + \Delta\rho_o) h_p^2 b_p \cos\theta + \frac{g}{2} [\rho_a (h_a + h_a + \Delta)^2$$

$$+ \Delta\rho_d h_d^2] b_d \cos\theta + (F^I_{x\ \text{wall}} + F^I_{x\ \text{bottom}}) - R^I_x - W^I_x \qquad 2\text{-}13$$

where:

$$U_p = Q_p / h_p b_p \qquad 2\text{-}14$$

$$U_a = Q_a / h_a b_d \qquad 2\text{-}15$$

$$U_d = Q_d / h_d b_d \qquad 2\text{-}16$$

$\zeta_{p,a,d}$ = the momentum correction factor

$F^I_{x\ \text{wall}}$ = the x-component of friction force along a side wall

$F^I_{x\ \text{bottom}}$ = the x-component of friction force along the channel bed

W^I_x = the x-component of weight

R^I_x = the reaction force exerted from a wall to the fluid

R^I_x and W^I_x are evaluated as follows:

$$R^I_x = \phi^I R^I \sin\delta = \phi^I p^I_d L \sin\delta \qquad 2\text{-}17$$

where

p_d^I = the pressure force per unit wall length at the downstream end of the plunge region

ϕ^I = the wall pressure correction factor

L = the length of plunge region.

$$W_x^I = G\rho_a(h_p + h_d + h_a + \Delta)\, Lb_p g \sin\theta/2 \qquad 2\text{-}18$$

where G = the weight correction factor. In the above expressions, superscript I denotes the property of C.V.I.

In rapidly varied flows, friction forces along boundaries are perhaps least significant. Thus ignoring all friction forces for simplicity, and substituting Eqs. 2-14 through 2-18 into 2-13:

$$\frac{2}{g}\left(\zeta_p \frac{Q_p^2}{h_p b_p} - \zeta_d \frac{Q_d^2}{h_d b_d} - \zeta_a \frac{Q_a^2}{h_a b_a}\right) +$$

$$(1 + \epsilon_o)h_p^2 b_p \cos\theta - (1 - \phi^I)[(h_a + h_d + \Delta)^2 +$$

$$\epsilon_d h_d^2]\, b_d \cos\theta - \phi^I[(h_a + h_d + \Delta)^2 + \epsilon_d h_d^2]\, b_p \cos\theta +$$

$$G(h_p + h_a + h_d + \Delta)\, Lb_p \sin\theta = 0 \qquad 2\text{-}19$$

A fractional depth (k) is defined as:

$$k = h_d/h_p \qquad 2\text{-}20$$

Geometric relationships of the plunge region are:

$$b_d = b_p + L \tan\delta \qquad 2\text{-}21$$

$$h_a = (1 - k)h_p + L \tan\theta \qquad 2\text{-}22$$

Substituting Eqs. 2-20, 2-21, and 2-22 into 2-19, the equation for the plunging flow in a diverging-slope channel is given by:

$$\frac{2\epsilon_o F_p^2}{\cos\theta}\left[\zeta_p - \frac{\zeta_d(1+\gamma)^2}{k(1 + L\sin\delta/b_p)} - \right.$$

$$\left. \frac{\zeta_a \gamma^2}{[(1-k) + L\sin\theta/h_p]\,(1 + L\sin\delta/b_p)}\right] + (1 + \epsilon_o) -$$

$$(1 - \phi^I)\left[(1 + \frac{L\sin\theta}{h_p} + \psi\frac{\epsilon_o}{2}F_p^2)^2 + \right.$$

$$\left.\frac{\epsilon_o}{1+\gamma}k^2\right]\,(1 + \frac{L\sin\delta}{b_p}) - \phi^I\left[(1 + \frac{L\sin\theta}{h_p} + \psi\frac{\epsilon_o}{2}F_p^2)^2 + \right.$$

$$\left.\frac{\epsilon_o}{1+\gamma}k^2\right] + G(2 + \frac{L\sin\theta}{h_p} + \psi\frac{\epsilon_o}{2}F_p^2)\,\frac{L\sin\theta}{h_p} = 0 \qquad 2\text{-}23$$

According to Eq. 2-23, the flow considered herein is very complex, and is dependent on the following parameters: ϕ^I, ψ, G, ϵ_o, F_p, θ, k, γ, L $\sin\theta/h_p$, L $\sin\delta/b_p$, ζ_p, ζ_d, and ζ_a.

In order to quantify the plunging phenomenon, further approximations are required.

A channel diverging angle of 7^{o} is considered to be a critical angle for flow separation based on experimental evidence presented later in this chapter; hence both δ and θ are less than 7^{o} in this analysis. θ of 7^{o} is a very steep slope in a natural channel and found infrequently. Approximately, for $\theta \leq 7^{o}$ on may use:

$$\sin\theta = \theta - \frac{\theta^3}{3!} + \ldots \qquad 2\text{-}24$$

$$\cos\theta = 1 - \frac{\theta^2}{2!} + \ldots \qquad 2\text{-}25$$

In non-suspension gravity currents (underflows), there is no unique normal slope due to entrainment of ambient water, and in fact an internal normal slope changes as the flow travels downstream. However, the amount of water entrainment is fairly small on a mild slope (Fig. 2-7).

Akiyama and Stefan [1984] estimated the internal critical slope to be 1/150 or $\theta \sim 0.38^{o}$ (Fig. 2-9) based on Ellison and Turner's [1959] shape factors (Fig. 2-8). Eq. 2-23 gives the following conditions:

1) For the channel bed slope θ.

   a) In a steep slope channel ($\theta \geq 0.38^{o}$).

   $$1 \sim \frac{L\theta}{h_p} > \psi \frac{\epsilon_o}{2} F_p^2$$

   b) In a mild slope channel ($\theta < 0.38^{o}$).

   $$1 \gg \frac{L\theta}{h_p} \sim \psi \frac{\epsilon_o}{2} F_p^2$$

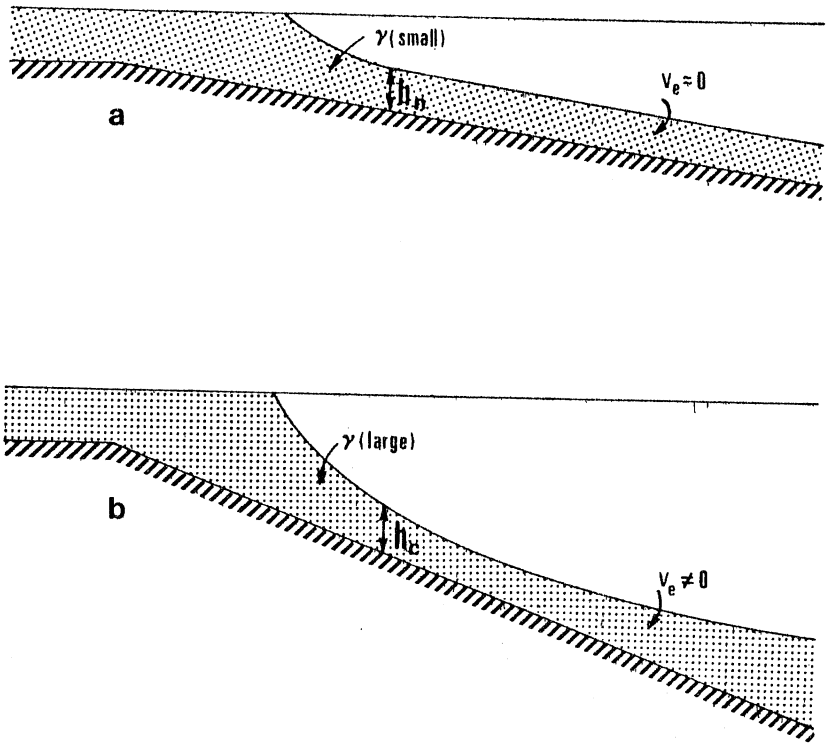

Fig. 2-7 Downstream condition in plunge region and its dependence on channel slope (constant width).
(a) mild slope
(b) steep slope

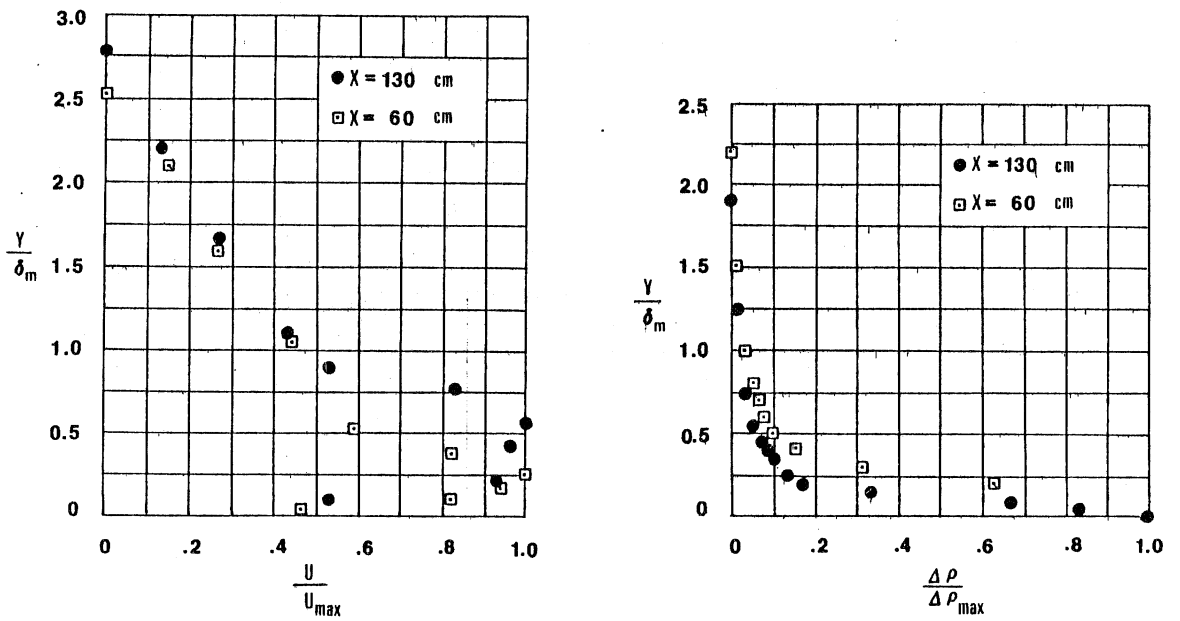

Fig. 2-8 Example of underflow velocity and density deficit distributions (after Ellison and Turner [1959]).

c) In a horizontal channel ($\theta = 0$),

$$1 >> \psi \frac{\epsilon_o}{2} F_p^2 > \frac{L\theta}{h_p} = 0$$

The approximate range of angles above is based on typical or possible variations of the following values. F_p can be at most unity, ϵ_o at most of order (0.01), and L/h_p at most of order 10 according to laboratory experiments.

2) For the diverging angle δ.

The effects of a diverging angle on plunging flow are dependent on b_p/L such that:

a) $\delta > \frac{b_p}{L}$

b) $\delta \sim \frac{b_p}{L}$

c) $\delta < \frac{b_p}{L}$

The length of the plunge region (L) can be judged mainly by the observed vertical instability of the interface provided that δ is small. The instability for a given density difference is primarily determined by the relative velocity between the upper and lower layer, and the dominant relative velocity component is not in the z-, but x-direction. Therefore, L can be related to the parameter which contains the vertical scale such as k. b_p is not only dependent on the hydrodynamics of plunging flow, but also on the geometry of the channel. b_p, can be large enough to satisfy the condition (c) above due solely to geometric reason.

This is the most unique feature on plunging flows in a diverging channel.

2.4 Plunging Flow in a Non-Diverging (Constant Width) Sloping Channel.

Setting $\delta = 0$ and $\phi^I = 0$ in Eq. 2-23, and assuming G = 1.0.

$$2F_p^2\left(\zeta_p - \frac{\zeta_d(1+\gamma)^2}{k} - \frac{\zeta_a\gamma^2}{(1-k) + L\theta/h_p} + \frac{\psi}{2} + \right.$$

$$\left.\frac{\zeta}{4}\left(\frac{L\theta}{h_p}\right) + 1 - \frac{k}{1+\gamma}\right) = 0 \qquad 2\text{-}26$$

In the derivation above, the approximation $((\epsilon_o F_p^2/2)^2 = 0)$ is made. Equation 2-26 can further be approximated dependent on the magnitude of θ and ψ.

If θ is small: $L\theta/h_p \sim 0$ and $\psi \sim 1.0$

If θ is large: $L\theta/h_p \sim 1.0$ and $\psi \sim 0$.

This indicates that the term $\psi/2$ in Eq. 2-26 is important in the subcritical flow on a mild slope, while the term $L\theta/h_p$ is important in the supercritical flow on a steep slope.

For accurate prediction of plunging flows, it is thus necessary to conduct experiments in order to examine the effects of these two parameters on h_p and γ.

Akiyama and Stefan [1984], however, neglected these two parameters in order to obtain an analytical formula for h_p. The model proposed by Akiyama and Stefan [1984] for plunging flow in a sloping parallel channel (b = const.), is briefly described in order to demonstrate the possible closure of the problem, by considering the downstream conditions of the plunge region.

A plunge flow is not a local phenomenon but influenced by downstream flow conditions, because F_p values obtained in experiments for both steep and mild slopes are less that the critical value. Two flow regimes below the plunge line can be distinguished depending on whether the slope is mild or steep. Each flow regime has a different plunge depth (Fig. 2-7).

(a) On a mild slope the underflow remains subcritical and assumes the internal normal underflow depth downstream of the plunge point. Entrainment is small and may be neglected for underflow along a mild slope. The plunging phenomenon in the Wellington Reservoir reported by Hebbert et al. [1979] is a good example of this case. The downstream condition on a mild slope is hence approximately equal to the depth (h_{dm}) of the underflow:

$$h_{dm} = \left(\frac{f_b}{SS_2} \frac{q_o^2}{\epsilon_o g}\right)^{1/2} (1 + \gamma) \qquad 2\text{-}27$$

where S_2 is the density deficiency coefficient defined by:

$$S_2 = \frac{1}{\epsilon_d h_d} \int_0^\infty \frac{\Delta\rho}{\rho_a} dy \qquad 2\text{-}28$$

(see Chapter 4)

(b) On a steep slope the plunging flow changes gradually from subcritical upstream of the plunge point (see Elder and

Wunderlich [1972]), to supercritical some distance downstream of the plunge point due to the acceleration of flow. It follows that the plunge point relates to the internal critical depth by passing through a critical section at some point. In particular, the densimetric Froude number of the hypothetical non-mixing plunge flow will be unity at the plunge point since the densimetric Froude number must decrease in the downstream direction. In a sense, the plunging flow on a steep slope is analogous to the outflow from a reservoir through a breach and into a steep channel. The downstream condition on a steep slope is hence approximately equal to the internal critical depth (h_{ds}).

$$h_{ds} = \left(\frac{1}{S_1} \frac{q_o^2}{\epsilon_o g}\right)^{1/2} (1 + \gamma) \qquad 2\text{-}29$$

where S_1 is the density deficiency coefficient defined by:

$$S_1 = \frac{1}{\epsilon_d h^2_d} \int_0^\infty 2 \frac{\Delta\rho}{\rho_a} y \, dy \qquad 2\text{-}30$$

(see Chapter 4)

Profile constants S_1 and S_2 defined in Eqs. 2-28 and 2-30 are dependent on the friction factor (f_b), bed slope (S), Richardson number ($R = F^{-2}$), and definition of the interface as shown in Chapter 4. Once an underflow flowing over a bed with consant f_b and S attains a normal

state ($R = R_n$), both profile constants are expected to be nearly constant. Examples of velocity and density deficiency profiles for the well-developed underflow are shown in Fig. 2-8.

In the plunging region, the depth ratio (k) between a plunge depth and the depth downstream of the plunge region is obtained by applying a control volume analysis (Eqs. 2-26 and 2-56) with the approximations regarding ψ and $L\theta/h_p$ described above.

$$k = h_p/h_d$$
$$= \frac{1}{2(1+\gamma)} \left[\frac{2+\gamma}{2} + F_d^2 + \left(\left(\frac{2+\gamma}{2} + F_d^2\right)^2 - \frac{4F_d^2}{1+\gamma}\right)^{1/2}\right] \qquad 2\text{-}31$$

where F_d is the densimetric Froude number downstream of the plunge region. F_d-values in the equation above are different dependent on channel slopes.

a) F_d-value for mild slopes (F_{dm})

$$F_{dm} = (S_2 S/f_b)^{1/2} \qquad 2\text{-}32$$

b) F_d-value for steep slopes (F_{ds})

$$F_{ds} = (S_1)^{1/2} \qquad 2\text{-}33$$

From Eqs. 2-31 and 2-32; dimensionless plunge depth (h_p^*) normalized by h_o are:

1) for a mild slope ($0 \leq S \leq \frac{f_b S_1}{S_2}$).

$$h^*_{pm} = k_m h^*_{dm} \qquad 2\text{-}34$$

2) for a steep slope ($S > \frac{f_b S_1}{S_2}$).

$$h^*_{ps} = k_s h^*_{ds} \qquad 2\text{-}35$$

3) for a critical slope ($S_c = \frac{f_b S_1}{S_2} \simeq 1/150$).

$$h^*_{pc} = h^*_{pm} = h^*_{ps} \qquad 2\text{-}36$$

An internally critical slope ($S_c \sim 1/150$) is estimated using experimental results obtained by Ellison and Turner [1959] (Fig. 2-8). The relationship between normal Richardson number (R_n) and bed slope (S) with $f_b = 0.02$ is shown in Fig. 2-9.

2.4.1 Comparison of Analytical Results with data for a Constant Width Channel.

Data used for comparison are from four sources: Laboratory experiments (S = 1/47 to 1/179) by Singh and Shah [1971], (S = 1/21) by Farrell and Stefan [1986], (S = 1/10 and 1/60) by Fukuoka et al. [1980],

field data from DeGray Lake (S = 12/10,000) by Ford and Johnson [1981], and data from Wellington Reservoir (S = 1/1,000) by Hebbert et al. [1979]. Equations used for comparison are summarized in Table 2-1, and data are in Appendix I.

The following analysis and comparsion is limited to the zero-initial mixing ($\gamma = 0$) plunging phenomenon, due to lack of information except Farrell and Stefan's [1986] data.

Non-dimensional plunge depths (h_p^*) are predicted by setting $\gamma = 0$ in Eqs. 2-34 and 2-35, with the result that:

$$h_{pm}^* = \left(\frac{f_t}{S\ S_2}\right)^{1/3} F_o^{2/3}$$

$$= (1.04 \sim 1.19)\ \left(\frac{f_t}{S}\right)^{1/3} F_o^{2/3} \qquad 2\text{-}37$$

for $S_2 = 0.6 \sim 0.9$, and

$$h_{ps}^* = \left(\frac{1}{S_1}\right)^{1/3} F_o^{2/3}$$

$$= (1.49 \sim 1.71)\ F_o^{2/3} \qquad 2\text{-}38$$

for $S_1 = 0.2 \sim 0.3$. Where $h_p^* = h_p/h_o$ and $F_o = \left(\frac{q_o^2}{\epsilon_o g h_o}\right)^{1/2}$

A coefficient α relating the critical depth (h_c) and plunge depth (h_p) is defined as:

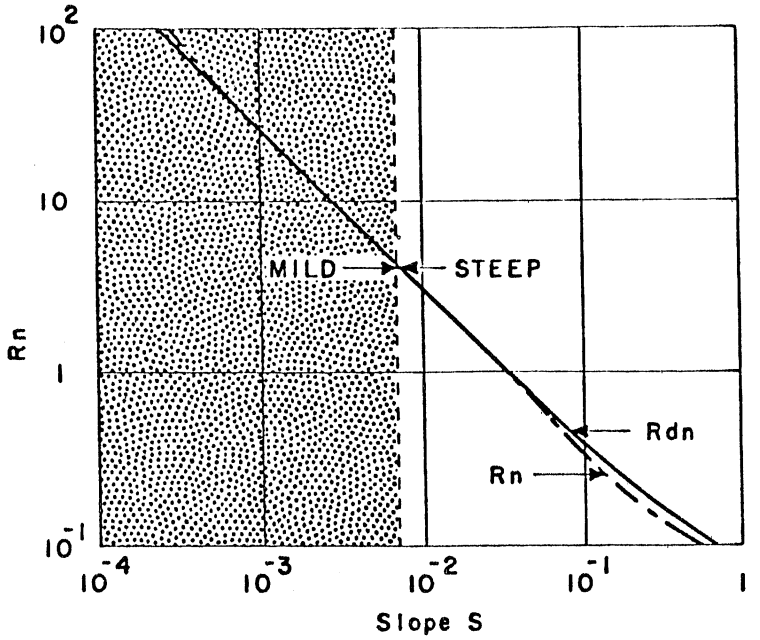

Fig. 2-9 Relationship between normal Richardson number (R_n) and channel slope (S).

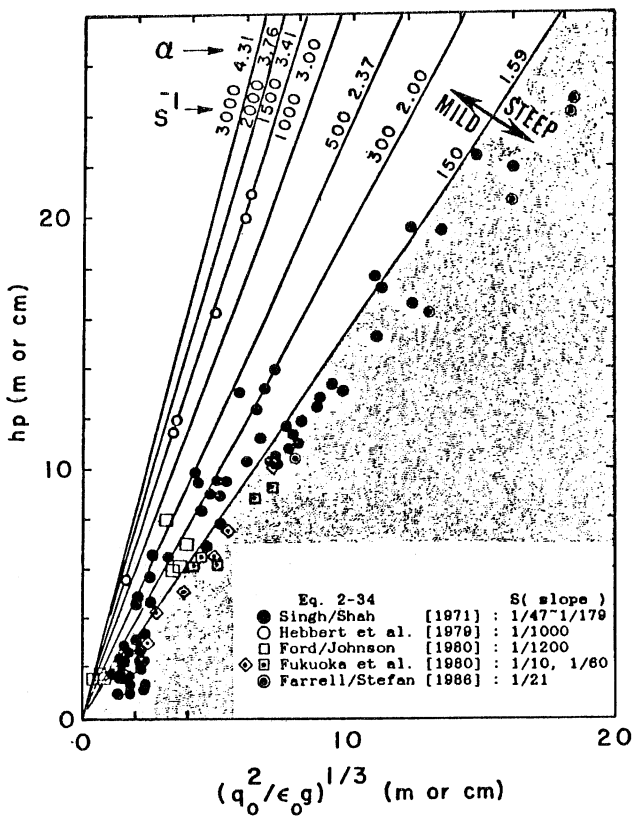

Fig. 2-10 Dependence of plunge depth (constant width), h_p, on channel slope, S.
(a) Laboratory data in cm
(b) Field data in m

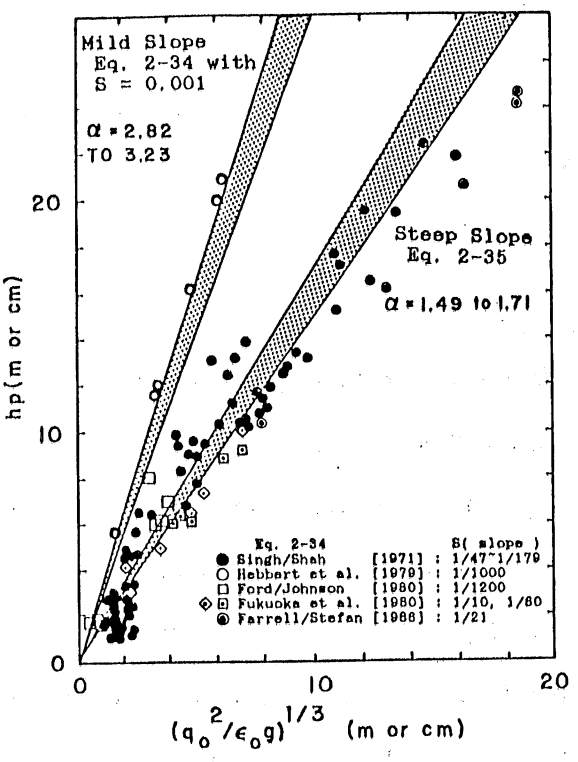

Fig. 2-11 Dependence of plunge depth (constant width), h_p, on profile constant S_1 and S_2.

(a) Laboratory data in cm
(b) Field data in m

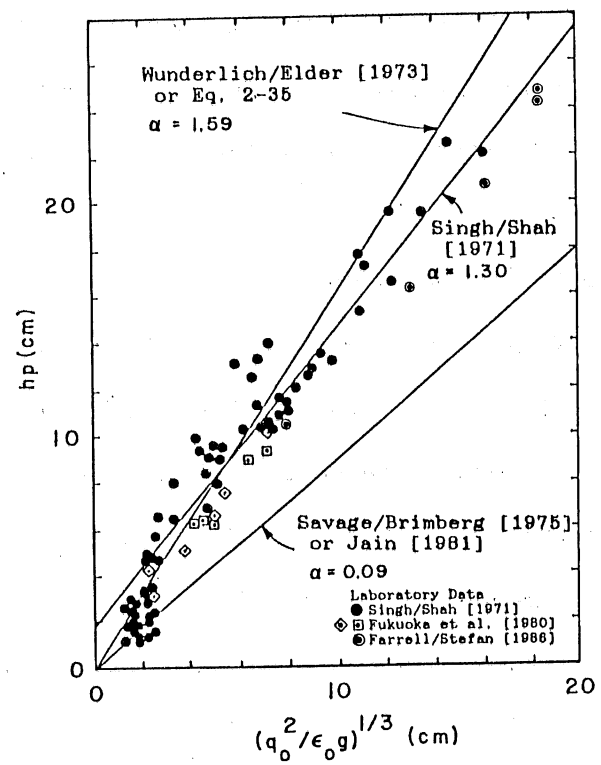

Fig. 2-12 Comparison of laboratory data with Eqs. for plunge depth (constant width) on steep slope.

$$\alpha = h_p/h_c = F_p^{-2/3} \qquad 2\text{-}39$$

where $h_c = (q_o^2/\epsilon_o g)^{1/3}$

Predicted plunge depths depend on the values of the profile constants S_1, S_2, and the total friction factor f_t ($=f_b + f_i$). Figure 2-10 shows variations in plunge depth with critical depth h_c and bed slope. Solid lines are calculated from Eqs. 2-37 and 2-38, with average values $S_1 = 0.25$, $S_2 = 0.75$, and $f_t = 0.02$. Bands shown in Fig. 2-11 give variations of the plunge depth with S_2 = from 0.6 to 0.9, $f_t = 0.02$ and $S = 1/1000$ for a mild slope, and for S_1 = from 0.2 to 0.3 for a steep slope.

Values of S_1 and S_2 are sensitive to the definition of the interface of an underflow. This is then reflected in the ambiguous location of the plunge point. Figure 2-11 indicates that bands of theoretical values are closely related to data points for reservoir and laboratory experiments.

(i) Comparison with Laboratory Data

Data are from Fukuoka et al. [1980], Farrell and Stefan [1986] and Singh and Shah [1971]. Singh and Shah [1971] did not specify bed slope in detail. Experiments are conducted in a channel with relatively steep slope ranging from 1/47 to 1/179. These data should be good examples of the plunge phenomenon on a steep slope. $S = 1/113$, $\alpha_i = 0.2$, and $f_b = 0.02$ are used with Savage and Brimberg's [1975] and Jain's [1981] results ($\alpha_i = f_i/f_b$), giving $\alpha = 0.90$ in both cases. Equation 2-38 using average values gives $\alpha = 1.59$. The assumption $\gamma = 0$ is justified

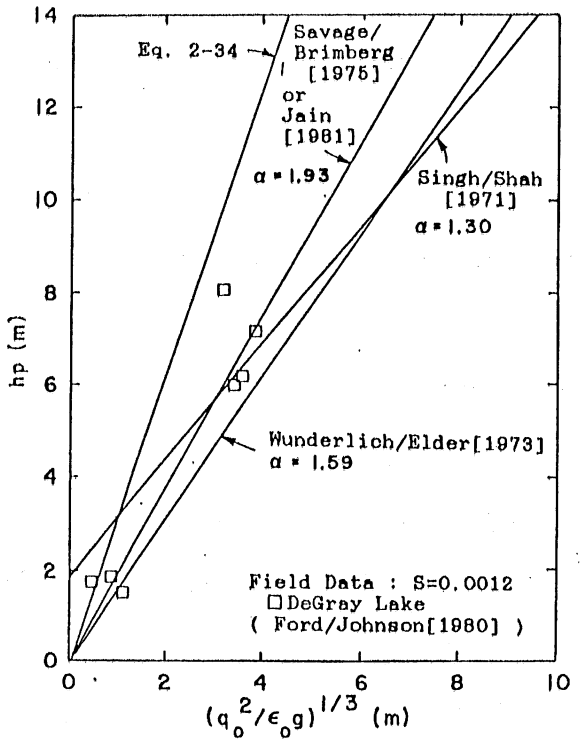

Fig. 2-13 Comparison of field data from DeGray Reservoir with Eqs. for plunge depth on mild slope.

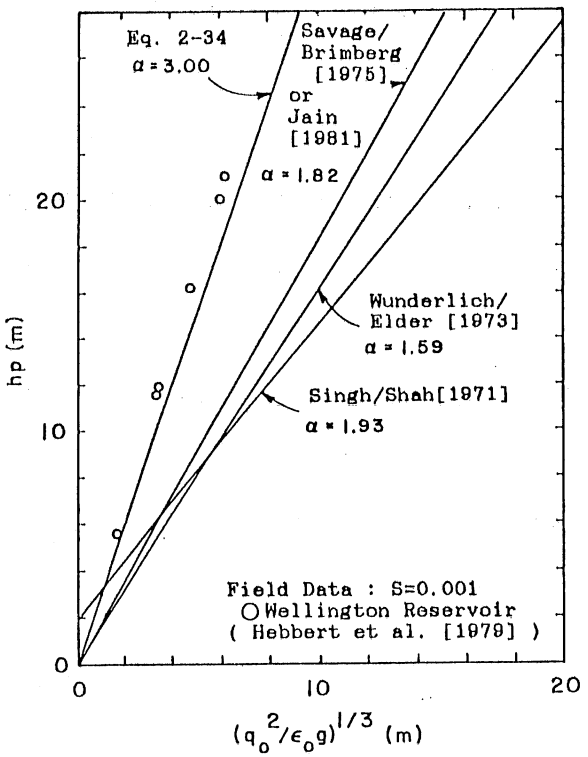

Fig. 2-14 Comparison of field data from Wellington Reservoir with Eqs. for plunge depth on mild slope.

for the mild slope (Eq. 2-37) but probably not realistic for the steep slope (Eq. 2-38).

The calculated results are shown in Fig. 2-12. The plotted line (Eq. 2-37) coincides with Wunderlich and Elder's [1973] equation. It lies approximately in the middle of the data and close to Singh and Shah's [1971] empirical formula.

(ii) Comparison with Field Data

Both data sets (DeGray Lake and Wellington Reservoir) may be regarded as examples of plunge flow on a mild slope. The equations of Savage and Brimberg and Jain are the same as above and were employed with the following variables:

a) $S = 0.0012$, $f_t = 0.02$ giving $\alpha = 0.2$ for DeGray lake and

b) $S = 0.001$, $f_t = 0.02$ giving $\alpha = 0.2$ for Wellington Reservoir.

Equation 2-38 with average values and $S = 0.0012$ and 0.001 is used for the present analysis. The results for DeGray Lake are shown in Fig. 2-13.

The results of Wellington Reservoir are shown in Fig. 2-14, the prediction with the proposed formula is much better than that with other formulas.

Ford and Johnson [1981] reported that the densimetric Froude number in the vicinity of the plunge point (F_p) ranges from 0.1 to 0.7 and Savage and Brimberg based on Singh and Shah's data gave a range from 0.3 to 0.8. This study shows that the F_p value can theoretically vary from 0.0 to 1.0.

2.5 Plunging Flow in a Horizontal-Diverging Channel

In order to understand the effects of channel divergence (δ) and energy dissipation near the plunge line on the plunging phenomenon, horizontal channels with several different δ's are considered theoretically (Fig. 2-15). We set $\theta = 0$ in Eq. 2-26, and assume that all momentum correction factors (ζ_a, ζ_d, ζ_p) are unity. Define the relative (fractional) width (m).

$$m = b_p/b_d = 1/(1 + L\delta/b_p) \qquad 2\text{-}40$$
$$(0 < m \leq 1)$$

With $\phi^I = 1$,

$$2F_p^2[k(1 - k) - \gamma^2 km - (1 + \gamma)^2 (1 - k)m] -$$

$$k(1 - k) [-1 + \psi F_p^2 + \epsilon_o F_p^4/4 + k^2/(1 + \gamma)] = 0 \qquad 2\text{-}41$$

Ignoring the term $\epsilon_o F_p^4/4$, which is at most of order ϵ_o:

$$F_p = \left[\frac{k(1 - k)(k^2/(1 + \gamma) - 1)}{(2 - \psi)k(1 - k) - 2m(k\gamma^2 - (1 - k) (1 + \gamma)^2\}}\right]^{1/2} \qquad 2\text{-}42$$

From Eqs. 2-3 and 2-40, the parameter m can be expressed in terms of inflow paramters (A_o, F_o), channel characteristics (δ), and characteristic properties in the plunging region (n, F_p).

$$m = \frac{1}{1 + \beta(nF_p)} \qquad 2\text{-}43$$

$$\beta = \tan\delta/(A_o F_o) \qquad 2\text{-}44$$

Where n is the non-dimensional plunge region length,

$$n = L/h_o \qquad 2\text{-}45$$

Equation 2-43 becomes:

$$\{n(2 - \psi)k(1 - k)\beta\} F_p^3 + [(2 - \psi)k(1 - k) - 2\{\gamma^2 k + (1 + \gamma)^2(1 - k)\}] F_p^2 - nk(1 - k)\{k^2/(1 + \gamma) - 1\}\beta F_p - k(1 - k)\{k^2/(1 + \gamma) - 1\} = 0 \qquad 2\text{-}46$$

Equation 2-46 has an asymptotic expression for constant width (parallel) channel in the limit $\beta \to 0$ ($A_o \to \infty$, $F_o \to \infty$, or $\delta \to 0$). Closure of the problem can be achieved in a diverging channel with a steep bed slope, using critical depth (h_c) as flow depth downstream of the plunge line. In a diverging channel with a mild slope, there is no unique downstream depth (internally normal depth) as in the constant width channel (Fig. 2-7). The behavior of underflows in a sloping-diverging channel will be investigated in Chapter 5. In the following analysis, effects of channel expansion on plunge flow in a horizontal channel will be investigated experimentally.

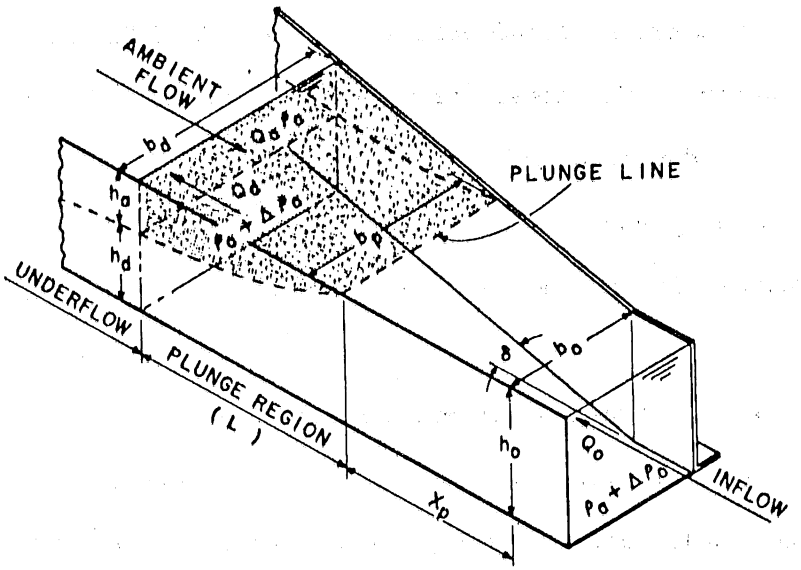

Fig. 2-15 Plunge flow in a diverging half-channel (schematic).

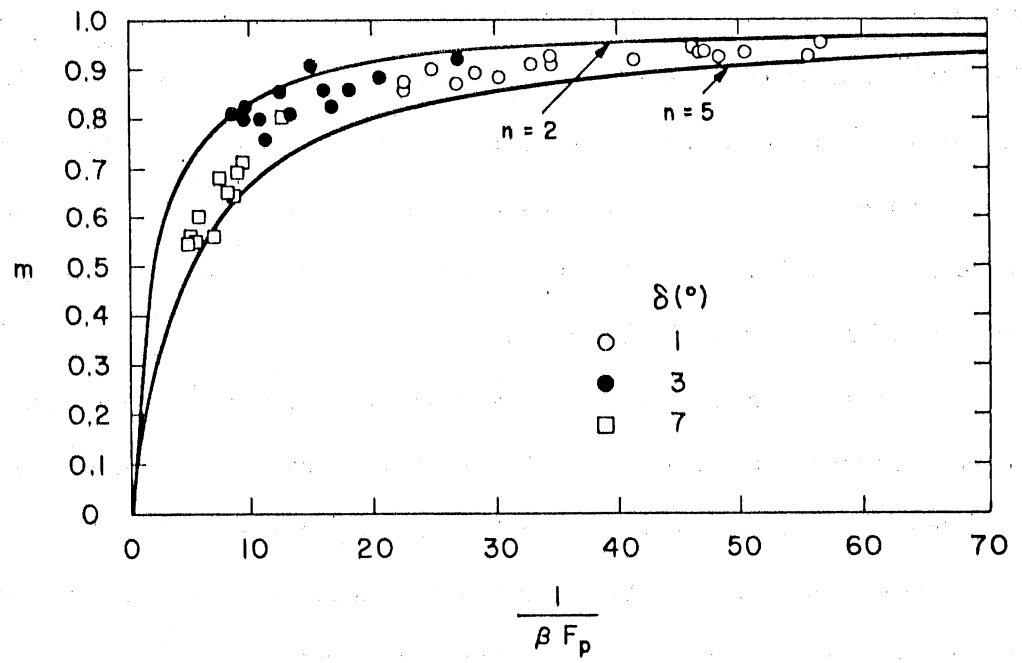

Fig. 2-16 Relationship between fractional depth (m) and $1/\beta F_p$.

Equation 2-43 and data are plotted in Fig. 2-16 in order to demonstrate the effects of m on the flow. Figure 2-16 also shows that n is independent of δ, and that n varies within about 2 to 5. For a given F_p and β, m can be calculated. Data shown in Fig. 2-16 are obtained in experiments described in the following section.

2.5.1 Experiments and Observations

Experiments were conducted in a diverging half channel inserted in a 24" wide, and 12" deep, laboratory flume schematically shown in Fig. 2-17. The width b_o of the inflow was always 5.3 cm. Density differences were created by temperature. Divergence angles of $\delta = 1^o$, 3^o, 7^o, and 15^o were chosen. The inflow discharge Q_o, the temperature profiles T(y) at the downstream end of the plunge region and at the plunge point, and the dimensions x_p, b_p, b_d, h_p, h_o, h_d, h_a, and L were measured. There was no measurable difference between h_o and h_p. The internal structure of the flow was visualized using multicolor dye injection. L was defined as the distance from the plunge line to the location where intermittent large eddies virtually disappear and an interface stabilized by buoyance effects is observed. L represents the length scale of the plunge region.

At the downstream end of the flume the underflow was carefully separated with the aid of a selective withdrawal plate and drained. The withdrawal rate was adjusted until a steady stratified flow condition was observed upstream. Data were taken after the plunge line, which was monitored during each run. Experimental conditions were varied by changing total inflow rate Q_o and/or temperatures T_o, T_a. During

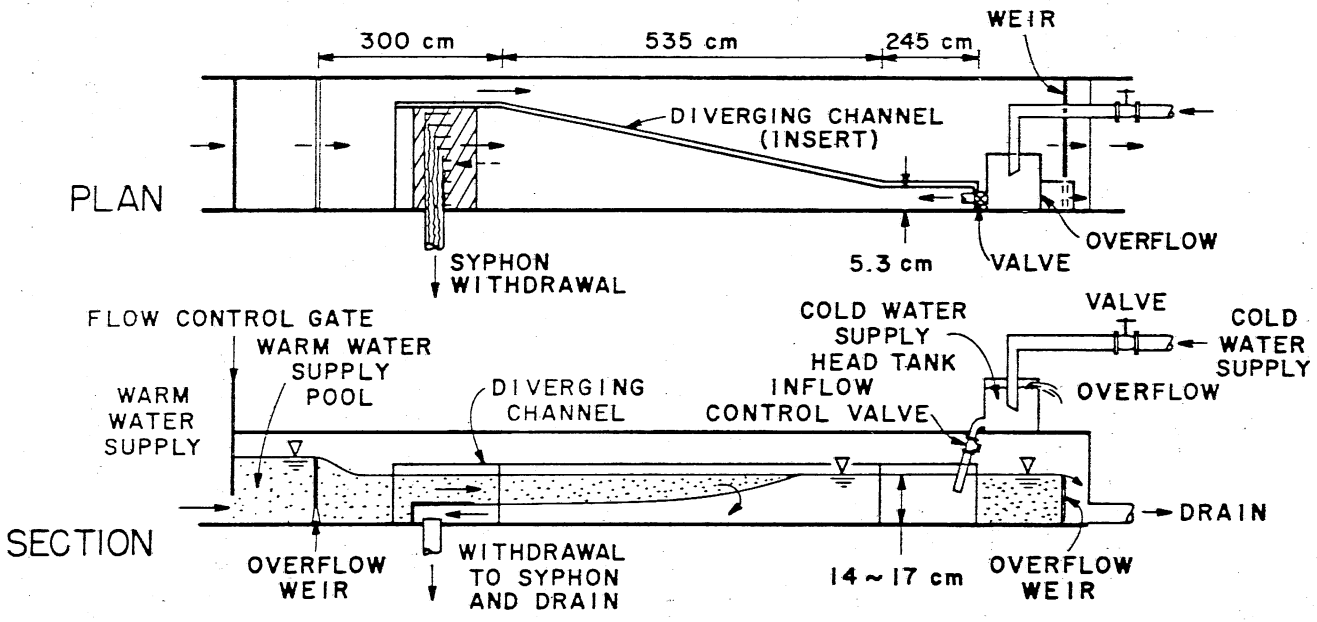

Fig. 2-17 Experimental set-up (not to scale).

measurements the temperature of the inflowing and ambient water was also monitored. But even after water temperatures had reached steady conditions, it was observed that the plunge line moved slightly back and forth. This tendency was found to be stronger at larger channel divergence angles δ ; it may be caused by unstable secondary flow, and by irregular entraining large eddies near the plunge line (Fig. 2-18).

At $\delta = 1^{o}$ and 3^{o}, no flow separation from the side wall could be detected, at $\delta = 15^{o}$, separation at the outlet was observed for all experimental conditions, and at $\delta = 7^{o}$ some weak internal flow separation occurred dependent on F_o.

In the experiments, dyes of different colors and particles were used as tracers to visualize the internal structure of the flow (Fig. 2-19). The overlapping region showing a dark color is a "mixing layer." It is a shear layer which grows from the plunge line to downstream. The plunge flow region displays three layers: the upper ambient h_a, the mixing h_m, and the lower flowing layer h_ℓ (Fig. 2-19).

The upper boundary of the mixing layer nearly coincided with the zero velocity point and was defined as an "interface." For analytical purposes the flow field was considered as two-layered: the upper ambient layer h_a and a layer below the zero velocity point ($h_d = h_m + h_\ell$), separated by this interface.

The details of the flow field structure appeared to be nearly independent of inflow conditions (e.g. F_o), however, strongly dependent on δ . The growth rate of the mixing layer downstream from the plungeline, for instance, was very small for $\delta = 1^{o}$ (Fig. 2-20, top), and much more for $\delta = 3^{o}$ and almost large enough to reach the channel

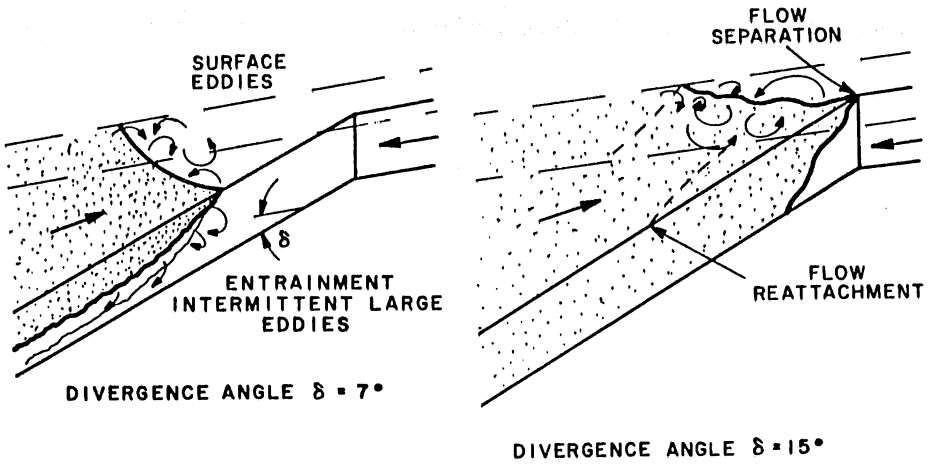

Fig. 2-18 Sketches of flow structures near the plunge line.

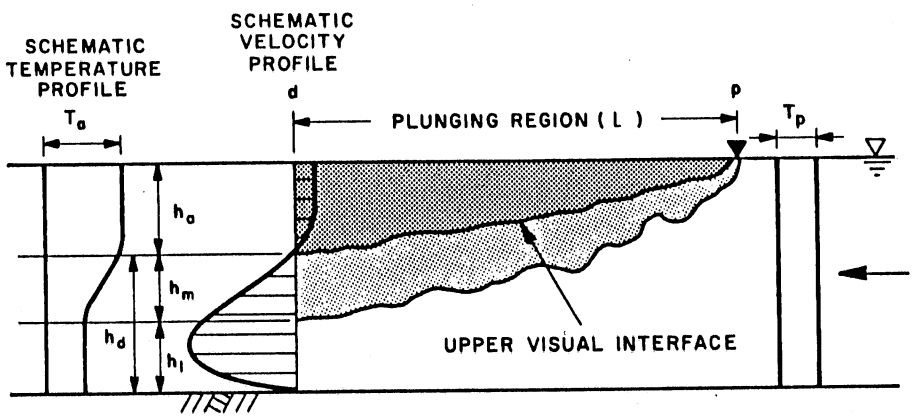

Fig. 2-19 Plunge region (horizontal)

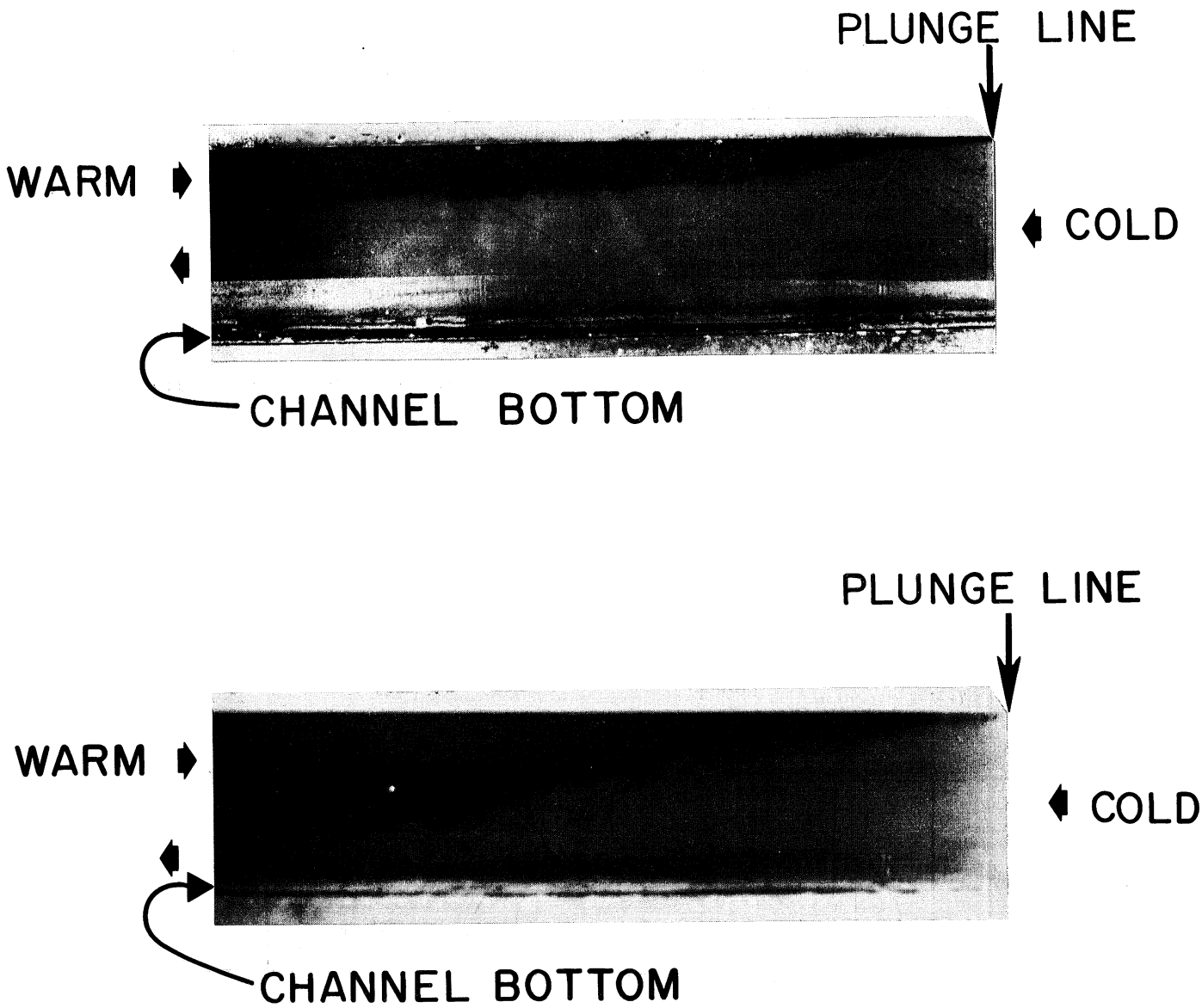

Fig. 2-20. Side view of plunging flows
Top: $\delta = 1^{o}$, $F_o = 1.08$, $F_p = 0.614$ (RUN 1-2).
Bottom: $\delta = 7^{o}$, $F_o = 2.11$, $F_p = 0.670$ (RUN 7-2).

bottom for $\delta = 7^{o}$ (Fig. 2-20, bottom). At $\delta = 7^{o}$ and particularly at $\delta = 15^{o}$, horizontal mixing together with vertical mixing was observed. Examples of measured temperature profiles are shown in Fig. 2-21. The symbols shown on each profile indicate the location of the observed interface.

Separation of the plunging flow from the water surface was very smooth. The water moving in the upper layer towards the plunge line was strongly sheared by the plunge flow below; thin layers of fluid were peeled off by the submerged current and partially entrained into the mixing layer before reaching the plunge line. In the vicinity of the plunge line, intermittent large eddies could be observed. They played a role in the pre-entrainment of the ambient water before plunging.

Data are summarized in Table 2-4. Data for $\delta = 15^{o}$ are not presented because the flow separated at the inlet in all experiments; T_p and T_d are measured to determine γ .

2.5.2 Experimental Results

(i) Location of Plungeline - The distance x_p of the plungeline from the inlet of the diverging channel can be estimated once the densimetric Froude number at the plungeline F_p is determined. No unique F_p value exists at least in the range of variables investigated experimentally and the dependence of F_p on k, m, and γ appears to be extremely complicated. An average F_p value ($\overline{F}_p$) of all data is, therefore presented herein for practical applications:

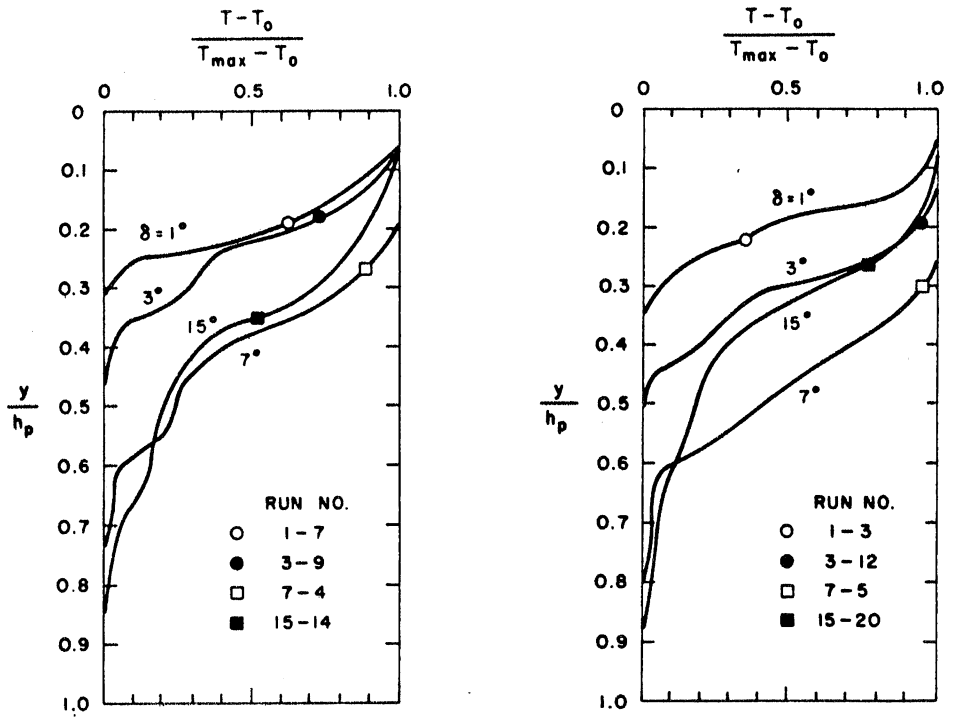

Fig. 2-21 Typical temperature profiles at the downstream end of the plunge region (Symbols shown indicate the location of visual interface).

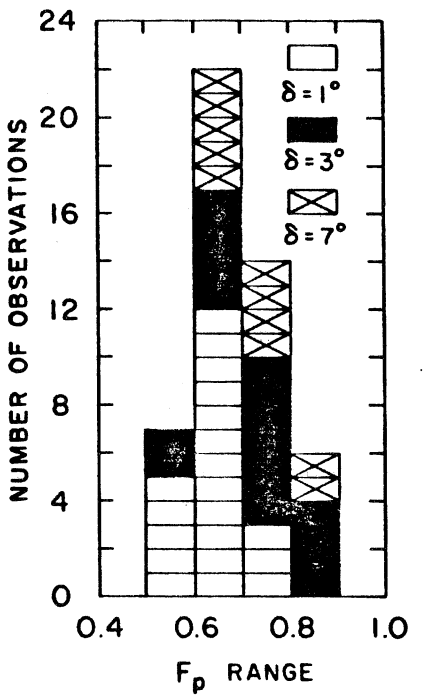

Fig. 2-22 Histogram of observations of F_p.

TABLE 2-2. Densimetric Froude Number at Plunging F_p

Field	F_p	Slope θ	Divergence Angle δ
Ford and Johnson [1980]	0.1 ~ 0.7	1/2000	N.R.
Itakura and Kishi [1979]			
Ishibasi et al. [1977]	0.54 ~ 0.69	N.R.	N.R.
Iwasaki et al. [1978]			
Laboratory			
Singh and Shah [1971]	0.30 ~ 0.80	1/47 ~ 1/179	0
Kan and Tamai [1981]	0.45 ~ 0.92	1/4 ~ 1/10	**
Fukuoka et al. [1980]	0.40 ~ 0.72	1/10	0
	0.37 ~ 0.68	1/60	
Farrell and Stefan [1986]	0.66 ~ 0.70	1/21	0
Akiyama and Stefan [1987]	0.56 ~ 0.89	0	1^o ~ 7^o

TABLE 2-3. Initial Dilution Rate, γ

Field	Dilution γ	Slope θ	Divergence Angle δ
Aki and Shirasuna [1981]	0.5 ~ 1.0	N.R.	N.R.
Elder and Wunderlich [1972]	0 ~ 1.0	~1/1470	N.R.
Ford and Johnson [1980]	1.0 ~ 5.0	~1/1200	N.R.
Iwasaki et al. [1978]	0.25	N.R.	N.R.
Hebbert et al. [1970]	nearly 1.0	~1/1000	N.R.
Laboratory			
Itakura and Kishi [1979]	0.2	N.R.	0
Kan and Tamai [1981]	0.1 ~ 2.0	1/4 ~ 1/10	**
Akiyama and Stefan [1987]	0 ~ 0.31	0	1^o ~ 7^o

N.R. = not reported
** = some experiments conducted in a diverging channel, db/dx =0.1

Table 2-4 Experimental Data

Exp. No.	Q_o (cm^3/s)	h_p (cm)	b_p (cm)	ε_o	k	m	γ	F_p	F_o
$\delta=1°$									
1-1	324.76	15.5	6.2	.001897	.65	.862	0	.63	.74
2	473.67	15.4	9.3	.001927	.87	.909	.02	.61	1.08
3	346.24	16.0	7.0	.001693	.81	.900	.032	.60	.79
4	542.35	16.1	9.3	.002202	.84	.909	.073	.62	1.08
5	646.21	16.1	9.7	.002608	.78	.909	.043	.65	1.18
6	480.57	15.8	9.6	.002012	.91	.926	.083	.57	1.03
7	363.30	14.7	12.0	.000854	.78	.935	.052	.59	1.33
8	553.02	14.8	7.7	.003635	.84	.893	.024	.67	.97
9	408.23	14.8	5.9	.002934	.80	.870	.030	.72	.80
10	378.70	13.1	6.9	.003498	.83	.885	.064	.63	.81
11	546.00	12.9	9.3	.003600	.77	.917	.019	.68	1.19
12	607.44	12.9	10.9	.004155	.77	.926	.008	.60	1.23
13	607.44	13.0	12.8	.003297	.88	.952	.033	.56	1.36
14	383.48	12.3	5.8	.004549	.73	.870	.008	.73	.80
15	383.48	12.3	6.5	.004203	.80	.885	0	.67	.83
16	573.06	12.3	10.1	.004097	.83	.935	.044	.66	1.25
17	381.56	14.3	11.5	.001202	.86	.943	.082	.57	1.23
18	477.55	14.4	13.8	.001261	.72	.926	.020	.56	1.40
19	326.58	14.8	7.0	.001369	.81	.909	.031	.71	.94
20	624.94	15.0	13.2	.001533	.80	.935	.037	.67	1.66
$\delta=3°$									
3-1	509.60	14.8	7.5	.002231	.86	.826	.14	.81	1.14
2	374.96	15.8	12.6	.000511	.80	.909	.06	.67	1.59
3	417.20	15.9	7.9	.001056	.65	.800	.13	.82	1.22
4	627.52	16.0	9.5	.001737	.86	.763	.09	.79	1.42
5	427.77	15.2	14.4	.000460	.85	.862	.18	.75	2.03
6	479.05	16.2	9.2	.001381	.83	.800	.17	.69	1.19
7	496.27	15.9	13.9	.000781	.83	.826	.14	.64	1.69
8	588.60	15.4	13.1	.001326	.85	.862	.10	.65	1.61
9	584.08	15.5	10.9	.001542	.81	.813	.15	.72	1.47
10	676.14	16.6	23.6	.000520	.86	.917	.10	.59	2.64
11	696.61	16.6	17.9	.000826	.82	.885	.11	.64	2.16
12	509.60	14.8	9.5	.001647	.70	.855	.20	.74	1.33
13	540.43	14.9	6.7	.003182	.71	.813	.10	.80	1.00
$\delta=7°$									
7-1	632.75	14.5	9.4	.002167	.77	.556	.20	.84	1.49
2	632.75	14.5	16.7	.001071	.77	.709	.26	.67	2.11
3	298.35	14.7	10.4	.000554	.75	.600	.31	.69	1.36
4	365.93	14.8	13.2	.000649	.70	.685	.30	.61	1.53
5	550.22	14.9	9.0	.001457	.73	.546	.19	.89	1.52
6	365.05	13.9	9.0	.001126	.68	.546	.28	.75	1.27
7	575.23	13.9	15.4	.001202	.71	.690	.17	.67	1.93
8	579.62	13.8	21.5	.000714	.86	.806	.21	.63	2.55
9	476.65	12.7	11.0	.001691	.66	.562	.29	.75	1.55
10	476.65	12.6	12.7	.001459	.78	.649	.26	.70	1.68
11	599.29	12.8	14.8	.001559	.73	.645	.18	.72	2.00

$$\bar{F}_p = 0.68 \pm 0.024 \text{ (95\% confidence interval)} \qquad 2\text{-}47$$

Measured values of F_p ranged from 0.56 to 0.89. Most frequently observed F_p values (Fig. 2-22) were in the range from $F_p = 0.60$ to 0.70. This is consistent with other results. F_p values calculated from experimental data are plotted against inflow densimetric Froude number F_p in Fig. 2-23 for three channel divergence angles. Plunging flows occur in a diverging channel only if $F_o > F_p$. F_p is a weak function of F_o and also dependent on δ. This is different from plunging flows in constant width channels. F_p values at a given δ decrease as F_o values increase because of inertial effects in the expanding channel (Eq. 2-46). The dependence of F_p on δ is more pronounced when F_p values are plotted against the channel aspect ratio at the section where plunging occurs, $A_p = b_p/h_p$ (Fig. 2-24). It is obvious that F_p decreases as A_p increases.

Channel aspect ratio A_p is also correlated to width ration $m = b_d/b_p$ (Fig. 2-25). Both channel divergence angle δ and F_o are related to F_p through the parameter m. To understand the role of m in the relationship between F_o and F_p consider plunging flow for fixed b_o, $\Delta\rho_o$, and δ. Plunging can occur in any section when a local force balance is attained and plunge width b_p naturally increases as F_o increases. The parameter m can therefore asymptotically approach unity, representing a constant width channel as shown in Fig. 2-25, and the effect of m on the flow will then vanish. The same tendency is also shown in a plot of m versus F_o (Fig. 2-26). Kan and Tamai [1981] conducted experiments on plunging flows in a diverging and sloping

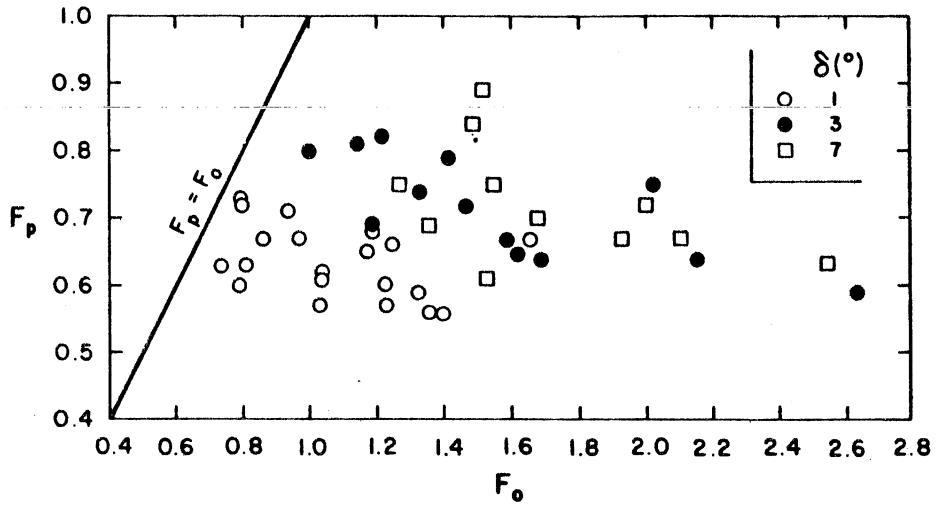

Fig. 2-23 Plunging densimetric Froude number (F_p) versus inflow densimetric Froude number (F_o).

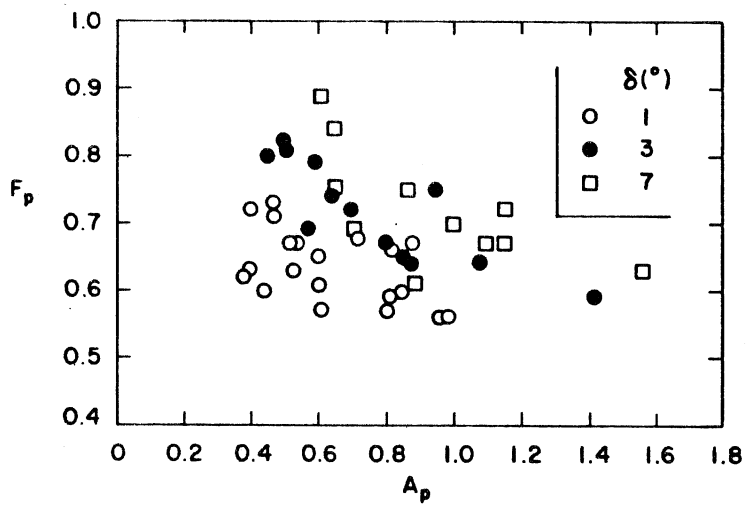

Fig. 2-24 Channel aspect ratio at plunge line (A_p) versus plunge densimetric Froude number (F_p).

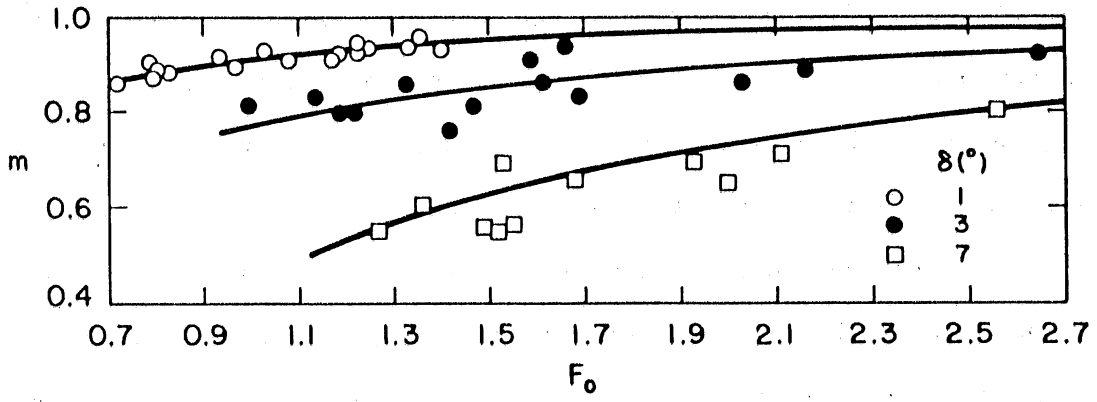

Fig. 2-25 Channel aspect ratioi at plunge line, (A_p).

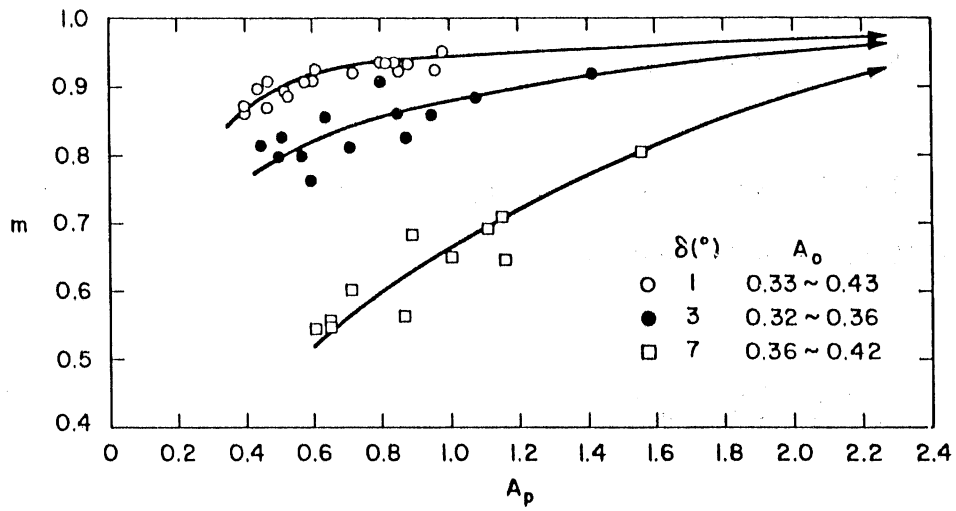

Fig. 2-26 Inflow densimetric Froude number, (F_o) versus fractional width (m).

channel (Table 2-2 and 2-3), and found identical results for constant width channels and diverging channels. Unfortunately data are not provided in their paper, so that it is impossible to follow their reasoning or to compare data with those presented herein. Effects of channel slope θ , large initial aspect ration A_o, or large A_p in the experiments will tend to mask effects of channel divergence. Based on the experimental results given herein, it is clear, however, that there is a domain where the divergence of the channel affects the structure of The flow. In that domain the width ratio m can be more important than the depth ratio $k = h_d/h_p$. Ignoring the change of water level Δh of order of ϵ_o between the sections "o" and "p," F_o and F_p are related through requirement of flow continuity, and b_o and b_p through a geometric relation.

$$F_p = (b_o/b_p)\ F_o \qquad 2\text{-}48$$

$$b_p = x_p \tan\delta + b_o \qquad 2\text{-}49$$

The distance from the plungeline to the inlet of the horizontal diverging channel therefore is:

$$\frac{x_p}{b_o} = \frac{1}{F_p \tan\delta}\ (F_o - F_p) \qquad 2\text{-}50$$

The variation of F_p is small compared to that of tan δ. It is therefore

meaningful to use an average $\bar{F}_p = 0.68$ in Eq. 2-50. Equation 2-50 and data are shown in Fig. 2-27.

(ii) Rate of Initial Dilution - The rate of initial dilution γ can be determined from measurment of temperature profiles at both the upstream "p" and downstream end "d" of the plunge region. Temperature data are analyzed by a two-layer uniform flow model. The measured temperature profiles are continuous as shown in Fig. 2-21. The observed upper boundary of the mixing layer near the zero velocity point (Fig. 2-19) is adopted as the interface for the two-layer flow model, and average temperatures in the upper layer ($\bar{T}_d$) are calculated. Dilution (entrainment) rate is calculated from a conservation of heat equation.

$$\gamma = (T_o - \bar{T}_a)/(\bar{T}_d - \bar{T}_{a)} - 1 \qquad 2\text{-}51$$

γ is assumed to apply also to conservation of mass. Figure 2-28 gives the relationship between γ and δ. γ-values depend also on F_o, A_o, and δ. The maximum value (γ_{max}) appears to be a function of δ. An empirical expression is:

$$\gamma_{max} = 0.089\delta^2 \qquad \text{for } 1^o \leq \delta \leq 15^o \qquad 2\text{-}52$$

where δ is given in degrees.

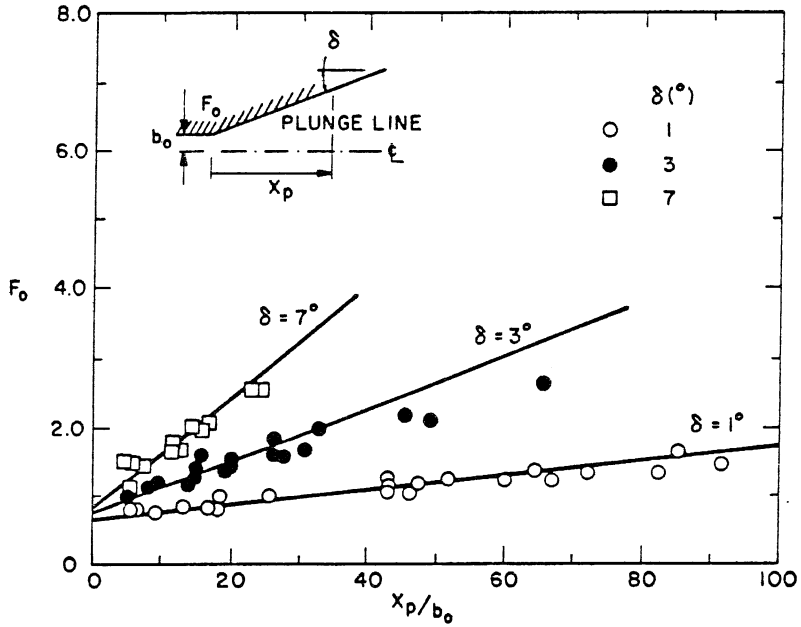

Fig. 2-27 Location of plunge line, (x_p).

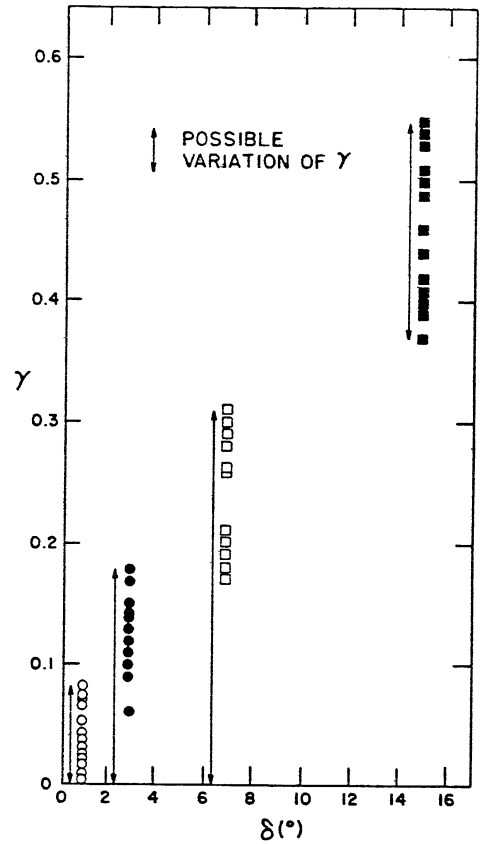

Fig. 2-28 Dependence of γ on δ.

2.5.3 Comparison between Theory and Experiments

(i) Comparison between oil slicks and plunging flows A hydrodynamic problem similar to a plunging flow is that of an arrested oil slick. The oil slick problem may be regarded as a plunging flow with zero or negligible mixing. Wilkinson [1972] investigated this problem experimentally and theoretically for constant width. His analysis demonstrates that an oil or hot water slick will not attain a stable thickness when the ambient water Froude number is greater than 0.527. When $F_p > 0.527$, the interface becomes unstable. This may be the case of a plunging flow. Wilkinson observed submergence of inflowing water beneath a slick in the range $F_p = 0.096$ to 0.56, including unstable oil slick data. Wilkinson's study implies the following: (a) good agreement between his theory and data indicates that correction factors for both momentum and pressure are not very significant at least in the non-mixing case, (b) F_p values can vary, dependent on flow conditions. F_p is larger in unstable or entraining plunging flows. Dilution is, therefore, an essential mechanism in the analysis of the plunging flow problem and necessary to explain the variation of F_p values in field and laboratory observations, and (c) plunging flow is not a local phenomenon, but related to downstream conditions (through k) because plunging flows occur in the range ($0 \leq F_p \leq 1.0$).

In Fig. 2-29 the effect of stagnation index ψ on the F_p - k relationship in the non-diverging, non-mixing case is shown. The effect m on the F_p - k relationship is shown in Fig. 2-30. Parameters (k, m, γ, F_p, and ψ) are closely associated with each other. Using Eq. 2-42

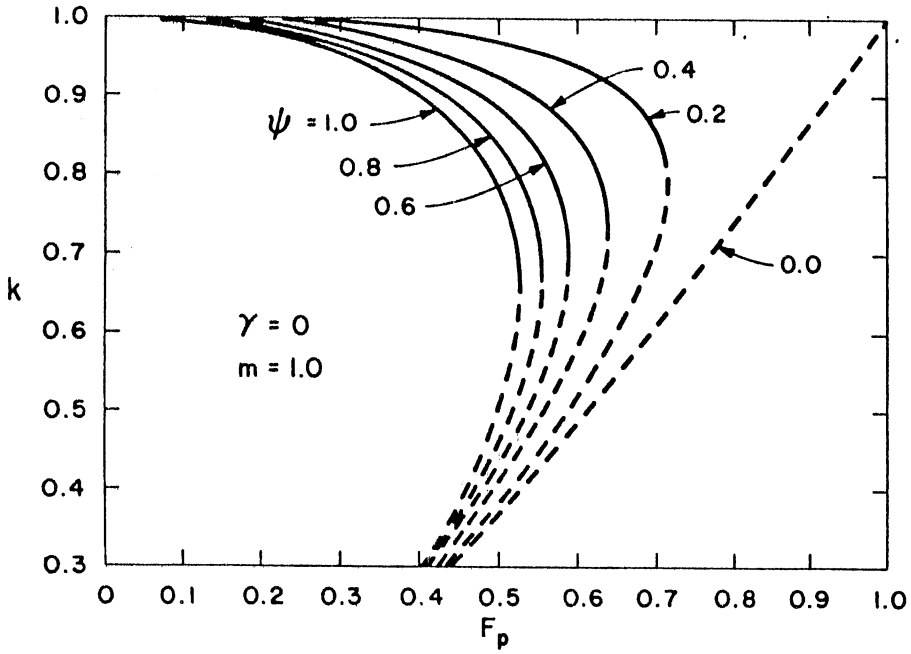

Fig. 2-29 Relationship between k and F_p in terms of ψ (Eq. 2-42).

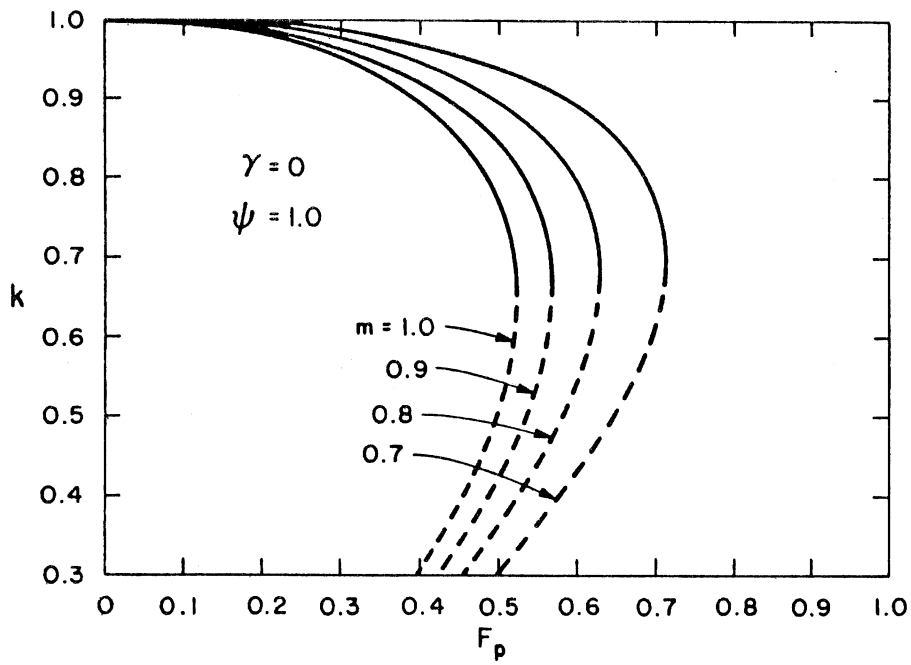

Fig. 2-30 Relationship between k and F_p in terms of m (Eq. 2-42).

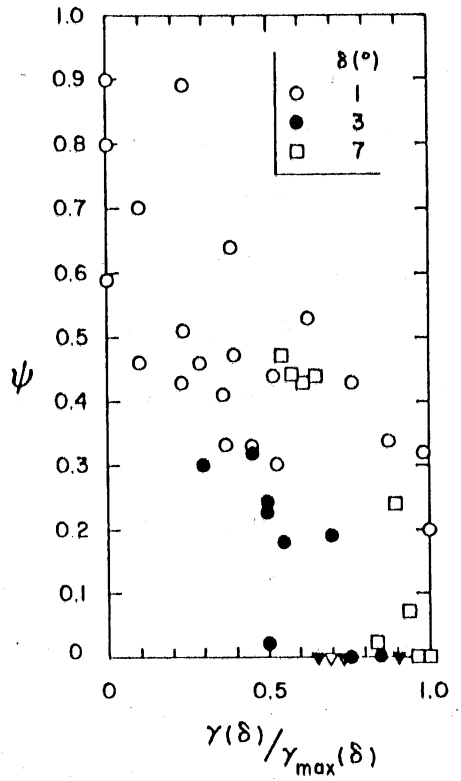

Fig. 2-31 Relationship between γ/γ_{max} and ψ for a given δ.

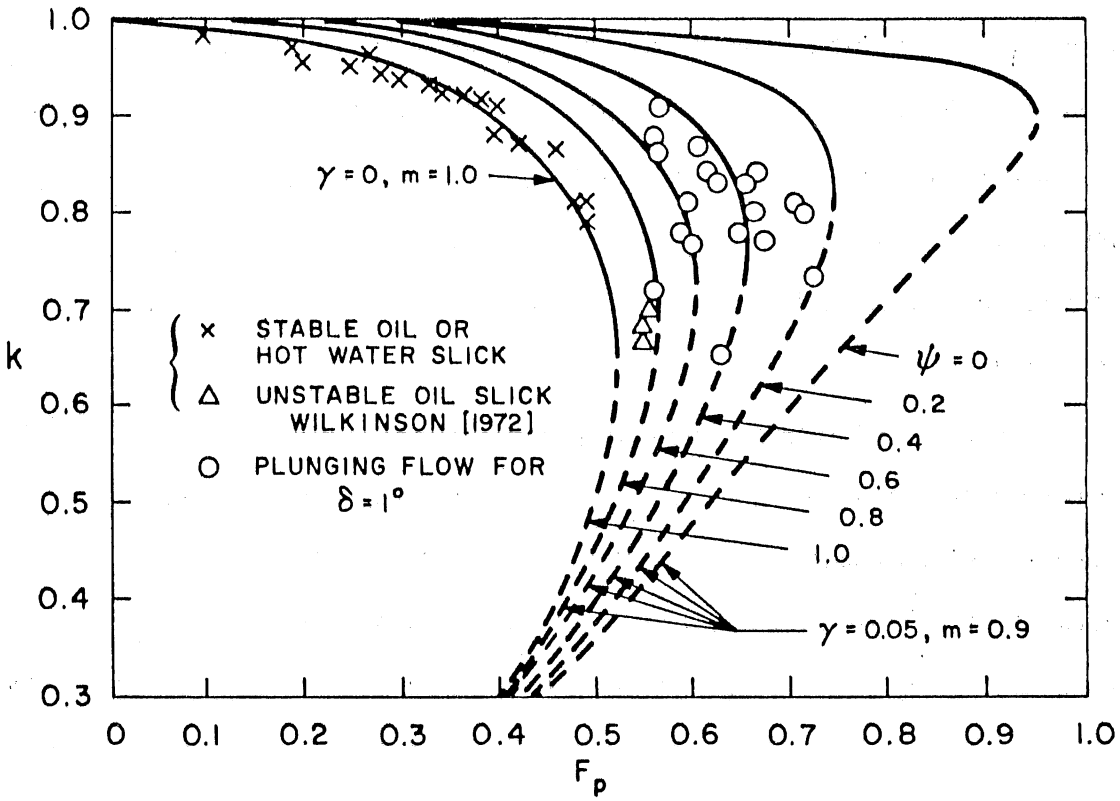

Fig. 2-32 Comparison between oil slick and plunge flow. Theory (Eq. 2-42) and data.

and data, ψ values have been back-calculated and plotted in Fig. 2-31. Inversed triangles indicate that values calculated from Eq. 2-42 are negative; they are shown as $\gamma = 0$:n Fig. 2-31. $\gamma(\delta)$ values for a given δ are normalized by maximum values $\tilde{\gamma}_{max}(\delta)$. There is much data scatter, but the trend is clearly that ψ decreases as γ/γ_{max} increases, and $\gamma = 0$ at $\psi = 1.0$. ψ values appear to vary typically from 0 to 0.45.

Larger F_p values are made possible in plunging flow by the dissipation of energy, according to Fig. 2-29. ψ and γ are strongly related to each other. Comparison between theory and the authors' data will be made with variable ψ values in order to explain the reason of data variation. The case of $\delta = 1^o$ is chosen for comparison because the influence of γ and m (approx. $\gamma = 0.05$, $m = 0.9$) on plunging flow is less important than for larger divergence angles. Wilkinson's and the authors' F_p ($\delta = 1^o$) data are plotted in Fig. 2-32. Data of stable slicks follow Eq. 2-42 with $m = 1$, $\gamma = 0$, and $\psi = 1$. Figure 2-32 indicates also that plunging flow can occur at F_p values from 0 to 1.0 depending on stagnation index ψ and the corresponding range of k against F_p.

(ii) Mixing plunging flows - According to Eq. 2-42 for the main control volume C.V.I., F_p is a function of ψ, γ and two nondimensional length scales (k and m). All four parameters are apparently an implicit function of channel divergence angle δ : $F_p(\delta) = \text{fun}\{m(\delta), k(\delta), \gamma(\delta), \psi(\delta)\}$. It is desirable to eliminate one of the length scales in order to reduce the complexity of the parametric relationship. An approach previously used (Akiyama and Stefan [1984])

is adopted for this purpose. It considers the force balance of ambient water, and a control volume II based on the assumption that there is only horizontal inflow Q_a at section "d" and outflow is only vertically downward; the horizontal velocity component of inflowing cold water is approximately zero, along the interface, based on experimental evidence.

Momentum Equation (Sub-Control Volume C.V.II) - The equation of horizontal momentum with respect to C.V.II (Fig. 2-6) is:

$$\frac{g}{2}\left((\rho_a + \Delta\rho_o)\ (h_a + \Delta)^2\ b_p - \rho_a(h_a + \Delta)^2\right)b_d =$$

$$\rho_a Q_a U_a - R^{II}_{x\ wall} + F^{II}_{x\ wall} + F^{II}_{x\ inter} \qquad 2\text{-}53$$

Where $F^{II}_{x\ inter}$ = the x-component of friction force along the interface. Reaction force R^{II}_x is, similarly, evaluated as:

$$R^{II}_x = \phi^{II} R^{II} \sin\delta = \phi^{II} P^{II}_d\ L\sin\delta \qquad 2\text{-}54$$

where P^{II}_d = the pressure force per unit length at the downstream end of the plunging region

ϕ^{II} = the wall pressure correction factor and:

$$P^{II}_d = \frac{g}{2}\rho_a(h_a + \Delta)^2 \qquad 2\text{-}55$$

Ignoring friction forces and assuming $\phi^{II} = 1$, Eq. 2-53 with 2-54 and 2-55 becomes:

$$m = \frac{(1 - k)^3}{2(\gamma F_p)^2} \qquad 2\text{-}56$$

In the derivation of Eq. 2-56, terms of $0(\epsilon_o)$ are dropped. It must be noted that in a strict sense Eq. 2-56 is valid for the mixing case only. Equation 2-56 is used to eliminate one of the nondimensional length scales, k or m in Eq. 2-42. An analytical expression for F_p in terms of γ, ψ, and k can then be obtained:

$$F_p = \left[\frac{\gamma^2 k((1 - k)^2 - 1 + k^2/(1 + \gamma)) + (1 + \gamma)^2(1 - k)^3}{\gamma^2 k(2 - \psi)}\right]^{1/2} \qquad 2\text{-}57$$

F_p in terms of γ, ψ, and m can alternatively be obtained with Eqs. 2-56 and 2-57 for the range of $0 < m, k \leq 1$. Equations 2-56 and 2-57 can be solved simultaneously by a numerical method. Comparison between theory and data in terms of k is given in Figs. 2-33 and 2-34 using $\psi = 0$ and 0.4. Equations and data in terms of m are plotted in Figs. 2-35 to 2-38, using $\psi = 0$, 0.2 and 0.4. Figure 2-38 indicates that γ for $\delta = 7^o$ will decrease along the calculated lines as m approaches 1; therefore γ values $\delta = 7^o$ can possibly vary from γ_{max} to 0, depending on F_o or A_o. Similar arguments can be made for the relationship between m and F_p. In mixing plunge flows, F_p can vary from about 0.53 to 1.0.

Agreement between theory and data appears to be good for the parametric relationships in terms of m and reasonably good in terms of k. This appears to indicate that the parameter m is more significant than k in the domain where the effects of divergence of channel on the plunge phenomenon are dominant. The variance of F_p, k, m, and γ

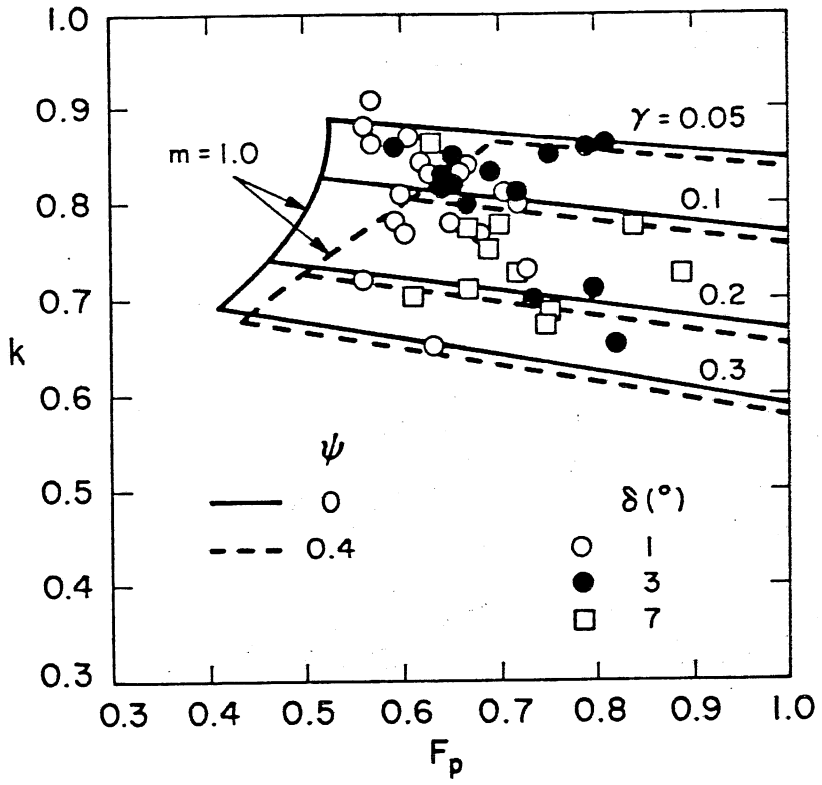

Fig. 2-33

Comparison between theory (Eqs. 2-56 and 2-57) and data in k - F_p - ψ relationship.

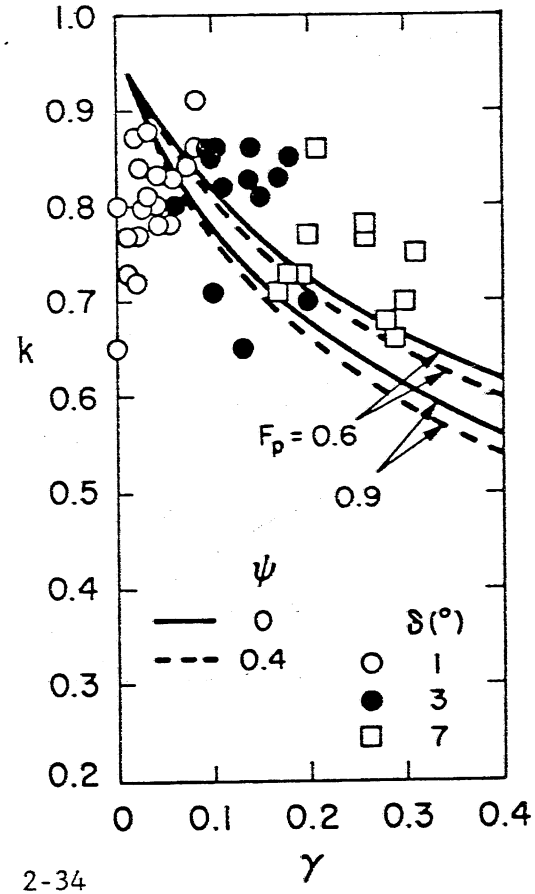

Fig. 2-34

Comparison between theory (Eqs. 2-56 and 2-57) and data in k - γ - ψ relationship.

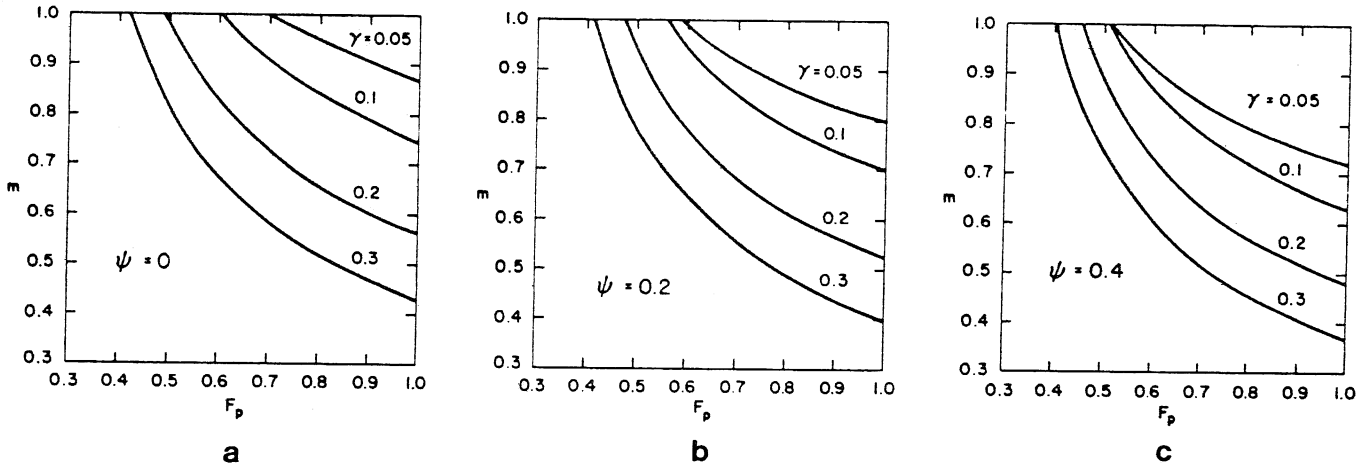

Fig. 2-35 Theoretical lines (Eqs. 2-56 and 2-57) for varible ψ in m - F_p - γ relationship.

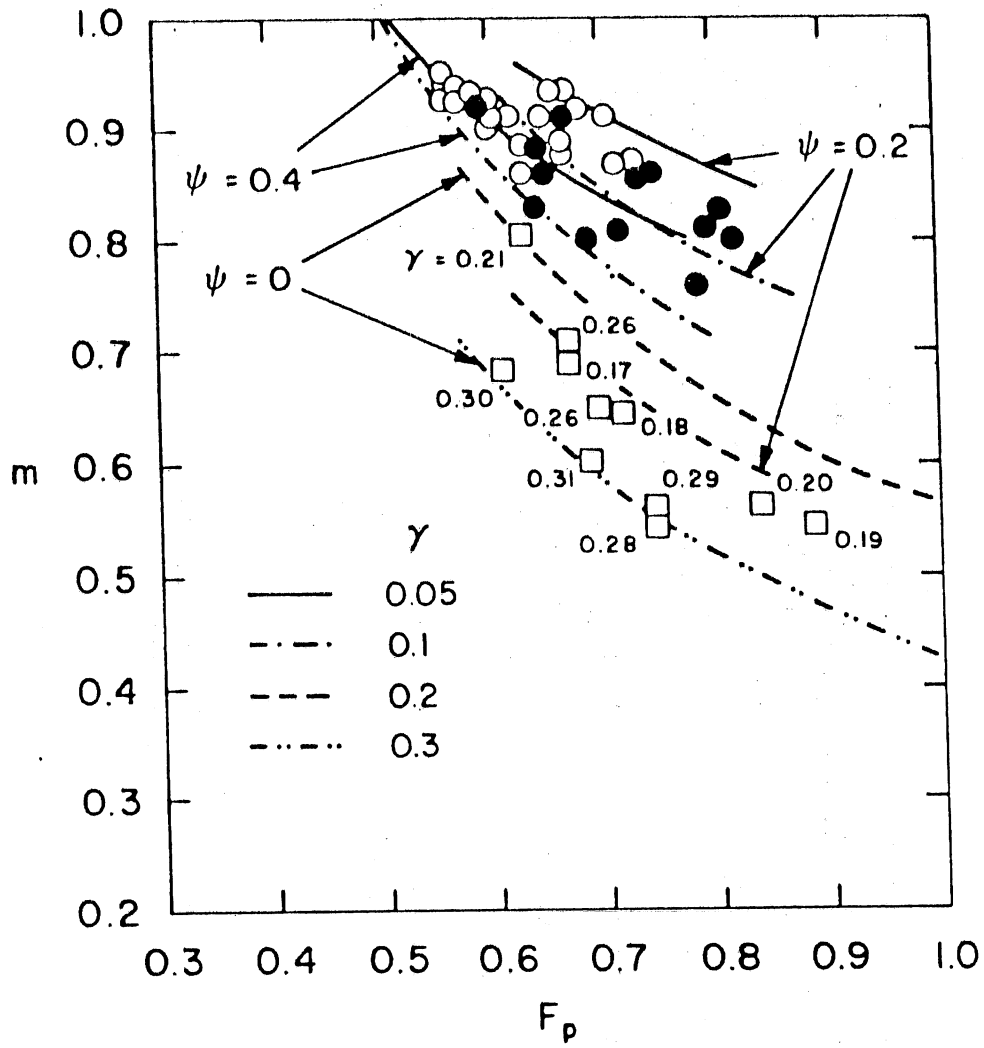

Fig. 2-36 Comparison between theory (Eqs. 2-56 and 2-57) and data in m - F_p - γ relationship.

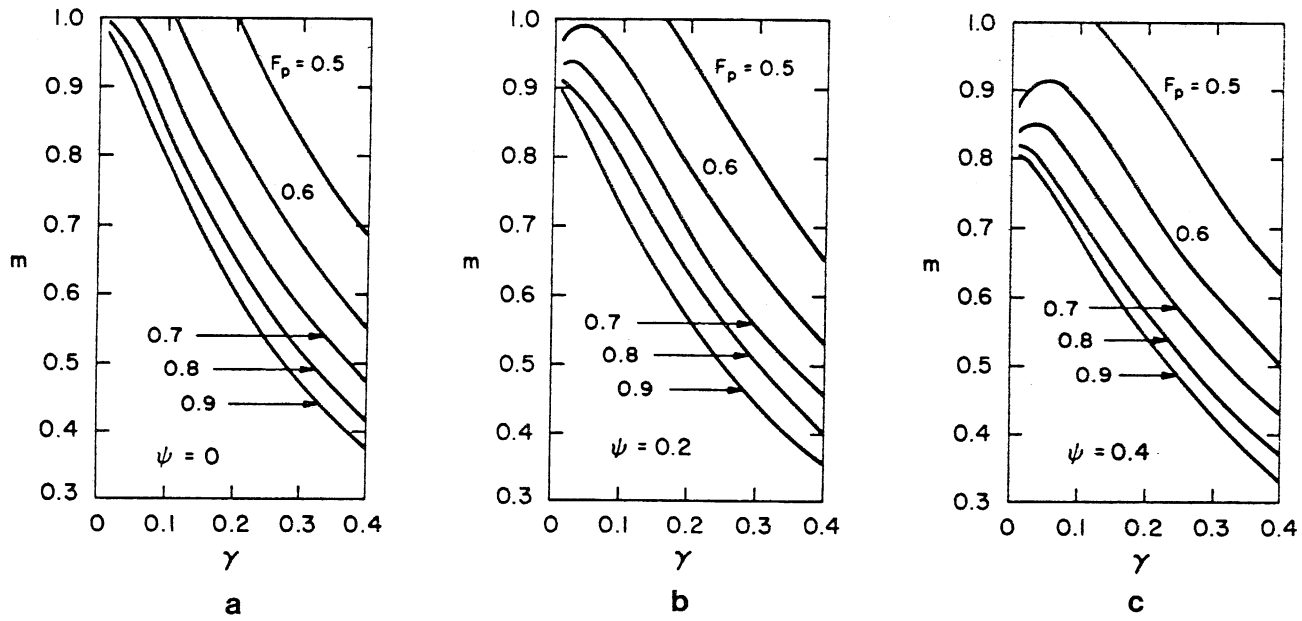

Fig. 2-37 Theoretical lines (Eqs. 2-56 and 2-57) for variable ψ in m - γ - F_p relationship.

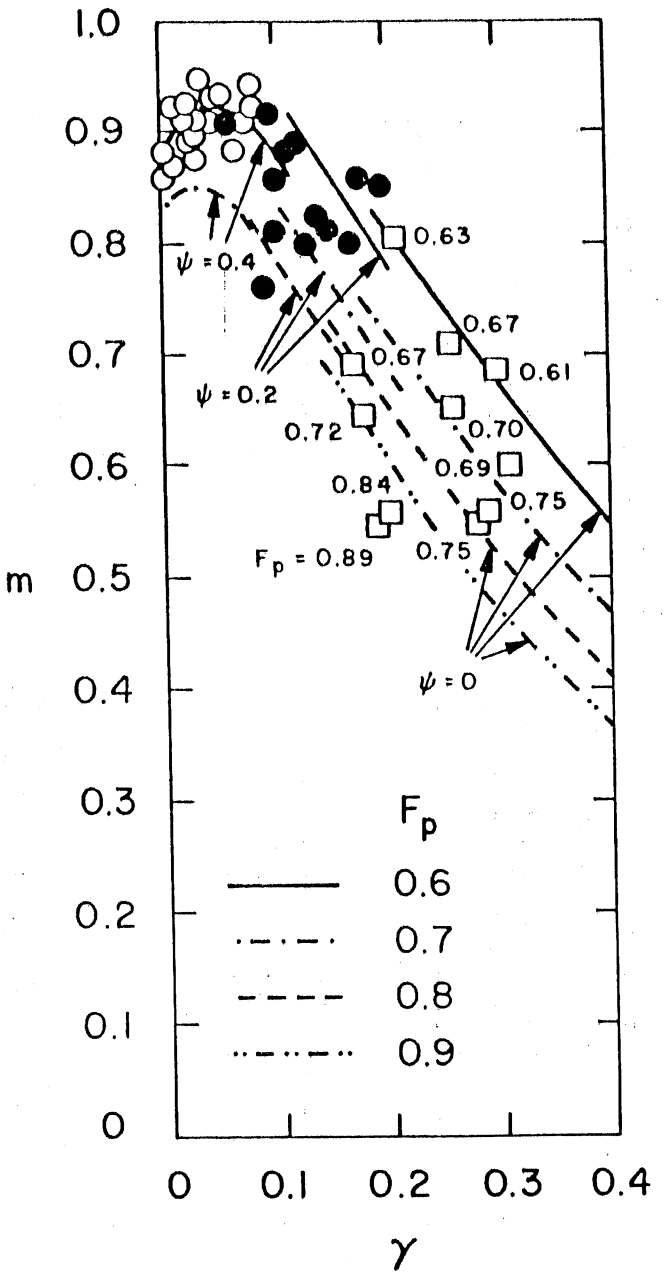

Fig. 2-38 Comparison between theory (Eqs. 2-56 and 2-57) and data in m - γ - F_p relationship.

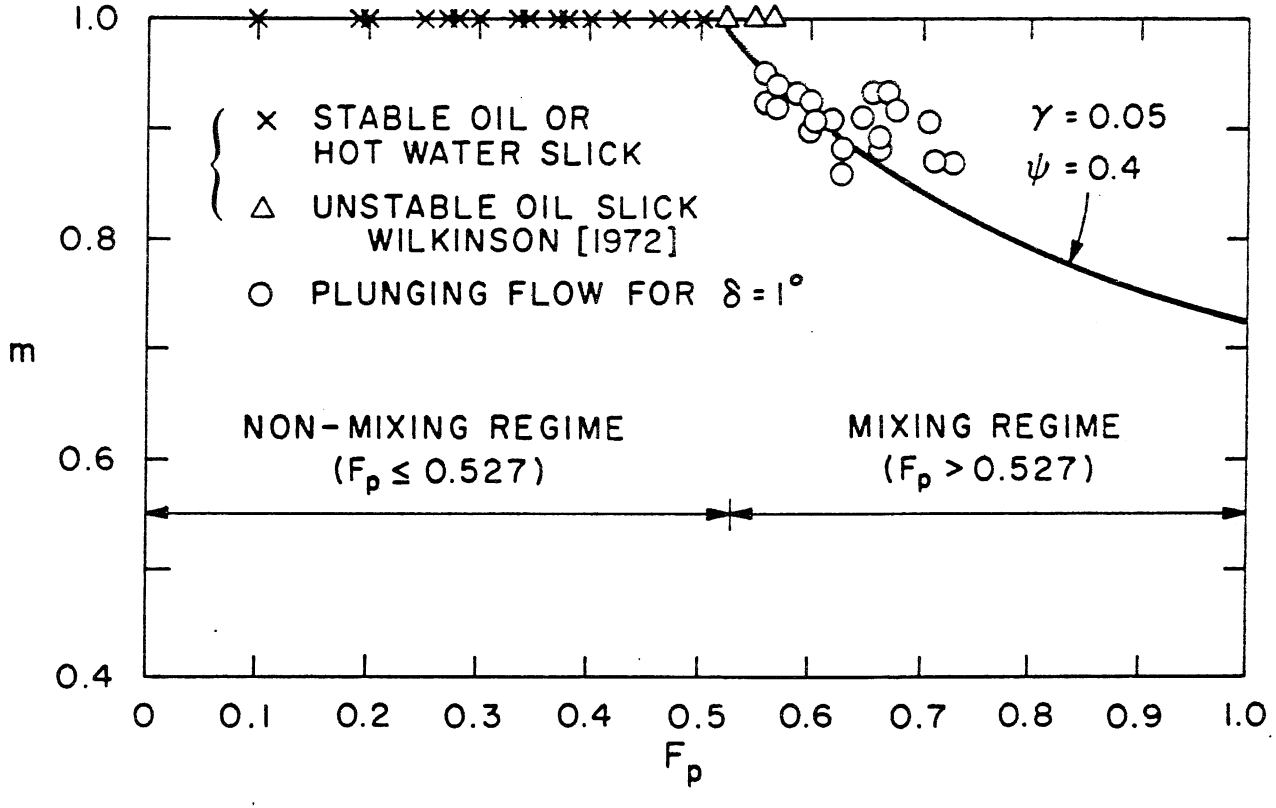

Fig. 2-39 Classification of flow domains for entraining and non-entraining flows.

data shown in Tables 2-2, 2-3, and 2-4 can be well explained in terms of the stagnation parameter ψ .

Figure 2-39 summarizes how the theory for immiscible flow (Eq. 2-38 with $\gamma = 0$) and for miscible flow (Eqs. 2-42 and 2-56) relate to each other. The calculated line with $\gamma = 0.05$ and $\psi = 0.4$ is added to the data, and divides Wilkinson's data for miscible (stable) and immiscible (unstable) cases. F_p values in miscible flow appear to approach $F_p = 0.53$ along the calculated lines, and further decrease, possibly to as low as zero, in immiscible flow.

2.6 Conclusions

(a) Plunging Flow in a Two-Dimensional Channel.

1. The configuration of plunge flow depends on both inflow and the resulting underflow characteristices uniquely determined by the channel configurations. Some empirical formulas reported may therefore be valid only in a specific type of reservoir.

2. Plunge depths depend on channel slope. On a mild slope underflow depth below the plunge point is approximately normal depth. On a steep slope underflow depth below the plunge point is the critical depth. Both are based on reduced gravity $g \cdot \Delta\rho/\rho_a$.

3. On a mild slope, the plunge depth is a function of bed friction, and inflow densimetric Froude number (Eq. 2-37). On a steep slope, the plunge depth depends on entrance mixing and inflow densimetric Froude number (Eq. 2-38).

4. The effect of entrance mixing (herein expressed through a parameter γ) is to deepen the plunge depth, and to increase F_p. γ is

small or negligible for flow over mild slopes; it is significant on steeper slopes.

5. Laboratory and field studies in which bed slope and roughness are measured and related to entrance mixing at the plunge point are necessary for better understanding of this problem.

6. The plunge depth equations Eqs. 2-37 and 2-38, based on both inflow and underflow characteristics, match experimental and field data covering a wide range of conditions.

7. Theoretical results presented herein are applicable only if these assumptions are met: a) no time change of inflow rate (storm events); b) negligible change of channel width and slope with distance; and c) well-mixed receiving reservoir, at least in the vicinity of the plunge point.

b) Plunging Flow in a Diverging Channel.

1. Densimetric Froude number at plunging, F_p, is an implicit function of inflow densimetric Froude number F_o, initial aspect ratio A_o and divergence angle δ. Plunging flow in a diverging channel without separation is affected by conditions upstream (F_o, A_o) and downstream (h_p and b_p) of the plunge region through the parameters k and m. F_p approaches asymptotically that of parallel flow as the effect of divergence diminishes (Fig. 2-36). In a horizontal diverging channel no unique F_p and γ values exist. F_p can vary approximately from 0 to 0.53 for immiscible flow and 0.53 to 1.0 for miscible flow (Fig. 2-39). According to experimental data, F_p most likely ranges from 0.6 to 0.7, and γ_{max} can vary from 0 to 0.3, dependent on where plunging occurs (Figs. 2-22 and 2-28).

2. Energy dissipation is an essential mechanism in plunging flow and is closely related to initial mixing (Fig. 2-31). The complex flow in a plunge region can be explained in terms of the parameter ψ, but it is very likely that the ψ values can fluctuate as the result of intermittent entrainment due to large eddy motion in the vicinity of the plunge line.

3. Empirical equations for the location of the plunge line, and for the rate of initial mixing were also obtained from the experimental data.

4. Closure of the problem using downstream conditions cannot be attained because no normal condition for underflow in a diverging channel exists (Chapter 5).

3. ENTRAINMENT FUNCTION OF NON-COHESIVE SEDIMENT

3.1 Outline and Review of Previous Studies

The problem of the entrainment of sediment into suspension from an erodable bed arises in a variety of contexts. The phenomenon of entrainment of sediment into suspension is often termed "resuspension."

Perhaps the simplest problem of interest is the entrainment induced by a lattice oscillating over a bed of fine material. Initially, the water is clear, but in time, entrainment from the bed leads to a developed distribution of suspended sediment, due to the turbulence generated by mechanical vibration. Among early investigators to consider this problem are Rouse [1938] and Dobbins [1944].

A closely related problem is that of steady flow of clear water from a non-erodible bed to an erodible bed (Fig. 3-1); in this case the flow picks up suspended sediment as it moves downstream over an erodible bed. This problem was analyzed by Mei [1969], Apman and Rumer [1970], and Hjelmfelt and Lenau [1970]. Resuspension is of considerable importance in natural bodies of water such as rivers, reservoirs, lakes, estuaries, and the ocean. Parker [1978], for example, considered the effect of lateral imbalance of entrainment and deposition on the formation and maintenance of river banks. Kerssens, Prins, and van Rijn [1979] studied the problem in the context of the filling of dredged channels in rivers and estuaries.

Sheng and Lick [1979] investigated wind-driven resuspension in Lake Erie. Lin, Huan, and Li [1983] included the effect of sediment entrainment in their mathematical model of suspended sediment transport in the tidal Qiantang Estuary.

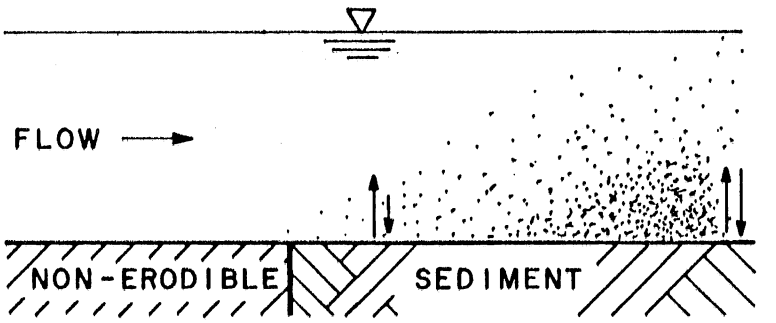

Fig. 3-1 Spatial development of suspension due to entrainment driven by shear flow.

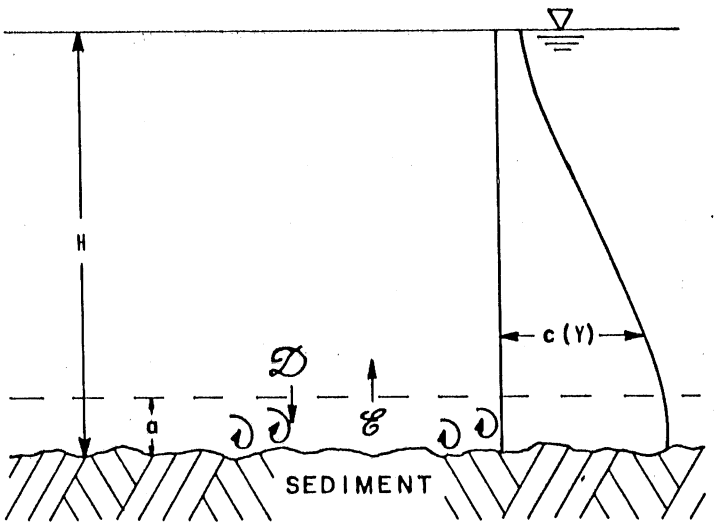

Fig. 3-2 Definition diagram.

Resuspension of particles is considered to be initiated when the vertical fluctuating velocity component (v') exceeds the settling velocity (V_f) of a particle.

Bagnold [1966], for example, proposed the following criteria for resuspension using the vertical turbulent intensity ($(\overline{v'}^{1/2})$)

$$\frac{(\overline{v'}^2)^{1/2}}{V_f} \sim \frac{u_{*cr}}{V_f} > 1$$

Where u_{*cr} is the critical bed-shear velocity. The ratio u_*/V_f is sometimes called "non-dimensional bed shear stress" or "suspension parameter (μ)", which is most significant in suspended sediment transport. According to Laursen [1958], the incipient μ (μ_{in}), at which sediments start to be in suspension, is about 0.8 and the critical value of μ (μ_c) at which suspended sediments start to increase abruptly, is about 2.0.

Many different approaches have been proposed by various investigators to determine the concentration profile of suspended sediments in uniform open channels for the purpose of predicting the sediment discharge due to suspended load. They are classified into diffusion (e.g., Rouse [1938], Lane and Kalinske [1941]), energy (e.g., Velikanov [1958]), or stochastic models (e.g., Yalin and Krishnappan [1973]). Among these models, the simplest and most widely used approach is a diffusion model.

The profile derived from the diffusion equation is sometimes referred to as Rouse's profile after H. Rouse [1938].

Rouse's profile can predict the relative concentration distribution satisfactorily except near a water surface, provided that the concentration (c_a) at the vicinity of the bed ($y = a$) is properly given, because Rouse's assumption for eddy diffusivity leads to a singularity at $y = 0$.

Rouse's profile is given by:

$$\frac{c}{c_a} = \left(\frac{H - y}{y} \cdot \frac{a}{H - a} \right)^Z \qquad 3\text{-}1$$

where

$$Z = \frac{V_f}{\beta \kappa u_*} \qquad 3\text{-}2$$

where H = the flow depth

κ = the Von Karman constant

V_f = the settling velocity of a sediment particle

β = the factor of proportionality (= the ratio of eddy viscosity to eddy diffusivity.)

a = the reference level

c_a = the reference concentration

Several different models to determine the reference level (a) and concentration (c_a) are proposed.

The reference level "a" is an artificial point which divides sediment transport into bed load ($0 \leq y < a$) and suspended load ($a \leq y < H$) as shown in Fig. 3-2.

There are basically four methods to select an arbitrary length scale "a".

1) to relate "a" to a typical bed grain size (D_s) (e.g., Einstein [1950])

2) to relate "a" to a bed-form height (Δ) (e.g., Rijn [1984])

3) to relate "a" to a length scale derived from hydrodynamic parameters (such as displacement thickness δ_D) (e.g., Coleman [1969])

4) to relate "a" to a flow depth (H) (e.g., Itakura and Kishi [1980])

There are basically two approaches to determine c_a.

1) to equate the upward flux of concentration due to the vertical fluctuating velocity component with the amount of downward sediment settlement (e.g., Lane and Kalinske [1941]).

2) to relate c_a to concentration in the bedload layer (e.g., Einstein [1950]).

Einstein [1950] circumvented the problem by choosing $a = 2D_s$, and proposed that c_a is the concentration of bedload layer, based on his experimental observations. This approach was followed by Engelund and Fredsoe [1976]. The pattern of fluid forces immediately adjacent to the bed, however, is extremely complicated. It is unlikely that Eq. 3-5 applies there, and measurement of concentration is extremely difficult. Van Rijn [1984] did not propose a unique choice of "a". Instead, he assumed "a" to be half the bed-form height (0.5Δ), or the equivalent roughness height (k_s) if the bed form dimensions are not known, while a minimum value of "a" ($a_{min} = 0.01H$) is used for reasons of accuracy. Coleman [1969] suggests that "a" correlates with displacement boundary

layer thickness (δ_D), based on laboratory and field data. Coleman's model is sometimes called a two-layer model, because of the experimental fact that concentration profiles are broken into two regions: an inner and outer. Recently, the two-layer approach is also followed by Samaga et al. [1985].

An alternative is to choose "a" as a small fraction of the flow depth H, such that Eq. 3-5 is still likely to apply there. Wills [1979], McTigue [1981], and Samaga et al. [1985] proposed a = 0.2H based on experimental data. Itakura and Kishi [1980] suggested the choice:

$$a = 0.05H \qquad 3\text{-}3$$

Eq. 3-3 is adopted in this analysis in order to determine a sediment entrainment function. This rather simple choice of "a" is based on the consideration that it is still difficult to confirm which method is most adequate.

Recently van Rijn's [1984] work may indicate that there is no unique reference level on movable bed, and the choice of "a" could change dependent on flow conditions, presence of bed forms, etc.

The entrainment rate normalized by the falling velocity of the sediment (V_f) is equal to the equilibrium bed concentration (c_{ae}). Typical examples of this type of approach are the studies done by Itakura and Kishi [1980] and Engelund and Fredsoe [1970]. Ikeda and Asaeda [1983] found that the concentration near the rippled bed increases with the power of eight against the cross-sectional mean velocity based on the bursting phenomenon of turbulence.

Herein, data from suspensions in open channel flows are used to determine an empirical relation for the entrainment of sediment into suspension. Data used in analysis are presented in Appendix II. Analysis is based on the diffusion equation, and data are reduced with the aid of dimensional analysis and similarity collapse method. The treatment is restricted to dilute suspensions of non-cohesive material, but both cases of uniform and mixtures are included. Only rectilinear flows are considered, although it is expected that the results could be applied to certain oscillating flows and furthermore, suspensions in moderate disequilibrium as well, although the relations will be determined for equilibrium flows. It is also noted that the sediment entrainment function (E_s) proposed herein is deduced when a = 0.05H and hence it may not be valid if a $\neq$ 0.05H.

3.2 Analysis

3.2.1 Governing Equations

The equation of sediment mass conservation can be, in general, written as

$$\frac{\partial c}{\partial t} + u\frac{\partial c}{\partial x} + (v - V_f)\frac{\partial c}{\partial y} + w\frac{\partial c}{\partial z} = \frac{\partial}{\partial x}\left(\epsilon_x \frac{\partial c}{\partial x}\right) + \frac{\partial}{\partial y}\left(\epsilon_y \frac{\partial c}{\partial y}\right) + \frac{\partial}{\partial z}\left(\epsilon_z \frac{\partial c}{\partial z}\right) \qquad 3\text{-}4$$

where $\epsilon_{x,y,z}$ is the turbulent eddy diffusivity. In many cases, in particular, gradually varied two-dimensional flows, the following relations are satisfied.

$$u\frac{\partial c}{\partial a} >> v\frac{\partial c}{\partial y} \text{ and } w\frac{\partial c}{\partial z}$$

$$\frac{\partial}{\partial y}(\epsilon_y\frac{\partial c}{\partial y}) >> \frac{\partial}{\partial x}(\epsilon_x\frac{\partial}{\partial x}) \text{ and } \frac{\partial}{\partial z}(\epsilon_z\frac{\partial c}{\partial z})$$

Equation 3-4 hence becomes

$$\frac{\partial c}{\partial t} + u\frac{\partial c}{\partial x} = \frac{\partial}{\partial y}F_y \qquad 3\text{-}5$$

where

$$F_y = -V_f c - \epsilon\frac{\partial c}{\partial y} \qquad 3\text{-}6$$

In the above equations, c denotes local concentration, and u denotes local flow velocity in the x direction, both averaged over turbulence; t denotes time. F_y denotes the vertical volumetric flux of suspended sediment. This flux consists of the two terms on the right hand side of Eq. 3-6; V_f denotes the particle fall velocity, taken to be constant herein, and ϵ denotes a vertical kinematic eddy diffusivity. Hereafter, ϵ denotes a vertical eddy diffusivity ϵ_y. The term $-\epsilon(\partial c/\partial y)$ provides a closed expression for the vertical Reynolds transport of sediment due to turbulent mixing. For equilibrium suspensions of non-cohesive material, c decreases with y, so the sediment flux due to turbulent mixing is directed upward, thus balancing the downward settling flux.

Considering the boundary condition at the water surface that $F_y(H) = 0$, Eq. 3-5 can be integrated in the vertical to yield

$$\frac{\partial}{\partial t}\int_a^H c\,dy + \frac{\partial}{\partial x}\int_a^H uc\,dy = F_y(a) = -\left[V_f c + \epsilon\frac{\partial c}{\partial y}\right]\Big|_{y=a} \qquad 3\text{-}7$$

Equation 3-7 provides a bulk sediment balance for the flow of sediment between $y = a$ and $y = H$. It is seen that sediment tends to settle out of this layer at the rate D, where

$$D(a) = V_f c\Big|_{y=a} \qquad 3\text{-}8$$

On the other hand, sediment is entrained by turbulence from the layer below at the rate E where

$$E(a) = -\epsilon\frac{\partial c}{\partial y}\Big|_{y=a} \qquad 3\text{-}9$$

Equation 3-7 can thus be written as

$$\frac{\partial}{\partial t}\int_a^H c\,dy + \frac{\partial}{\partial x}\int_a^H uc\,dy = E(a) - D(a) \qquad 3\text{-}10$$

It is seen that $D(a)$ is always positive; the entrainment rate $E(a)$ is always positive when c decreases in the vertical.

The suspension between $y = a$ and $y = H$ neither gains nor loses sediment if deposition due to settling equals entrainment; i.e.

$$E(a) = D(a) \qquad 3\text{-}11$$

Eq. 3-10 is of greatest interest when "a" approaches zero, for this provides a description of sediment entrainment from, and deposition on, the bed. There are a variety of reasons why the parameter "a" should not be set precisely equal to zero.

It is clear from Eq. 3-10 and Fig. 3-2 that at this value of "a," E(a) and D(a) represent entrainment from, and deposition to, a thin fluid layer above the bed rather than the bed itself. The equation for the conservation of sediment mass below y = a can be written as

$$(1 - \lambda)\frac{\partial \eta_b}{\partial t} + \frac{\partial}{\partial t}\int_0^a c\,dy + \frac{\partial}{\partial x}\int_0^a uc\,dy = D(a) - E(a) \qquad 3\text{-}12$$

where η_b denotes bed elevation and λ denotes bed porosity. The integral terms in Eq. 3-12 represent the effect of storage of sediment in the thin layer between the bed and the flow above y = a. If this storage is small, as is certainly the case for $a/H \ll 1$, Eq. 3-12 may be approximated as

$$(1 - \lambda)\frac{\partial \eta_b}{\partial t} = D(a) - E(a) \qquad 3\text{-}13$$

Thus, D(a) and E(a) can be interpreted as rates of deposition on, and entrainment from, the bed.

Herein, it is assumed that the simplification from Eq. 3-12 to Eq. 3-13 is valid for the choice a = 0.05H.

It is often assumed that settling is inhibited by forces generated near the bed. Indeed, the electrochemical forces in a cohesive suspension can sometimes prevent settling completely (Partheniades [1965]). For the noncohesive sediments considered herein, the only possible inhibiting forces are mechanical. If the thin layer near the bed is below its capacity to hold suspended sediment, extra sediment supplied from above may be held there rather than settling on the bed. The total capacity of a thin layer to hold sediment, however, is very small, and a state of near-capacity should be reached much more rapidly in such a layer than in the thicker flow above. Thus, Eq. 3-13 should be accurate as long as a characteristic time scale of the imposed disequilibrium is much larger than a characteristic time required for the thin layer to reach capacity.

3.2.2 Entrainment From a Bed of Uniform Material

The rate of bed deposition is a property of the water-sediment flow, and it is given by Eq.3-8. The rate of entrainment, however, is a function of the fluid forces acting on the bed and the characteristics of the bed itself. The case of a bed completely covered with uniform material of grain size D_s is considered first. A dimsionless entrainment rate E_s can be defined such that

$$E(a) = V_f E_s \qquad 3\text{-}14$$

In general, it can be assumed that E_s should be a function of the parameters of the flow itself. Following the general dimensional analysis of Parker and Anderson [1977], E_s is taken to be a function of the specific gravity of a submerged particle

$$\sigma = \left(\frac{\rho_s}{\rho_w} - 1\right) \qquad 3\text{-}15$$

particle Reynolds number

$$R_p = \frac{D_s\sqrt{\sigma g D_s}}{\upsilon} \qquad 3\text{-}16$$

and two dimensionless hydraulic parameters. In the above relations, ρ_w denotes water density, ρ_s denotes sediment density, g denotes the acceleration of gravity, and υ denotes the kinematic vicosity of water.

Herein, the two hydraulic parameters are taken to be the ratio μ of shear velocity $u_* = \sqrt{\tau/\rho_w}$, τ is shear stress on the bed) to fall velocity V_f

$$\mu = \frac{u_*}{V_f} \qquad 3\text{-}17$$

and the dimensionless depth H/D_s. That is,

$$E_s = f(\mu, \frac{H}{D_s}, R_p, \sigma) \qquad 3\text{-}18$$

For suspensions of natural material, σ is usually close to 1.65; thus this parameter can be dropped.

It is desired to determine the functional relationship E_s empirically. This can be done by measuring the near-bed concentration c_a at a = 0.05H for equilibrium suspensions, for according to Eqs. 3-8, 3-11, and 3-14,

$$E_s = c_{ae} \qquad 3\text{-}19$$

where c_{ae} denotes the value of c_a at equilibrium.

Laboratory data on suspensions of uniform material were used to evaluate E_s for the equilibrium case. The concentration c_{ae} at a = 0.05H was determined directly from the measured distributions of suspended sediment, with a minimum of interpolation or extrapolation. A typical example is shown in Fig. 3-3. The data used are those given by Einstein and Chien [1955], Vanoni and Nomicos [1960], Vanoni [1941], and Straub, Anderson, and Flammer [1958].

The data were plotted as a function of μ, with R_p as a secondary parameter in Fig. 3-4. Values of H/D_s range from 50 to 1400; over this range very little dependence of E_s on H/D_s could be discerned. The relationship to μ and R_p, however, is strong. The variation of R_p are relatively small for large sediment (D_s = 0.274, 0.94, 1.3 mm) and relatively large for small sediment (D_s = 0.1, 0.16 mm). In fact, the experiment of Straub et al. [1958] was made to find the dependence of concentration on the temperature, that is, R_p. As shown in Fig. 3-4, the dependence of μ on E_s is larger than on R_p. In order to find the

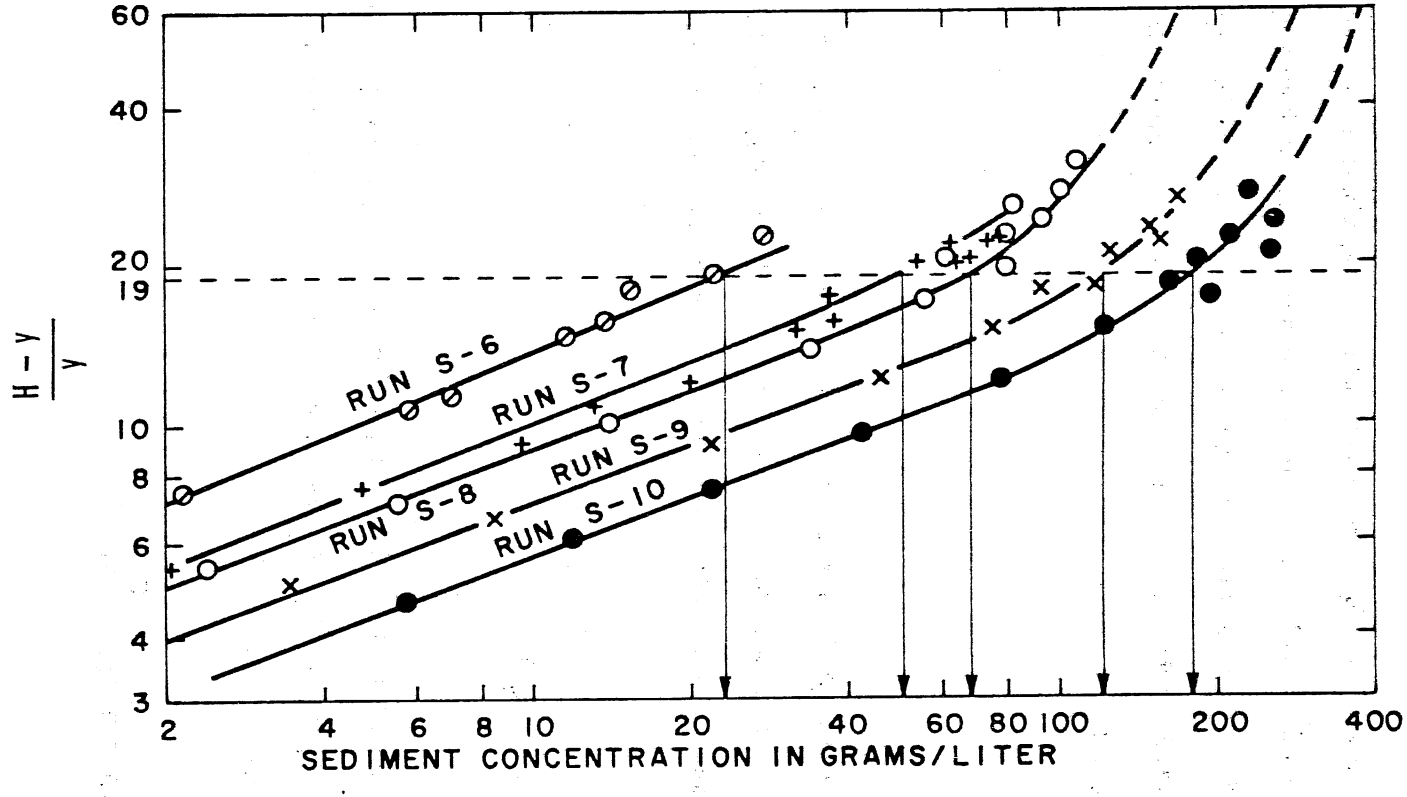

Fig. 3-3 Typical diagram showing the method by which c_a is determined at $z = a = 0.05h$. The arrows point to the appropriate value of concentration in grams per liter; this must be converted to volumetric concentration. From Einstein and Chien [1955].

effect of R_p on E_s, the relationship between μ and E_s is determined by using the data for large sediments in which the variation of R_p is small. Those relations are shown in Fig. 3-4 by straight lines. A similar relation is applied to the data for small sediment. In Fig. 3-5, the values of μ for $E_s = 0.01$ are plotted against $\bar{R}_p$, where $\bar{R}_p$ is the average value of R_p for each size of sediment. It is found that the effect of R_p on E_s changes with the square root of R_p. It is expected that the sand entrainment rate E_s is a function of the similarity variable Π, where

$$\Pi = \mu R_p^{0.5} \qquad 3\text{-}20$$

In Fig. 3-6, the data of E_s are plotted as a function of Π. A regression relation for the data in Fig. 3-6 is obtained by using the method of the least squares fitting. The relation is found to be extremely steep.

$$E_s = 3.70 \times 10^{-13} \Pi^{10.6} \qquad 3\text{-}21$$

Equation 3-21 is added in Fig. 3-6. Equation 3-21 does not give any critical value of Π_c where E_s becomes zero. Thus, the following modified forumla is proposed:

$$E_s = 3.0 \times 10^{-12} \Pi^{10} \left(1 - \frac{\Pi_c}{\Pi}\right) \qquad 3\text{-}22$$

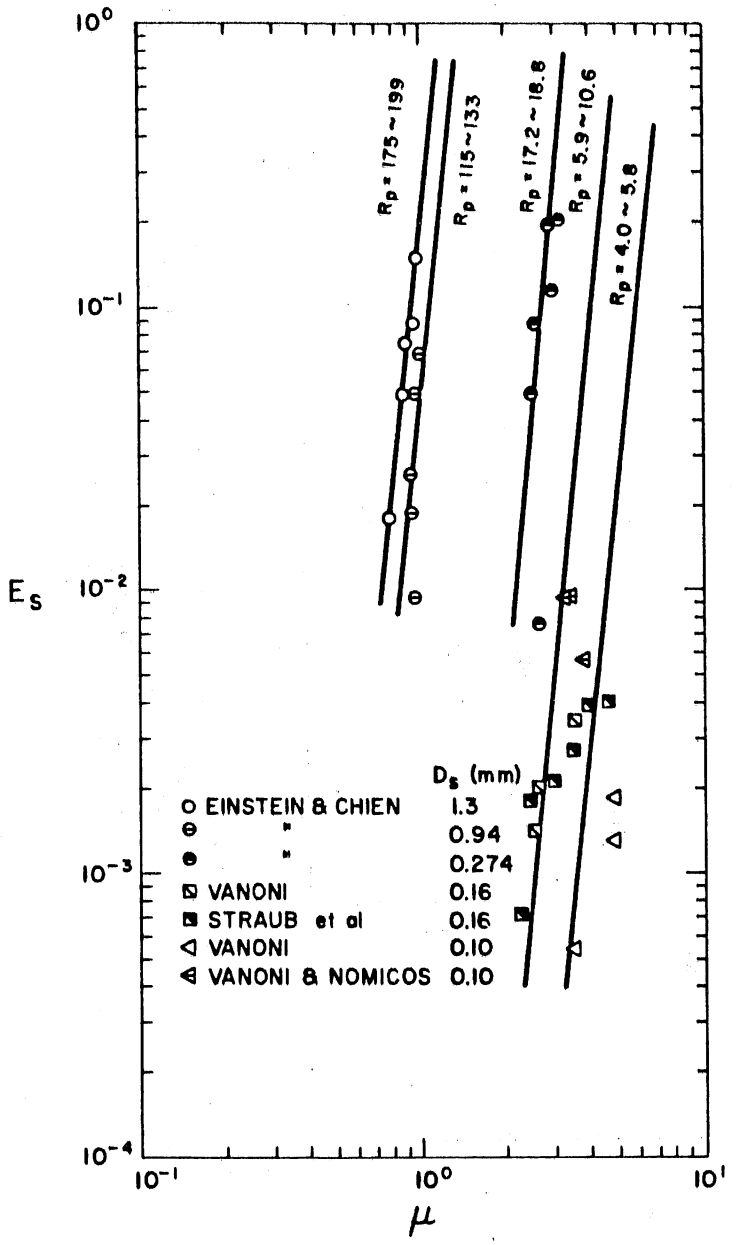

Fig. 3-4 Equilibrium entrainment rate versus non-dimensional bed shear stress with different particle Reynolds numbers.

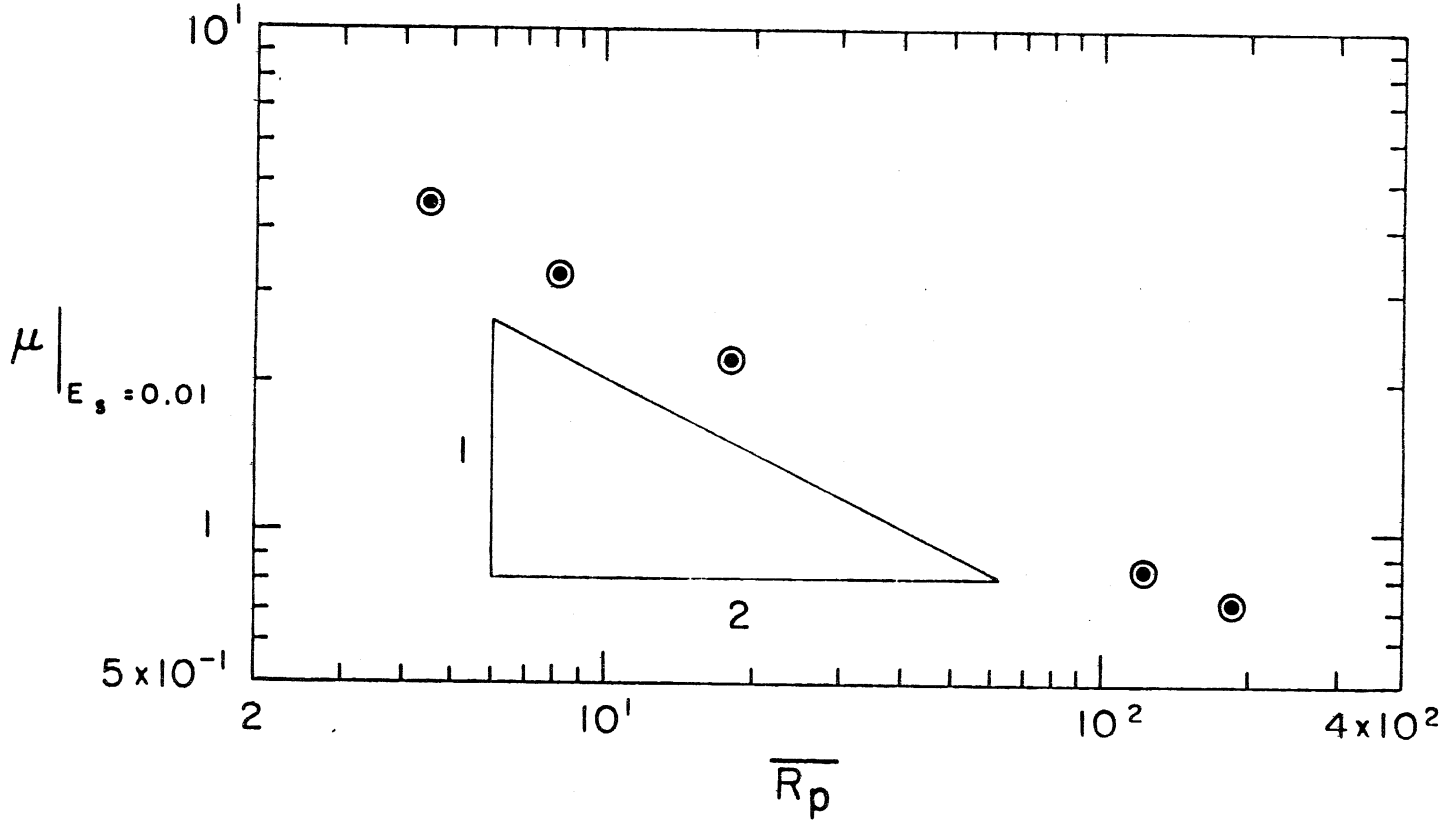

Fig. 3-5 Nondimensional shear stress versus averaged value of the particle Reynolds number for the same size of sediment.

where Π_c is a critical value of Π, found to be equal to five.

3.2.3 Entrainment From a Bed Consisting of a Mixture

In the natural environment, sediment mixtures are common. Let the bed material be divided into N size ranges, such that fraction p_i of the bed material is contained to the ith range, which has mean size D_i. Then, Eq. 3-18 is generalized to

$$E_{si} = f(\mu_i, \frac{H}{D_{50}}, R_{p50}, P_i, \frac{D_i}{D_{50}}) \qquad 3\text{-}23$$

where E_{si} denotes the entrainment rate for the ith grain size range,

$$\mu_i = \frac{u_*}{V_{fi}} \quad ; \quad R_{p50} = \frac{D_{50}\sqrt{\sigma g D_{50}}}{\upsilon} \qquad 3\text{-}24$$

and D_{50} denotes the mean grain size of the mix, and V_{fi} denotes the fall velocity associated with the size D_i.

The integral form of mass conservation equation for the ith range of sediment mixture can be written as

$$\frac{\partial}{\partial t}\int_a^H c_i dy + \frac{\partial}{\partial x}\int_a^H uc_i dy = v_{si}(P_i E_{si} - c_{ai}) \qquad 3\text{-}25$$

where c_{ai} denotes the value of c_a for the ith range of sediment mixture. For equilibrium suspension, Eq. 3-25 gives the following relation

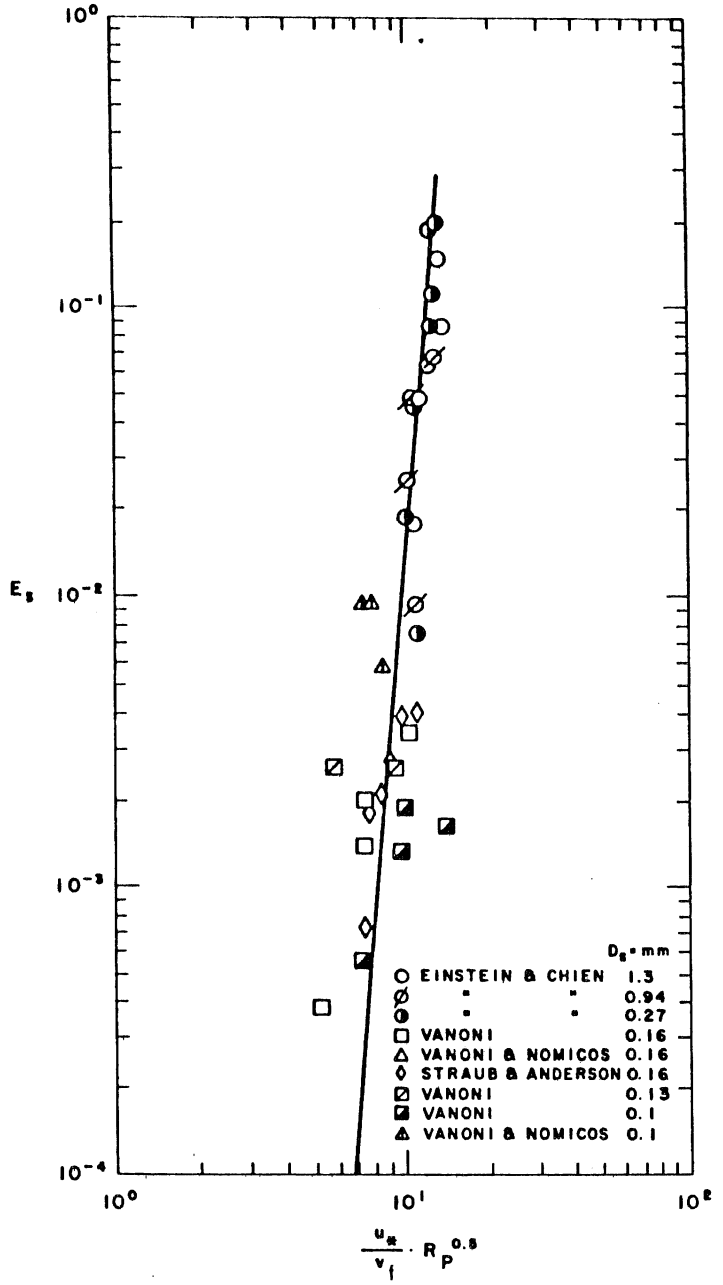

Fig. 3-6 Entrainment relation for laboratory suspensions of uniform material.

$$E_{si} = \frac{c_{aei}}{P_i} \qquad 3\text{-}26$$

where c_{aei} is the value of c_{ae} at equilibrium.

Field data on suspensions for two reaches on the Rio Grande (Nordin and Dempster [1983]) and one reach on the Niobrara River (Colby and Hembree [1955]) were analyzed similarly to the laboratory data to determine E_{si}. Three grain size ranges were used. For range 1, 0.0625 mm $< D_s <$ 0.125 mm, and D_1 = 0.088 m. For range 2, 0.125 mm $< D_s <$ 0.25 mm, and D_2 = 0.18 mm. For range 3, 0.25 mm $< D_s <$ 0.5mm, and D_3 = 0.35 mm. The corresponding values of P_i, along with D_{50}, show some variation from day to day. The value of E_{si} on a given day was related to the corresponding values of P_i and D_{50} for that day. Typical values of P_i and D_{50}, based on an average of all size distributions reported for the reach in question, are shown on the Table 3-1.

Field data were plotted against μ in Fig. 3-7. Again, E_{si} was found to be independent of H/D_{50} over the examined range (1250 ~ 3000). Using the same analysis as for the experimental data, the power of D_i/D_{50} is found to be 1.4. The similarity variable for the sediment mixture is given by

$$\Pi_i = \mu_i R_{p50} \left(\frac{D_i}{D_{50}}\right)^{1.4} \qquad 3\text{-}27$$

For the case of uniform sand, Π_i reduces to Π. The empirical sand entrainment function for uniform sand may be applied also to the sediment mixture in the following form

$$E_{si} = 3.0 \times 10^{-12} \Pi^{10} \left(1 - \frac{\Pi_c}{\Pi_i}\right) \qquad 3\text{-}28$$

In Fig. 3-8, the dimensionless entrainment rate of the field data were plotted as a function of Π_i. The empirical formula (Eq. 3-28) was added as a solid line. Fig. 3-8 shows that Eq. 3-25 is a good approximation of the data.

3.3 Observations and Discussion

The entrainment relation obtained herein covers a range of dimensionless entrainment rates varying from 0.0004 to 0.2. It is characterized by its extreme steepness, such that a fifteen percent change in shear velocity can produce an order of magnitude change in the entrainment rate.

As noted previously, at equilibrium the entrainment rate equals the near bed concentration c_{ae}. This value can never exceed the value for packed, static sediment (~ 0.7). It has often been suggested that E_s should not exceed a value of about 0.3 for a true suspension (e.g., Engelund and Fredsoe [1976]). Figures 3-6, and 3-8, however, reveal no tendency for c_{ae} to level off, even at values as high as 0.2. It can only be assumed that some mechanism internal to the suspension acts to limit the increase in E_s as shear velocity is increased further.

Equations 3-8 and 3-9 define the bed boundary condition for suspensions flowing over an erodible bed. For uniform material

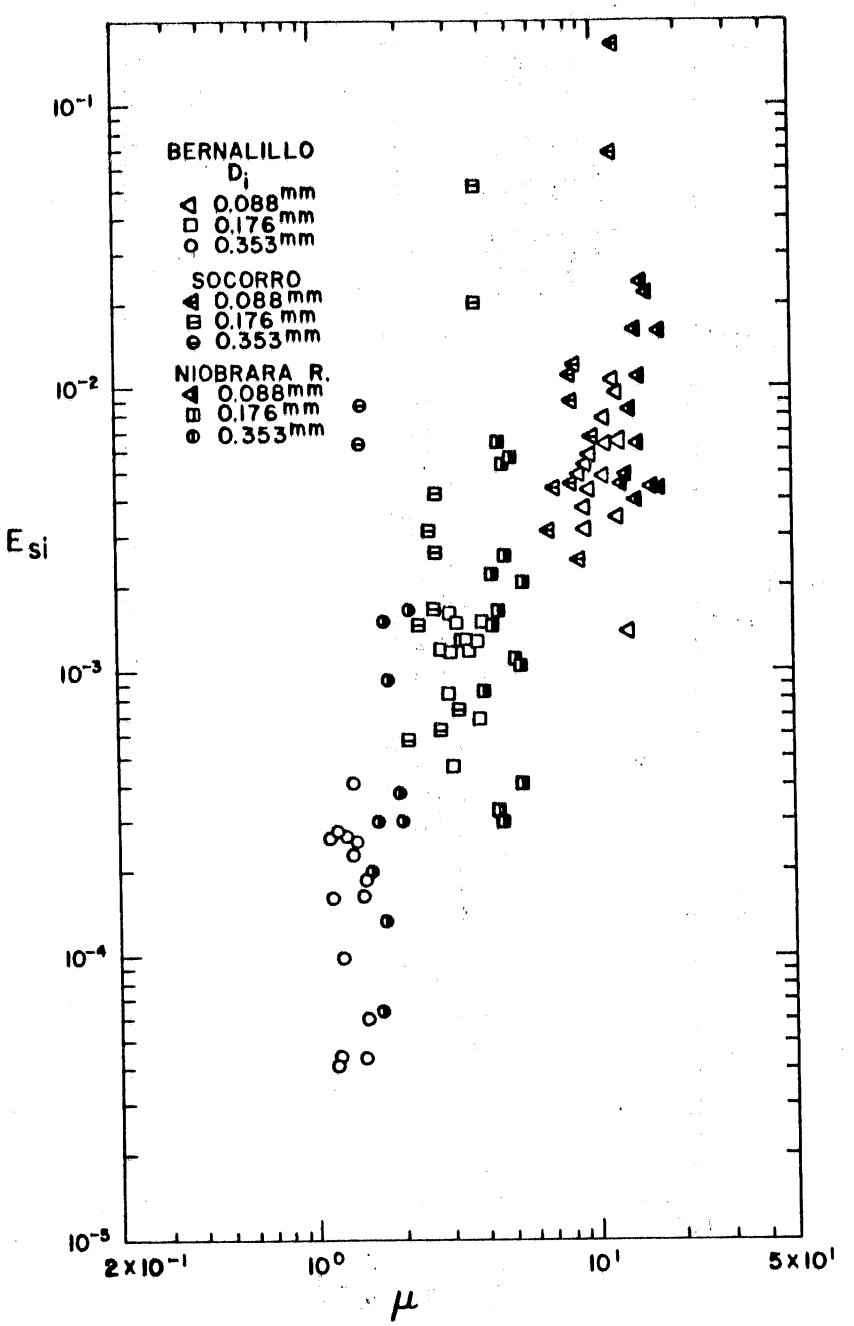

Fig. 3-7 Equilibrium entrainment rate versus the non-dimensional bed stress for the field data obtained by Colby and Hembree [1955] and Nordin and Dembster [1963].

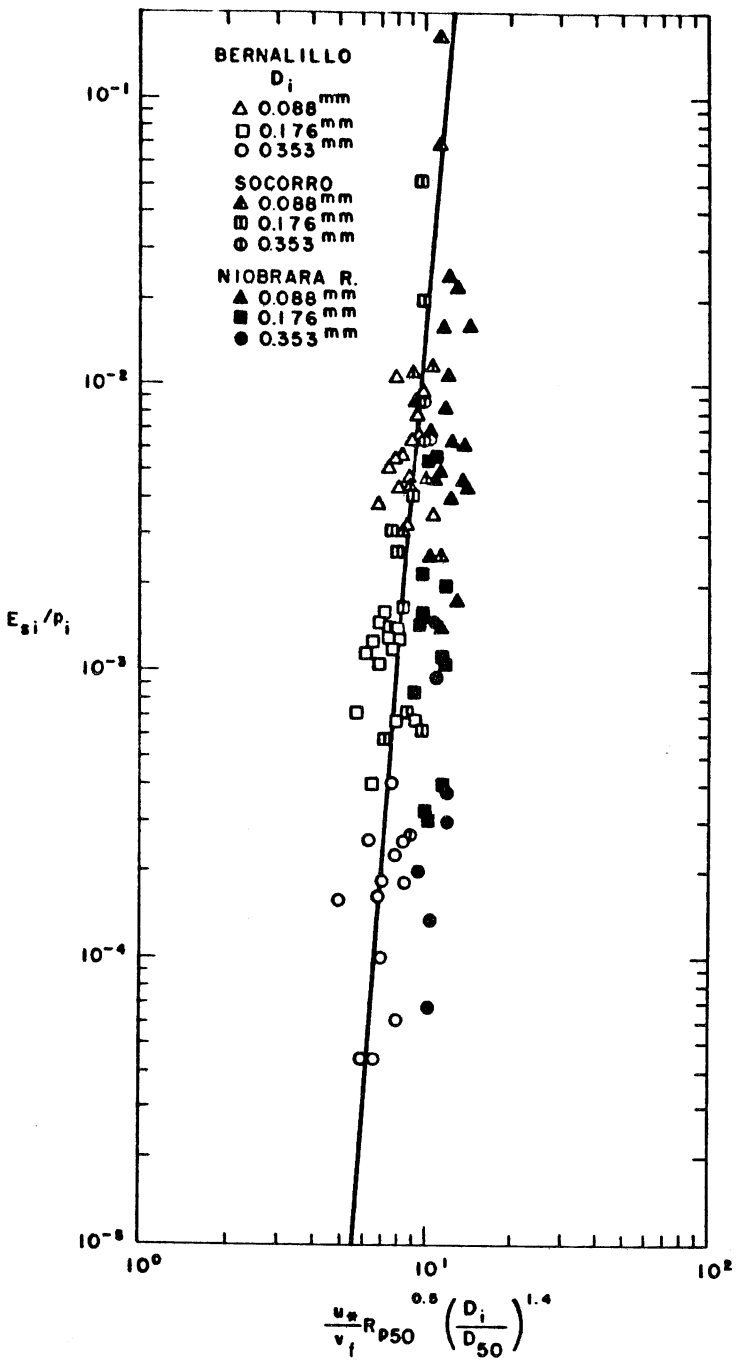

Fig. 3-8 Entrainment relation for suspensions of mixtures in rivers.

$$-\epsilon\frac{\partial c}{\partial y}\bigg|_{y = a} = V_f E_s \qquad 3\text{-}29$$

In the case of mixtures, let c_i denote the local mean volumetric concentration of material in the ith grain size range. Equation 3-29 then generalizes to

$$-\epsilon\frac{\partial c_i}{\partial y}\bigg|_{y = a} = V_f P_i E_{si} \qquad 3\text{-}30$$

Equations 3-22 and 3-28 apply for both equilibrium and disequilibrium suspensions. It is suggested herein that E_s can be evaluated via Eq. 3-22 (and E_{si} via Eq. 3-28) for suspensions in moderate disequilibrium, even though Eqs. 3-22 and 3-28 were determined for equilibrium suspensions. The assertion is similar to the often-used assumption of open channel flow that a relation for friction factor determined for normal flow can also be used for varying flow, as long as the variation is not too great.

The necessity of a boundary condition of the type of Eq. 3-7 was recognized by Dobbins [1944], Parker [1982], and Sheng and Lick [1979], to mention a few. Many others, however, have taken the bed boundary condition for disequilibrium suspensions to be such that $c|_{y = a}$, rather than $\epsilon\partial c/\partial y|_{y = a}$, as a prescribed function of flow conditions. Among proponents of this approach are Engelund [1976] and Hjemfelt and Lenau [1970]. Parker [1978] provided a simple example to explain the superiority of Eq. 3-10 to a specification of c_a as a function of flow

conditions because the concentration boundary condition cannot give the correct solution of steady uniform overloading suspension flow.

In principle, any functional relationship for the equilibrium bed concentration c_{ae} as a function of the flow conditions also determines a form for E_s that can be used in Eq. 3-10. Itakura and Kishi [1980], and Engelund and Fredsoe [1976] have determined such relationships based on semi-theoretical approaches. In Fig. 3-9, their relations are compared with Eq. 3-22 for several grain sizes.

The exponents of Π reported in Eqs. 3-22 and 3-28 are large, but of the same order as reported by other investigators (Engelund and Fredsoe [1976]; Itakura and Kishi [1980]). Ikeda and Asaeda [1983] investigated experimentally the relationship between c_a and mean flow velocity U. They also found that the concentration near the rippled bed increases with the eighth power of U. It seems that the steep slope of the relationship is strongly related to the nature of the suspension phenomenon, regardless of the different values of Π_c.

It is of some value to know whether the suspensions used herein to determine Eqs. 3-22 and 3-28 follow Rouse's [1938] distribution. A simple test was devised as follows. Let C denote the vertically averaged concentration of suspended sediment;

$$C = \frac{1}{h} \int_a^H c \, dz \qquad 3\text{-}31$$

where $a = 0.05H$. Parker [1982] used Rouse's distribution with a value of von Karman's constant of 0.4 to obtain the approximate relation

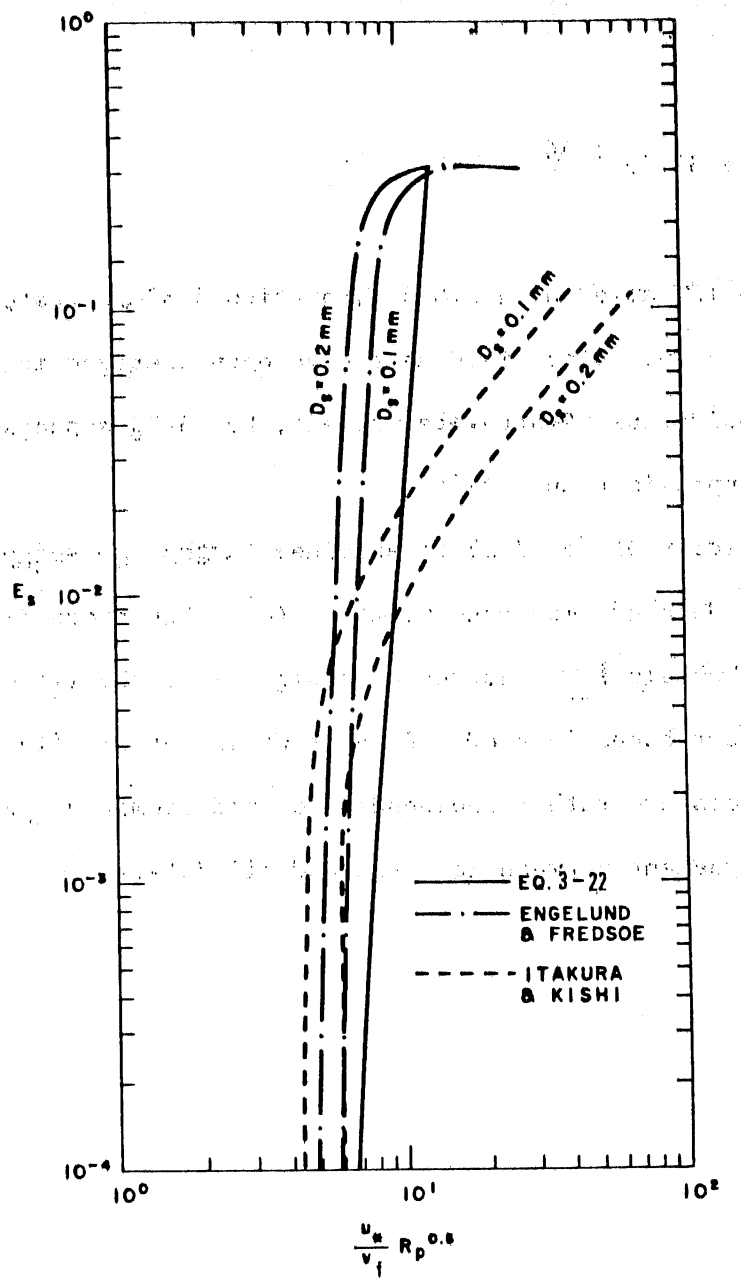

Fig. 3-9 Comparison of Eq. 3-22 with the relations by Itakura and Kishi [1980] and Engelund and Fredsoe [1976].

$$c_{ae} = r_o C \qquad 3\text{-}32$$

where

$$r_o = 1 + 31.5\mu^{-1.46} \qquad 3\text{-}33$$

The relation is valid for $\mu > 0.5$. Equation 3-33 is tested against the data in Fig. 3-10. (The field data have been averaged in groups.) Although considerable scatter is present, Eq. 3-33 appears to provide a reasonable approximation.

The validity of Eq. 3-22 is examined further, based on available experimental data of mean concentration (C). Equations 3-32 and 3-33 were used to obtain c_{ae}. As shown in Fig. 3-11, the fit of Eq. 3-22 appears to be reasonably good. Data of Willis et al. [1972] indicate that c_{ae} values are rather independent of bed geometry. Figure 3-12 shows the agreement between Eq. 3-22 and all data.

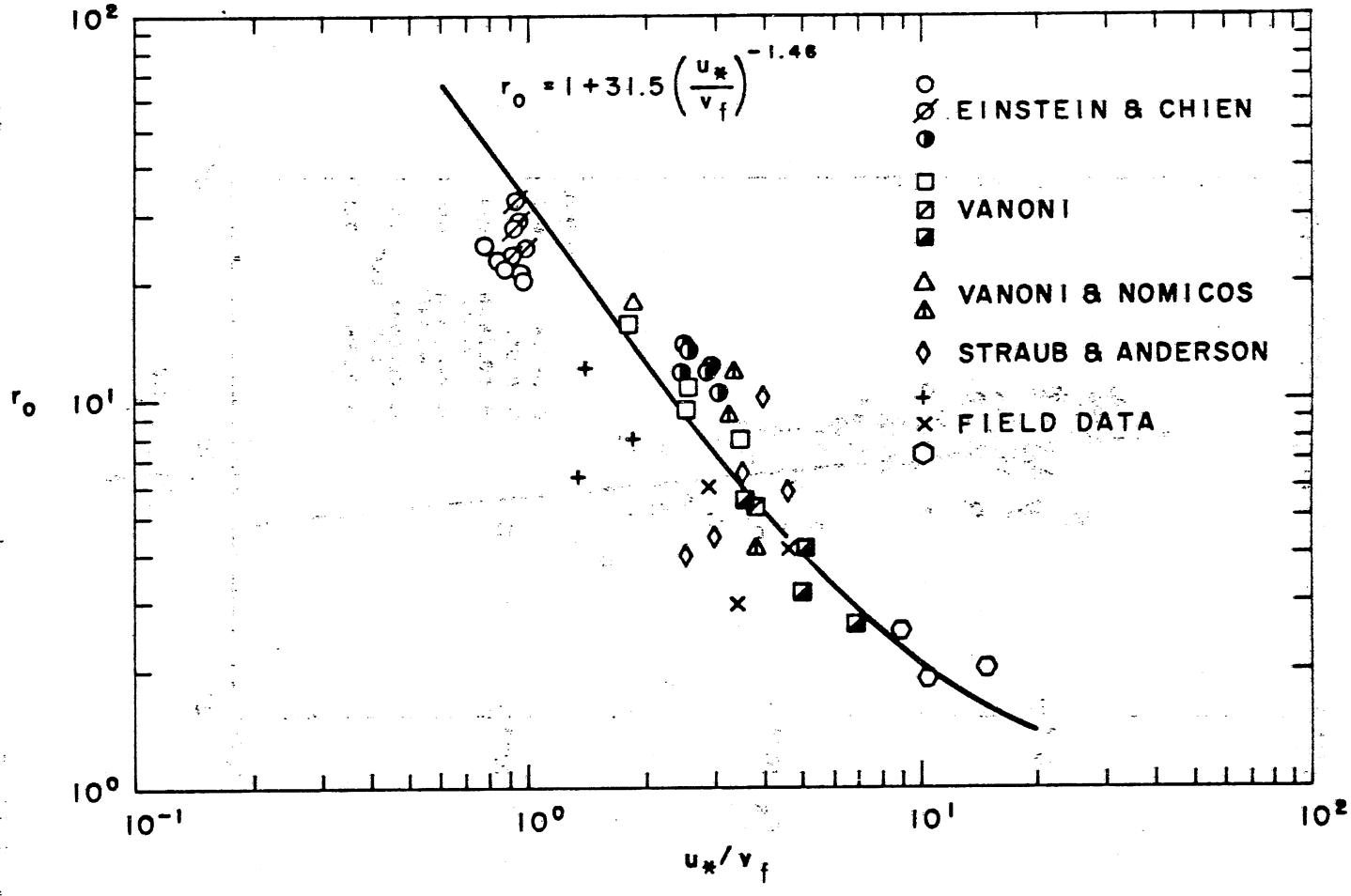

Fig. 3-10 Plot of r_o versus μ . The field data have been group-averaged.

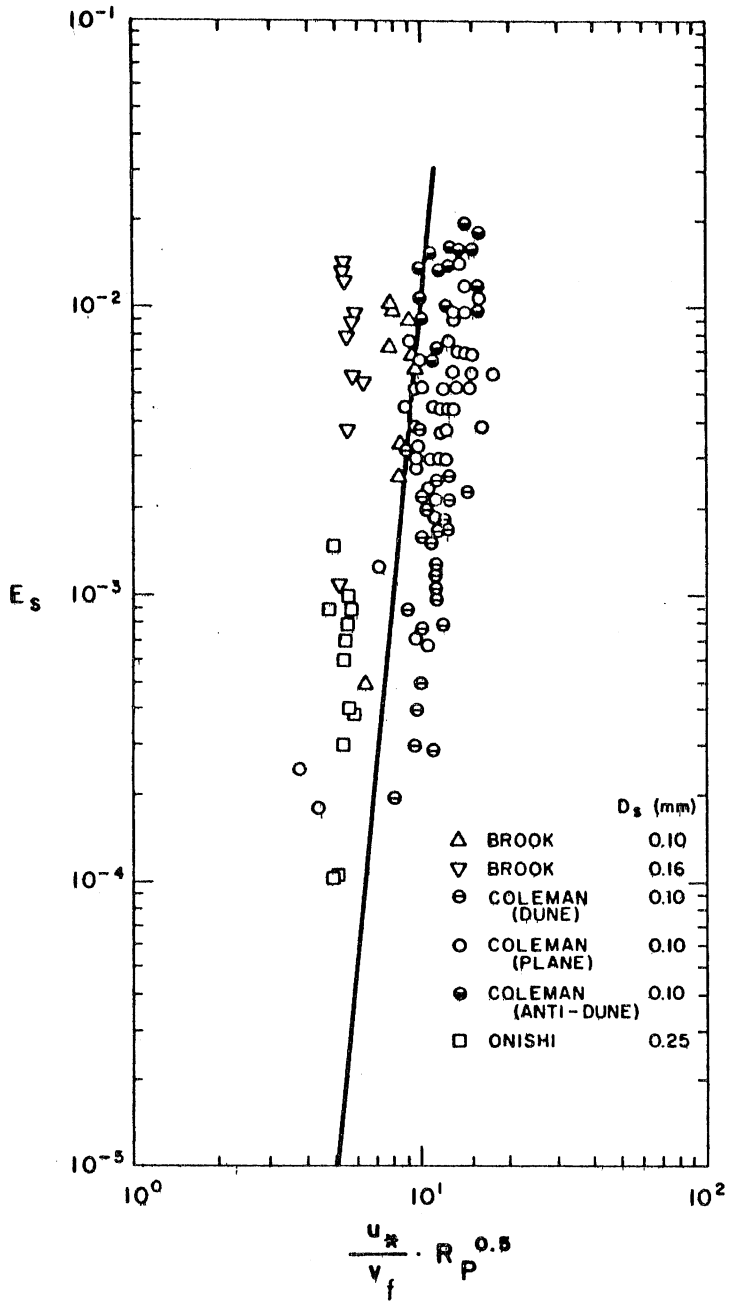

Fig. 3-11 Entrainment relation for suspension of uniform material obtained from mean concentration.

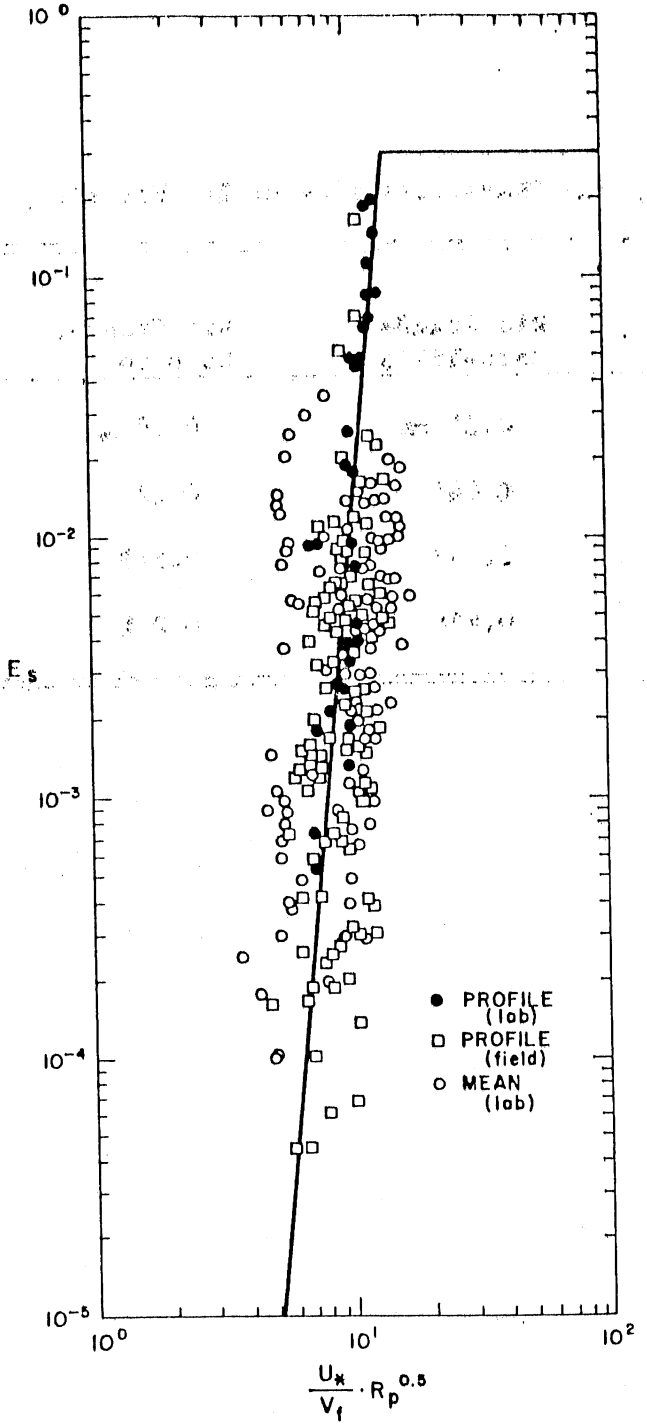

Fig. 3-12 Entrainment relation for all data.

TABLE 3-1 Typical Characteristics of Bed Material, Natural Streams

	Rio Grande, Bernalillo	Rio Grande, Socorro	Niobrara River
D_{50}	0.31 mm	0.19 mm	0.30 mm
p_1	0.046	0.129	0.023
p_2	0.297	0.573	0.367
p_3	0.484	0.218	0.453

4. GRADUALLY VARIED EROSIVE AND DEPOSITIVE TURBIDITY CURRENTS

4.1 Definition and Outline

Turbidity currents are gravity currents consisting of a sediment-water mixture flowing down a sloping bottom. Similar gravity induced currents can be produced by salinity or temperature differences and have been referred to as "inclined plumes," "underflows," or "dense bottom currents."

In this thesis, a density current, which is generated by salinity or temperature differences is called "non-suspension gravity current," or "underflow" and a density current caused by suspended particles is called "suspension gravity current," or "turbidity current."

a) Non-suspension type gravity currents (underflows).

If there is no sink or source of heat, salinity, or dissovled matter along the bottom slope, the buoyancy flux is preserved and remains constant over the downslope. This type of density current includes inclined plumes and underflows.

b) Suspension type gravity currents (turbidity currents).

In suspension type gravity currents buoyancy flux is not always preserved downslope. Suspended particles make the density of the mixture greater than the density of the surrounding water and provide the driving force; the particles bearing flow must generate enough turbulence to hold them in suspension. Suspension type currents are, therefore, turbulent flows. The presence of the suspended particles has a major effect on the dynamics of the current.

Some similarities between suspended sediment transport in open channels and subaquaeous suspended sediment transport exist. Major

differences between the two flows must however, also be noted. In open channel flow, the transport rate of suspended sediment can be calculated separately from hydraulic conditions. This is possible because turbulent energy is transported from the water to the sediment phase, and the presence of suspended sediment has minor effect on the flow. In turbidity currents, on the contrary, the direction of energy transfer is reversed, and hence, hydraulic conditions and the transport rate of suspended sediment are coupled. This is why turbidity currents are sometimes called "self-generated flows." A flow of a gravity current may be regarded as analogous to the free-surface open channel flow of a homogeneous fluid in reduced gravitational field, due to buoyancy effects. Turbidity currents are essentially non-uniform flows due to the entrainment of ambient water. This is another major difference between two flows. Non-uniformity allows the flow to entrain or deposit suspended matter. Settling of material to the bed reduces the effective density of the suspension and hence reduces the driving force of the current. On the other hand, entrainment of material from the bed into the current increases the effective density of the suspension and the driving force of the current.

This type of density current exists not only as subaqueous flow but also as atmospheric turbidity current and powder flow. A suspension type gravity can be:

a) An eroding current, which entrains material from the bed into the flow, or

b) A depositing current, which deposits suspended material onto the bed, or

c. An equilibrium current, which neither entrains nor deposits material.

When the settling velocity of the suspended particle is negligible, the suspension type gravity current becomes a non-suspension type. Turbidity currents made of clay particles correspond to this case in first approximation (Stefan [1973]). Non-suspension gravity currents can be considered as a special case of suspension type gravity current.

In nature, suspension type gravity currents are more frequently observed than non-suspension type gravity currents. The latter have been, however, investigated theoretically and simulated in laboratory flumes by many researchers. Understanding the behavoir of non-suspension gravity currents is the first step in investigating the more complex flow of a suspension type current.

4.2 Significance of Turbidity Currents in Nature

Turbidity currents have been observed in nature: in the atmosphere, in lakes, reservoirs, coastal regions, estuaries, and the ocean.

In the air, dust storms, volcanic ash from eruptions and powder snow avalanches are examples. Atmospheric turbidity currents are usually large in scale and often cause natural disasters. They are of significance in the field of meterology.

In lakes and reservoirs, the inflow of turbid water influences the biological activity and sand and clay silts up reservoirs and reduces their storage capacity.

In the ocean, turbidity currents have been suggested as significant agents in the distribution of sediments on the ocean floor, and in

shaping of submarine topography. Much of the silt and clay size sediments in the sea are introduced by rivers and transported primarily as suspended load.

In coastal regions, storm waves erode beaches and sands are transported away into the deep parts of the ocean.

Understanding modes and pathways of particle transport in the deep sea is of considerable importance to a wide variety of marine problems.

4.3 Possible Causes of Turbidity Currents in Nature

When turbidity currents occur in nature, a large amount of suspended sediment is required in order to initiate the movement.

Sediment or dissolved matter required for turbidity currents is introduced by the following mechanisms:

a) Direct inflow of sediment laden river water, or of dissolved matter from waste water outlets. (e.g., Linth River into Walensee in Switzerland, Congo Submarine Canyon).

b) Artificial discharge of industrial waste (mine tailings, ash). (e.g., Silver Bay in Lake Superior).

c) Underwater land slides caused by earthquakes. (e.g., the Grand Banks event in 1929, Wester New Britten Trench in 1966 and 1968, Orleansville in 1954).

d) Resuspension of sediment by waves, and currents during storm events or by ship passages. (e.g., Scripps Submarine Canyon).

4.4 Type of Turbidity Currents

Turbidity currents have been classified into two types, depending on magnitude of the velocity and concentration.

a) Low-velocity, low-concentration turbidity currents

The currents under reduced gravity force are, in general, slow as observed e.g., in Lake Mead (Howard, 1953), and in other reservoirs. In Lake Mead, turbidity currents have nevertheless been observed to flow distances of over 100 miles.

The suspended material is wash load originating from erosion of the catchment area rather than material derived from erosion of the stream bed.

This type of current has been observed where the bed slope is relatively mild and suspended sediments are very fine materials such as clay or silt. Low-velocity turbidity currents are capable of transporting large amounts of fine sand and clay into deeper parts of lakes, reservoirs, or the oceans, where transported materials are then deposited.

b) High-velocity, high-concentration turbidity currents

High-velocity, high-concentration turbidity currents are usually large in dimension and often carry suspended sediment material introduced near the shore to the deep sea, and even have erosive power enough to carve out submarine canyons.

Regardless of the type of basin (lake, reservoir, or the ocean), it has been observed in the field the the bottom slope changes from a steeper to a milder slope as schematically shown in Fig. 1-1. High-velocity, high-concentration turbidity currents are, therefore,

expected to become low-velocity, low-concentration ones as the result of depositing suspended material onto the bed as the currents travel downstream.

4.5 Review of Previous Related Studies

4.5.1 Theoretical and Semi-Theoretical Investigations.

(i) Non-Suspension Gravity Current (underflows)

Ippen and Harleman [1952] investigated steady, uniform, laminar underflows ($Re = UH/\upsilon < 1000$) under infinite ambient water depth without entrainment of ambient water, and discussed important characteristics of underflows such as velocity profile, the location of maximum velocity, and interfacial and bottom friction coefficients.

Schijff and Schonfeld [1953] considered the movement of not only the lower layer, but also of the upper ambient layer.

This type of analysis is referred to as "two-layer model," and has been used by many researchers. The two-layer approach is usually applied to cases that satisfy the following conditions; the movement of the upper layer is not negligible; there is a distinct interface between the two layers and hence the mixing through the interface is weak.

Ellison and Turner [1959] dealt with a more realistic situation of gravity currents and developed equations for gradually varied underfow in a manner similar to open channel hydraulics in their layer integrated model using continuity, diffusion, and equation of motion together with the concept of an entrainment for water (E_w) introduced by Morton, Taylor, and Turner [1956]. They found that the overall Richardson number (R) becomes almost invariant with x in a short distance from

the initial discharge point, and termed such a Richardson number "normal Richardson number, (R_n)." Once R attains R_n, the behavior of gravity currents is described by simple relationships. They also discovered experimentally that E_w is an exponential decay function of R; and that entrainment of water is almost negligible when R is larger than about 0.8.

Lofquist [1960] made measurments of the shear stress between a single layer flowing along a horizontal plane and a stationary layer above, and showed that this interfacial friction is much smaller than the bottom stress. He also showed a possible method to calculate shear from the equation of motion under some assumptions. However, his results appear to be only valid for slowly moving density currents.

Stefan [1973] obtained interfacial profiles of turbdity currents and approximated the effect of depth of submergence by analysis of laminar two-layer flow.

Tsubaki and Komatsu [1979] further elaborated on Ellison and Turner's model, considering mean and turbulent energy equations in addition to continuity, diffusion, and momentum equations. Unlike other researchers, they did not assume the form of entrainment function. They treated it as one of the unknowns and did obtain a relationship similar to Ellison and Turner's [1959]. The above studies dealt with one- or two-dimensional gravity currents. Some efforts have been made to solve the three-dimensional problem.

Fietz and Wood [1969] studied mainly fundamental mechanisms of three-dimensional underflows highlighting relations with important parameters and providing useful information for modeling.

Alavian [1985] extended the two-dimensional model by Ellison and Turner [1959] to three-dimensional gravity currents, considering vertical as well as lateral entrainment of water. His model, however, appears to be limited to three-dimensional gravity currents with relatively weak lateral spreading, which occur on steep slopes.

(ii) Suspension Gravity Current (Turbidity Currents)

Bagnold [1962] introduced the concept of "auto-suspension," which is a criterion to determine approximately whether a turbidity current can be maintained or not, considering a simple energy balance: the power needed by the turbidity current to maintain full suspension must be greater than or equal to the power available from gravity, minus the power lost by the settling of the particles, minus the power lost through bottom friction.

Hinze [1960] considered only the upper portion of the current (above the velocity maximum) assuming that the point of zero shear stress coincides with the point of the velocity maximum, and that the portion below the velocity maximum is close to the bed and hence negligible. Velocity profiles of turbidity currents are obtained under the assumption of constant eddy diffusivity.

Ashida and Egashira [1975] analyzed velocity and concentration profiles of the turbidity current made of a fine suspended material by dividing velocity profiles into three sub-regions in order to understand the basic transport mechanism of fine suspended sediment due to slow gravity currents in lakes and reservoirs as typically observed in Lake Mead.

Chu, Pilkey, and Pilkey [1979] derived equations for a non-conservative turbidity current, and demonstrated analytically that there are four stages to be distinguished during the history of a turbidity current according to the variation of the densimetric Froude number: flow establishment, uniform flow, hydraulic jump, and flow decay.

Pantin [1979] and Parker [1983] took erosion and deposition into account, and provided the foundation for analysis of non-conserving turbidity currents.

Fukushima et al. [1985] considered that turbulence is essential in a turbidity current and developed a spatially varied model of turbidity currents considering equations of volume, mass, momentum, and energy in a manner similar to the model of non-suspension density currents by Tsubaki and Komatsu [1979].

Akiyama and Stefan [1985, 1986] extended Ellison and Turner's models and developed the generalized model which includes non-suspension gravity currents as a special type of suspension gravity currents, considering continuity, diffusion with sink and source, and momentum equations together with the sediment exchange between the flow and the bed at the lower boundary as well as water entrainment at the upper boundary. They found that suspension type currents consist of accelerating-erosive, decelerating-erosive, and decelerating-depositive currents dependent on channel bed slope (θ), viscosity of water (υ), particle size (D_s), specific weight of particles (ρ_s), channel bed friction coefficient (C_{bo}), and initial conditions (H_o, B_o, R_o). They applied the model to man-made turbidity currents in Sivler Bay, Lake

Superior in order to explain the distribution of suspended sediment on the lake floor and the formation of a delta.

4.5.2 Field and Laboratory Experimental Studies

Typical field and laboratory experimental studies are briefly reviewed in order to understand the nature of turbidity currents.

(i) Field Studies

Typical field observations and investigations of low velocity turbidity currents were conducted by Howard [1953]. Sediment-laden Colorado River water flows into Lake Mead and forms turbidity currents, which carry fine material consisting mainly of particles with diameters less than 0.02 mm. According to the 1948-49 Lake Mead survey, the volume of sediment deposited in the first 14 years of storage amounted to over 1,420,000 area feet. About 67% of deposited sediment is considered to transported by turbidity currents.

Normark and Dickson [1976] investigated man-made turbidity currents and resulting turbidities produced by the discharge of taconite tailings from a mining operation into Lake Superior at Silver Bay, Minnesota. The resulting fan covers about 20 sq km along the northwestern shore of Lake Superior and extends to a water depth of 285m. Normark and Dickson also reported that the slope has no prominent channels, but divers observed a 3 to 5 m deep turbidity current, which is considered to have played a dominant role in the formation of the delta fan.

Lambert et al. [1976] measured velocity and direction of turbidity currents induced by sediment-laden river inflow in Lake of Walenstadt. The highest current velocity of 30 cm/s was obtained where the channel

bed slope is about 2^{o}. They also found a strong correlation between river discharge and speed of turbidity currents. Topographical cross-sections of the site and recorded flow velocities are shown in Fig. 1-2.

Inman et al. [1976] reported that a sustained current of 1.9 m/s along Scripps Submarine Canyon was measured for two and one half hours at a depth of 44 m on 24 November 1968 before all instruments were lost. The turbidity currents are affected by the persistent rip currents at the canyon head. They argued that a unique combination of air-sea-land interaction may cause strong down-canyon currents.

More detailed descriptions of turbidity currents in Lake Superior and Scripps Submarine Canyon are presented in Chapter 6.

(ii) Laboratory Experiments

Among the earliest of laboratory experiments is the work of Bonnefille and Goddet [1959]. They examined velocity and concentration profiles of underflow and turbidity currents experimentally, based on data obtained from laboratory experiments and field experiments in a canal.

Georgiev [1972] obtained the vertical distribution of mean velocity, turbulent fluctuation, and shear stress in a saline solution underflow, and reported that both maximum velocity gradient and interfacial friction coefficient vary with Reynolds number, (Re). He also demonstrated the relationship between total (interfacial and bottom) friction coefficient and Reynolds number from 3 to 1000. In the laminar range ($Re < 1000$) the result matched that of Ippen and Harleman

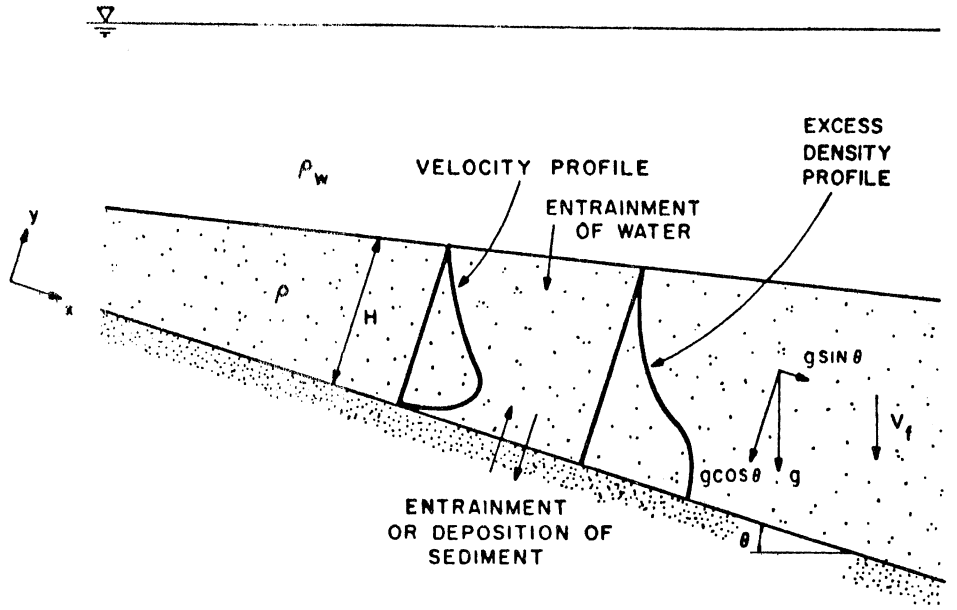

Fig. 4-1 Gradually varied turbidity current (schematic).

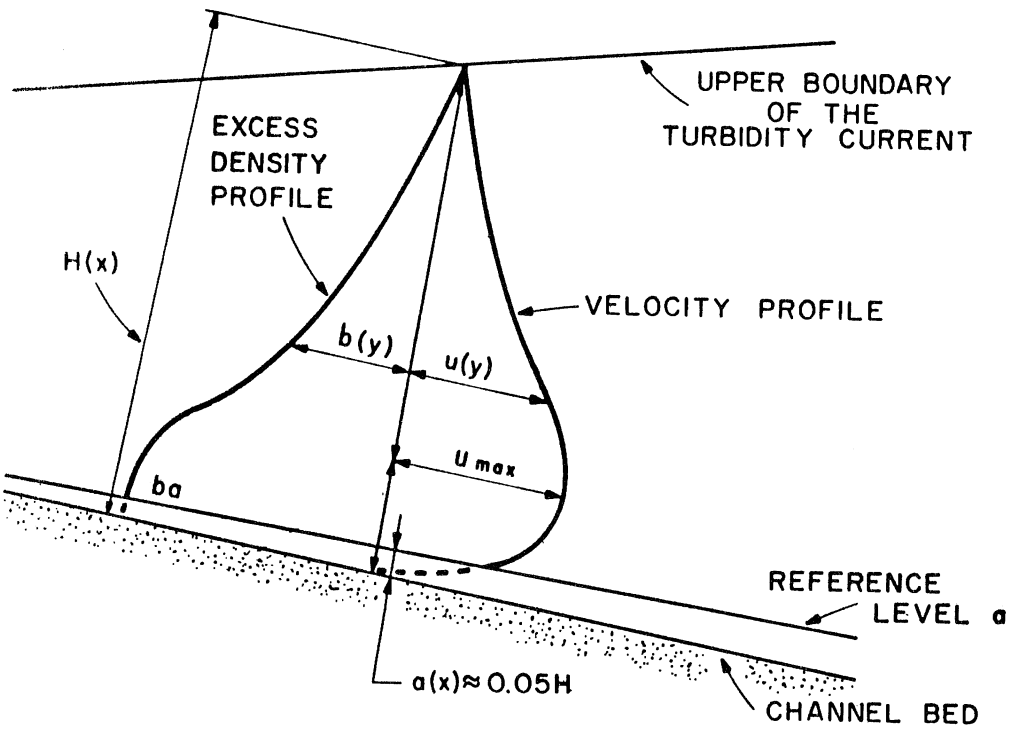

Fig. 4-2 Velocity and buoyancy (density) profile in a turbidity current.

[1952]. When Re > 2000, total friction coefficient was almost independent of Re and had a nearly constant value of 0.005.

Middleton [1966] performed experiments of saline underflow using the tilting flume. Channel slope was varied from 0.0025 to 0.04. Density differences, flow thickness, and flow velocity ranged from 0.0265 to 0.061, 0.9 to 4.7 cm, and from 6.7 to 26.3 cm/s respectively. Based on these experimental data, the magnitude of the friction coefficient and its dependence on densimetric Froude number are discussed.

Tesaker [1969] conducted experiments of continuous turbidity currents using clay slurries ($D_s < 75\mu$) with varing amounts of fine sand ($D_s < 600\mu$) in a channel with slope ($S = 0.05 \sim 0.125$), and obtained velocity and concentration profiles of depositing turbidity currents.

Recently, Garcia [1985] has carried out large scale experiments of continuous turbidity currents using two different particle sizes ($D_s \sim 30$ and $\sim 60\mu$) in a channel with a slope of 0.05 ~ 0.08 in order to verify the existence of eroding currents. Because of the limited length of the channel test section, he was unable to produce such currents. His results suggest that much larger scale experiments may be necessary to create eroding turbidity currents. However, some useful information for both velocity and concentration profiles of relatively fast turbidity currents was obtained. Based on the above information, water and sediment entrainment functions, and bottom friction coefficient for this type of flow have been obtained.

4.6 Analysis

4.6.1 Background and Important Parmeters of the Model

The flow dynamics of a steady-state, two-dimensional, gradually varied turbidity current produced by a uniform material including the exchange of non-cohesive sediment between the current and the bed are analyzed. The main features of the turbidity current are defined in Fig. 4-1.

To develope the turbidity current model, four basic relationships will be used:

a) Conservation of volume.

b) Diffusion equation with sink and source term to describe the mechanism of sediment exchange between the flow and the bed.

c) Equation of motion.

d) Turbulent energy equation, which is used to explain Bagnold's autosuspension concept.

Among these equations, the diffusion equation is of particular significance becuase it incorporates the erosive and depositive character of the currents. The equations are first given in two-dimensional form, then vertically integrated. The layer averaged equations are transformed into gradually varied flow equations.

They represent the extended form of those given by Ellison and Turner [1959], which describe the behavior of non-suspension gravity currents.

In the layer integrated model, there are three unknowns; total layer thickness (H), layer averaged mean velocity (U), and concentration (C) for the equations above, or alternatively; total layer thickness

(H), buoyancy force (B), and overall Richardson number (R), which are defined below.

In the analysis, the latter combination of unknowns is selected. Two empirical functions are required for entrainment of ambient water (E_w) and of sediment (E_s), which are boundary conditions at the upper and lower boundaries of the current, in order to close the system. Unknowns can then be obtained for given intial conditions denoted by o , namely, H_o, B_o, and R_o. Important parameters are properties of water (density (ρ_w) and viscosity (υ)), of sediment (density (ρ_s) and settling velocity (V_f)), of the channel (bed slope (θ) and bed friction coefficient (C_b), and acceleration of gravity (g).

Gravity currents flowing down an incline, are in general scaled by densimetric Froude number (F) or Richardson number (R). F or R are defined as:

$$F^2 = \frac{U^2}{BH\cos\theta} = \frac{1}{R}$$

where B = layer averaged buoyancy force per unit mass:

$$(= \frac{\rho_s - \rho_w}{\rho_w} gC).$$

Density currents in a manner similar to open channel flows have supercritical and subcritical regimes (Stefan [1973]). The flows are controlled from down to upstream in subcritical flows, and from upstream to downstream supercritical flows. In internal hydraulic jump is the

mechanism by which a density current changes from the former to the latter regime. The condition of transition is determined by the magnitude of F or R. The typical behavior of a turbidity current that changes from supercritical to subcritical flow is schematically illustrated in Fig. 1-1.

As will be seen later, the critical value of F or R (F_c or R_c) is not necessarily equal to unity in density currents, because of non-uniformity of both velocity and density profiles as schematically shown in Fig. 4-2.

Flow regimes are distinguished dependent on the magnitude of R:

$R > R_c$: internally subcritical.

$R = R_c$: internally critical.

$R < R_c$: internally supercritical.

The calculation of turbidity currents with erosion and deposition is possible when the flows remain supercritical, but impossible when the flows become subcritical unless proper upstream and downstream conditions are imposed, and the distance between two sections is known. Because subcritical turbidity currents are expected to become decelerating-depositive, it is implied that the turbidity currents vanish at some distance downstream after they become subcritical.

4.6.2 Model Assumptions

The model is based on the folloowing assumptions and approximations:

1. Boundary and Boussinesq approximations are made for the two-dimensional steady-state governing equations.

2. Sediment concentration is assumed to be small enough to treat the mixture as a newtonian fluid.

3. Bed load transport and related phenomena such as additional shear stress due to bedforms are not considered.

4. The bed friction coefficient is estimated from experimental results of homogeneous wall jets and non-susupension type gravity currents, and treated as constant over the entire flow domain (turbulent flow).

5. Bagnold's auto-suspension term [Bagnold, 1962] is accounted for by an additional shear stress in the momentum equation based on a simple turbulent energy consideration.

6. All shape factors are treated invariant over the entire flow domain, because of the lack of information for both velocity and density distributions.

7. The material suspended in the turbidity current is non-cohesive.

8. A water entrainment function (E_w) is obtained from density currents driven by salinity or temperature differences.

9. The sediment entrainment function (E_s) is used in the model is derived from data of suspended sediment transport in open channel flow.

10. The assumptions 8 and 9 are based on consideration of a free shear layer type velocity profile above the velocity maximum and a boundary layer type profile below it. It is reasonable to assume that each entrainment mechanism depends primarily on the shear near the boundary where it takes place, and that the interaction between the shear layers (bottom and interface) is not strong.

11. Fall velocity (V_f) of sediment particles is assumed constant.
12. Viscosity of water (υ) does not change in magnitude due to the change of suspended sediment concentration, and is a function of water temperature only.

Turbidity currents have been analyzed as flows in three phases: clear ambient water, turbid water (mixture), and the sediment (bed material). Water and mixture are related through water entrainment and, mixture and bed material through sediment erosion and deposition. Actually a turbidity current entrains and deposits at the same time, but there is a net flux either to the bed (depositing current) or from the bed (eroding current).

The velocity profile of a turbulent turbidity current consists of two subregions. The point of maximum velocity and minimum shear provides the division (Fig. 4-2).

Water entrainment is closely associated with turbulence generated in the upper portion of the current (the outer layer region), while sediment entrainment is related to turbulence generated near the channel bottom (the inner layer region).

Density profiles can be linear or exponential in the outer layer and similar to suspended sediment distribution in open channel flow in the inner region.

4.6.3 Governing Two-Dimensional Equations

Figure 4-2 shows that velocity and buoyancy force distributions in a turbidity current are at least two-dimensional.

For a steady-state flow the governing equations including boundary and Boussinesq approximations are:

(a) Continuity equation

$$\frac{\partial u}{\partial x} + \frac{\partial v}{\partial y} = 0 \qquad 4\text{-}1$$

(b) Diffusion equation

$$\frac{\partial (bu)}{\partial x} + \frac{\partial (bv)}{\partial y} - V_f \frac{\partial b}{\partial y} \cos\theta = - \frac{\partial}{\partial y} \overline{v'b'} \qquad 4\text{-}2$$

(c) Momentum equation in x-direction

$$\frac{\partial (u^2)}{\partial x} + \frac{\partial (uv)}{\partial y} = - \frac{\partial}{\partial x} \int_y^\infty b\cos\theta \, dy + b\sin\theta + \frac{1}{\rho_w} \frac{\partial \tau}{\partial y} \qquad 4\text{-}3$$

In the above equations x, y = coordinates, u, v = velocity components, τ = shear stress, ρ_w = density of ambient (clear) water, and V_f = particle settling velocity. Fluctuating components are designated by primes. Important parameters and the definition of the coordinate system are shown in Fig. 4-1 and 4-2. Buoyancy force is defined as

$$b = \frac{\rho - \rho_w}{\rho_w} gc \qquad 4\text{-}4$$

where g = acceleration of gravity.

The density of the suspension ρ is related to concentration of suspended sediment c, density of solids ρ_s and density of water ρ_w. Using a normalized ($0 \leq c \leq 1$) concentration:

$$\rho = \rho_s c + \rho_w (1 - c) \tag{4-5}$$

or

$$\frac{\rho}{\rho_w} = 1 + \sigma c \tag{4-6}$$

where σ is the specific gravity of submerged sediment particles

$$\sigma = \frac{\rho_s - \rho_w}{\rho_w}. \tag{4-7}$$

Thus, b becomes

$$b = \sigma g\, c \tag{4-8}$$

and the corresponding fluctuating component is:

$$b' = \sigma g c' \tag{4-9}$$

Over the sloping bottom sediment particles are lifted upward perpendicular to the channel bed, i.e., in the y-direction, but fall downward in the direction of the gravity vector independent of the slope

of the channel bed. The sine component of the turbulent diffusion term $\overline{u'b'}$ is ignored in equations 4-2 and 4-3. The following analysis, is valid only up to moderately steep slopes.

The governing equations are examined individually and integrated vertically in order to derive their one-dimensional form.

4.6.4 Vertical Integration of the Governing Equations

Continuity and diffusion equations are integrated vertically from 0 to H(x). The upper boundary of the turbidity current (y = H) is chosen such that $u_H \simeq 0$ and $b_H \simeq 0$, based on experimental evidence (Ashida and Egashira [1975]; Bonnefille and Goddet [1959]). Consequently H is by definition the turbidity current layer thickness in this analysis (Fig. 4-2). Equations 4-1 and 4-2 yield.

(a) Continuity

$$\frac{d}{dx}\int_0^H udy + v_H = \frac{d}{dx}\int_0^a udy - u_a\frac{da}{dx} + v_a \qquad 4\text{-}10$$

(b) Diffusion

$$\frac{d}{dx}\int_0^H ubdy - (\overline{v'b'} - V_f\, b\cos\theta)_a = b_a\left(\frac{d}{dx}\int_0^a udy + v_a\frac{da}{dx}\right)$$

$$+\int_0^a udy\,\frac{db_a}{dx} \qquad 4\text{-}11$$

Equation 4-11 includes the assumption that $b(x,y) = b_a(x)$ from y = 0 to a(x), i.e., the buoyancy force in the immediate vicinity of the bed is considered as constant in the y-direction. If the right-hand side of Eq. 4-10, and the second term in the right-hand side of Eq. 4-11 are negligible, the continuity and diffusion equations give:

$$\frac{d}{dx}\int_0^H udy = - v_H = v_e \qquad 4\text{-}12$$

where v_e is an entrainment velocity with negative direction along the y-axis, and:

$$\frac{d}{dx}\int_0^H ubdy = (\overline{v'b'} - V_f\, b\cos\theta)_a \qquad 4\text{-}13$$

If the above assumptions are valid "a" must be small. In open channel flow "a" has sometimes been chosen as 5% of the total flow depth. If the same fraction is used for the turbidity current, a = 0.05H.

To determine the suspended sediment diffusion $\overline{v'b'}$ let us consider an equilibrium condition.

$$\overline{v'b'} = b\, V_f \cos\theta \qquad 4\text{-}14$$

V_f is constant along the y-direction. We define E_s^* as the sediment entrainment function for buoyancy force at location y = a(x) near the bed.

$$\overline{v'b'}\Big|_a = E_s^* V_f \qquad 4\text{-}15$$

Then equation 4-13 becomes:

$$\frac{d}{dx}\int_a^H budy = V_f(E_s^* - b_a \cos\theta) \qquad 4\text{-}16$$

Three conditions can be distinguished dependent on the sign of the right hand side term of Eq. 4-16.

(a) $E_s^* - b_a \cos\theta = 0$

An equilibrium current, which neither deposits sediment onto the bed nor removes material from the bed.

(b) $E_s^* - b_a \cos\theta > 0$

An eroding current, which removes material from the bed.

(c) $E_s^* - b_a \cos\theta < 0$

A depositing current, which deposits sediment onto the bed.

(c) Momentum

Similarly the momentum equation yields:

$$\frac{d}{dx}\int_0^H u^2\, dy = -\frac{d}{dx}\int_0^H yb\cos\theta\, dy + \int_0^H b\sin\theta - \frac{\tau_b}{\rho_a} \qquad 4\text{-}17$$

In the momentum equation no interfacial shear stress appears because $u \simeq 0$ at $y = H$.

Ashida and Egashira [1975], as well as Bonnefille and Goddet [1959], studied density currents consisting of very fine material with negligible settling velocity, i.e., a turbidity current without deposition and erosion. In a more general situation deposition and erosion would be significant only in the near-bed portion of the current, especially the flow below the velocity maximum. It is the turbulence created in the lower shear layer which controls erosion and deposition provided that the flow meets Bagnold's "autosuspension criterion" across the layer. Herein "suspension" is distinguished from "erosion" and "deposition."

4.6.5 Summary of 1-D (Vertically Integrated) Governing Equations

The layer integrated equations of the turbidity current are given below:

(a) Conservation of volume

$$\frac{d}{dx}(f_1 UH) = E_w U \qquad 4\text{-}18$$

(b) Conservation of buoyany flux

$$\frac{d}{dx}d(f_2 BUH) = V_f(E_s^* - b_a \cos\theta) \qquad 4\text{-}19$$

(c) x-Momentum equation

$$\frac{d}{dx}(f_3 U^2 H + \frac{1}{2}S_1 BH^2 \cos\theta) = S_2 BH \sin\theta - \frac{\tau_b}{\rho_w} \qquad 4\text{-}20$$

Layer averaged properties as used above are denoted by capital letters (Fig. 4-3). E_w in Eq. 4-18 is defined in Eq. 4-59. Shape factors f_1 through f_3 and S_1 and S_2 are introduced to account for velocity and density distributions. Shape factors are defined as follows:

$$f_1 = (UH)^{-1} \int_0^H u \, dy \qquad 4\text{-}21$$

$$f_2 = (UBH)^{-1} \int_0^H ub \, dy \qquad 4\text{-}22$$

$$f_3 = (U^2H)^{-1} \int_0^H u^2 \, dy \qquad 4\text{-}23$$

$$S_1 = (BH^2)^{-1} \int_0^H 2by \, dy \qquad 4\text{-}24$$

$$S_2 = (BH)^{-1} \int_0^H b \, dy \qquad 4\text{-}25$$

In turbidity currents, shape factors defined above are not constant but are expected to be at least a function of Richardson number (R), friction coefficient (C_b).

Defining the volume flux (Q_f), buoyancy flux (B_f), and flow force (F_f) respectively as:

$$Q_f = f_1 UH \qquad 4\text{-}26$$

$$B_f = f_2 BUH \qquad 4\text{-}27$$

$$F_f = f_3 U^2 H + \frac{1}{2} S_1 B H^2 \cos\theta \qquad 4\text{-}28$$

in Eqs. 4-18, 4-19, and 4-20.

Three typical density currents, namely a surface buoyant jet, a non-suspension gravity current, and a suspension gravity current are shown schematically and their relationship to Q_f, B_f, and F_f in Fig. 4-4.

In a surface buoyant jet, Q_f increases in the flow direction due to the water entrainment and thus an initial volume flux $(Q_{fo}) \neq Q_f$. While, both B_f and F_f are maintained at the initial value: B_{fo} and F_{fo}.

In a non-suspension gravity current, B_f can be maintained as B_{fo}, but neither Q_f nor F_f is not conserved due to the water entrainment and the wall boundary shear stress at the bed.

In a suspension gravity current, none of the properties can be preserved due to the water entrainment, wall boundary shear, and sediment exchange at the bed. Consequently, the behavior of flows are complex.

4.6.6 Considerations on Velocity Profiles in Turbidity Currents

The velocity profile for turbidity currents has two boundaries: an upper, free boundary and a lower, solid boundary as shown schematically in Fig. 4-5.

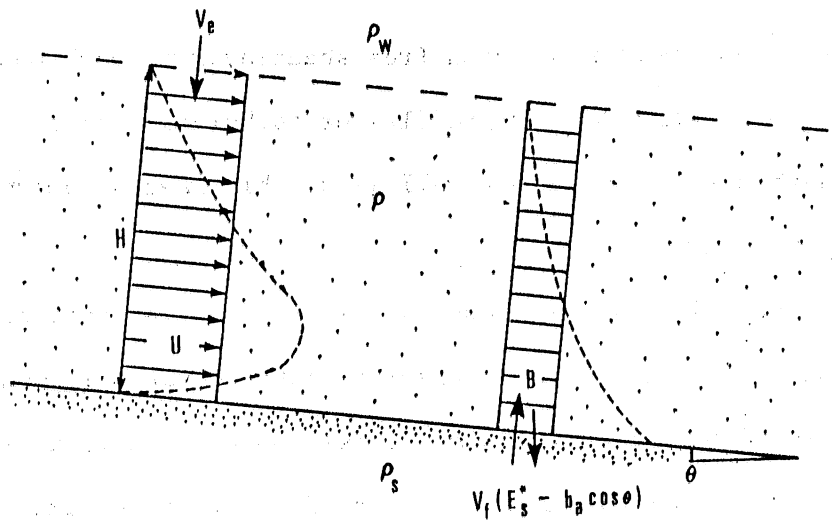

Fig. 4-3 Definition of layer averaged properties.

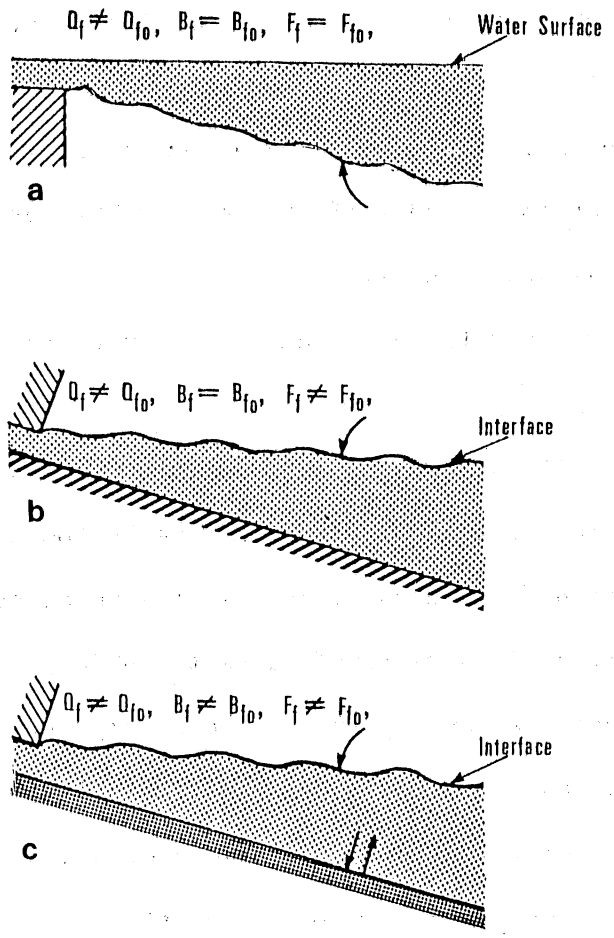

Fig. 4-4 Typical density currents with reference to volume flux (Q_f), buoyancy flux (B_f), and flow force (F_f).

The flow, therefore, has a free shearlayer and a boundary layer. In this sense, the velocity profiles of turbulent turbidity currents resemble those of homogeneous wall jets, which are also composed of a two-layer shear flow.

The location of the velocity maximum is often chosen as the dividing point. It has been observed that the velocity maximum does not always match with the zero shear stress point, but is at least close to it. It is reasoned that the velocity field is non-symmetrical because of different boundary conditions at the upper and lower edges of the flowing layer. The location of the velocity maximum has been arbitrarily chosen for dividing the flowing layer into two subregions.

The region from the wall to the maximum velocity will be referred to as the inner or wall region (H_1) and the region from the maximum velocity point to the edge of the flow as the outer or free mixing region (H_2) as shwon in Fig. 4-5.

Defining the ratio of thickness of inner to outer layer as χ:

$\chi = H_1/H_2$.

If shear stress distribution is assumed to be linear (Fig. 4-5), χ is also the ratio of shear stress at the bottom to at the point where $u = \frac{1}{2} u_{max}$, which point usually coincides with or at least is close to visual interface in stratified flows ($H_2 \sim 2H_3$). Glauert [1956] had predicted that the inner part and the outer part of a homogeneous wall jet could not possibly have the same similarity form. Dividing the flow into two, Eskinazi and Kuruka [1962], showed a definite improvement of the similarity collapse of velocity profiles.

As shown in Table 4-1 and Fig. 4-6, the outer part of the velocity distribution approximately follows a Gaussian profile, while the inner part of the velocity distribution follows a logarithmic profile, regardless of type of flow (homogeneous or stratified).

Tables 4-2 and 4-3 show that χ-values are not unique, due to effects of stratification (amount of water entrainment across an upper boundary) and effects of channel bottom condition (smooth or rough bed). It must be noted that χ-values in Tables (4-2 and 4-3) are mean values obtained from each profile. χ-values are expected to be controlled by the growth of both a free shear layer and a boundary layer.

The parameter χ for turbidity currents, for example, is examined by Middleton [1966], based on Michon et al.'s data [1955], which are from experiments with clay suspension in two smooth flumes. Middleton [1966] found that there is a moderate correlation between densimetric Froude number (F) and χ.

The approximated trend obtained by Middleton [1966], using overall Richardson number (R), can be expressed as

$$R = (2.5\chi - 0.8)^{-2} \qquad \text{for} \qquad 0.5 \leq R \leq 1.0.$$

It is obvious that the relationship above at least holds in supercritical underflows or turbidity currents made of sediment with negligible V_f, flowing over a smooth bed.

Tesaker's [1969] as well as Garcia's [1985]velocity profiles for supercritical turbidity currents show very noticeable variations of both velocity and concentration profiles in a manner similar to Michon et al.'s data. Variations in Tesaker's data are shown in Fig. 4-5, and indicate that no similarity profiles exist.

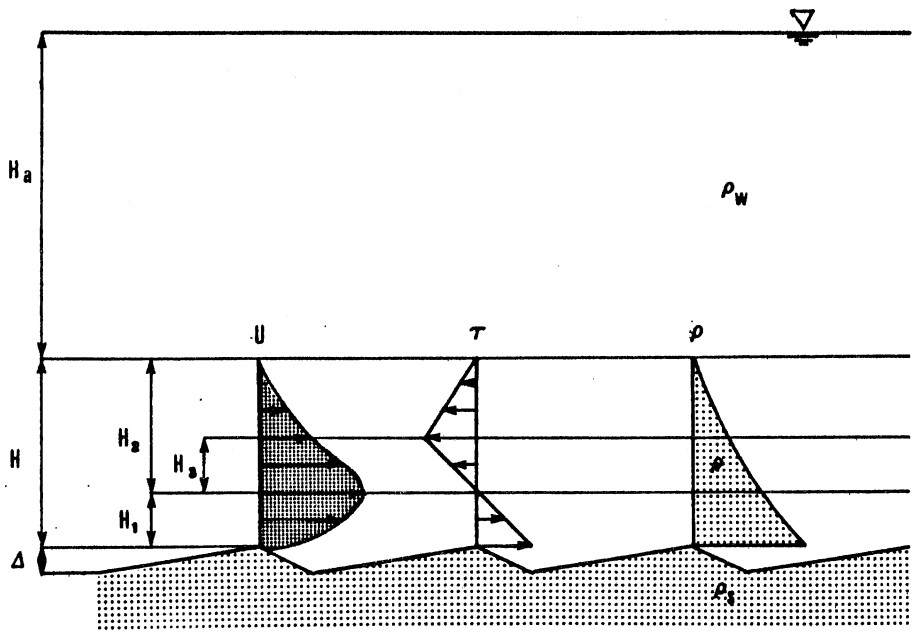

Fig. 4-5 Profiles of velocity (U), shear stress (τ), and density profiles (ρ).

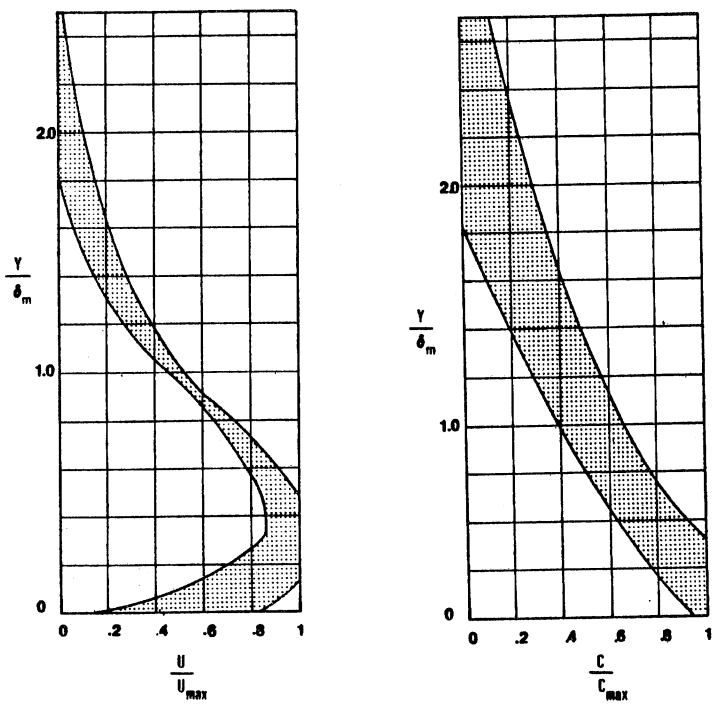

Fig. 4-6 Variation of velocity and concentration profiles for depositing supercritical turbidity current.

The effect of an upper boundary condition on the χ-value is explained as follows. Entrainment of ambient water, which determines the growth rate of the flow, is adequately described by two parameters: Richardson number (R) and Reynolds number (Re). The dependence of the Re number on water entrainment is experimentally observed when the turbulence length scale is comparable to the viscosity length scale. Therefore, Re number is closely related to the mixing mechanism across the upper intermittent free boundary.

Water entrainment is a function of the Re number when entrainment is controlled by viscosity dominated mechanisms such as breaking internal waves, or molecular diffusion. Lofquist's experiments [1960] are a good example of this type of underflow. In turbulent density currents, it has been experimentally well verified that entrainment of ambient water is a function of Richardson number (R) only (e.g., Ashida and Egashira [1977]). Experimental data obtained by various investigators essentially show that the amount of entrainment will increase, as the Richardson number decreases. Consequently, the ratio χ decreases, provided the rest of the conditions such as bed roughness are kept invarient. This is an explanation for the trend pointed out by Middleton [1966], and explains also the variations of velocity profiles, resulting from the growth rate of an outer layer.

Another factor which influences χ-values is the roughness (k_s) of the bed, which is a lower boundary condition of the flowing layer. k_s is the parameter to determine the growth rate of the inner layer as known in boundary layer theory. The dependence of χ-values on roughness can be seen in Tables 4-2 and 4-3 (Rajaratnam [1965] and Ashida and

TABLE 4-1. SUMMARY OF OUTER LAYER VELOCITY PROFILE

NAME OF INVESTIGATOR	A
Chu and Vanvari [1976] (2-D surface buoyant jet)	0.694
Rajaratnam and Subramanyan [1983] (2-D surface buoyant jet)	0.693
Patel and Newman [1961] (2-D homogeneous wall jet)	0.693
Tesaker [1969] (2-D turbidity current)	0.693
Tsubaki and Komatsu [1978] (2-D surface buoyant jet)	0.694

$u/u_{max} = \exp(-A(y/\delta_m)^2)$

where $\delta_m = y$ at $u = (1/2)\, u_{max}$.

(note: all of the flows are supercritical)

TABLE 4-2. LOCATION OF U_{max} IN A HOMOGENOUS WALL JETS

NAME OF INVESTIGATOR	x
(1) Smooth Wall	
Eskinazi and Kuruka [1962]	0.110
Forthmann [1934]	0.105
Irwin [1973]	0.108
Patel and Newman [1961]	0.100
Schwarz and Cosart [1961]	0.140
Verhoff [1963]	0.095
(2) Rough Wall	
Rajaratnam [1965]	0.300

TABLE 4-3. LOCATION OF U_{max} IN A STRATIFIED GRAVITY CURRENT

NAME OF INVESTIGATOR	χ
Asida and Egashira [1975]	0.380 (k_s = 0.10 cm)
(subcritical turbidity current)	0.480 (k_s = 0.59 cm)
Ellison and Turner [1959] (supercritical underflow)	0.370
Garcia [1985] * (supercritical turbidity current)	0.300
Georgiev [1973] (subcritical underflow)	0.450
Lofquist [1960] (subcritical underflow)	0.530
Tesaker [1969] * (supercritical turbidity current)	0.340
Wilkinson and Wood [1970] (internal hydraulic jump)	0.330

k_s = the roughness height

* indicates the existence of bed forms

Egashira [1975]). The former is a homogeneous wall jet, and the latter is a turbidity current made of very fine materials (D_s = 32 and 27 μ). Tables 4-2 and 4-3 suggest that the presence of roughness tends to increase χ-values. This implies that the parameter k_s/H or D_s/H is of significance.

χ-values of turbidity currents are expected to be further complicated than those of underflows (or turbidity currents made of non-settling particles) when bed forms (Δ) are presented. In fact, well-defined ripples and dunes have been observed in large scale laboratory experiments by Tesaker [1969] and Garcia [1985] as well as at field sites.

The effect of bed forms can be described by Shields' parameter (τ_*), particle Reynolds number (R_p), and submerged specific gravity (σ).

The shape Factors (f_1, f_2, f_3, S_1, S_2) defined in Eqs. 4-22 through 4-25 are, therefore, not constant, but at least a function of R, D_s/H, τ_*, σ, which are not maintained unique in erosive and depositive turbidity currents (Fig. 4-8).

4.6.7 Consideration on the Shear Stress at the Bed

In Eq. 4-20, the form of bed shear stess (τ_b) has not been determined and hence is considered in this section.

When both suspended and bed load are presented in an alluvial stream, the shear stress (τ_b) at the bed is, in general, considered to be made of three components under the assumption of linear composition of shear stresses:

$$\tau_b = \tau_{bo} + \tau_{b1} + \tau_{b2} \qquad 4\text{-}29$$

where τ_{bo} is the shear stess due to the skin friction roughness (k_s) of the bed surface, τ_{b1} is the component of shear stress due to the form (pressure) drag behind bars such as ripples and dunes, and τ_{b2} is the component of shear stress caused by the diffused material, which is equivalent to the work done against buoyancy force, which has been commonly referred to as "Bagnold's autosuspension term" from the energy balance point of view.

Bagnold's suspension criterion will be discussed in more detail in this chapter.

In Eq. 4-20, τ_b is constant for the uniform flow condition ($d(S_1 BH^2 \cos\theta)/dx = 0$). For the sediment transport in open channel, hydraulic conditions such as flow velocity and depth are known.

Types of bed form and the magnitude of the associated shear stress (τ_{b1}) are often unknown even in an equilibrium and uniform flow.

Yalin [1977], for example, has classified the role of shear stress, depending on the stage of channel bed development:

(a) Plane bed in the early stage

$$\tau_b \sim \tau_{bo} \qquad 4\text{-}30$$

(b) Irregular bed in the intermediate stage.

$$\tau_b \sim \tau_{bo} + \tau_{b1} \qquad 4\text{-}31$$

(c) Plane bed in the advanced stage.

$$\tau_b \sim \tau_{bo} + \tau_{b2} \qquad 4\text{-}32$$

Define each shear stress as:

$$\tau_{bi}/\rho_w = C_{bi}U^2 \qquad \text{where } i = 0, 1, 2 \qquad 4\text{-}33$$

and

$$\tau_b/\rho_w = C_b U^2 \qquad 4\text{-}34$$

where C_{bo} = skin friction coefficient, C_{b1} = drag coefficient, and C_{b2} = additive friction coefficient due to the presence of suspended sediment.

The resistance of a movable bed is, in general, considered to be controlled by the following dimensionless parameters: $\{C_b, R_p, \tau_*, K, J, \sigma\}$

where:

$$C_b = \frac{u_*}{U}, \quad R_p = \frac{D_s(\sigma g D_s)^{1/2}}{\upsilon}, \quad \tau_* = \frac{u_*^2}{\sigma g D_s}, \quad K = \frac{D_s}{H}, \quad J = \frac{\Delta}{H}, \quad \sigma = \frac{\rho_s}{\rho_w} - 1$$

where:

τ_* = non-dimensional tractive force (Shields' parameter). R_p = particle Reynolds number. σ = submerged specific gravity. C_b = total friction coefficient. Δ = bed form height. Ripples are sometimes found

to be superimposed on dunes. The development process of bed forms is expected to be controlled by tractive forces. Therefore, $C_b = f(\tau_*, K, J, R_p)$. σ is generally constant (= 1.65), and is dropped. The Shield's parameter, τ_* is equivalent to the parameter V_f/u_*.

In sediment transport in open channels, the dimension of ripples (Δ_r) and dunes (Δ_d) are found to be controlled by different parameters such that $\Delta_r \sim D_s$ and $\Delta_d \sim H$ dependent on R_p.

On the other hand, the flow depth of a steady turbidity current is not uniform and consequently the sediment concentrations and, the fluid force exerted on the bed vary with distance.

If a turbidity current is made of uniform material C_{bo} can be constant because $D_s \sim k_s$, and the channel bed may be even regarded as smooth bed. Because turbidity currents in nature are usually large in dimension ($K = D_s/H \sim 0$), neither C_{b1} nor C_{b2} can be constant with x.

The parameter J is considered to be also a function of τ_*, K, and R_p. C_{b1} may, therefore, be expected to be in the form:

$$C_{b1}(x) = f(\tau_*(x), K(x), R_p) \qquad 4\text{-}35$$

in a turbidity current.

Equation 4-35 implies that bed forms change in flow direction, and as a result C_{b1} can vary.

The determination of C_{b1} is impossible with present knowledge. It will be necessary in the future to investigate experimentally the effect of an interface on the formation of dunes in order to understand the role of bed forms on turbidity currents.

4.6.8 Estimation of the Friction Coefficient (C_{b2}) for an Additive Shear Stress (τ_{b2})

Bagnold [1962] introduced the concept of autosuspension for turbidity currents from the energy balance point of view. The Bagnold term $\Delta\rho gH(V_f/U)$ measures the power required to hold sediment in suspension. Bagnold's term originates from the buoyancy flux term $\overline{v'b'}$ in the turbulent energy equation:

$$u\frac{\partial}{\partial x}(k) + v\frac{\partial}{\partial y}(k) = - \overline{u'v'}\,\frac{\partial u}{\partial y}(1 + R_{f\ell}) - \frac{\partial}{\partial y}\,\overline{v'\,(k - \frac{p'}{\rho_w})} - E \qquad 4\text{-}36$$

where p = pressure and E = turbulent energy dissipation due to viscosity. Fluctuating components are designated by primes. Turbulent kinetic energy (k) and flux Richardson number ($R_{f\ell}$) are defined respectively:

$$k = \frac{1}{2}\,(\overline{u'^2} + \overline{v'^2} + \overline{w'^2}) \qquad 4\text{-}37$$

$$R_{f\ell} = \frac{\overline{b'v'}}{\overline{u'v'}\,\frac{\partial u}{\partial y}} \qquad 4\text{-}38$$

The buoyancy flux term ($\overline{b'v'}$) describes work done against buoyancy force due to vertical density gradient. Considering an equilibrium state, Eq. 4-13 yields:

$$V_f b \cos\theta = \overline{b'v'} \qquad 4\text{-}39$$

Similarly, considering a turbulent energy balance, Eq. 4-36 with 4-39 yield:

$$\int_0^H (-\overline{u'v'})\frac{\partial u}{\partial y}\, dy = \int_0^H bV_f \cos\theta\, dy + \int_0^H E\, dy \qquad 4\text{-}40$$

$$P = I + D$$

where P = layer integrated turbulent energy production (= mean flow energy loss)

I = layer integrated work done against buoyancy force

D = layer integrated turbulent energy dissipation

Total energy available from gravity is $S_2BHU\sin\theta$, and I is $S_2BV_fH\cos\theta$, considering the mean energy equation, which can be calculated from Eq. 4-3.

The total energy balance in an equilibrium state is, therefore, given by:

$$S_2BHU(\sin\theta - V_f\cos\theta) = D \qquad 4\text{-}41$$

or

$$\frac{S_2BH\sin\theta}{U^3} - S_2R\left(\frac{V_f}{U}\right) = \frac{D}{U^4} \qquad 4\text{-}42$$

The Bagnold term can be explicitly obtained from the energy balance. However, the magnitude of the turbulent dissipation term (D) cannot be evaluated properly without the knowledge of turbulence. The magnitude of Bagnold's term is relatively small. It is difficult therefore to verify Bagnold's concept through small scale laboratory experiments [Middleton, 1966] as one can see from the functional form (Eq. 4-42). It also must be noted the Bagnold's auto-suspension criteria is not a "sufficient" but "necessary" condition for auto-suspension as clearly seen from its origin.

Bagnold's term cannot be obtained directly from the momentum equation, because it associates with turbulence energy within the flow.

Some alternative considerations for C_{b2} are given in the following paragraph.

From Eqs. 4-38 and 4-39, $R_{f\ell}$ becomes:

$$R_{f\ell} = \frac{V_f \, b\cos\theta}{u_*^2 \frac{du}{dy}} \sim \left(\frac{BH\cos\theta}{U^2}\right) \left(\frac{V_f}{U}\right) = R\left(\frac{V_f}{U}\right) \qquad 4\text{-}43$$

The velocity profile of a turbidity currents is similar to that of a homogenous wall jet (Fig. 4-7). A difference between the two profiles will be caused by flux Richardson number defined in Eq. 4-43. The velocity profile of a turbidity current may be skewed by this factor, and consequently production of turbulence increases in magnitude. This additional turbulence must be used for the suspension of sediment particles.

The shear stress of a turbidity current (τ_b) and homogeneous wall jet ($\tilde{\tau}_b$) are assumed to be related in the form:

$$\frac{\tau_b}{\tilde{\tau}_b} = \text{fct } (R_f) \qquad 4\text{-}44$$

$$\tau_b = \tau_{bo} + \tau_{b2} = (1 + m_1 R_f)\ \tilde{\tau}_b \qquad 4\text{-}45$$

Where m_1 is a correction factor.

Comparing Eqs. 4-42 and 4-45, the coefficient in Eq. 4-45 ($m_1 C_{bo}$) is equal to S_2, Eq. 4-45 can be expressed as

$$C_b U^2 = (C_{bo} + C_{b2})\tilde{U}^2 = (C_{bo} + S_2 R_f)\tilde{U}^2 \qquad 4\text{-}46$$

4.6.9 Estimation of the Friction Coefficient (C_{bo}) for the Shear Stress (τ_{bo}) due to Skin Friction

Determination of the drag coefficient C_{bo} is of significance in the momentum formulation. Many detailed measurements in homogeneous wall jets are available in the literature (e.g. Schwarz and Cosart [1961], Irwin [1973]). The friction factor (f_b) for a homogeneous wall jet as defined and given by Schwarz and Cosart [1961] is:

$$f_b = \frac{\tilde{\tau}_b}{\frac{1}{2}\rho_w u^2_{max}} = 0.01109 \qquad 4\text{-}47$$

on a smooth bottom. Based on the analogy of velocity profiles between

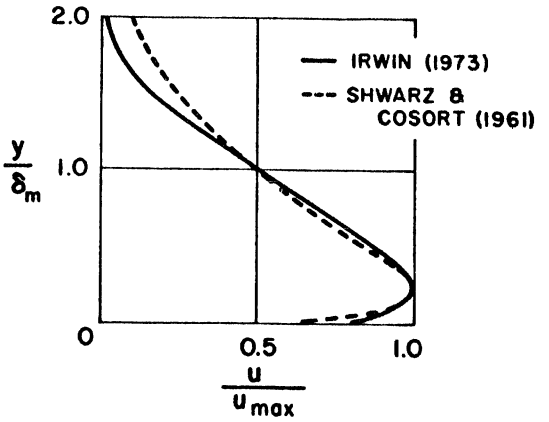

Fig. 4-7 Typical velocity profiles of plane wall jets.

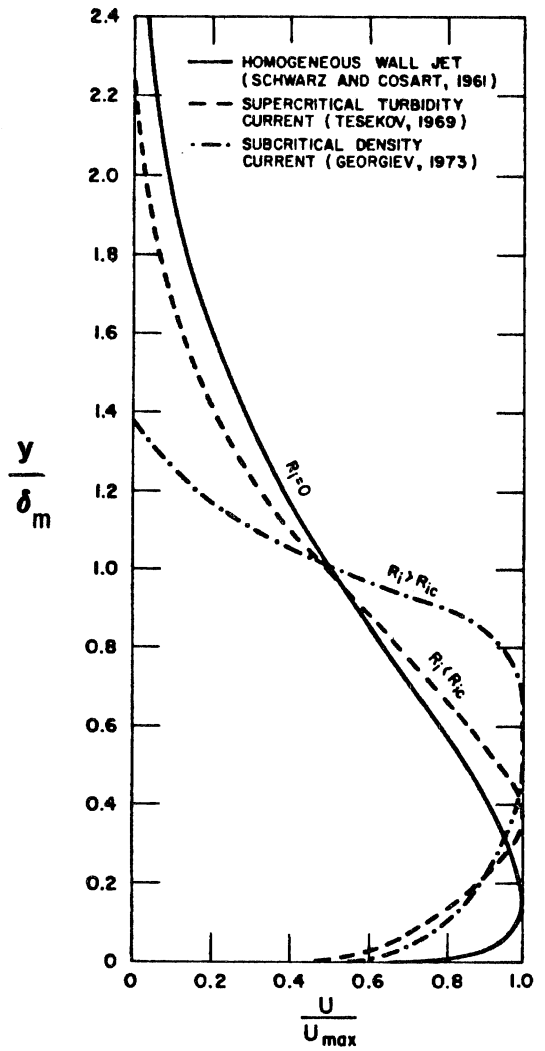

Fig. 4-8 Comparison of velocity profiles at different Richardson numbers.

high-velocity turbidity currents and homogeneous wall jets (Fig. 4-8), Eq. 4-47 is used to estimate C_{bo}. By equating $\tilde{\tau}_b$ in 4-47 with τ_{bo} one finds

$$C_{bo} = (\frac{u_{max}}{U})^2 \cdot \frac{f_b}{2} \qquad 4\text{-}48$$

The ratio of u_{max} to U is typically 2.0 (Fig. 4-7). Hence, $C_{bo} = (2)\cdot(1.109\text{x}10^{-2}) \simeq 0.02$. Ellison and Turner [1959] found this same value in their laboratory experiments (Fig. 2-8). Hebbert, Imberger, Loh, and Patterson [1979] obtained $C_{bo} = 0.0151$ for their plunging flow study.

$C_{bo} = 0.02$ is considered to be a reasonable value for the flow over a smooth bed; however, a natural bed may be hydraulically rough, due to grain roughness and bed forms. In nature, the condition $D_s/H \ll 1$ can however, be satisfied for a flat bed.

4.6.10 Gradually Varied Flow Equation for a Turbidity Current (Constant Width)

The vertically integrated governing equations given in section 4.6.5 are developed into the following gradually varied flow equations.

$$\frac{dR}{dx} = \frac{3R}{H}\left[\frac{\frac{1}{f_1}\left(1 + \frac{S_1}{2f_3}R\right) E_w - \frac{S_2}{f_3}R\tan\theta + \frac{C_{bo}}{f_3}}{1 - \frac{S_1}{f_3}R} + \right.$$

$$\left. \frac{\left\{\left(1 + \frac{S_1}{2f_3}R\right)\frac{1}{3f_2}\frac{(E_s^* - b_a\cos\theta)}{B} + \frac{S_2}{f_3}R\right\} V_f\left(\frac{R}{BH\cos\theta}\right)^{1/2}}{1 - \frac{S_1}{f_3}R}\right] \qquad 4\text{-}49$$

$$\frac{dH}{dx} = \frac{\frac{E_w}{f_1}\left(2 - \frac{S_1}{2f_3}R\right) - \frac{S_2}{f_3}R\tan\theta + \frac{C_{bo}}{f_3}}{1 - \frac{S_1}{f_3}R} +$$

$$\frac{\frac{R}{f_2} V_f\left(\frac{R}{BH\cos\theta}\right)^{1/2}\left\{\frac{S_1}{2f_3}\frac{(E_s^* - b_a\cos\theta)}{B} + \frac{f_2 S_2}{f_3}\right\}}{1 - \frac{S_1}{f_3}R} \qquad 4\text{-}50$$

$$\frac{dB}{dx} = -\frac{B}{f_1}\frac{E_w}{H} + \frac{V_f}{f_2}\frac{(E_s^* - b_a\cos\theta)}{H}\left(\frac{R}{BH\cos\theta}\right)^{1/2} \qquad 4\text{-}51$$

The second term on the right-hand side of Eqs. 4-49 , 4-50 , and 4-51 is in addition to the density underflow. From Eqs. 4-49 and 4-50, the relationship between dH/dx and dR/dx is derived:

$$\frac{dH}{dx} = \frac{E_w}{f_1} + \frac{H}{3R}\frac{dR}{dx} - \frac{V_f}{3f_2}\left(\frac{R}{BH\cos\theta}\right)^{1/2}\left(\frac{E_s^* - b_a\cos\theta}{B}\right) \qquad 4\text{-}52$$

The last term on the right-hand side of Eq. 4-52 is in addition to the simple underflow equation, and its contribution to dH/dx is negative when the flow is erosive and is positive when it is depositive. According to the Eq. 4-49, it is clear that a normal Richardson number does not exist in erosive and depositive turbidity currents.

For the limiting case of $V_f = 0$, the set of Eq. 4-50, 4-51, and 4-52, is reduced to those for ordinary underflows obtained by Ellison and Turner [1959] which is an extended form of the gradually varied flow equation for free surface (open channel) flow. Therefore, it can be expected that the behavior of erodible accelerating currents will approach that of simple density currents, as $V_f/U \to 0$.

4.6.11 Additional Relationships for the Model

(i) Evaluation of Sediment Entrainment Function (E_s^*) for Buoyancy Force or (E_s) for Concentration

We define $E_s^* = E_s \sigma g$, where E_s is the entrainment function for concentration.

$$E_s = f\left(\frac{V_f}{u_*}, \frac{H}{D_s}, R_p, \sigma\right) \qquad 4\text{-}53$$

where D_s = grain size of sediment particles

u_* = shear velocity at the bed ($= \sqrt{\tau_b/\rho_w}$)

H = flow depth

R_p = particle Reynolds number ($= D_s\sqrt{\sigma g D_s}/\upsilon$)

υ = kinematic viscosity of water

Relationships of the form of Eq. 4-53 have been proposed by Engelund and Fredsoe [1976], Itakura and Kishi [1980], and Ikeda and Asaeda [1983]. All functions have in common a very steep slope of E_s with respect to u_*/V_f or mean velocity U (Ikeda and Asaeda, [1983]). An empirical formula which was obtained by analysis of suspended sediment data for open channel flow will be used (see Chapter 3). For uniform sediment particles:

$$E_s = 3.0 \cdot 10^{-12} \cdot \Pi^{10}(1 - \frac{5}{\Pi}) \qquad \text{for } \Pi \leq 0.3 \qquad 4\text{-}54a$$

$$E_s = 0.3 \qquad \text{for } \Pi > 0.3 \qquad 4\text{-}54b$$

where

$$\Pi = (\frac{u_*}{V_f})\, R_p^{0.5} \qquad 4\text{-}55$$

E_s changes very strongly for small variations of u_*/V_f. Equation 4-54 and data are shown in Fig. 3-12.

(ii) Determination of Buoyancy Force (b_a) or Concentration (c_a) at y = a above the bed.

A relationship between concentration near the bed (c_a) and mean concentration C in the current can established by integrating the concentration profile. Parker [1982] obtained a relation by integrating Rouse's [1938] profile for open channel flow from a = 0.05H to H .

$$c_a = [1 + 31.5 \left(\frac{V_f}{u_*}\right)^{1.46}] C \qquad 4\text{-}56$$

The concentration profiles in open channel flow and in turbidity currents are different, in particular, in the upper portion. The concentration profile in the turbidity current is a combination of free shear flow (upper part) and open channel flow (lower part), provided that there is enough turbulence to meet the condition $V_f < \sqrt{\overline{v'^2}}$. Therefore, Eq. 4-56 is modified to:

$$c_a = \frac{m_2}{S_2}[1 + 31.5\left(\frac{V_f}{u_*}\right)^{1.46}] C \qquad 4\text{-}57$$

where m_2 is a factor to account for the difference of concentration profiles and reference level "a," and S_2 is the shape factor. In self-perserving flow such as surface jets (see e.g., Tsubaki and Komatsu, [1979], or Chu and Vanvari, [1976]) or underflows, the shape factor (S_2) for buoyancy flux has approximately the same value of 0.75. It coincides with the mean value of Ellison and Turner's result [1959]. Equation 4-57 gives the c_a value for a noneroding or depositing density current when $V_f/u_* \to 0$.

(iii) Entrainment Function of Water (E_s)

Entrainment of water is a term to describe the process when turbulence spreads into adjacent non-turbulent fluid.

It is therefore, a characteristic property of virtually all free turbulent flows, e.g., boundary layers, jets and wakes. Herein, turbulent flows implies that Re number is insignificant. If the entrainment velocity (v_e) is a function of these turbulent parameters, as well as the buoyancy difference across the interface (the flow is stratified), then entrainment of water in terms of mean flow velocity (Fig. 4-3) is expressed as:

$$v_e/U = \text{fct}(R) \qquad 4\text{-}58$$

An entrainment function of water (E_w) is customarily defined (Morton, Taylor and Turner, [1952]) as:

$$E_w = v_e/U \qquad 4\text{-}59$$

Thus from Eqs. 4-58 and 4-59,

$$E_w = \text{fct}(R) \qquad 4\text{-}60$$

Richardson number (R) can be interpreted as the ratio of the rate of increase of potential energy due to the entrainment and the rate of production or dissipation of turbulent energy which causes the

entrainment. Different functional forms of E_w have been investigated, and proposed by various investigators.

One functional form of E_w is:

$$E_w = \beta R^n \qquad 4\text{-}61$$

where both β and n are empirical constants.

Ashida and Egashira [1977], proposed $\beta = 0.0015$ and $n = -1.0$ based on experimental results obtained under different flow conditions by Kato and Phillips [1969] (a turbulent shear flow produced by a surface shear stress), Ellison and Turner [1959] (a turbulent underflow and overflow), Lofquist [1960] (a turbulent underflow), and their own data as shown in Fig. 4-9.

4.6.12 Summary of Equations

1. Gradually Varied Turbidity Current Equations

Equations 4-49, 4-50, and 4-51 are the gradually varied turbidity current equations.

2. Sediment Entrainment Function for Buoyancy Force (E_s^*)

Equation 4-56 is used to describe sediment entrainment from the bed.

3. Fall Velocity

Particle fall velocity is calculated by Dietrich's [1984] empirical equation derived from extensive data on arbitrarily shaped, natural particles.

$$V_f = (\sigma g \upsilon W_*)^{1/3}$$

where $\log W_* = -3.7617 + 1.92944 (\log D_*) - 0.09815 (\log D_*)^{2.0} - 0.00575 (\log D_*)^{3.0} + 0.00056 (\log D_*)^{4.0}$ 4-62

and

$$D_* = \sigma g D_s^3 / \upsilon^2 \qquad 4\text{-}63$$

4. Water Entrainment Function (E_w)

Ashida and Egashira's [1977] formulation of the water entrainment function is used.

$$E_w = \frac{\beta}{R}, \quad \beta = 0.0015 \qquad 4\text{-}64$$

5. Buoyancy Force Near the Bed (b_a)

The buoyancy (concentration) near the bed.

$$b_a = \frac{m_2}{S_2} \{1 + 31.5 (\frac{V_f}{u_*})^{1.46}\} B \qquad 4\text{-}65$$

6. Drag Coefficient at the Bed (C_{bo})

$$C_{bo} = 0.02 \qquad 4\text{-}66$$

4.7 Aggradation and Degradation due to Turbidity Currents

The bed elevation (η_b) of a channel in which a turbidity current is flowing can change due to erosion or deposition. The bed slope is gradually modified by the currents when continuous currents are produced for a certain time interval (Δt_s).

The aggradation and degradation of the bed due to over- and underloading of the erosive and depositive turbidity current is expressed by:

$$\frac{d\eta_b}{dt} + \frac{1}{1 - \lambda} \frac{dq_s}{dx} = 0 \qquad 4\text{-}67$$

where η_b is the bed level. λ is the porosity. q_s is the sediment discharge.

From Eqs. 4-16 and 4-67,

$$\frac{d\eta_b}{dt} + \frac{1}{1 - \lambda} V_f (E_s - c_a \cos\theta) = 0 \qquad 4\text{-}68$$

Equation 4-68 indicates that the sediment bed elevation and the flow are coupled. The following conditions are distinguished:

1) aggradation depositive current

$$\frac{d\eta_b}{dt} > 0 \quad \text{when} \quad c_a \cos\theta > E_s \qquad 4\text{-}69$$

2) degradation erosive current

$$\frac{d\eta_b}{dt} < 0 \qquad \text{when} \qquad c_a\cos\theta < E_s \tag{4-70}$$

The time interval (Δt) during which a turbidity current continues is:

$$\Delta t = \frac{1}{1 - \lambda}\frac{V_f}{\Delta\eta_b}(c_a\cos\theta - E_s) \tag{4-71}$$

The time interval Δt_s is in general expected to be short. Thus, the condition $\Delta t_s < \Delta t$ is assumed in the calculations in this chapter, so that the change of the bed slope in x-direction is assumed to be small within Δt_s. Some considerations on aggradation and degradation due to turbidity currents are provided in Chapter 5.

4.8 Sample Calculation and Discussions

Equations 4-49, 4-50, and 4-51 in conjunction with the other equations of Section 4.6.12 were simultaneously solved by using a fourth order Runge-Kutta method. The calculation step (Δx) was chosen to be 5 percent of the initial depth H_o until $x = 100\ H_o$, and 10 percent of H_o thereafter. In the numerical computation all of the shape factors (f_1, f_2, f_3, S_1, and S_2) were set equal to unity (first approximation). Viscosity of water (υ) was kept constant ($= 1.0 \times 10^{-6}$ m^2/s) in all calculations except Fig. 4-23. In this section the model has been used to illustrate the qualitative effects of sediment erosion and deposition, and the influence of settling velocity of suspended sediment on the flow. A comparison with ordinary density currents has been made

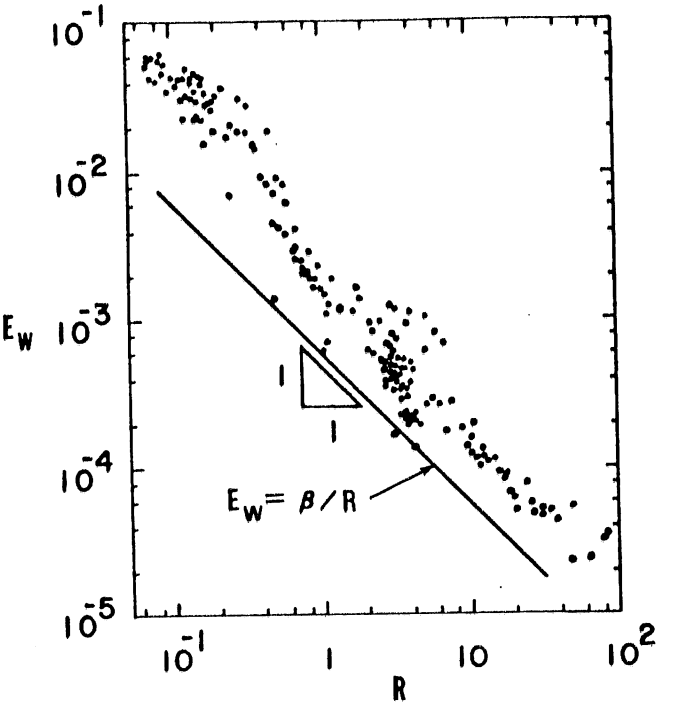

Fig. 4-9 Entrainment coefficient (E_w) versus Richardson number (R) in two layer stratified flow (after Ashida and Egashira [1977]).

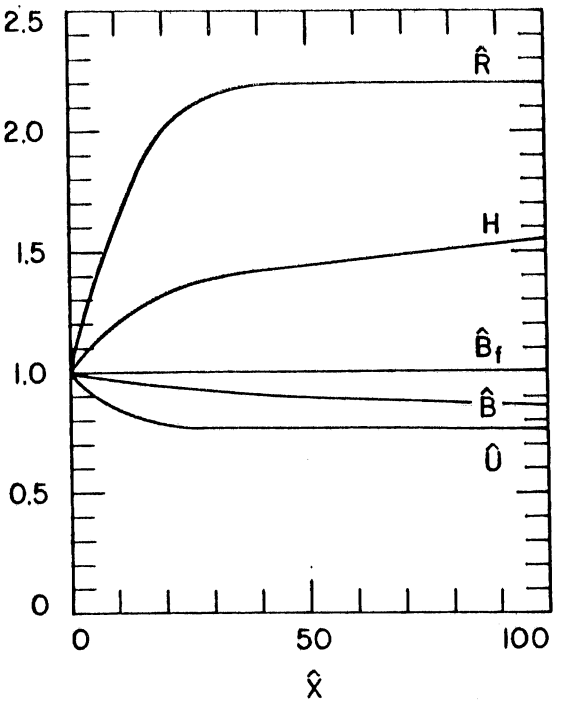

Fig. 4-10 Sample calculations for a density current (R_o = 0.3, B_o = 0.3 m/s^2, H_o = 1.0 m, θ = 2°, υ = 1.0 x 10^{-6} m^2/s).

where possible. A sample calculation for a constant buoyancy flux (nonentraining or depositing) density current is plotted in Fig. 4-10. All values in Fig. 4-10 are normalized as follows:

$$\hat{H} = H/H_o,\ \hat{B} = B/B_o,\ \hat{U} = U/U_o,\ \hat{B}_f = \hat{H}\hat{B}\hat{U},\ \hat{R} = R/R_o,\ \hat{x} = x/H_o$$

It is known that the density current will reach a normal state within a short distance (Ellison and Turner, [1959]), (Tsubaki and Komatsu, [1979]). In a normal state gravity force, bottom shear, pressure force, and momentum due to water entrainment are in balance. Normal flow condition is achieved when the flow experiences constant bed shear stress: constant friction coefficient, flow velocity, and wetted area. Water entrainment acts like a shear force in the momentum formulation, but small. Setting $V_f = 0$ in Eqs. 4-40, 4-50 and 4-51, gives the relationships for the normal state as:

$$\frac{dH}{dx} = E_w/f_1 \qquad 4\text{-}72$$

$R = R_n$ = constant

B_f = UBH = buoyancy flux = constant

From Eq. 4-64 and 4-72, $dH/dx = \beta/(R_n f_1)$. Once a normal state has been reached ($R = R_n$), the depth and the buoyancy force of the density current follow a linear relation with x as can be seen in Fig. 4-10, and the flow velocity (U) is constant with x . The behavoir of the flow, therefore, follows a very simple relation.

The situation is, however, more complex for the turbidity current because of additional terms in the governing equation. These terms contain the perturbation parameter $V_f(R/BH\cos\theta)^{1/2} = V_f/U$. Sample

computations of accelerating turbidity currents are given in Fig. 4-11, 4-12, and 4-13. The behavior of turbidity currents is similar to that of density currents in some respects, e.g., for depth $\hat{H} = H/H_o$. However, differences for $\hat{B}_f$, $\hat{B}$, and $\hat{U}$ are quite obvious. In particular, the buoyancy flux $\hat{B}_f$ is not constant but increases almost linearly with x as the result of active sediment entrainment. Figures 4-11, 4-12, and 4-13 also demonstrate the effect of initial conditions (B_o, R_o, H_o, channel bed slope (θ), and the size of suspended sediment particle (D_s) on the accelerating (supercritical) turbidity currents. In Figure 4-14 an example of a decelerating-erosive supercritical flow is given. In this example $\hat{B}_f$ is almost constant, similar to a density underflow. The flow is still entraining some sediment from the bed, and the rate of decrease of $\hat{B}$, therefore, is not as rapid as in the case of Fig. 4-15, which is a sample calculation of supercritical decelerating-depositive turbidity currents. The results show that in supercritical flows ($R > 1$), sediment deposition does not occur, if $D_s < 1.5$mm.

A comparison of R numbers for density currents and turbidity currents in channels of different slopes θ is provided in Figs. 4-16 and 4-17 respectively. Density currents maintain supercritical conditions at $\theta > 1^o$; in turbidity currents at $\theta > 4^o$ is required for D_s = 0.1 mm. In turbidity currents the steeper channel slope is required in order to achieve higher velocity necessary to entrain and suspended sediments. Another important feature of Figs. 4-16 and 4-17 is the magnitude of the Richardson number after $\hat{x} > 100$ in the turbidity currents. The Richardson number in a density currents becomes a normal value after a short distance. That of turbidity currents require much

a

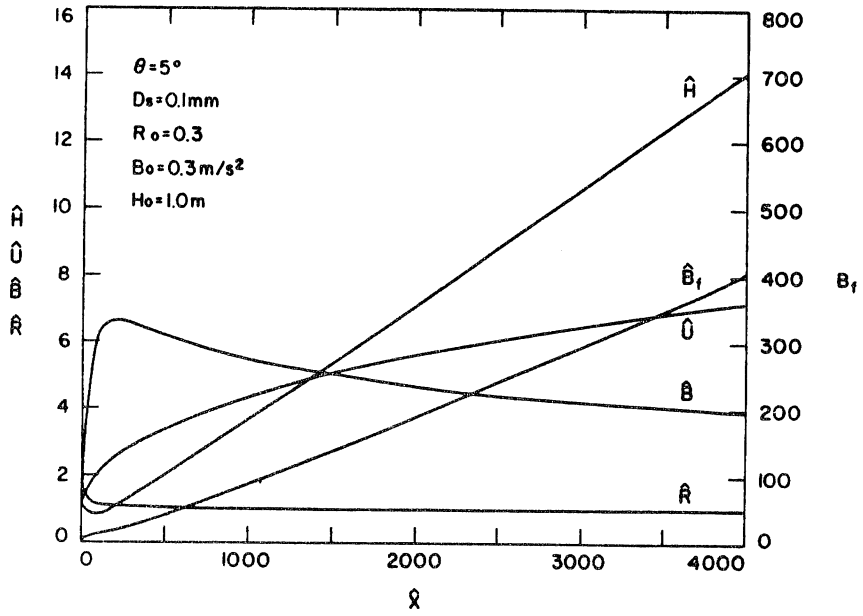

b

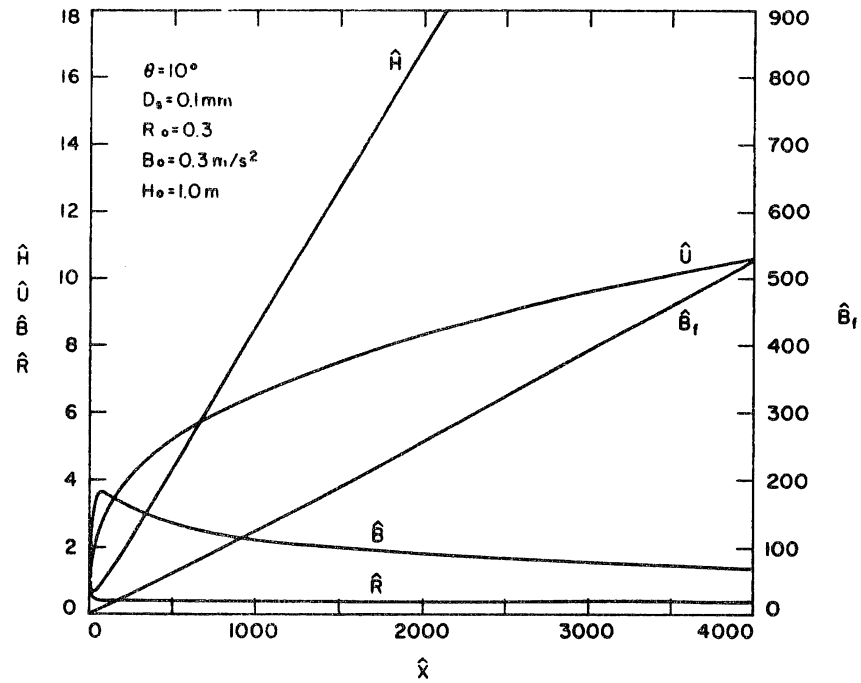

Fig. 4-11 Sample calculations for accelerating supercritical turbidity currents. (D_s = 0.1mm. θ = 5° (a) and θ = 10° (b)).

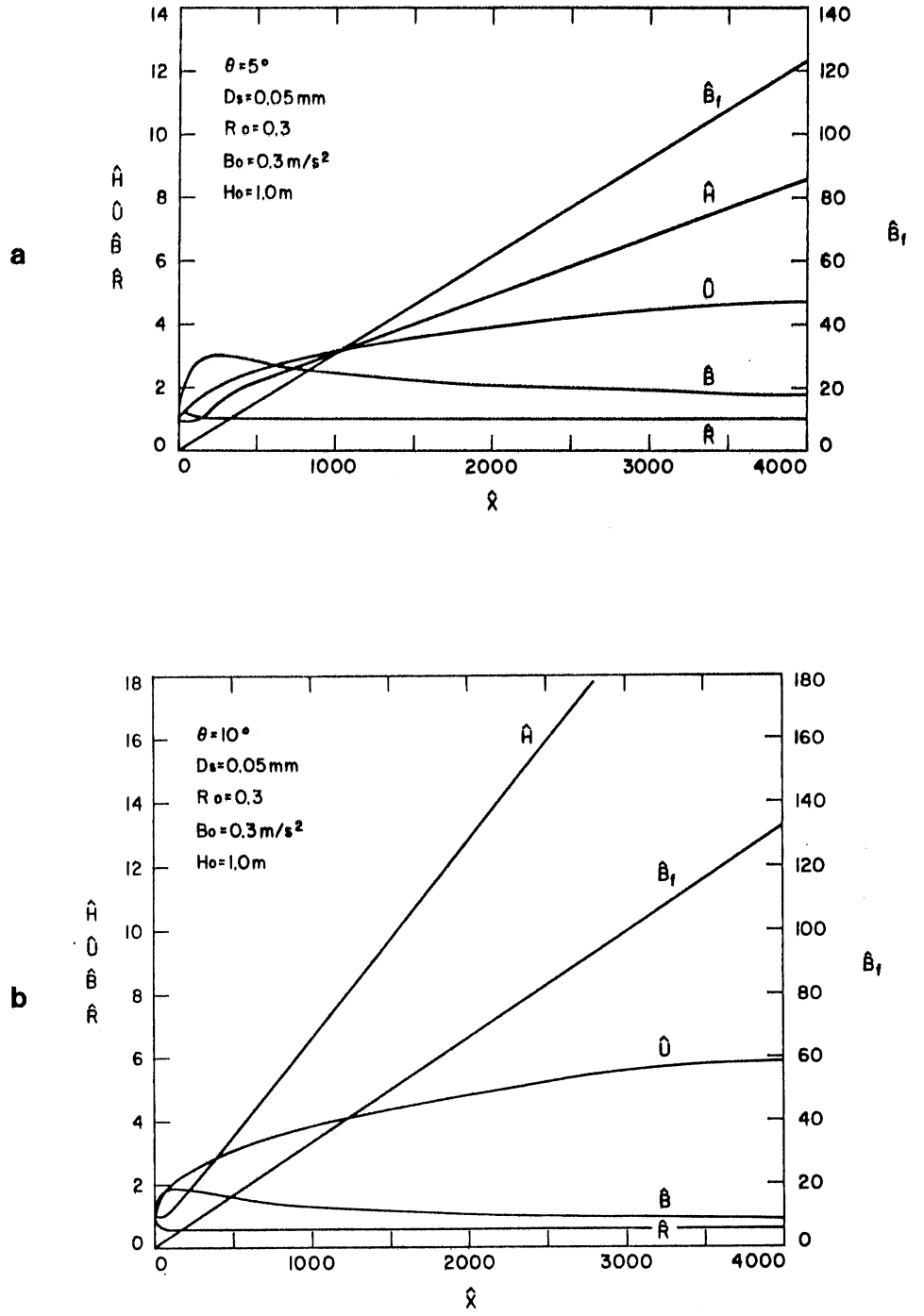

Fig. 4-12 Sample calculations for accelerating supercritical turbidity currents, as in Fig. 4-11, except particle size (D_s = 0.05 mm, θ = 5° (a) and θ = 10° (b)).

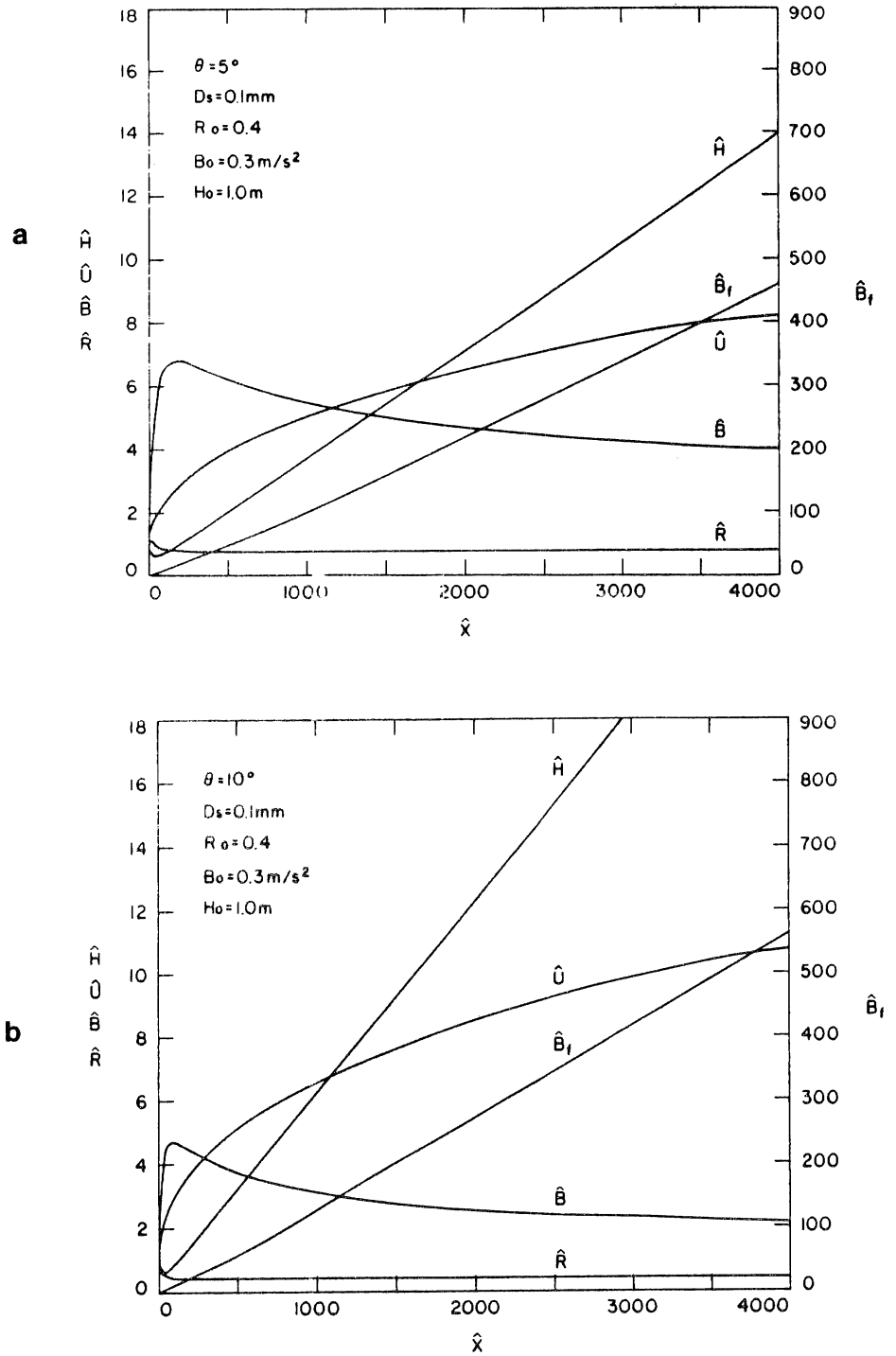

Fig. 4-13 Sample calculations for accelerating supercritical turbidity currents, as in Fig. 4-11, except initial condition (R_o) (D_s = 0.1 mm, θ = 5° (a) and θ = 10° (b)).

longer distances in order to become near normal value of R. After $\hat{x}$ = 1000, R numbers asymptotically approach values for density currents. This is obviously due to the fact that V_f/U approaches zero as U increases.

The convergence rate is fast for steep slopes and slow for mild slopes. R numbers at $\hat{x}$ = 4000, where the Richardson number is denoted as R_f for different channel slopes are plotted in Fig. 4-18. Under any given initial conditions a turbidity current with D_s = 0.1mm cannot maintain a supercritical condition if θ is less than 2^o. Density currents require a slope of 1.2^o only.

In Fig. 4-19 the growth rate $d\hat{H}/d\hat{x}$ of the layer thickness is plotted against θ. For turbidity currents, the growth rates are determined at $\hat{x}$ = 4000, and for density currents after normal conditions have been reached. $d\hat{H}/d\hat{x}$ of turbidity currents is smaller than that of underflows as indicated by Eq. 4-52. The ratio of growth rate is found to be about 2 to 3 in the range of $\theta = 2 \sim 20^o$. The significance of initial conditions and particle size to accelerating turbidity currents is demonstrated in Fig. 4-20a, b, c, and d. In Fig. 4-20a, for $\theta = 10^o$ all cases maintain supercritical accelerating conditions, and converge rapidly to R_f. For $\theta = 5^o$ relatively higher initial velocity is required, and the convergence is not as swift as in the case of $\theta = 10^o$. At slopes of $\theta = 3^o$, no erosive currents could form. Increasing the initial buoyancy force from 0.1 to 0.3, all flows (except for $\theta = 3^o$) converge to the same R_f in Fig. 4-20b.

The effect of particle size is examined in Figs. 4-20c and 4-20d. Initial conditions are the same as in Fig. 4-20b. For D_s = 0.15mm (Fig.

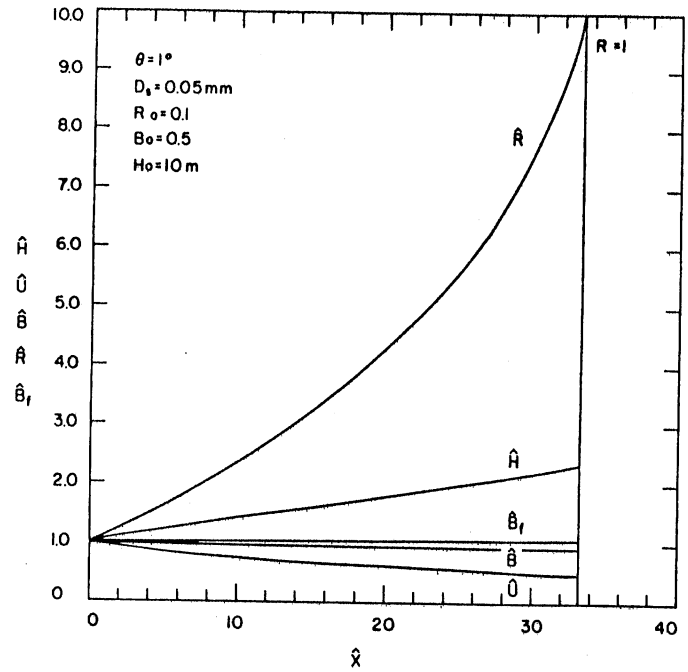

Fig. 4-14 Sample calculation for a decelerating-erosive supercritical turbidity current.

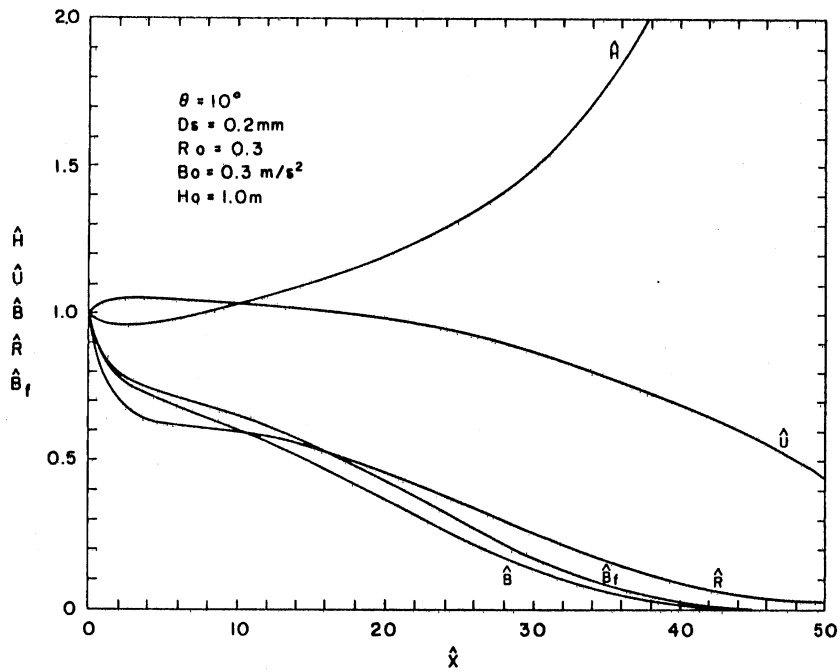

Fig. 4-15 Sample calculation for a decelerating-depositive supercritical turbidity current.

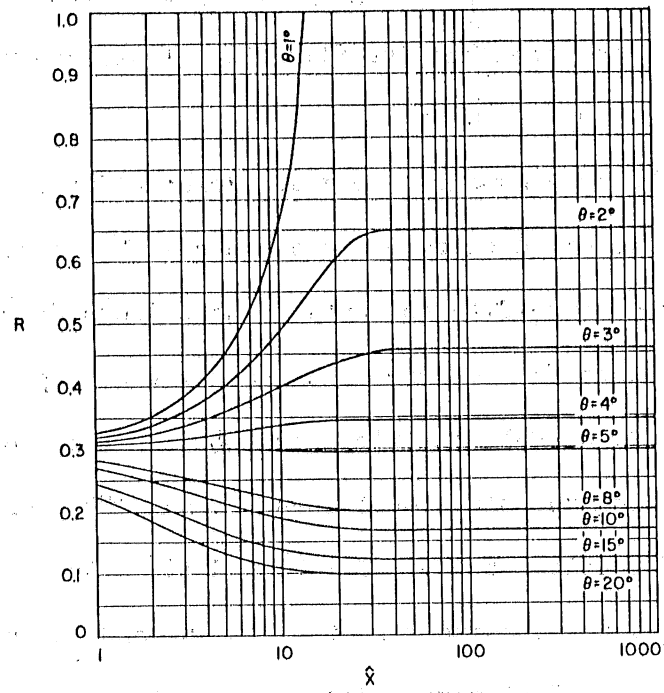

Fig. 4-16 Dependence of Richardson number, (R) on channel bed slope, (θ) for underflows.

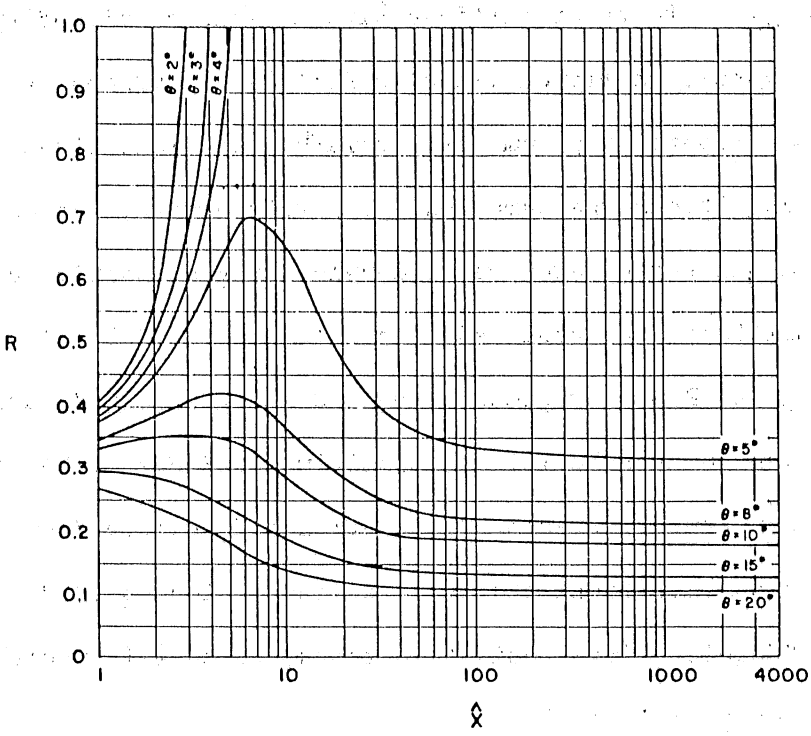

Fig. 4-17 Dependence of Richardson number, (R) on channel bed slope, (θ) for turbidity currents with same initial conditions as Fig. 6-16.

4-20d) all currents become depositing subcritical flows if the channel slope is less than 3^{o}. Accelerating flows, however, converge similar to the case of D_s = 0.05mm.

Richardson number is a good indicater to determine the type of flow. However, Richardson number alone cannot describe the flow dynamics of turbidity currents. The effects of sediment particle size (D_s) are therefore examined in the relationship with flow velocity (U), buoyancy force (B), and flow depth (H) in Figs. 4-21 and 4-22.

Keeping the flow conditions the same, two channel bed slopes are chosen for this purpose: $\theta = 7^{o}$ and 10^{o}. As seen in the figures, particle size is quite sensitive to U and B, but not to R and H. The behavior of different density underflows is also shown for comparison in Fig. 4-21 and 4-22.

Effects of particle size as well as viscosity of water are systematically examined in Fig. 2-23. Viscosity of water is found to be an important parameter for larger particle sizes. Keeping all conditions the same, except particle size, the change from accelerating-erosive to decelerating-depositive currents can be seen for different channel bed slopes ($\theta = 1^{o} \sim 20^{o}$). The calculated lines which go to R = 1, represent "decelerating-erosive" currents, which will vanish as subcritical depositive currents. The lines which approach R = constant, represent "accelerating-depositive" currents, which remain in a supercritical state. The lines which go to R = 0, represent "decelerating-erosive" currents, which will vanish while remaining supercritical flows.

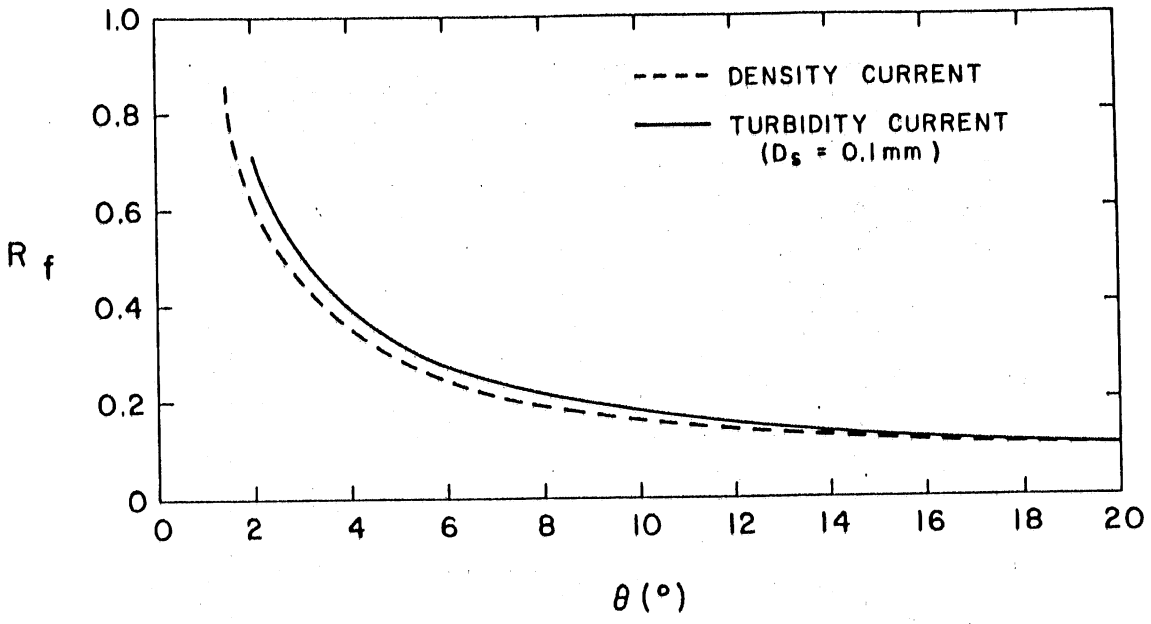

Fig. 4-18 Comparison of Richardson number, (R_f) at $\hat{x}$ = 4000, between underflows and turbidity currents (D_s = 0.1 mm).

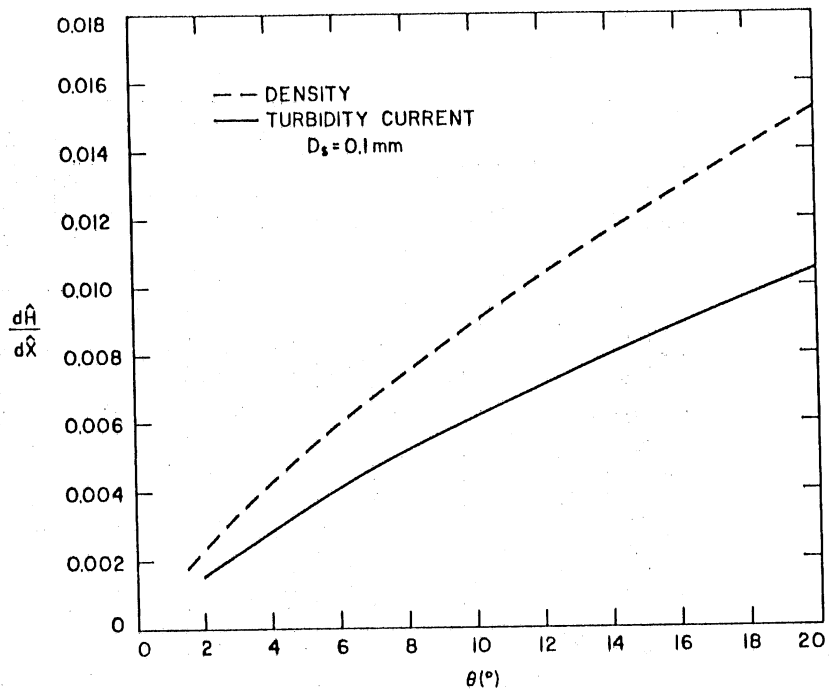

Fig. 4-19 Comparison of growth rate of flow thickness ($d\hat{H}/d\hat{x}$) at $\hat{x}$ = 4000, between underflows and turbidity currents (D_s = 0.1 mm).

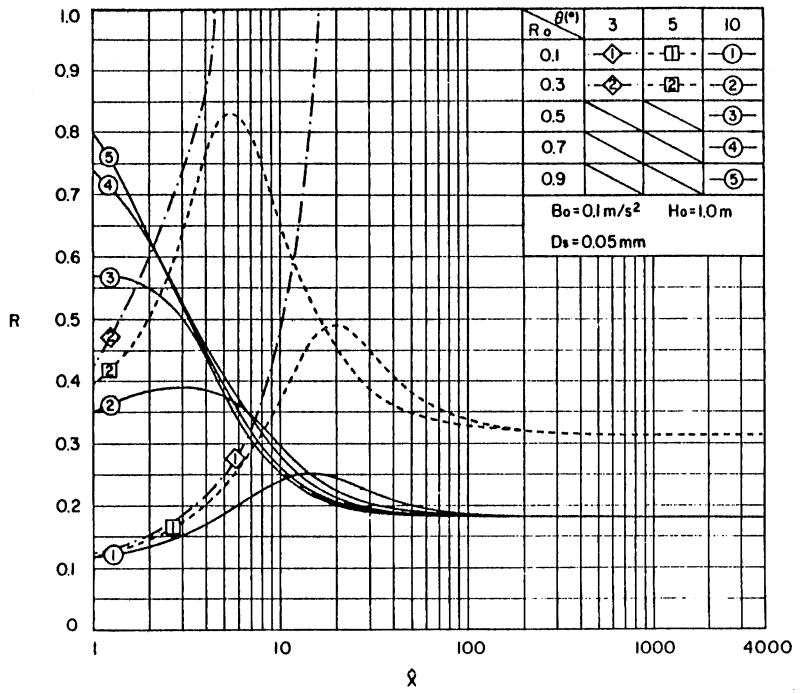

Fig. 4-20 Particle size effects on turbidity currents:
(a) D_s = 0.05mm. B_o = 0.1m/s², H_o = 1.0m

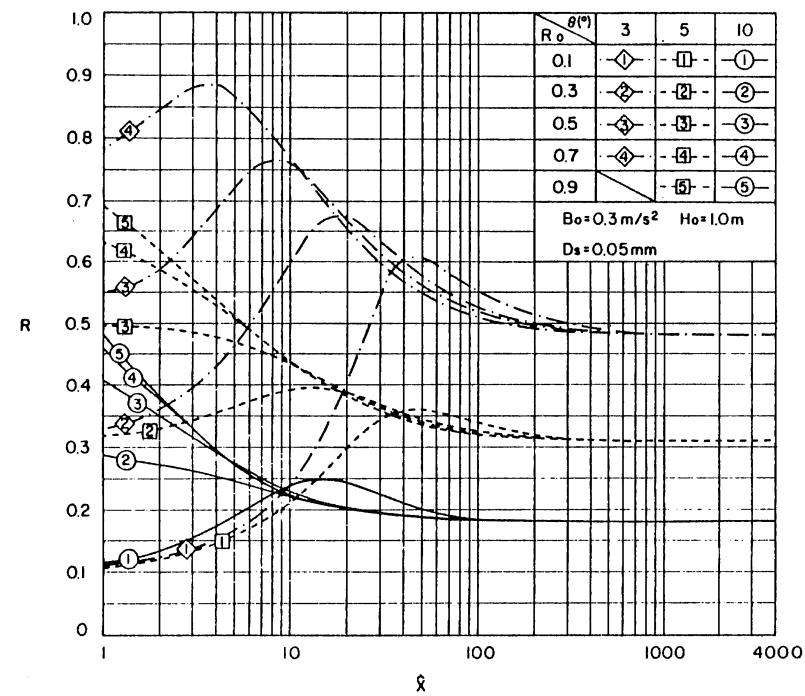

(b) D_s = 0.05mm, B_o = 0.3m/s², H_o = 1.0m

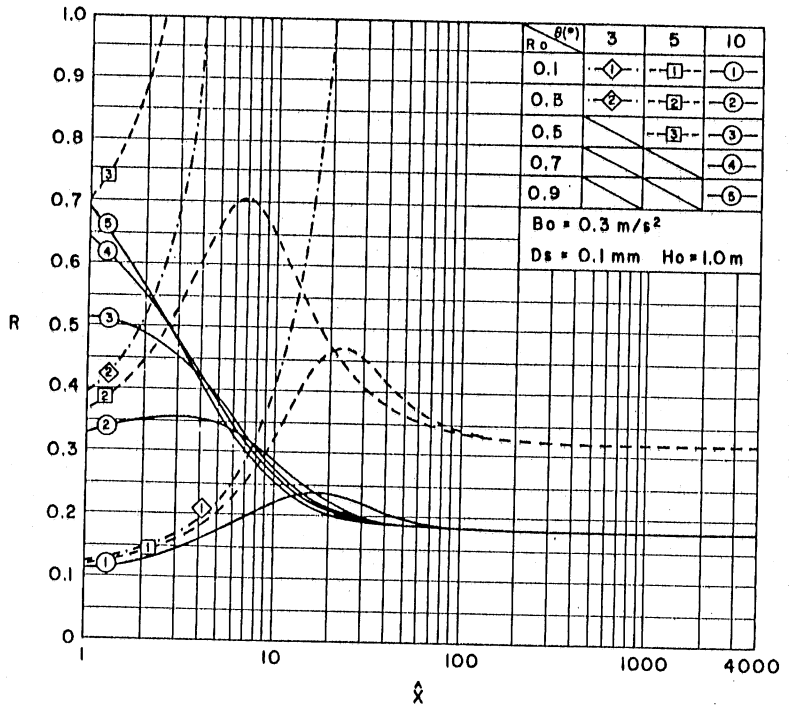

(c) D_s = 0.10mm, B_o = 0.3m/s², H_o = 1.0m

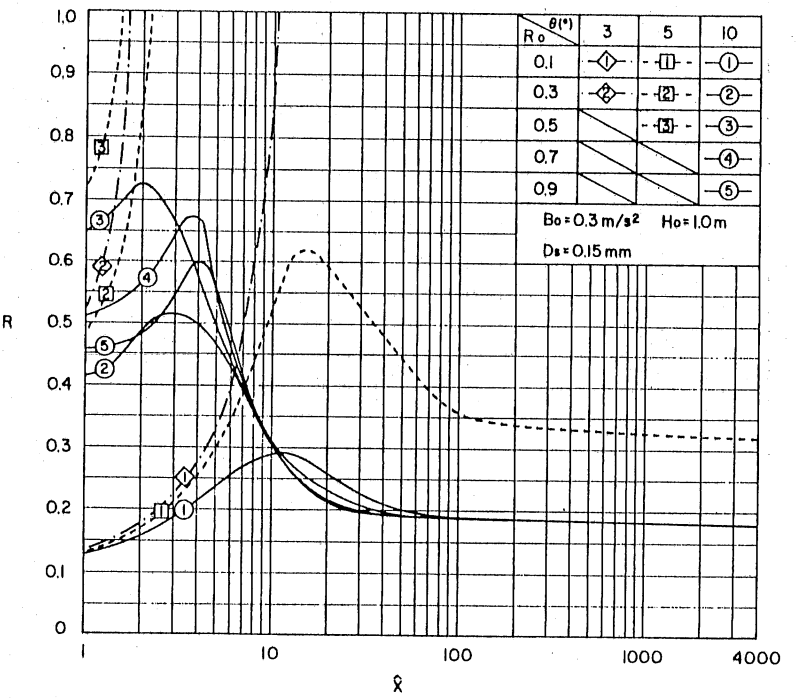

(d) D_s = 0.15mm, B_o = 0.3m/s², H_o = 1.0m

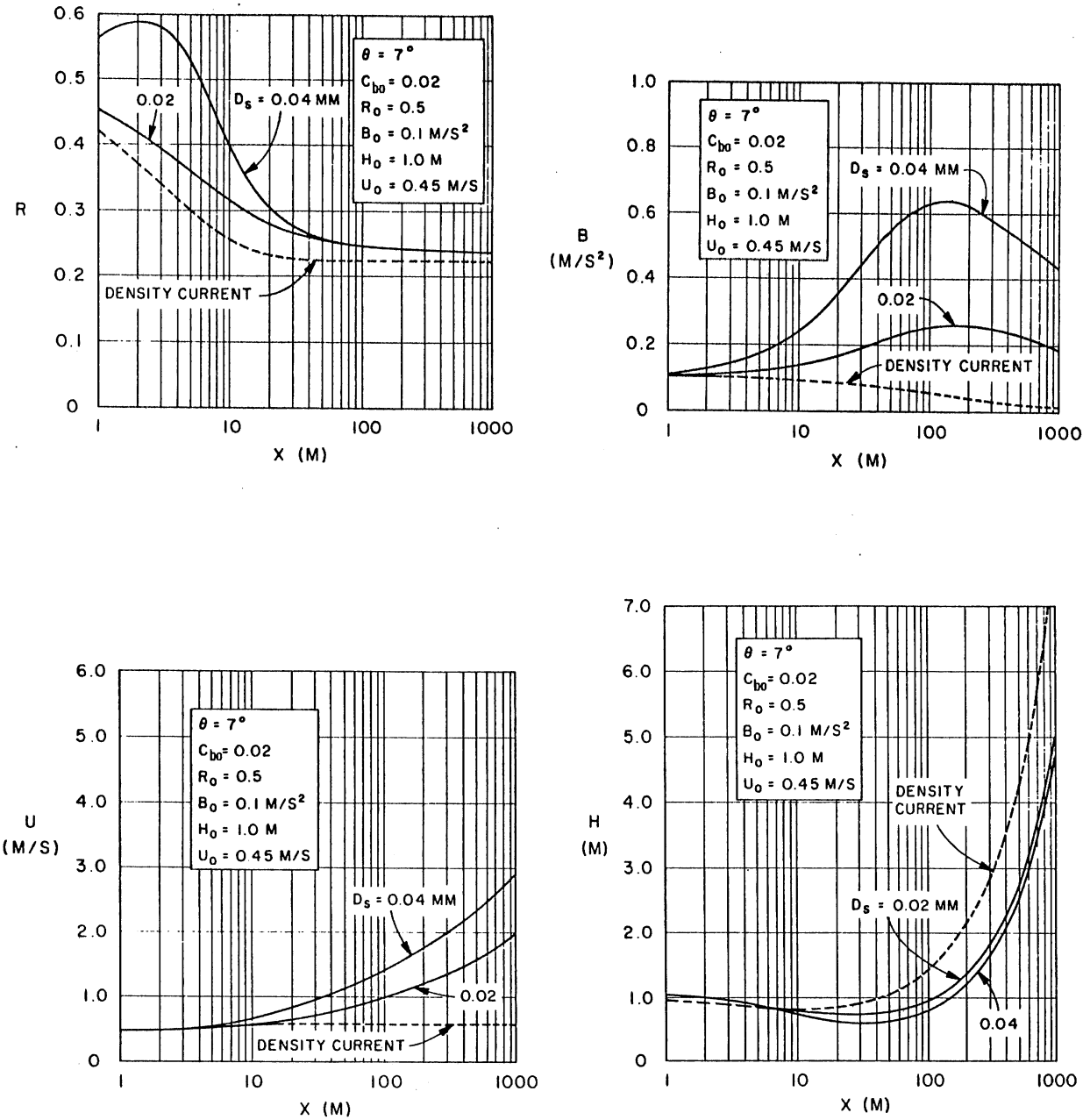

Fig. 4-21 Effect of sediment particle size, (D_s) ($\theta = 7^o$, $R_o = 0.5$, $B_o = 0.1 m/s^2$, $H_o = 1.0m$).

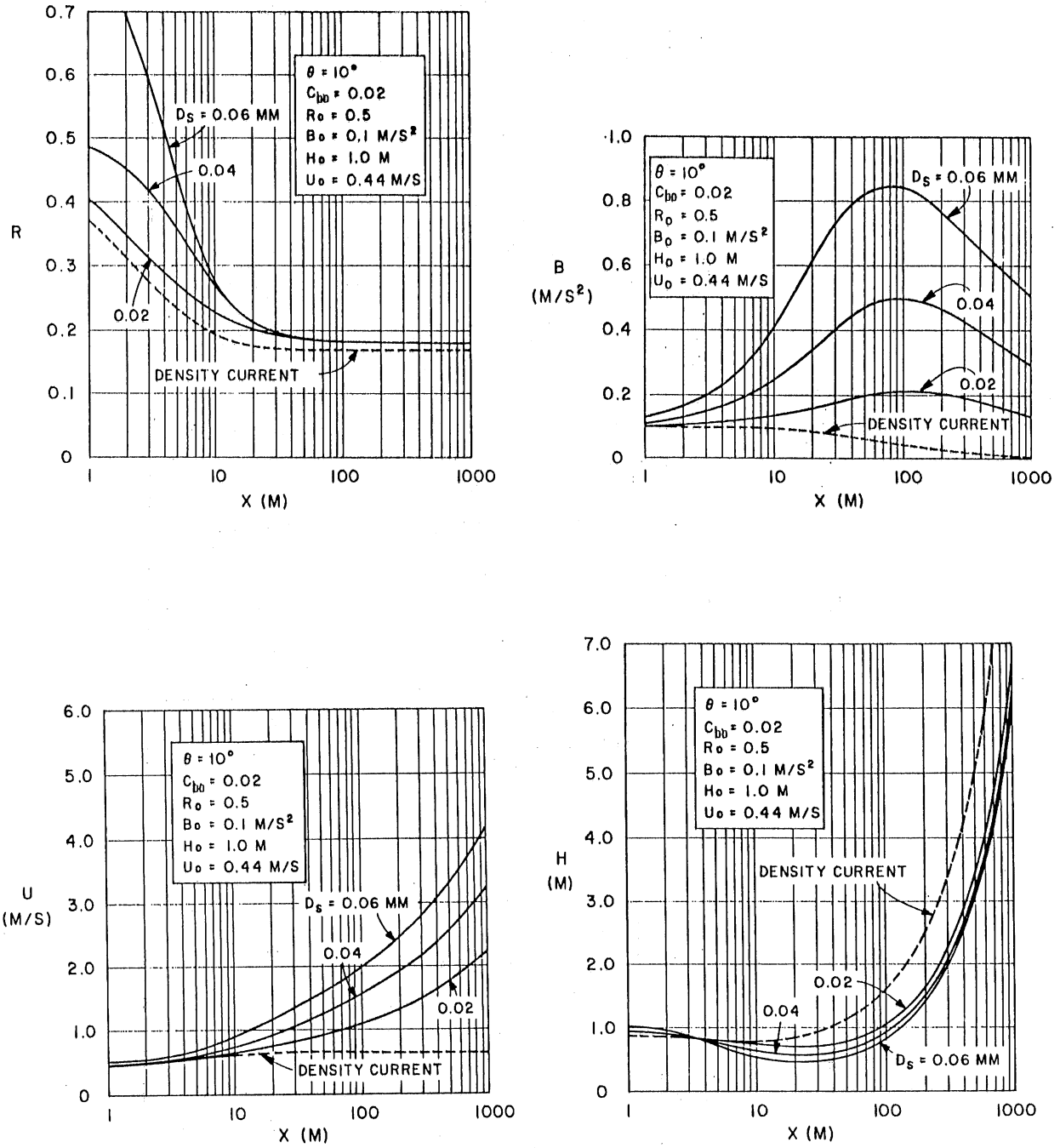

Fig. 4-22 Effect of sediment particle size, (D_s) ($\theta = 10^o$, $R_o = 0.5$, $B_o = 0.1 m/s^2$, $H_o = 1.0m$).

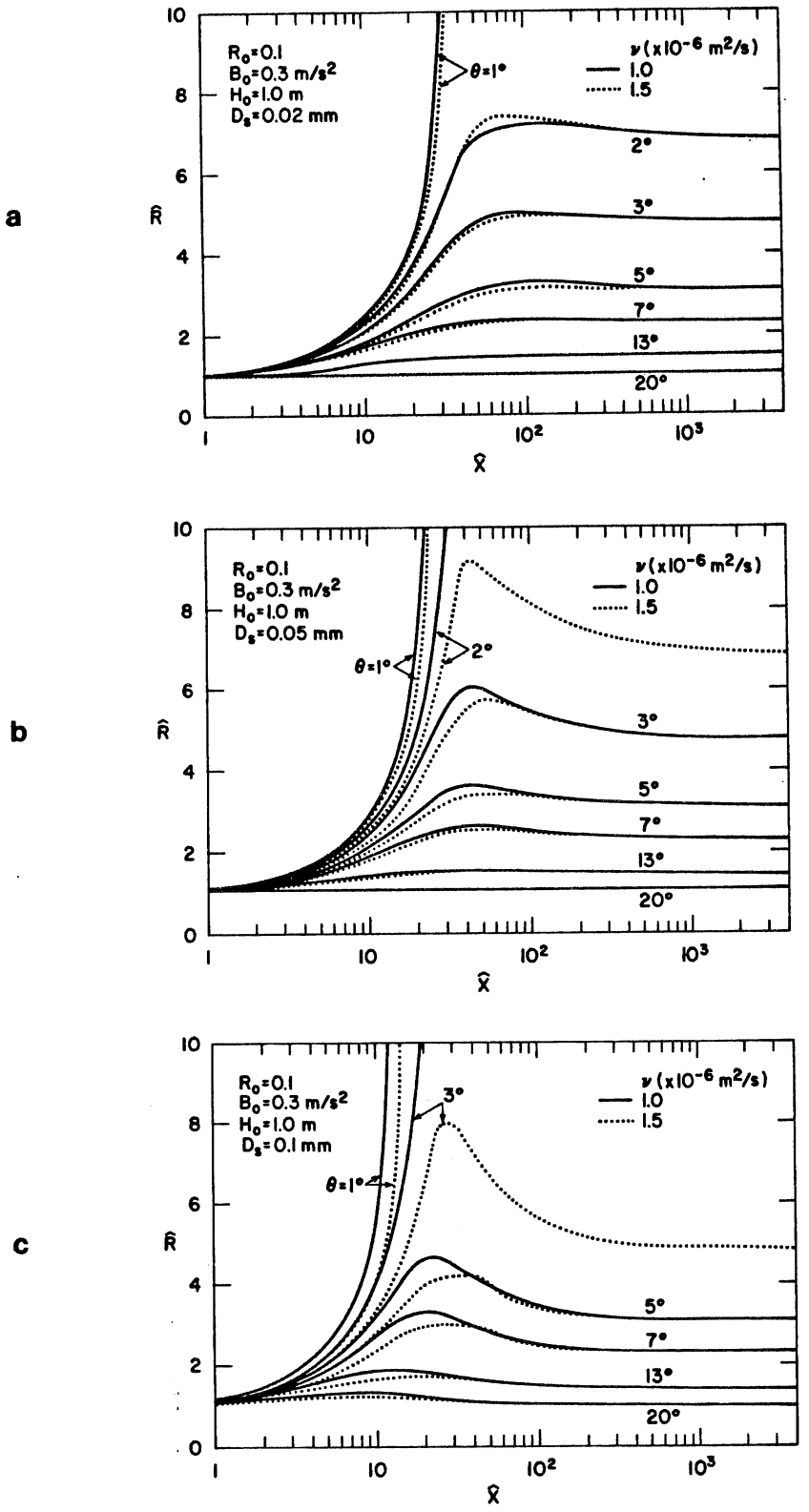

Fig. 4-23 Effect of sediment particle size (D_s) and viscosity (υ) for different θ .

d

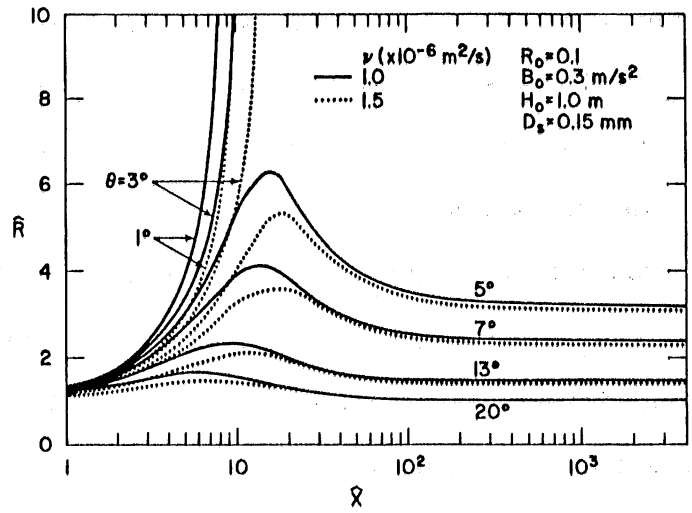
ν (x10⁻⁶ m²/s)
1.0
1.5
R₀=0.1
B₀=0.3 m/s²
H₀=1.0 m
Dₛ=0.15 mm
θ=3°
1°
5°
7°
13°
20°
R̂
X̂

e

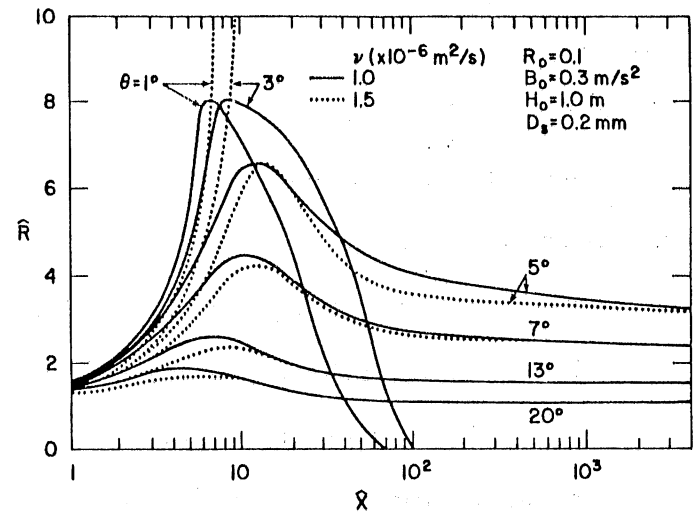
ν (x10⁻⁶ m²/s)
1.0
1.5
R₀=0.1
B₀=0.3 m/s²
H₀=1.0 m
Dₛ=0.2 mm
θ=1°
3°
5°
7°
13°
20°
R̂
X̂

f

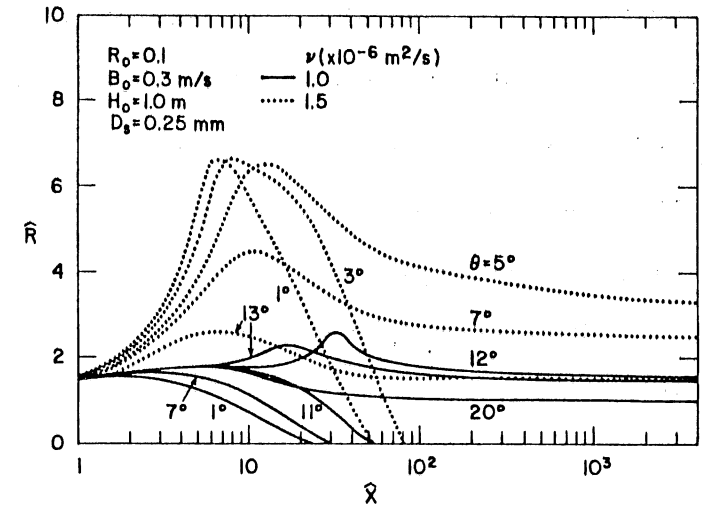
R₀=0.1
B₀=0.3 m/s
H₀=1.0 m
Dₛ=0.25 mm
ν (x10⁻⁶ m²/s)
1.0
1.5
θ=5°
3°
1°
13°
7°
12°
7°
1°
11°
20°
R̂
X̂

Subcritical turbidity currents can pass through an internal hydraulic jump with sediment exchange. This has not been investigated yet. It is difficult to conclude at this stage that subcritical currents can be erosive or depositive, although it is most likely that they are depositive.

Subcritical turbidity currents must be of the decelerating type, because it is impossible that subcritical currents become supercritical by entraining sediments from the bed provided that the bed slope remains constant in the flow direction.

The turbidity currents flowing over a bed of constant slope are of the following types:

a) Subcritical Currents

Decelerating depositive

b) Supercritical Currents

Decelerating Depositive (e.g., Fig. 4-15)

Decelerating Erosive (e.g., Fig. 4-14)

(Supercritical → Jump → Subcritical)

Accelerating Erosive (e.g., Fig. 4-11)

All currents except accelerating erosive turbidity currents will vanish somewhere downstream. Accelerating erosive turbidity currents will grow in flow direction. When the bed slope changes from steep to mild turbidity currents (Fig. 1-1) are:

a) Subcritical Currents

Decelerating Depositive

b) Supercritical Currents

Decelerating Depositive → vanish

Decelerating Erosive

(Supercritical → Jump → Subcritical)

Accelerating Erosive.

4.9 Conclusions

Spatially varied turbidity currents with erosion and deposition of sediment are simulated. The model is fundamentally the extension of Ellison and Turner's [1959] formulation.

The model presented includes and quantifies all mechanisms which control accelerating and decelerating turbidity currents, such as the cause of turbite deposits, submarine canyons, and other subsurface factors. Whether the flow of a turbidity current made of uniform particles increases in speed or not is dependent on three factors: (1) initial conditions (H_o, B_o, R_o); (2) the size of suspended sediment particle (D_s): the viscosity of water (υ) and (3) the channel slope (θ). The situation varies dependent on these parameters. For example, the flow on a mild slope will accelerate when intial buoyancy force is large enough, but will decelerate when it is not, under otherwise the same conditions, i.e., particle size, bottom slope, initial layer thickness, and Richardson number.

The model can explain clearly the differences and the similarities between gravity currents and erosive and depositive turbidity currents. The main conclusions are:

(1) The buoyancy flux (UBH) is not constant in erosive/depositive turbidity currents;

(2) In turbidity currents Richardson number will asymptotically approach nearly the same constants as density currents. In particular, the magnitudes of the final Richardson number are almost identical. This occurs because the effects of settling of suspended materials and of entrainment in large scale flow become unappreciable, as the result of acceleration.

(3) The buoyancy force in a turbidity current does not decrease as rapidly as in the case of ordinary density currents because of supply of sediment from the bed for high velocity turbidity currents (even decelerating cases).

(4) There are three basic types of turbidity currents: (a) accelerating-erosive; (b) decelerating-erosive; and (c) decelerating depositive turbidity currents. The buoyancy flux (B_f) increases for type (a), decreases for type (b) and (c). In underflows B_f remains constant.

(5) The method outlined in this chapter is the starting point for the analysis of complicated problems, caused by turbidity currents, such as engineering design of mine tailing disposal and reservoir sedimentation. The depositional or erosive features are presented in the model. This is an extension of the state-of-the-art of subsurface or reservoir flow models. With this feature it is possible, e.g., to analyze where along its path a turbidity current will deposit material and where it will occur.

5. GRADUALLY VARIED EROSIVE AND DEPOSITIVE TURBIDITY CURRENTS IN A DIVERGING CHANNEL

5.1 Introduction

Turbidity currents are normally non-uniform and in disequilibrium as they travel over the sloping bed. Imbalance in sediment concentration makes turbidity currents erosive or depositive, accelerating or decelerating. Consequently, the initial buoyancy flux of the flow is usually not conserved. Mechanics of such turbidity currents occurring in constant width channels without side wall frictions were investigated in Chapter 4.

Herein, the model is extended to a laterally expanding turbidity current. The effects of side wall frictions, channel divergence, and initial channel aspect ratio on the mechanics of the flow are investigated in both turbidity currents and underflows.

Aggradation and degradation of the channel bed by the expanding turbidity current is also simulated.

5.2 Definitions

Natural channels or basins in which turbidity currents occur often change both width and cross-sectional shape. A simplified geometry of such a three-dimensional channel has a rectangular cross-section and is diverging as shown in Fig. 5-1.

Reservoirs and lakes in which turbidity currents form often gradually expand in flow direction (Akiyama and Stefan [1987]). In the ocean, turbidity currents often flow down within submarine canyons (Inman et al. [1976]), which are diverging. When a channel is slightly

widening, the physics of the turbidity currents are different from a constant width channel. Nevertheless, the entrainment functions for water and sediment, used for two-dimensional turbidity currents, can be applied in first approximation.

In this analysis, the sediment exchange between the flow and the bed is taken into account, but the erosion from the banks (side walls) is not included. Since, the time scale of bank erosion is often much greater than that of the bed erosion side walls are treated as rigid boundaries, while the bed is a loose boundary. The channel considered herein is also assumed to be deep enough so that turbid water will not overflow

Under these circumstances, the flow physics of an erosive-depositive turbidity current, made of uniform suspended material without bed load is controlled by the following parameters: bed slope (θ), side wall (δ), kinematic viscosity of water (υ), particle size (D_s) and submerged specific density of sediment particle (σ), and initial conditions such as (depth (H_o), width (W_o), layer averged buoyancy force (B_o), overall Richardson number (R_o)), and friction coefficient (C_b) at the bottom and (C_w) at the walls. The coordinate system used in this analysis and some of the important parameters of the problem are shown in Fig. 5-2.

Similar to the non-diverging case (Akiyama and Stefan [1985, 1986]), boundary and Boussinesq's approximations are made for the sediment transport (diffusion) equation and the equations of motion (x-, y-, and z-component). The scaling conditions of the governing equations for slightly diverging flows are:

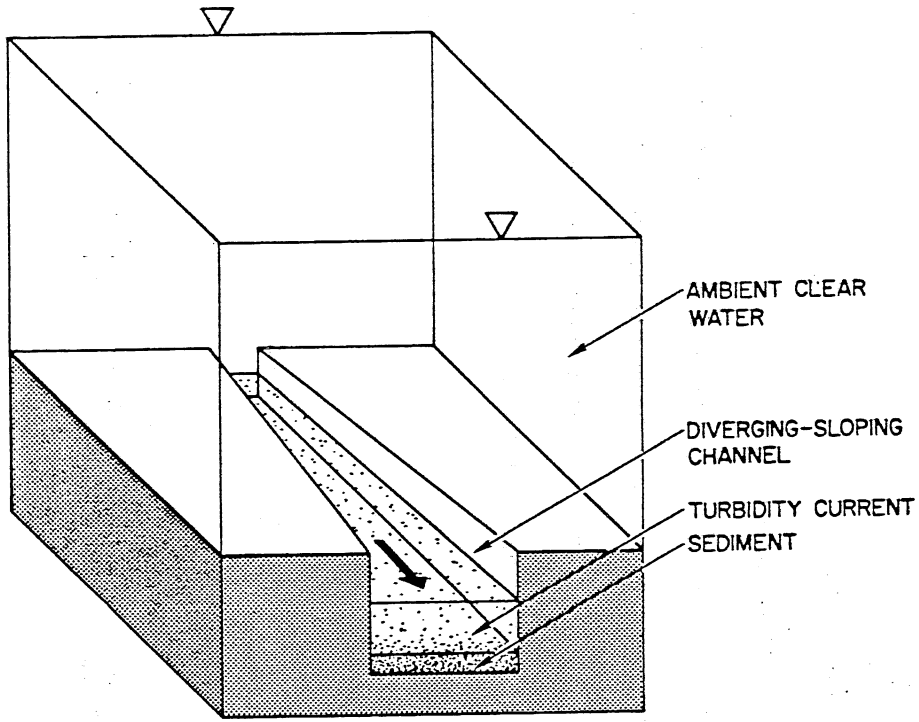

Fig. 5-1
Schematic of turbidity current in a slightly diverging and sloping channel.

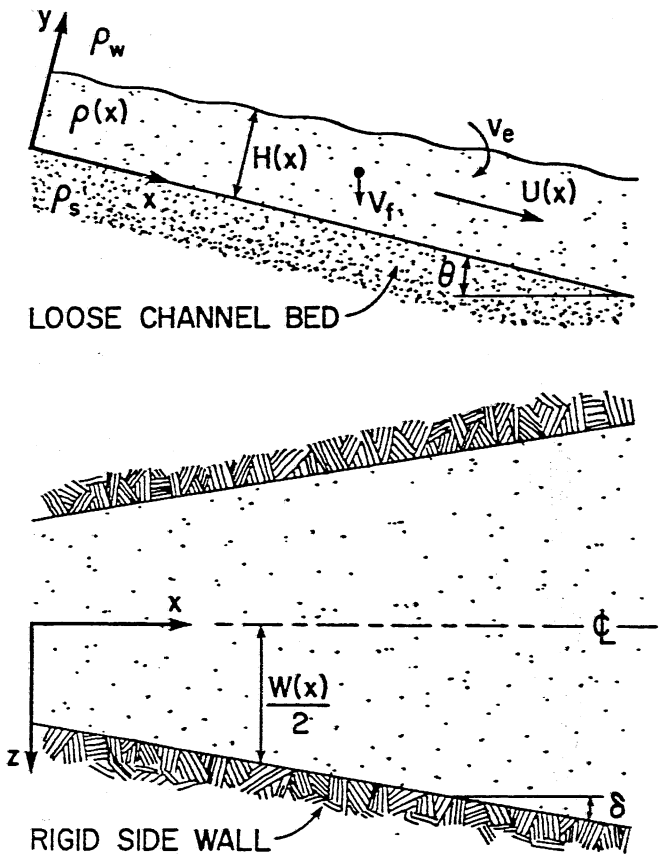

Fig. 5-2 Definition sketch.

$$O[\frac{d(W(x)/2)}{dx}] \sim O[\frac{dH(x)}{dx}] << 1,$$

and

$$O[u]' \sim O[v'] \sim O[w'] \sim O[u_*],$$

where W(x) is the channel width, H(x) is the flow depth, u', v', and w' are fluctuating velocity components, and u_* is the shear velocity. The scaling condition above implies that the flow depth is independent of transverse (z) direction.

5.3 Analysis

5.3.1 Governing Equations

The governing three-dimensional equations of a steady-state turbidity current in a slightly diverging sloping channel including boundary and Boussinesq's approximations are:

(a) Continuity equation

$$\frac{\partial u}{\partial x} + \frac{\partial v}{\partial y} + \frac{\partial w}{\partial z} = 0 \qquad 5\text{-}1$$

(b) Diffusion equation

$$\frac{\partial ub}{\partial x} + \frac{\partial}{\partial y}(v - V_f\cos\theta) + \frac{\partial wb}{\partial z} = - \frac{\partial \overline{v'b'}}{\partial y} - \frac{\partial \overline{w'b'}}{\partial z} \qquad 5\text{-}2$$

(c) Momentum equation in x-direction

$$u\frac{\partial u}{\partial x} + v\frac{\partial u}{\partial y} + w\frac{\partial u}{\partial z} = -\frac{\partial}{\partial x}\int_y^\infty b\cos\theta\, dy + b\sin\theta +$$

$$\frac{1}{\rho_w}\left(\frac{d\tau_y}{dy} + \frac{d\tau_z}{dz}\right) \qquad 5\text{-}3$$

In the preceeding equations, x, y, and z = longitudinal, vertical, and transverse coordinates respectively, u, v, and w = velocity components, V_f = particle settling velocity, ρ_w = density of water, and τ_y, τ_z = shear stesses. Fluctuating components are designated by primes. b is the reduced gravity (buoyancy) force defined by:

$$b = \frac{\rho - \rho_w}{\rho_w} g \qquad 5\text{-}4$$

The density of the suspension ρ is related to concentration of suspended sediment c , density of solids ρ_s and density of water ρ_w. Using a normalized ($0 \leq c \leq 1$) concentration

$$\rho = \rho_w(1 + \sigma c) \qquad 5\text{-}5$$

where σ is the specific gravity of submerged sediment particles defined by:

$$\sigma = \frac{\rho_s - \rho_w}{\rho_w} \qquad 5\text{-}6$$

Thus b becomes:

$$b = \sigma g c \qquad 5\text{-}7$$

(d) Geometric relationship

The growth rate of the flow in z-direction is determined solely by the geometry of the channel proved that δ is small and the flow is attached to both side walls. The flow width (W(x)) is, therefore, given by:

$$W = W_o + 2x\tan\delta \qquad 5\text{-}8$$

where W_o is an initial channel width. Subscipt o denotes properties of initial point.

5.3.2 Integrated Governing Equations over the Cross-Section

Integrating Eqs. 5-1 to 5-3 in the y- and z-directions, and using the same relationships as in two-dimensional turbidity currents (Chapter 4), one obtains:

(a) Conservation of volume

$$\frac{d}{dx}(f_1 WHU) = Wv_e = WE_w U \qquad 5\text{-}9$$

(b) Conservation of buoyancy flux

$$\frac{d}{dx}(f_2 BHUW) = WV_f(E_s^* - b_a \cos\theta) \qquad 5\text{-}10$$

(c) x-Momentum equation

$$\frac{d}{dx}(f_3 WU^2 H + \frac{S_1}{2} WBU^2 H \cos\theta) = S_1 BH^2 \frac{d(W/2)}{dx}\cos\theta +$$

$$S_2 WBH\sin\theta - \frac{W}{\rho_w}\tau_b + \frac{2H}{\rho_w}\tau_w \qquad 5\text{-}11$$

In the preceeding Equations v_e = entrainment velocity, E_w = entrainment function for water, b_a = buoyancy force at y = a, and E_s^* = sediment entrainment function for buoyancy force. Herein, E_s^* is defined by:

$$E_s^* = E_s \sigma g \qquad 5\text{-}12$$

where E_s is the sediment entrainment function defined by Eq. 3-22. The lower limit of vertical integration is chosen to be y = a in Eq. 5-10. This implies that the sediment storage in the thin layer between y = 0 and a is negligible. This assumption requires that $a/H \ll 1$. a = 0.05H is selected in order to meet this requirement. E_s is, therefore, the sediment entrainment function estimated at y = 0.05H.

Define the shear stress (τ_b) at the bottom and (τ_w) at the wall as:

$$\tau_b/\rho_w = \tau_{bo} + \tau_{b2} = (C_{bo} + S_2 R(\frac{V_f}{U}))U^2 \qquad 5\text{-}13$$

$$\tau_w/\rho_w = - C_{wo}U^2 \qquad 5\text{-}14$$

The first term of the right-hand side term of Eq. 5-13 is due to the pure friction shear stress (τ_{bo}) at the bed. The second term of the right-hand side term of Eq. 5-13 is equivalent to Bagnold's auto-suspension term (Bagnold [1962]), which is obtained from a simple energy balance. In this analysis, Bagnold's term is treated as an additional shear stress (τ_{b2}) due to the diffused sediment material in the momentum equation. The presence of bed forms are ignored in anlysis as clearly can be indicated in Eq. 5-13. The x-momentum equation hence becomes:

$$\frac{d}{dx}\{f_3WU^2H + \frac{S_1}{2}WBH^2\cos\theta\} = S_1BH^2\frac{d(W/2)}{dx}\cos\theta + S_2WBH\sin\theta -$$

$$W(C_{bo} + \frac{2}{A}C_{wo} + S_2R(\frac{V_f}{U}))U^2 \qquad 5\text{-}15$$

Where A is the channel aspect ratio defined by $A(x) = W(x)/H(x)$. The behavior of a turbidity current in a slightly diverging-sloping channel is described by Eqs. 5-8, 5-9, 5-10, and 5-15.

In equation 5-15, the difference between the non-diverging and diverging gravity current are distinguished by the term such as $S_1BH^2\frac{d(W/2)}{dx}\cos\theta$, which repesents the reaction force from the wall to the fluid, and the term $2HC_{wo}U^2$, which represents the shear stress at the walls. Herein, cross-sectionally averaged properties are denoted by capital letters. Shape factors f_1 through f_3 and S_1 and S_2 are

introduced to account for non-uniformity of velocity and density distributions. They are defined as follows.

$$f_1 = (UHW)^{-1} \int_0^H \int_{-W/2}^{W/2} u\,dy\,dz \qquad 5\text{-}17$$

$$f_2 = (UBWH)^{-1} \int_0^H \int_{-W/2}^{W/2} ub\,dy\,dz \qquad 5\text{-}18$$

$$f_3 = (U^2HW)^{-1} \int_0^H \int_{-W/2}^{W/2} u^2\,dy\,dz \qquad 5\text{-}19$$

$$S_1 = (BH^2W)^{-1} \int_0^H \int_{-W/2}^{W/2} 2by\,dy\,dz \qquad 5\text{-}20$$

$$S_2 = (BHW)^{-1} \int_0^H \int_{-W/2}^{W/2} b\,dy\,dz \qquad 5\text{-}21$$

For the shape factors (f_1, f_2, f_3, S_1, S_2) defined above, the lower integral limit is approximated as $y = a = 0$.

To close the problem, additional relationships are required for water entrainment function (E_w). sediment entrainment function (E_s), sediment concentration near the bed (c_a), settling velocity of sediment particle (V_f), friction coefficient at the bed and side walls (C_{bo}, C_{wo}).

5.3.3 Gradually Varied Flow Equations for a Turbidity Current in a Slightly Diverging Sloping Channel

The vertically and horizontally integrated governing equations (Eqs. 5-9, 5-10, 5-15) and other equations, together with the geometric relationship (Eq. 5-8) are developed into the following gradually varied flow equations.

$$\frac{H}{3R}\frac{dR}{dx} = \frac{\frac{1}{f_1}\left(1 + \frac{S_1}{2f_3}R\right) E_w - \frac{S_2}{f_3}R\tan\theta + \frac{C_{bo}}{f_3}}{1 - \frac{S_1}{f_3}R} +$$

$$\frac{\left\{\left(1 + \frac{S_1}{2f_3}R\right)\frac{1}{3f_2}\frac{(E_s^* - b_a\cos\theta)}{B} + \frac{S_2}{f_3}R\right\} V_f\left(\frac{R}{BH\cos\theta}\right)^{1/2}}{1 - \frac{S_1}{f_3}R} +$$

$$\frac{\left\{-\frac{2}{3}\left(1 + \frac{2S_1}{f_3}R\right)\sin\delta + \frac{2C_{wo}}{f_3}\right\}\frac{H/W_o}{1 + 2(x/W_o)\sin\delta}}{1 - \frac{S_1}{f_3}R} \qquad 5\text{-}22$$

$$\frac{dH}{dx} = \frac{\frac{E_w}{f_1}(2 - \frac{S_1}{2f_3}R) - \frac{S_2}{f_3}R\tan\theta + \frac{C_{bo}}{f_3}}{1 - \frac{S_1}{f_3}R} +$$

$$\frac{\frac{R}{f_2}V_f(\frac{R}{BH\cos\theta})^{1/2}(\frac{S_1}{2f_3}\frac{(E_s^* - b_a\cos\theta)}{B} + \frac{f_2S_2}{f_3})}{1 - \frac{S_1}{f_3}R} +$$

$$\frac{(-2\sin\delta + \frac{2C_{wo}}{f_3})\frac{H/W_o}{1 + 2(x/W_o)\sin\delta}}{1 - \frac{S_1}{f_3}R} \qquad 5\text{-}23$$

The second and third terms of the right-hand side of Eq. 5-22 and 5-23 are the effects of erosion/deposition, and of channel divergence on the underflow, respectively. The buoyancy force equation becomes:

$$\frac{dB}{dx} = -\frac{B}{H}\frac{E_w}{f_1} + \frac{V_f}{f_2}\frac{(E_s^* - b_a\cos\theta)}{H}(\frac{R}{BH\cos\theta})^{1/2} \qquad 5\text{-}24$$

The relationship between dH/dx and dR/dx is derived as:

$$\frac{dH}{dx} = \frac{E_w}{f_1} + \frac{H}{3R}\frac{dR}{dx} -$$

$$\frac{1}{3}\{4\frac{H/W_o}{1 + 2(x/W_o)\sin\delta}\sin\delta + \frac{V_f}{f_2}(\frac{R}{BH\cos\theta})^{1/2}(\frac{E_s^* - b_a\cos\theta}{B})\} \qquad 5\text{-}25$$

In the derivations above, the approximation $\frac{d(W/2)}{dx} = \tan\delta \sim \sin\delta$ is used.

The behavoir of a turbidity current in a slightly diverging channel is more complicated than that in a non-diverging channel. The most significant aspect of the flow is the dependence on the parameters such as H/W_o and x/W_o. Small parameters such as $\sin\delta$ and V_f/U influence and modify, substantially, the behavoir of the current.

The effect of channel divergence on the flow vanishes if the channel is initially very wide ($A_o \to \infty$) or if the flow progresses very far downstream ($x/W_o \to \infty$).

5.3.4 Aggradation and Degradation due to Turbidity Currents with Erosion and Deposition

The bed elevation (η_b) of a channel in which a turbidity current is flowing can be aggrading and degrading due to erosion or deposition similar to sediment transport in open channel hydraulics (e.g., Graf [1971]). The bed slope is gradually modified by the currents. In turn, a change of the bed elevation will affect the behavior of the turbidity currents when continuous turbidity currents are produced for a certain time interval. In this sense, the sediment bed and the flow are coupled.

Assuming that the bed elevation is changed only by deposition or resuspension of suspended sediment in a turbidity current, the sediment continuity equation for a channel of variable width is given by:

$$\frac{d\eta_b}{dt} = -\frac{1}{W(1-\lambda)}\frac{d(q_s W)}{dx} \qquad 5\text{-}26$$

where λ is the bed porosity. η_b is the bed elevation from an original bed. q_s is the sediment discharge per unit width ($= f_2 CHU$). From Eqs. 5-10 and 5-26,

$$\frac{d\eta_b}{dt} = \frac{V_f}{1-\lambda}(c_a \cos\theta - E_s) \qquad 5\text{-}27$$

If the time interval (Δt_s) for the occurence of a continuous turbidity current is expected to be long enough to satisfy the condition:

$$\Delta t_s >> \Delta t = \frac{1}{1-\lambda}\frac{V_f}{\Delta\eta_b}(c_a \cos \quad - E_s) \qquad 5\text{-}31$$

then the bed slope changes sufficiently to affect the behavoir of the turbidity current.

According to Eq. 5-28, the following conditions can be distinguished:

(a) Aggradation — Depositing Current

$$\frac{d\eta_b}{dt} > 0 \quad \text{when} \quad c_a \cos\theta > E_s \qquad 5\text{-}28$$

(b) Degradation — Eroding Current

$$\frac{d\eta_b}{dt} < 0 \quad \text{when} \quad c_a \cos\theta < E_s \qquad 5\text{-}29$$

5.4 Sample Calculations

The physics of an erosive and depositive turbidity current made of uniform material in a slightly diverging and sloping channel are controlled by the following parameters:

$$\{\delta,\ \theta,\ \upsilon,\ D_s,\ \sigma,\ A_o,\ H_o,\ B_o,\ R_o,\ C_{bo},\ C_{wo}\}$$

Among these δ, A_o, C_{wo} are unique parameters for the turbidity current in a slightly diverging-sloping channel. The effects of these three parameters on the behavoir of underflows and turbidity currents will be further examined. Equations 5-22, 5-23, 5-24, and 5-27 together with the empirical relationships for E_w, E_s, C_a, V_f, C_{bo}, and C_{wo} were solved simultaneously by using a forth order Runge-Kutta method. The calculation step ($\hat{\Delta x}$) was chosen to be 5% of the initial depth H_o until $\hat{x} = 100$, and 10% of H_o thereafter. In the numerical calculation all shape factors (f_1, f_2, f_3, S_1, and S_2) are set equal to unity (first approximation). The shape factors may not be constant with x. The model has not yet been verfified experimentally because laboratory and field data available in the literature are limited and not sufficient to determine these shape factors for a wide range of variations on both Richardson number, bed roughness, and sediment size. The model has, therefore, been used to simulate the qualitative effects of sediment erosion and deposition and of channel divergence on the flow, and on aggradation and degradation of the channel bed.

(i) Non-Suspension Gravity Currents (Underflows)

Non-suspension gravity currents will be examined for the purpose of

understanding the role of A_o and δ on the flow physics. C_{bo} and C_{wo} have been fixed at 0.02.

Figure 5-3 shows the significance of initial width (W_o) or initial channel aspect ration (A_o). A side slope $\delta = 3^o$ is chosen to illustrate this effect. The case $A_o \to \infty$ or $\delta = 0$ with $C_{wo} = 0$ corresponds to the two-dimensional underflow investigated by Ellison and Turner [1959]. No normal condition exists in underflows in a diverging channel, and the behavoir of the flow depends on A_o.

The effect of channel diverging angle (δ) is examined in Fig. 5-4. Two-dimensional underflow is represented by $A_o \to \infty$, or $\delta = 0^o$ and $C_{wo} = 0$. The condition $\delta = 0^o$ alone does not yield two-dimensional underflow, because of side wall friction. When a laterally confined two-dimensional underflow travels in the downstream direction, flow depth will increase after some point as shown in Fig. 5-4. The flow experiences more shear forces from side wall boundaries, as A_o is decreased. For a normal state the friction coefficient, flow velocity, and wetted area must be constant. However, this is not the case for the diverging underflows.

The flow sometimes cannot maintain supercritical condition, and hence an internal hydraulic jump occurs as shown in Fig. 5-4. However, such effects of the side walls may be compensated by the channel expansion. This may be seen in Eq. 5-23, where the contribution of the channel expansion is negative and proportional to the growth rate of H.

In Fig. 5-5, the effect of initial conditions for different channel bed slopes in examined. The effect of channel divergence is more obvious where bed slope is smaller. Two-dimensional underflow will

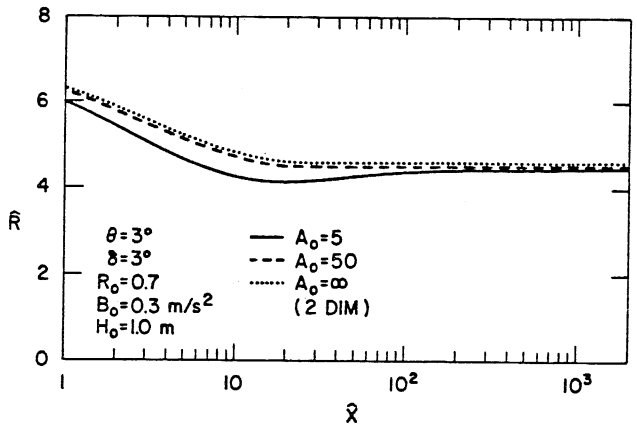

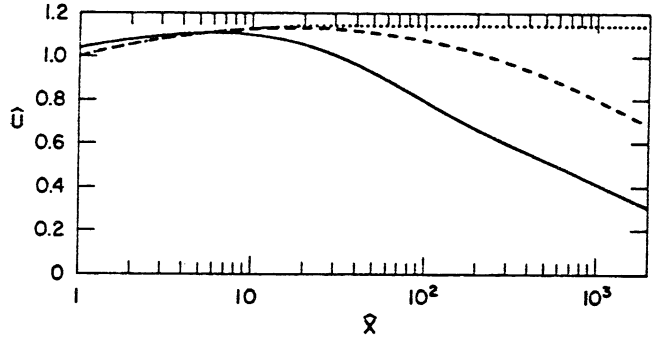

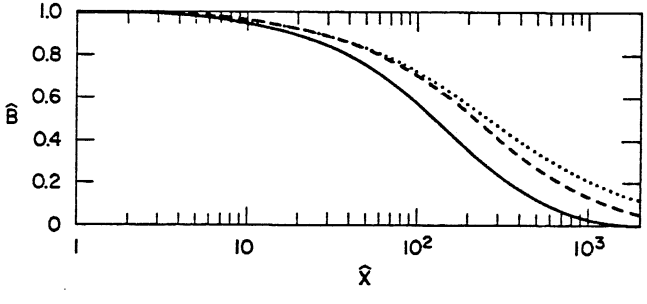

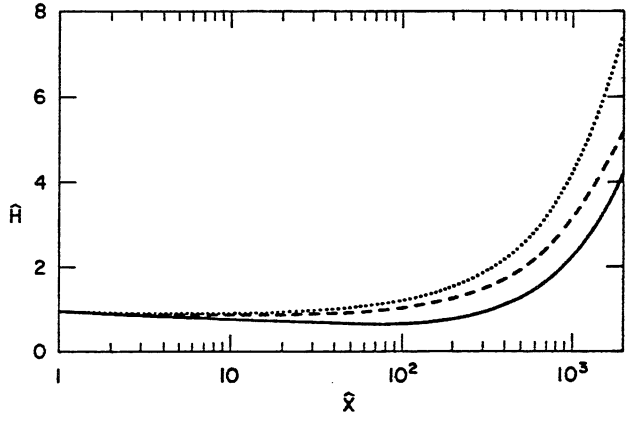

Fig. 5-3 Effects of initial aspect ratio A_o on underflows.

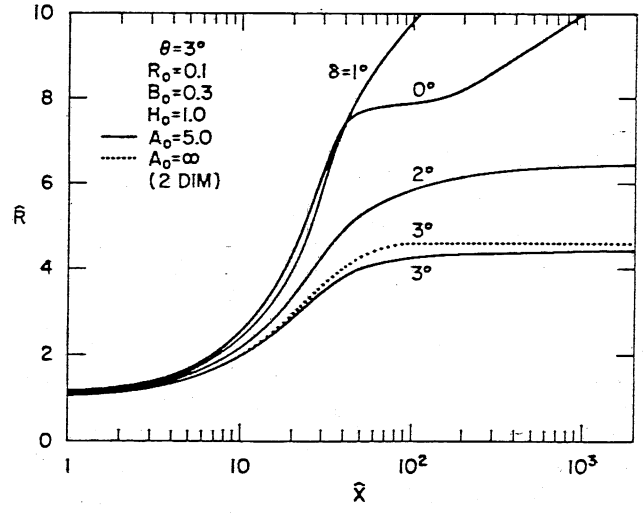

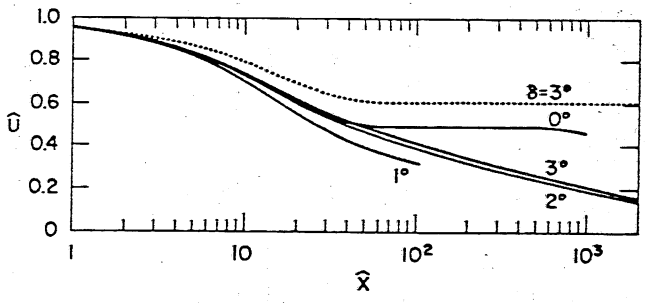

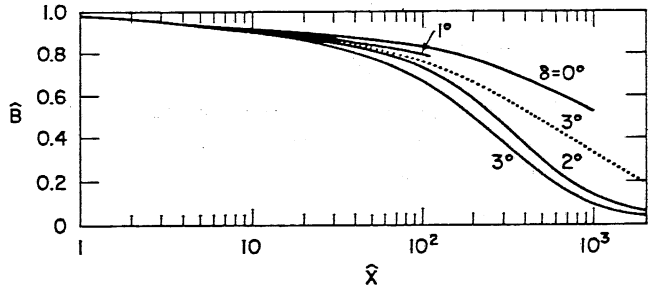

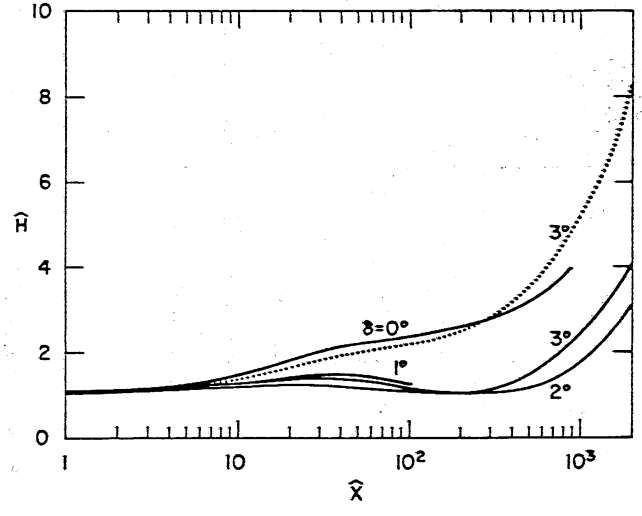

Fig. 5-4 Effects of diverging channel angle δ on underflows.

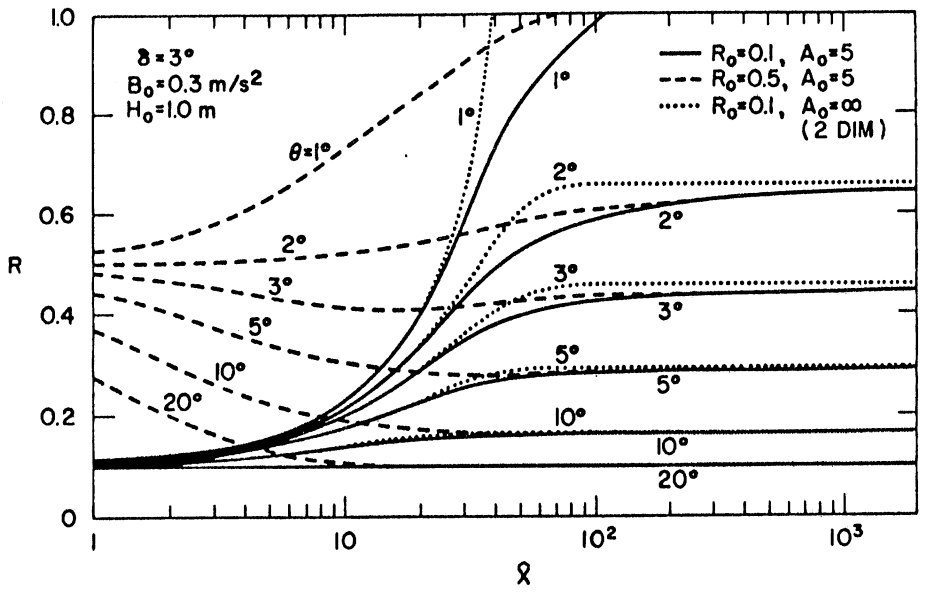

Fig. 5-5 Comparison between Richardson numbers for diverging and constant-width underflows.

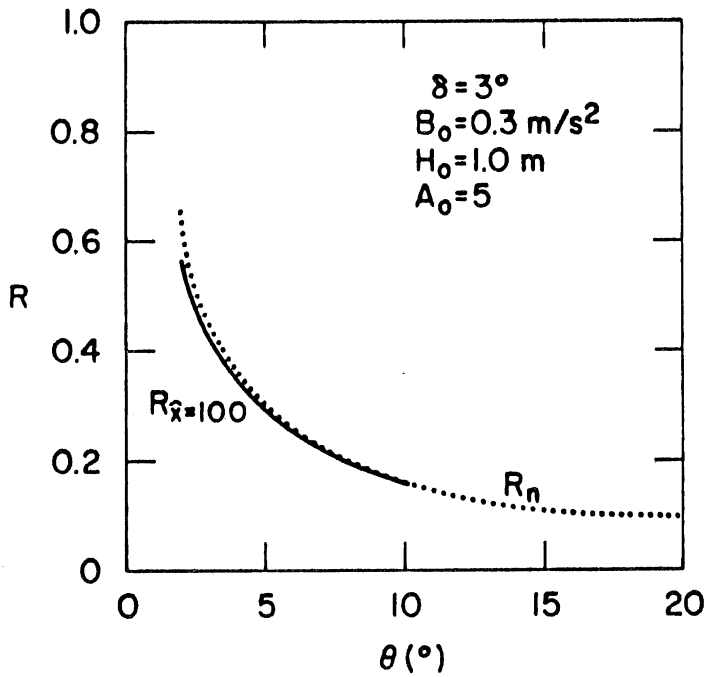

Fig. 5-6 Comparison between normal Richardson number and Richardson number at $\hat{x} = 100$ for diverging underflow and their dependences on the bed slope θ.

reach a normal state about $\hat{x} = 100$, regardless of channel bed slope. However, diverging underflow has no such state.

As can be seen in Fig. 5-6, the differences in Richardson number R at $\hat{x} = 100$ are subtle, but this does not imply that the behavoir of the currents is identical as already seen in Figs. 5-3 and 5-4.

(ii) Suspension Gravity Currents (Turbidity Currents)

The sensitivity of suspension gravity currents (turbidity currents) to several parameters will be examined. C_{bo} and C_{wo} have been fixed at 0.02. Effects of A_o are examined in Fig. 5-7. Figures 5-8 and 5-9 show the effect of channel divergence δ for two different channel bed slopes ($\theta = 3^o$ and 10^o).

Effects of initial conditions are examined in Fig. 5-10. Regardless of the difference of initial conditions, Richardson numbers become the same around $\hat{x} = 500$ even in the diverging flows when δ and θ are the same.

Figure 5-11 shows the Richarson numbers for two-dimensional turbidity currents with and without the effects of side walls. Several bottom slopes are examined.

Figure 5-12 shows the effect of particle size on erosive and depositive turbidity currents. Keeping all conditions the same except sediment particle size, the change from accelerating-erosive to decelerating-depositive currents can be seen for different channel bed slopes. For $D_s = 0.25$ mm, all flows vanish by depositing suspended sediment onto the bed on the very steep slope ($\theta = 20^o$). On a slope

$\theta = 20^{o}$ the flow still possess enough driving force to maintain erosive power.

Figure 5-13 shows that there are three types of turbidity currents in the supercritical state in a diverging channel. Type 1 is the decelerating erosive current which becomes subcritical through an internal jump (D_s = 0.15 mm), Type 2 is the accelerating erosive current which remains in the supercritcal state (D_s = 0, 0.05, and 0.1 mm), and Type 3 is the decelerating depositive current which vanishes (D_s = 0.2 and 0.25 mm). The Richardson number $\hat{R}$ for a two-dimensional underflow is also shown for composition.

Figure 5-14 demonstrates effect of water viscosity on the flow. Viscosity is changed by both concentration and the temperature of water.

Examples of supercritical depositive turbidity currents, which are important for the formation of delta due to coarse material, and of aggradation and degradation are shown in Fig. 5-15 and 5-16, respectively.

λ is a function of D_s. For the sediments under consideration (D_s = 0.05 ~ 0.25 mm) λ is about 0.3 ~ 0.5, according to data for open channel flow. λ = 0.44 is used for D_s = 0.25, based on the empirical equation proposed by Komura [1963]. In this case, the deposition of suspended sediment starts to occur around $\hat{x}$ = 110. The flow vanishes around $\hat{x}$ = 160, droping almost all sediment material onto the bed. Both deposition and erosion processes are very fast, because of the relatively large sediment size (D_s = 0.25 mm).

The depositional area (downstream) is smaller than the erosion area (upstream). This is due to channel expansion. The deposition area

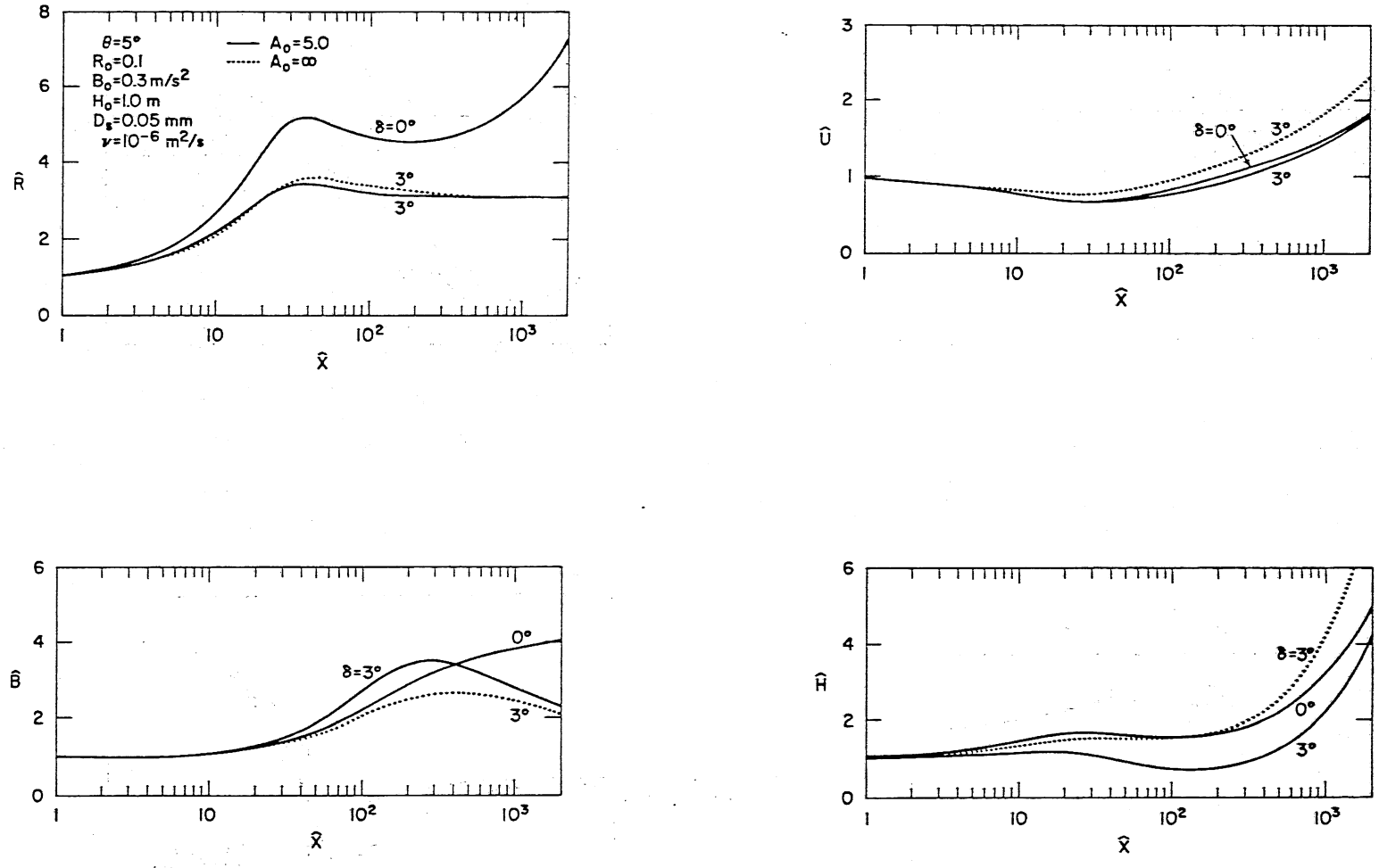

Fig. 5-7 Effects of initial aspect ratio A_o on turbidity currents.

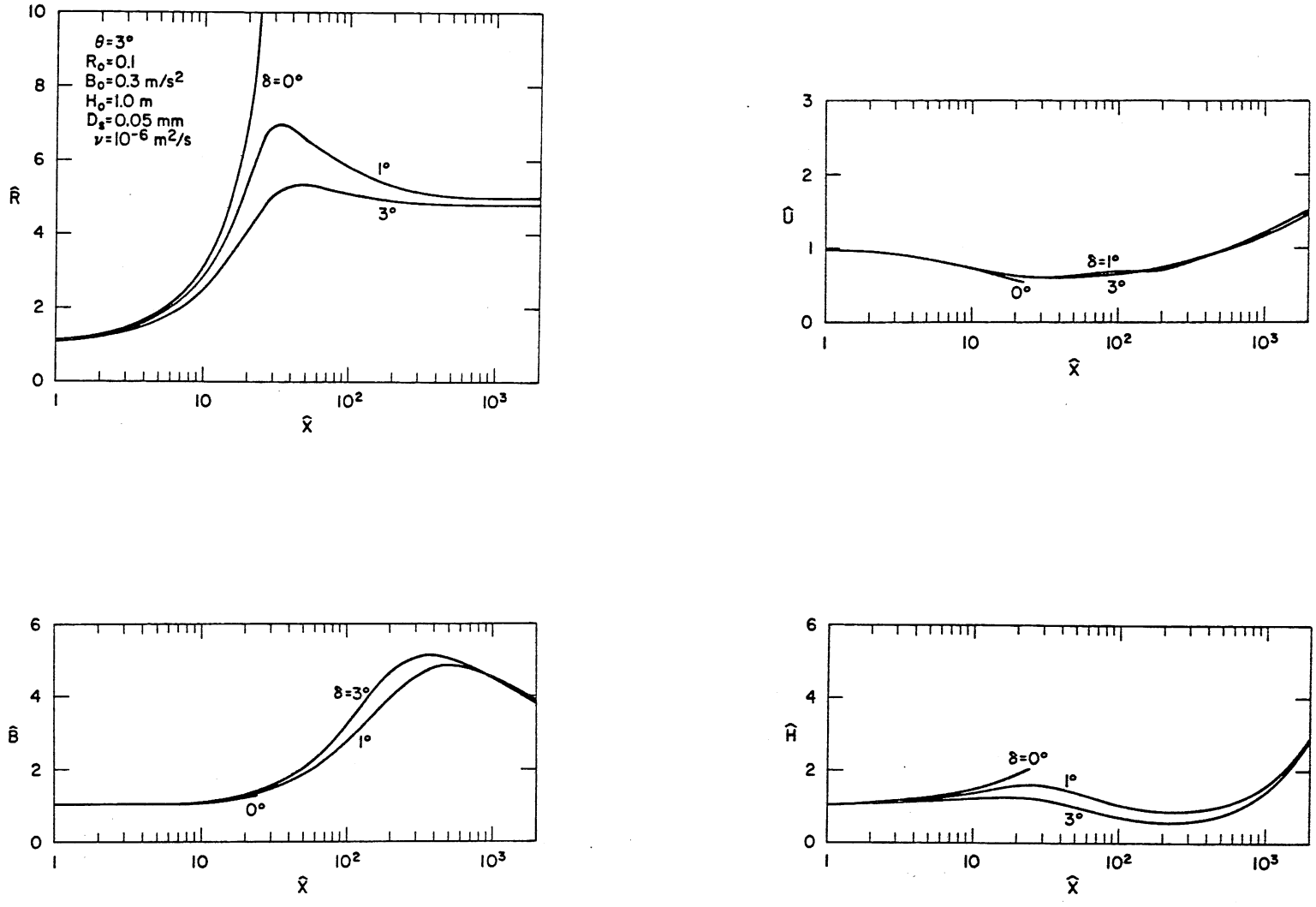

Fig. 5-8 Effects of δ on turbidity currents ($\theta = 3^{o}, D_{s} = 0.05$mm).

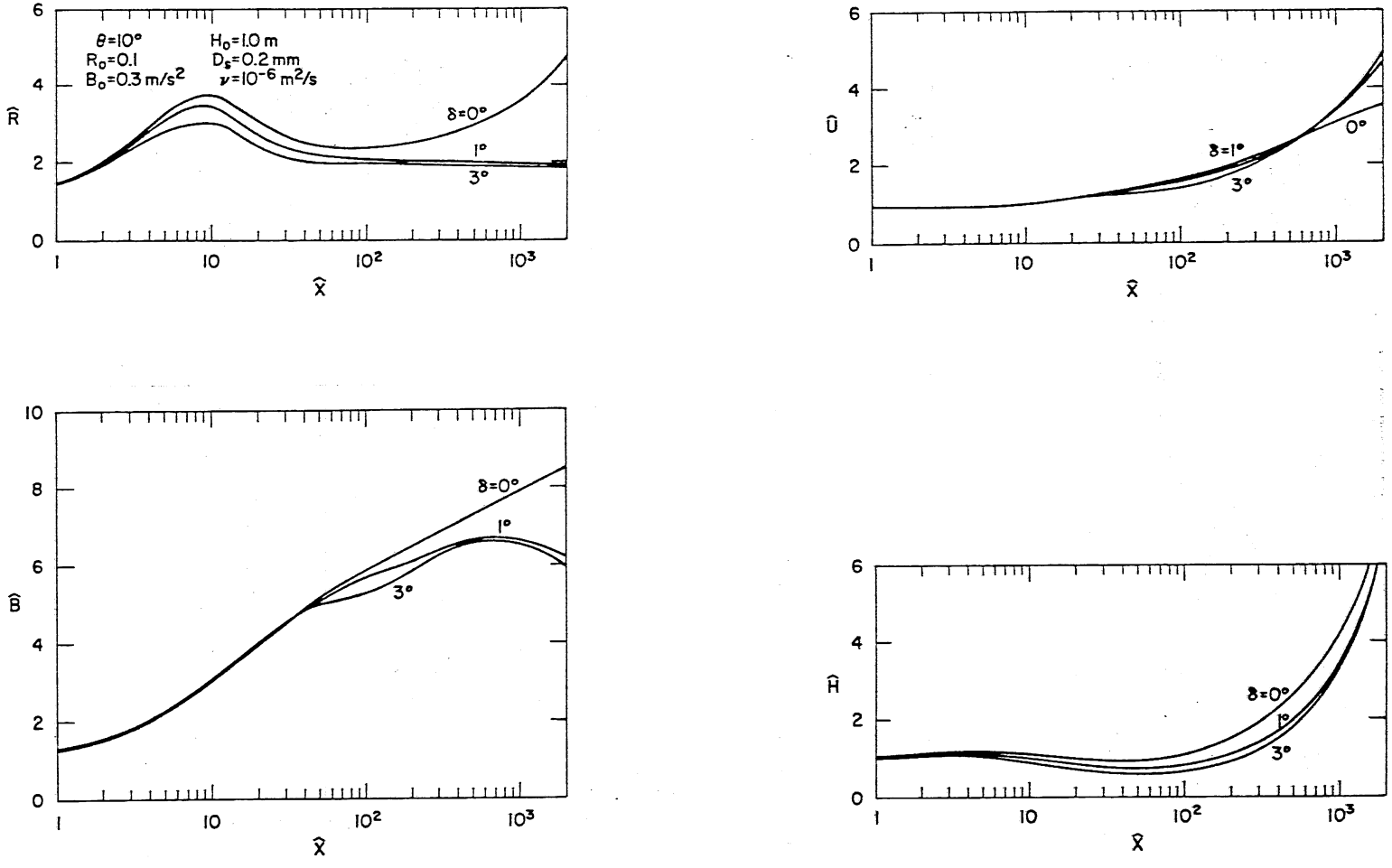

Fig. 5-9 Effects δ on turbidity current ($\theta = 10^{o}$, $D_s = 0.20$mm).

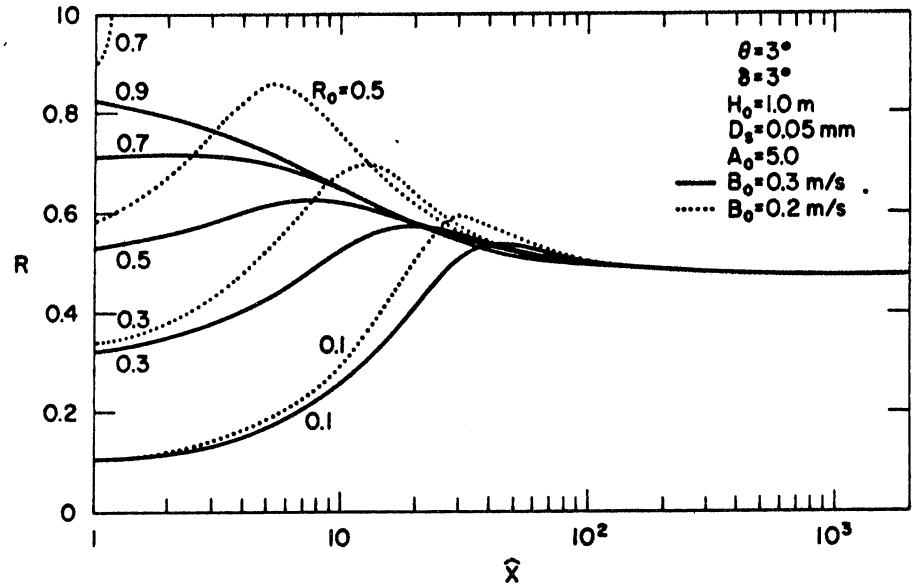

Fig. 5-10 Effect on initial conditions (R_o and B_o)

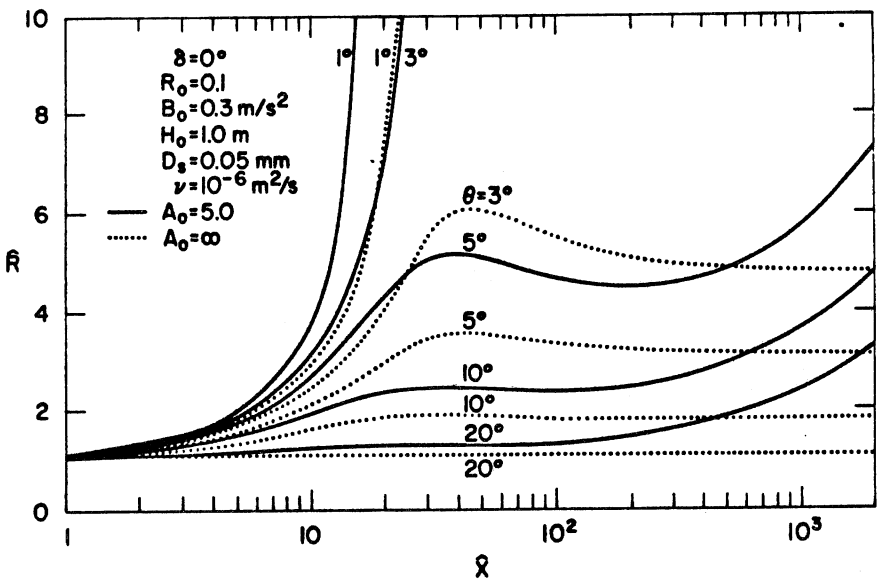

Fig. 5-11 Comparison between a constant width turbidity current with finite and with infinte A_o.

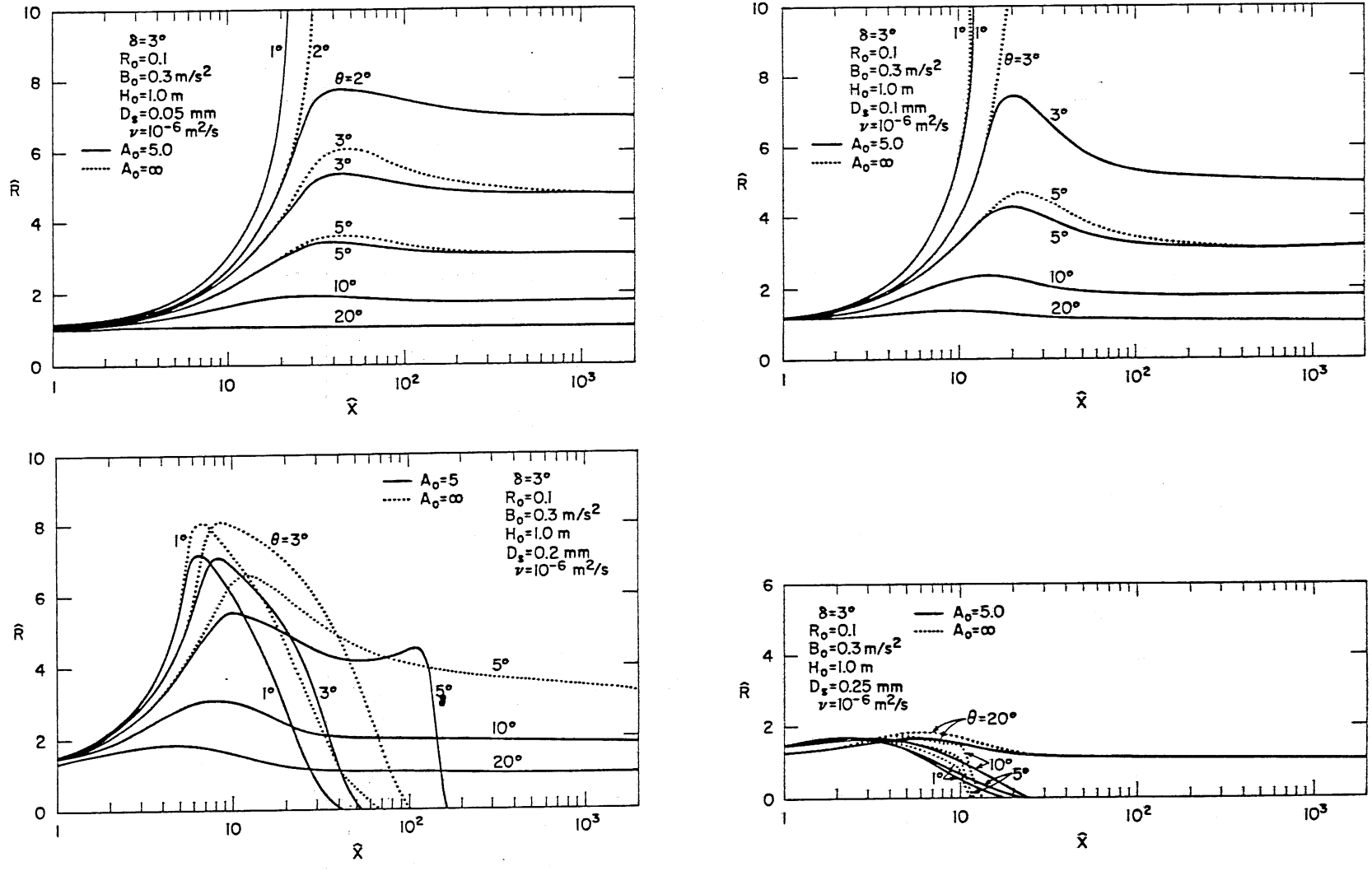

Fig. 5-12 Dependence of Ri number on the bed slope θ for different particle sizes D_s.

(a) D_s = 0.05mm. (c) D_s = 0.20mm (b) D_s = 0.10mm (d) D_s = 0.25mm

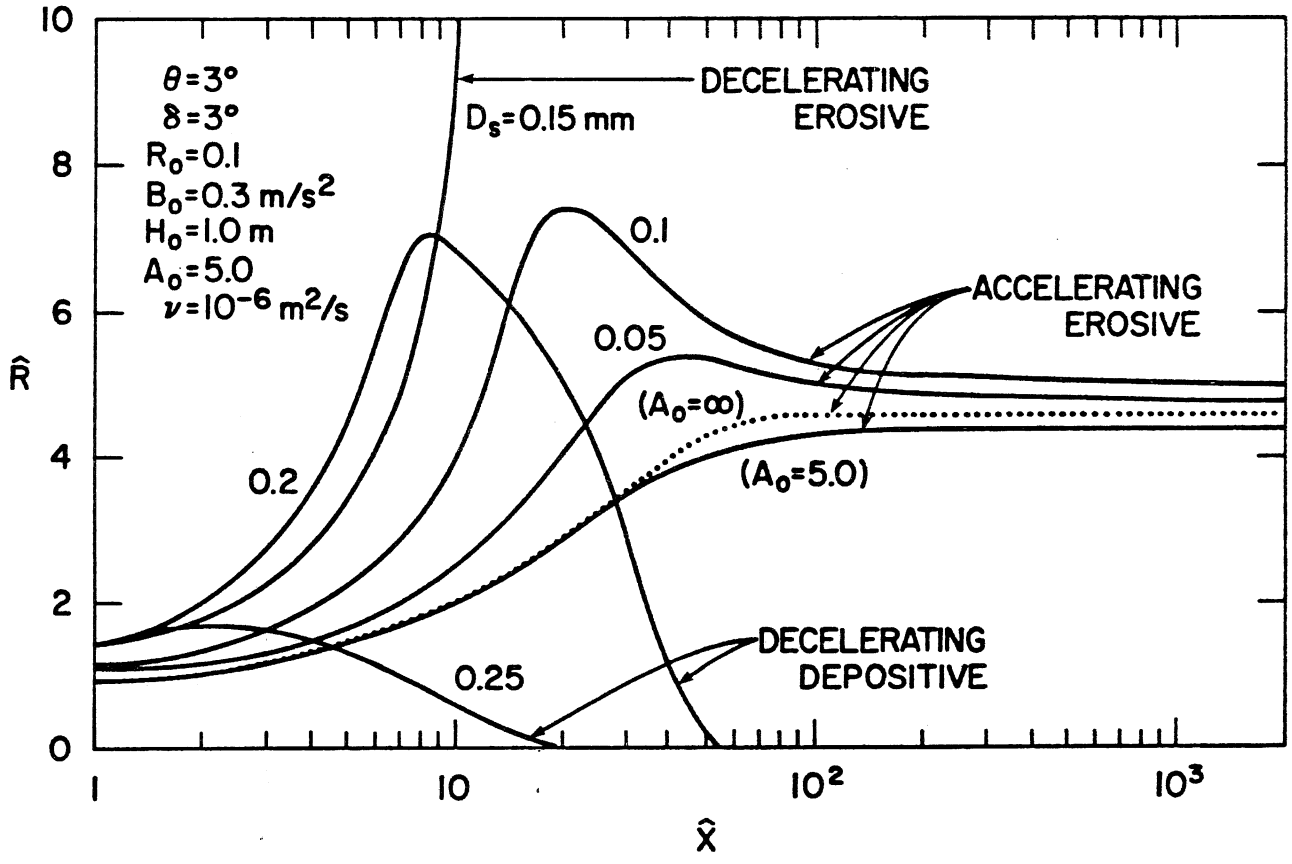

Fig. 5-13 Dependence of Richardson number (R) on particle size (D_s).

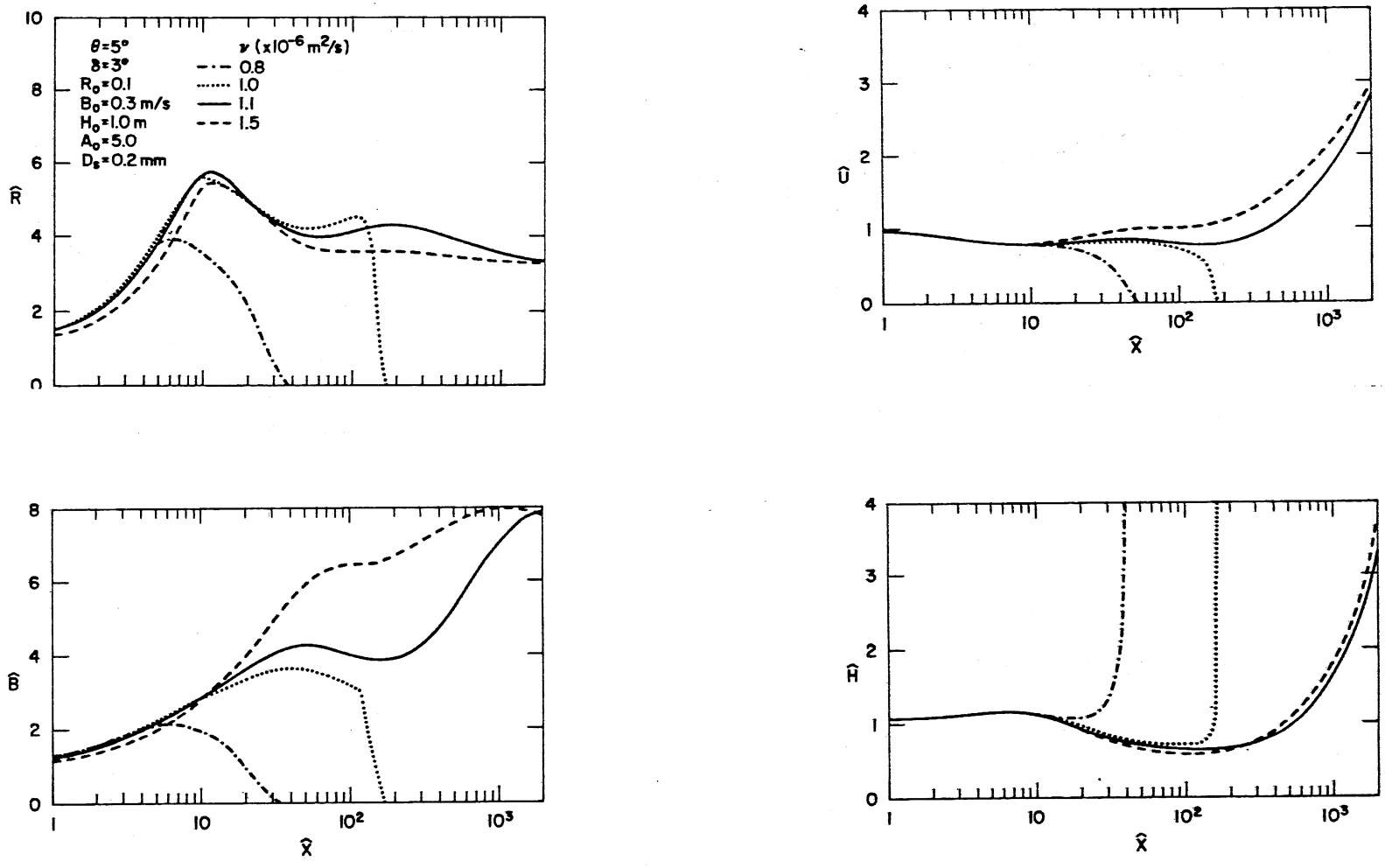

Fig. 5-14 Effect of viscosity on the behavior of turbidity currents.

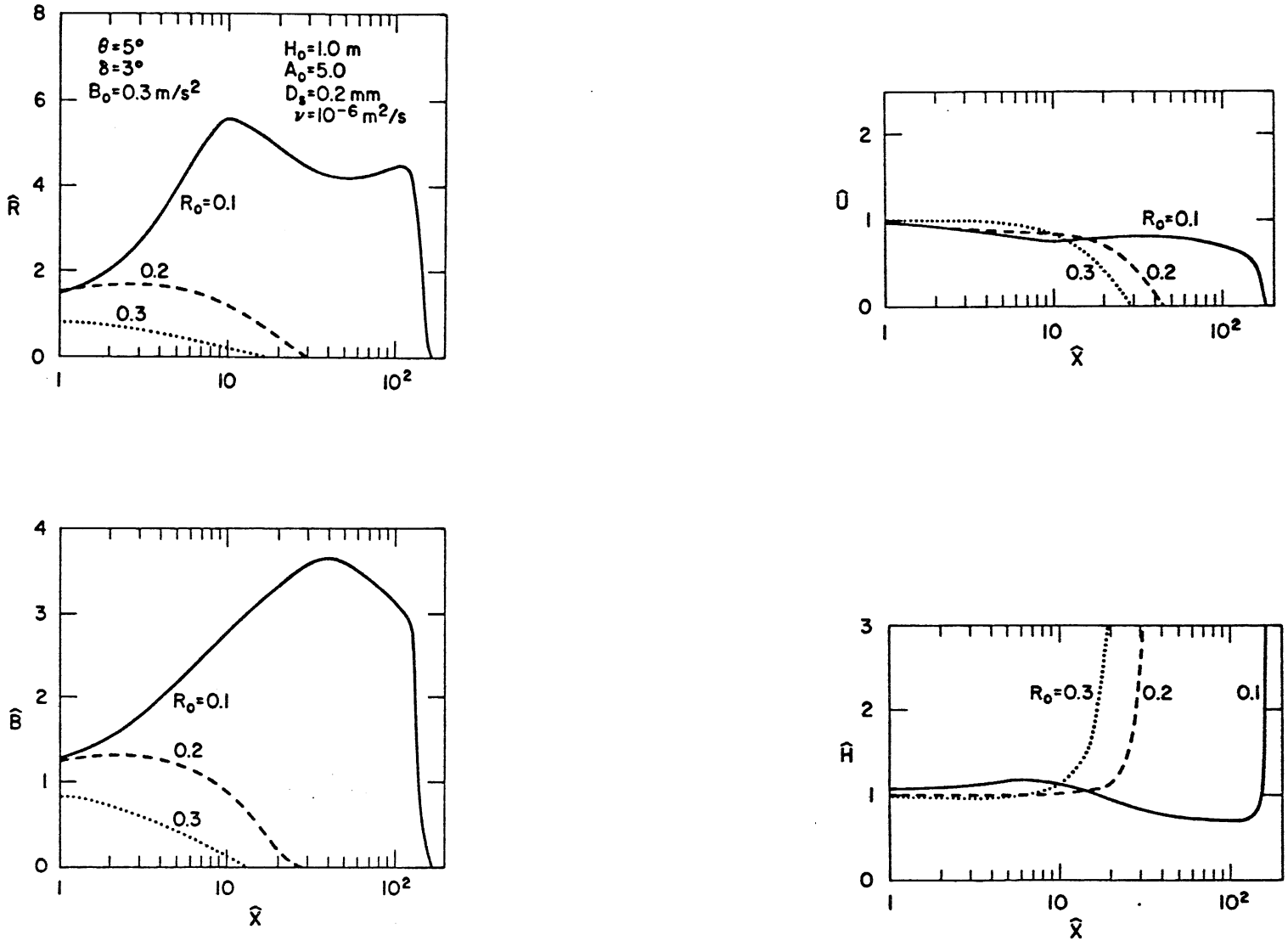

Fig. 5-15 Example of a supercritical depositive turbidity current.

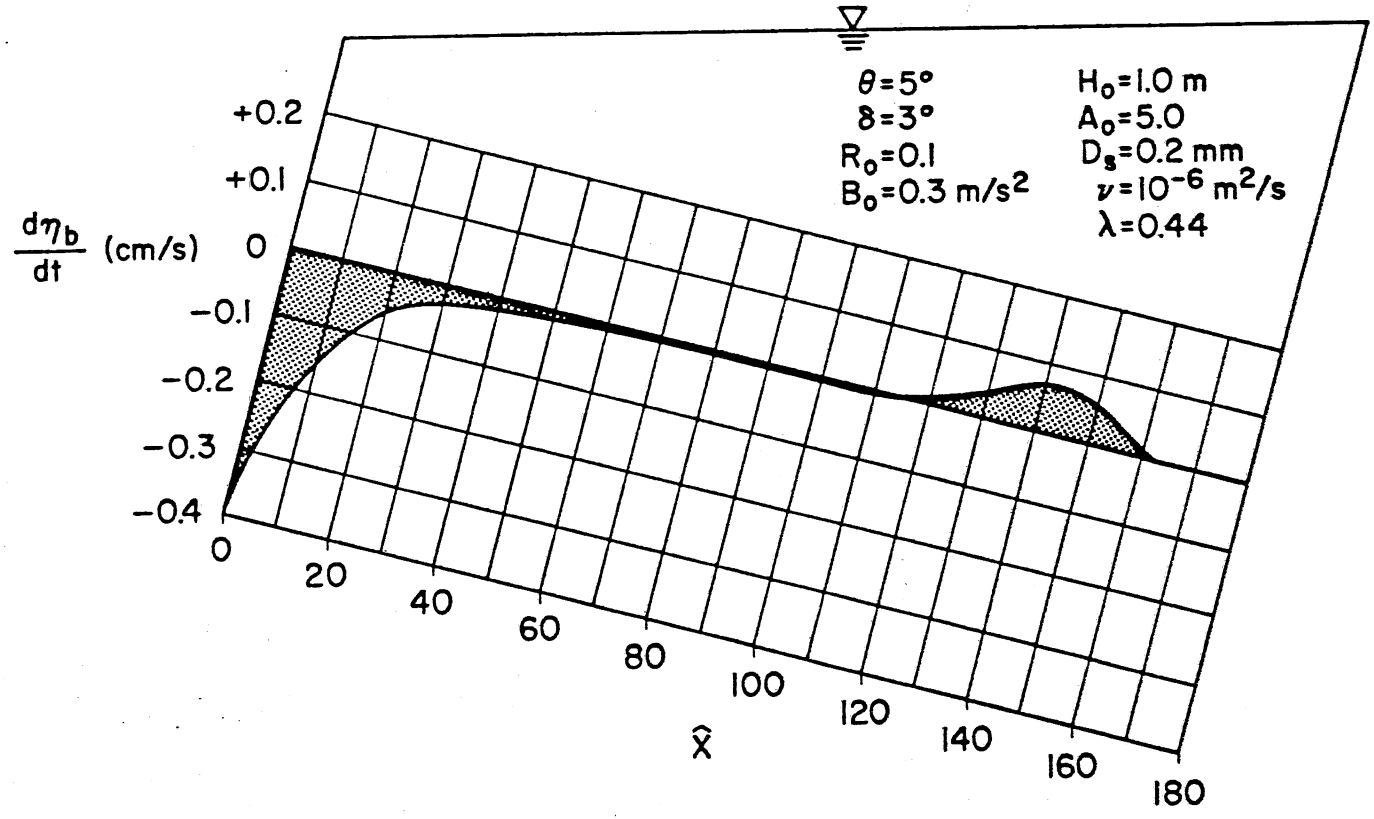

Fig. 5-16 The rate of change of bed elevation produced by a supercritical depositive turbidity current.

forms a delta and the channel upstream of the delta develops a milder bed slope if the same initial conditions are maintained at the upstream end.

5.5 Conclusions

Spatially varied turbidity currents with erosion and deposition of sediment occurring in slightly diverging-sloping channels with a rectangular cross-section are simulated. The model consists of cross-section integrated equations for conservation of volume and mass, x-momentum equation, continuity equation for sediment, and empirical relationships for water entrainment and sediment entrainment. The continuity equation for the sediment bed is coupled with the equations for the flow in order to simulate the change of bed elevation due to erosion and deposition of turbidity currents.

The gradually varied equations are numerically solved with the following results.

(1) Underflows occurring in a diverging channel do not have a normal state, because both the flow velocity and wetted area are not constant.

(2) Channel divergence may prevent underflows from becoming subcritical flows, because of smaller flow depth and resulting smaller side wall friction.

(3) The initial channel aspect ratio is of importance in gravity currents in a diverging channel.

(4) Three different types of turbidity currents occur: They are declerating-erosive, accelerating-erosive, and decelerating-depositive.

(5) Aggradation and degrading due to turbidity currents occuring in a slightly diverging channel can be calculated and an example is presented. According to the example, supercritical decelerating-depositive turbidity currents can form a delta, and modify the original bed substantially.

(6) It is desirable to determine the dependence of the drag coefficient (C_{b1}) on bed forms and shape factors for a wide range of Richardson numbers, bed roughnesses, and sediment sizes for quantitative predication.

6. APPLICATION OF THE MODEL TO FIELD CASES

6.1 Background

Investigations of bed topographies of lakes and the ocean floor by geologists and marine scientists suggest that turbidity currents occuring in nature are meandering, braiding over delta fans, and overflowing from subaqueous channels. It seems that they possess many features also observed in free surface river flows. As discussed in Chapter 4 and 5, a subsurface suspended sediment transport is more complicated than sediment transport in open channel flow. Very few data sets were. therefore, found to be useful for both calibration of the model and the comparison of the model to data. This implies that it is still impossible to predict quantitatively the behavoir of turbidity currents in the field, it is possible only to estimate qualitatively the characteristic features, utilizing experimental information obtained from somewhat similar phenomena such as non-suspension gravity currents and sediment transport in open channel flow.

As discussed in Chapters 5 and 6, the behavior of turbidity currents made of uniform material is dependent on channel bed slope (θ), side wall angle (δ), particle size (D_s), submerged specific weight (σ) of sediment particles, kinematic viscosity of water (υ), friction coefficient at the bed (C_{bo}) and at the wall (C_{wo}), and initial conditions (depth H_o, buoyancy force B_o, Richardson number R_o, channel aspect ratio A_o) if the currents are laterally confined in channels of rectangular cross-sectional shape and without bed forms. Among these parameters, one of the most crucial parameters is C_{bo} and its magnitude

is of particular significance for both the force balance and the rate of sediment entrainment or deposition.

The channel bottom shear stress is related to surface (grain) roughness and bed features such as ripples and dunes, similar to sediment transport in open channel hydraulics.

Turbidity currents are essentially turbulent flows; therefore, C_{bo} is a function of relative roughness (k_s/H or D_s/H), provided that no bed feature is present (flat bed). Considering the dimensions of typical turbidity currents in the field, k_s/H is small enough to regard the bed as smooth.

The entrainment parameter E_s does not appear to be a function of bed form in an explicit manner (Chapter 3), but the bed-form effect on E_s is considered to be absorbed in the shear velocity (u_*). The reason for this may be that E_s is determined at the reference level $a = 0.05H$, where suspended sediment concentration and bed are not presumably strongly correlated.

Therefore, the model appears to be still applicable to turbidity currents in the presence of bed forms as long as their height (Δ) is reasonably small, i.e., $\Delta \ll 0.05H$.

Treating the channel bed as a smooth boundary, the model requires the following properties; shape factors (f_1, f_2, f_3, S_1, S_2) and initial conditions (R_o, B_o, H_o, A_o) or (U_o, C_o, H_o, A_o). Properties such as θ, δ, υ, σ, and D_s are usually known from field surveys. On the other hand, values for C_{bo}, C_{wo}, and initial conditions are not obvious.

In the following simulation C_{bo}, initial conditions, and shape factors (S_1, S_2) are varied in order to understand the model's

sensitivity to these parameters, by applying the model to two field cases: the mine tailing discharge into Lake Superior (Fig. 6-1) and Scripps Submarine Canyon (Fig. 6-2) as an example of turbidity currents in Lakes and in the ocean, respectively. Kinematic viscosity of water (υ) is fixed as $\upsilon = 1.0 \times 10^{-6}$ m^2/s and $\delta = 0$ are used in all calculations.

Scripps Submarine Canyon can be regarded as a diverging channel. The model developed in Chapter 5 is more adequate than that in Chapter 4. Unfortunately, the exact orientation of the turbidity current is not known at this site. Therefore, $\delta = 0$ is chosen. A turbidity currents in a constant width channel is dependent on bed slope, θ, so that initial conditions will have less effect on the behavior of the current than for a diverging channel ($\delta \neq 0$).

Field investigations in Lake Superior and Scripps Submarine Canyon were conducted by Normark and Dickson [1976] and Inman et al. [1976], respectively. Furthermore, turbidity currents at these sites can be considered as nearly steady flows composed of nearly uniform sediment material.

The bathymetry at these sites is shown in Figs. 6-1 and 6-2. Taconite tailings from a mining operation had been discharged into Lake Superior and deposited off Silver Bay from 1955 to early 1980. Turbidities had modified the original shore line to form a delta. Much of the coarse fraction of the tailings is deposited on the subaerid dalta and the remaining, nearly uniform, sediment is carried to the Lake edge by turbidity currents.

Studies done by Normark and Dickson [1976] show that the delta has progressed about 1 km into water 180 m deep. At 180 m depth, there is an abrupt change in slope from $\bar{S} = 17^{o}$ to about 1.5^{o} in the prodelta area, where the tailings deposit exhibits a topography analogous to a submarine fan.

The three distinct morphologic aspects of the tailing deposit, the delta, fan and lake trough, reflect different modes of sedimentations. The slope has not prominent channels, but divers have observed 3 to 5 m thick density currents flowing down the delta slope.

In Scripps Submarine Canyon, the sand is temporarily deposited in the canyon head and along its rim by shelf currents and by strong rip currents that form over the canyon heads. Sediment is well-sorted quartz with a median diamter near $D_s = 0.15$ mm. Sediment is suspended during a unique combination of wind-sea-land interactions consisting of a pile-up of water along the shoreline caused by strong onshore winds; down-canyon pulses of water associated with groups of high incident waves; excitation of standing edge waves that produce longer period up- and down-canyon currents.

The strongest down-canyon current measured 1.9 m/s at a depth of 44m, being recorded during the passage of a storm front on 24 November 1968. The current meter failed at down-canyon velocity of 50 cm/s at site 1 (Fig. 6-2) and was lost in the turbidity current (Fig. 6-3).

Turbidity currents in Lake Superior and Scripps Submarine Canyon are controlled by the following conditions:

Lake Superior:

Average channel bed slope $\theta = 17^{o}$ in delta slope region and 1.5^{o} in delta fan, grain size $D_s = 0.04$ mm, submerged specific gravity of taconite tailings $\sigma = 2.1$.

Scripps Submarine Canyon:

Average canyon axis slope $\theta = 4.59^{o}$, grain size $D_s = 0.15$ mm, submerged specific gravity of sediment $\sigma = 1.65$.

6.2 Effect of Bed Shear Coefficient

The value of C_{bo} normally regared as reasonable for gravity currents ranges roughly from 0.0035 to 0.02. Initial conditions are arbitrarily chosen to yield accelerating erosive currents; $R_o = 0.5$, $B_o = 0.1$ m/s, $H_o = 1.0$ m for Lake Superior (Fig. 6-4 and 6-5), $R_o = 0.5$, $B_o = 0.8$ m/s, $H_o = 1.0$ m for Scripps Submarine Canyon (Fig. 6-6). Unrealistic small C_{bo} values such as 0.0002 and 0.0005 are used to examine the role of bed shear stress in both the resistance force and sediment exchange mechanism in Fig. 6-4. In Figs. 6-5 and 6-6, several different C_{bo} values are employed for the purpose of examining the effects of C_{bo}. Buoyancy flow and current depth are most affected by the choice of C_{bo}, flow velocities the least.

Flow behavior is more sensitive to bedshear coefficient C_{bo} in the Scripps Canyon case than in the Lake Superior situation. This is due to the larger sediment particle size, which requires higher turbulence intensity level in order to sustain sediment.

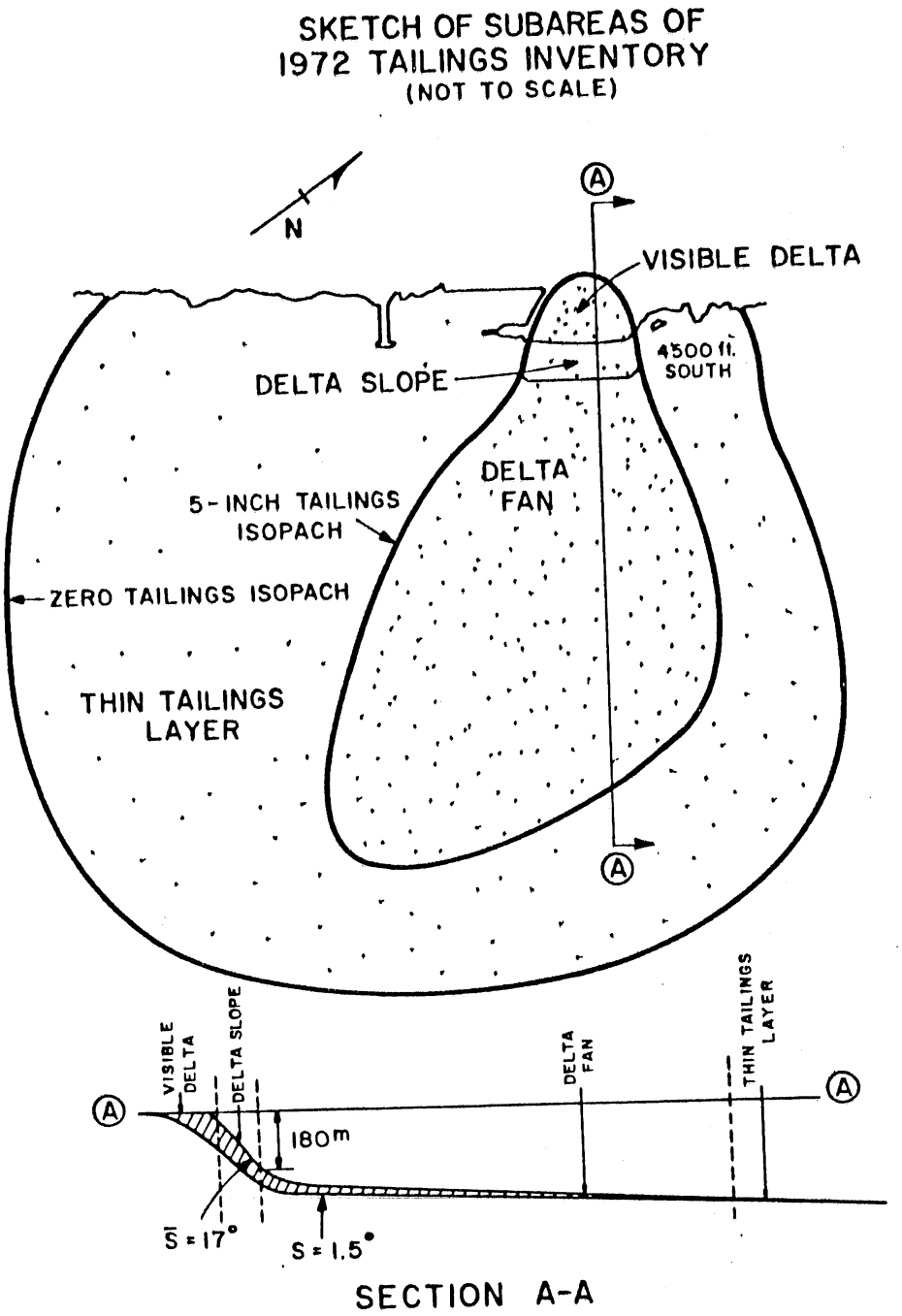

Fig. 6-1 Topography of Lake Superior at Silver Bay, Minnesota (after Normark and Dickson [1976]).

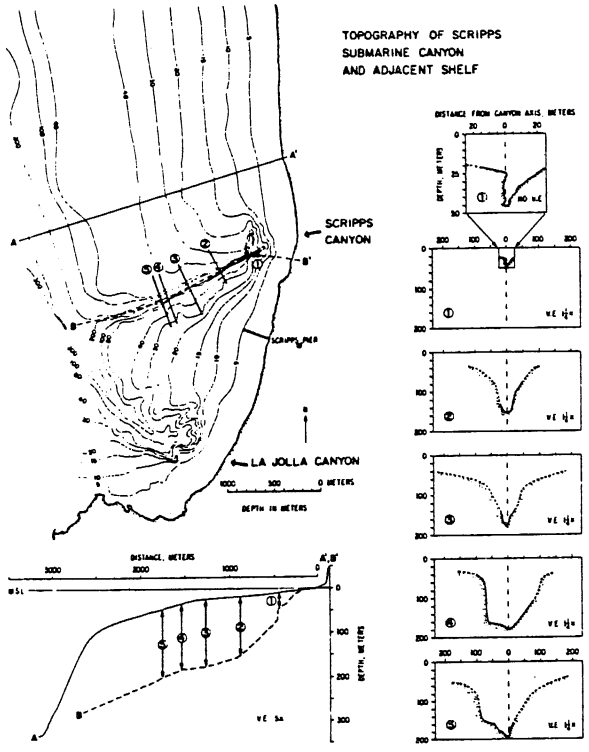

Fig. 6-2
Detailed topography of Scripps Submarine Canyon and shelf. Numbered lines indicate the position of canyon profiles measured by closely spaced lead line soundings (after Inman et al. [1976]).

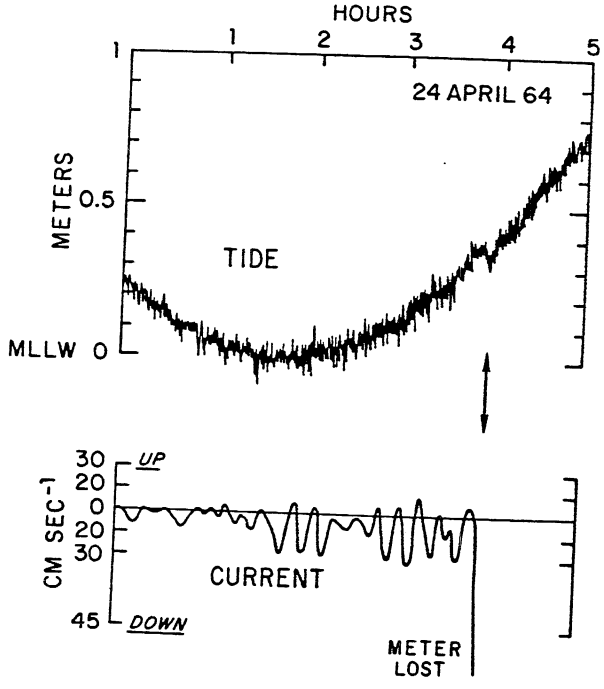

Fig. 6-3
Analog record of first sustained down-canyon currents of 24 April 1964 (site 1) (after Inman et al. [1976]).

At a given site, whether the flow velocity increases or decreases at an appropriate, predetermined C_{bo} value is dependent on two factors: (i) initial conditions, (ii) shape factors. The effects of these two will therefore be examined.

6.3 Effect of Initial Conditions (R_o, B_o, H_o)

Figures 6-7 and 6-9 illustrate the significance of initial conditions on acceleration or deceleration of the currents.

Figure 6-7 is for Lake Superior, and Fig. 6-9 for Scripps Canyon, where channel bed slope and properties of the sediment are known. The subareas on the right-hand and left-hand side of the lines H_o = 0.5, 1.0, and 2.0 correspond to accelerating-erosive and decelerating-erosive flow regimes in Fig. 6-7, respectively, and similarily to accelerating-erosive and decelerating-depositive flow regimes in Fig. 6-9. C_{bo} = 0.02 for Lake Superior, and C_{bo} = 0.002 (Inman et al., [1976]). For Scripps submarine canyon are used in the calculations.

The sensitivity of the model to C_{bo} for a given set of initial conditions (R_o = 0.5, B_o = 0.1, H_o = 1.0) in the case of Scripps Submarine Canyon is examined in Fig. 6-6.

In Figures 6-8 and 6-10, Richardson number changes in the B - R plain, depending on initial conditions, are shown. According to the simulation, decelerating-erosive currents are not able to maintain supercritical condition, so that they become subcritical flows within a short distance from an initial point x_o. It is reasonable to expect that an internal hydraulic jump takes place in the transition from supercritical to subcritical state. The role of internal hydrualic

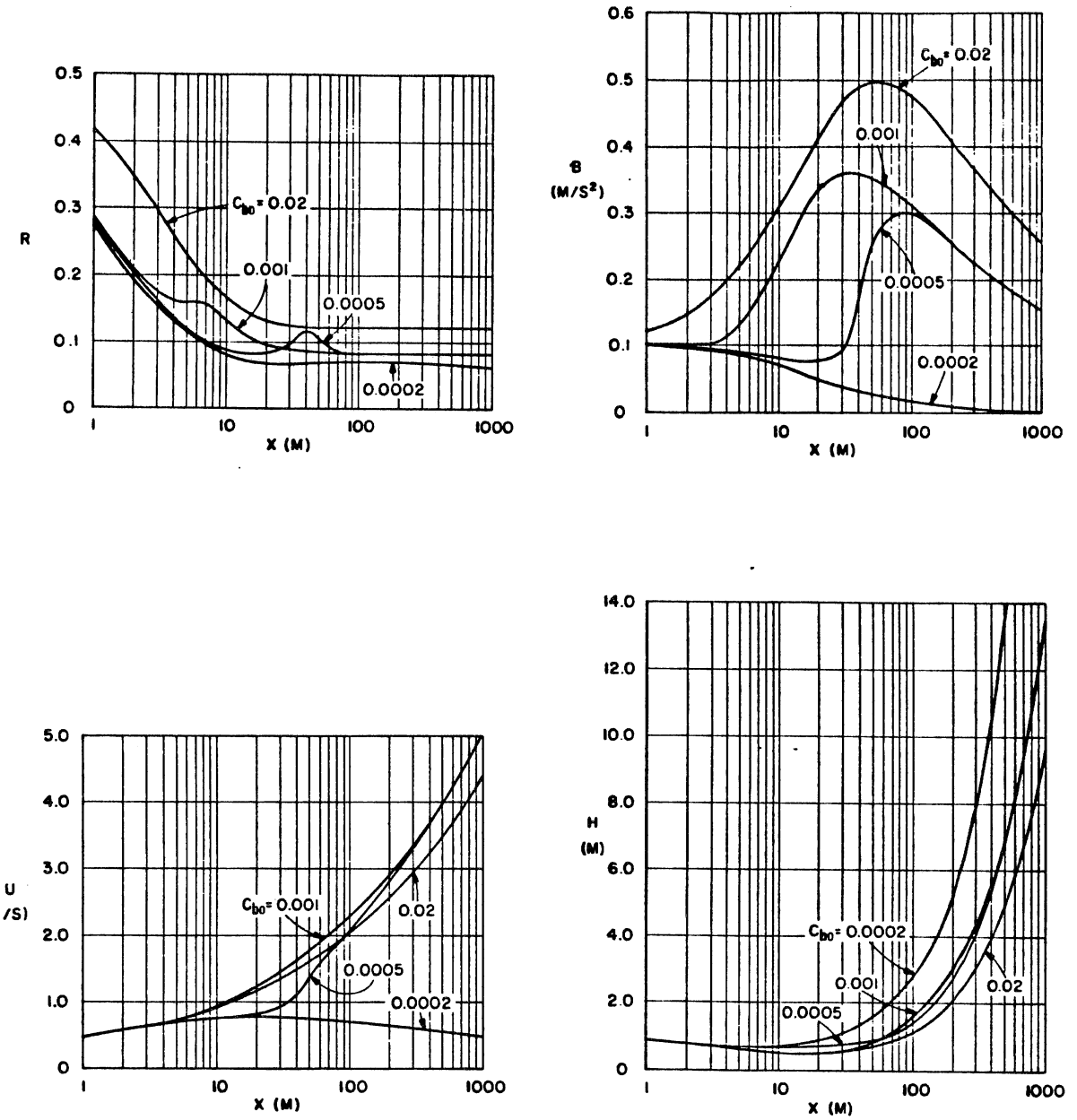

Fig. 6-4 Effect of friction coefficient (C_{bo}) on Lake Superior turbidity current (initial conditions: $R_o = 0.5$, $B_o = 0.1$, $H_o = 1.0$).

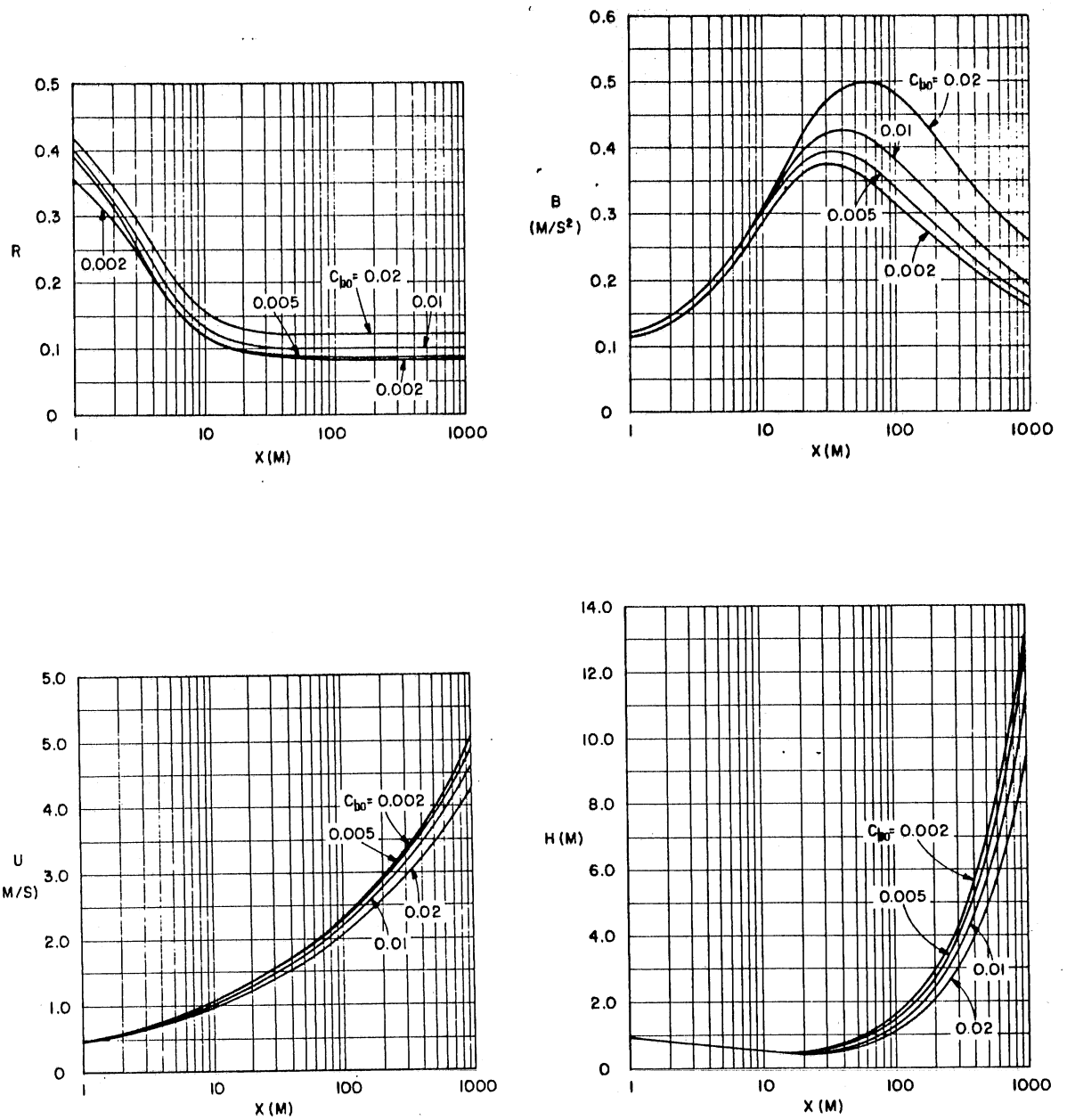

Fig. 6-5 Effect of friction coefficient (C_{bo}) on Lake Superior turbidity current (initial conditions: R_o = 0.5, B_o = 0.1, H_o = 1.0).

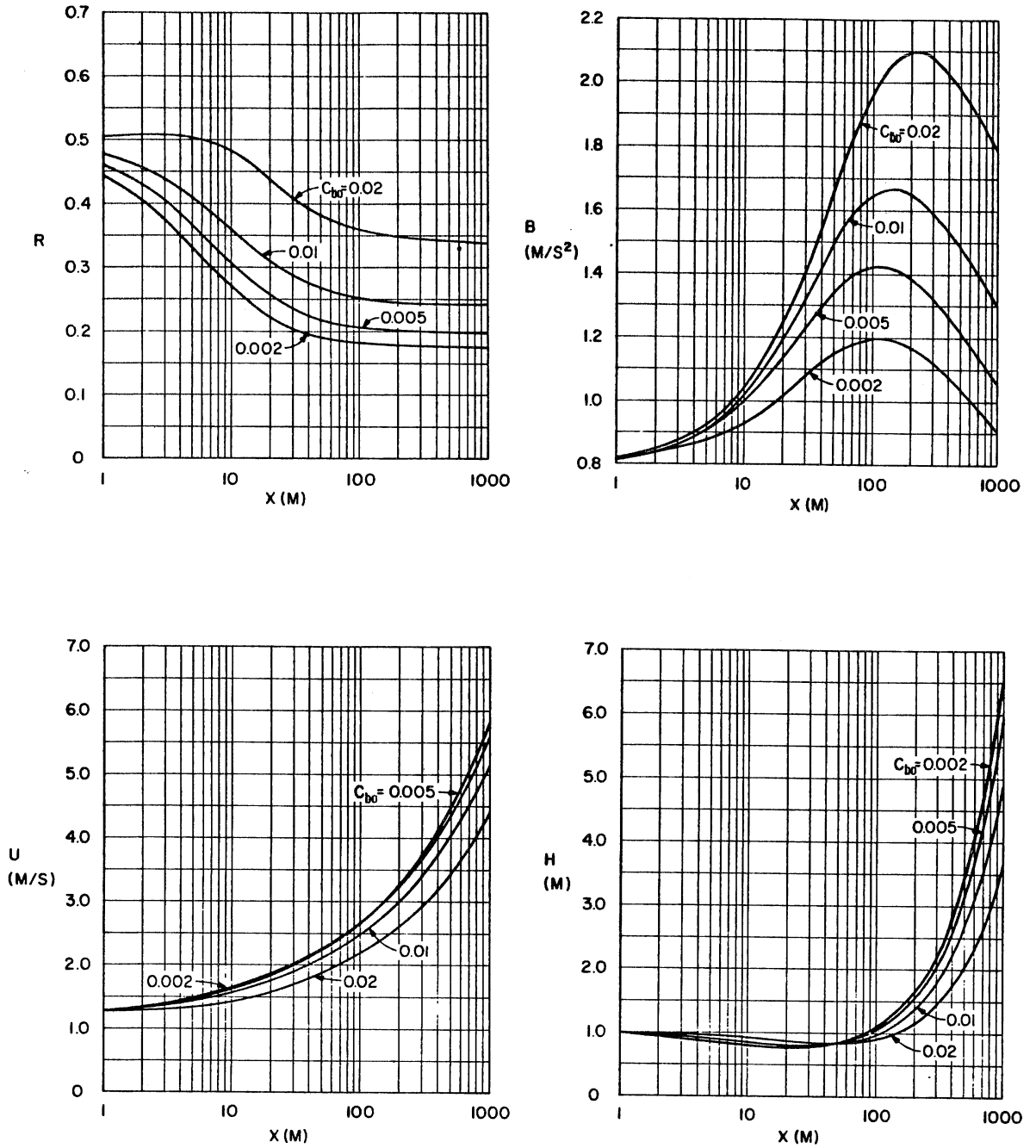

Fig. 6-6 Effect of friction coefficient (C_{bo}) on Scripps Canyon turbidity current (initial conditions: $R_o = 0.5$, $B_o = 0.8$, $H_o = 1.0$).

jumps in sediment laden flows is not well known. It is reasonable to speculate that a certain amount of sediment deposition might occur as the result of energy dissipation in an internal hydraulic jump. It is not implied that subcritical turbidity currents are non-erosive, but that they could be erosive or depositive, depending on the condition of flow after the jump.

The model can be applied for subcritical turbidity currents provided that upstream boundary conditions after the internal hydraulic jump and downstream boundary conditions before the flow completely vanishes, as well as the distance between the two sections are known through field investigations.

It is, therefore, very desirable to clarify the role of the internal hydraulic jump in sediment erosion and deposition. Without this knowledge, any kind of simulation for subcritical turbidity currents is not very meaningful.

Typical supercritical accelerating-erosive and decelerating depositive turbidity currents in Scripps Canyon are shown in Fig. 6-11. Supercritical decelerating-depositive turbidity currents may be of importance for the delta slope due to relatively coarser suspended sediment. Values in the very vicinity of the dividing line (Fig. 6-9) are chosen as initial conditions. The flow is, therefore, unstable until a driving force definitely overcomes a resistance force (see Fig. 6-11 for small x). Once such a condition has been attained, the behavoir of the currents is found to be virtually identical regardless of initial conditions. In decelerating-depositive currents (Fig. 6-12),

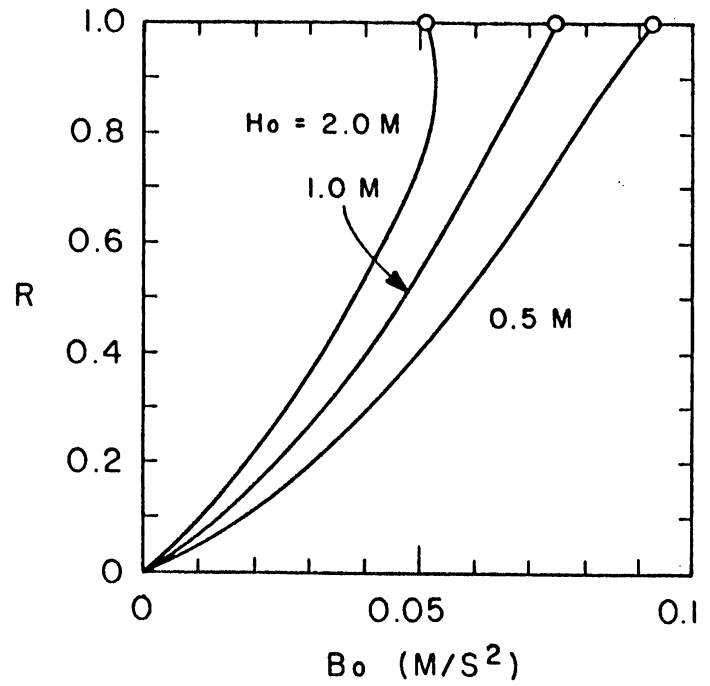

Fig. 6-7 Diagram of regimes for Lake Superior turbidity currents.

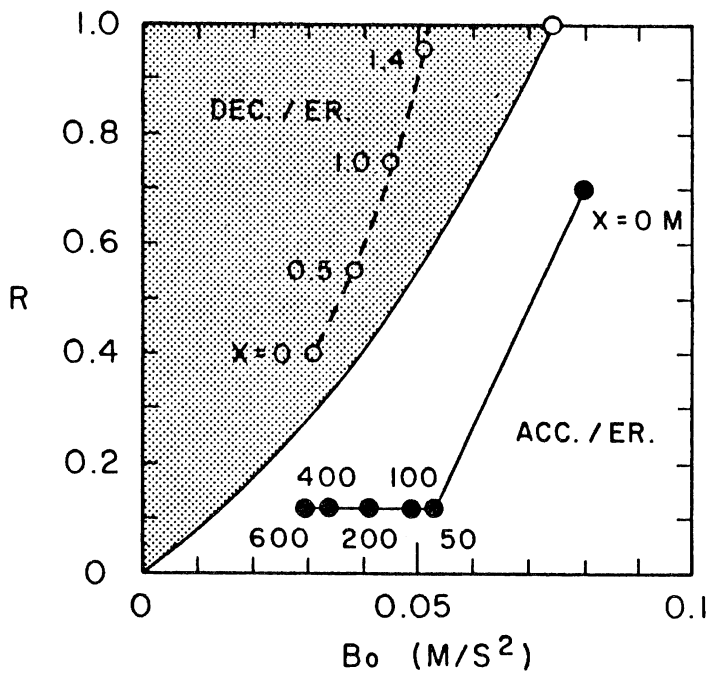

Fig. 6-8 Behavior of Richardson number in the R - B plane for Lake Superior turbidity currents.

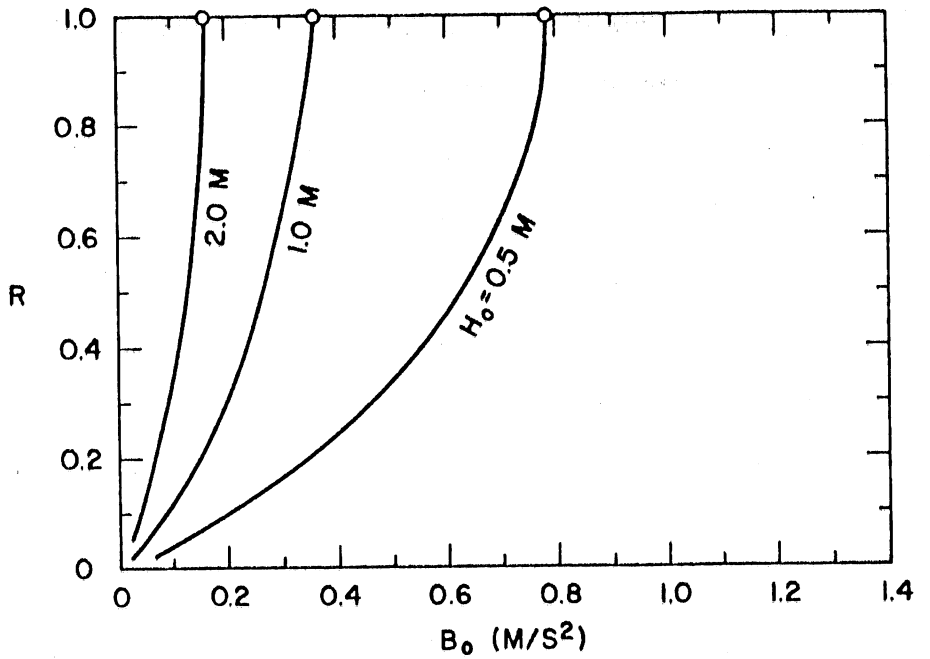

Fig. 6-9 Diagram of regimes for Scripps Canyon turbidity currents.

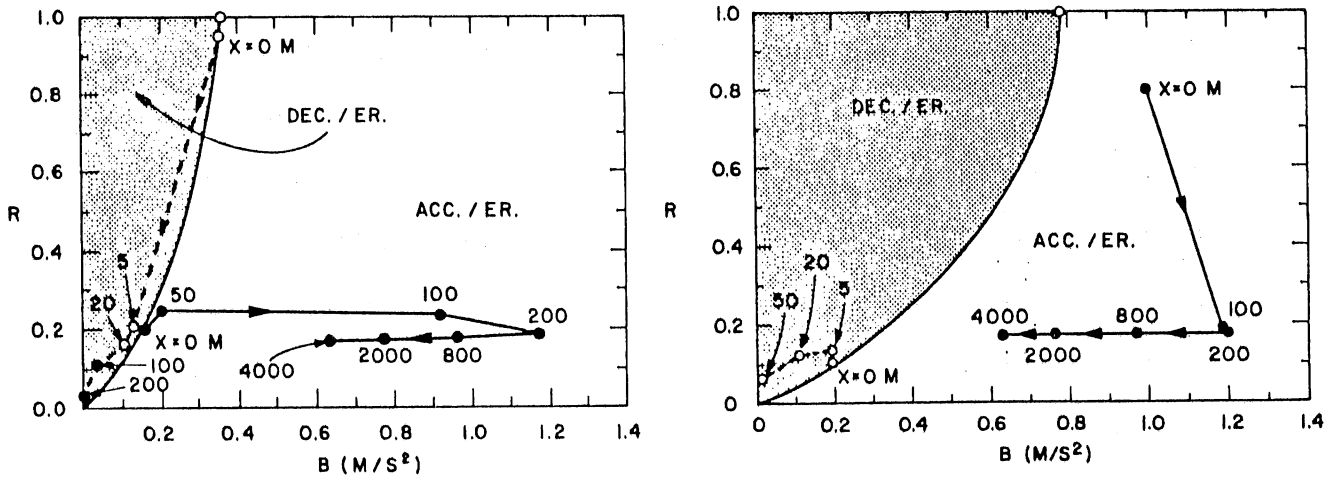

Fig. 6-10 Behavior of Richardson number in the R - B plane for Scripps Canyon turbidity currents.

buoyancy flux B_f (= BHU) decreases as the flows travels downslope, and turbidity currents vanish as a result of sediment deposition.

In Fig. 6-13, the effects of initial Richardson number R_o are examined systematically. The condition R = 0 indicates that decelerating depositive currents will vanish. More favorable conditions for decelerating-depositive flow, namely larger B_o, H_o, and smaller R_o prevent flows from vanishing as currents travel downslope.

Different initial Richardson numbers for the accelerating current, on the other hand, merge into, the value 0.17 around x = 200 m.

The effect of initial conditions on Lake Superior turbidity currents is further investigated in Fig. 6-14 and 6-15. Initial flow depths H_o = 1.0 in Fig. 6-14 and 0.5 in Fig. 6-15 were selected. The influence of the initial conditions on the current is small by the time the currents reach x = 600, where the channel bed slope θ changes from 17^o (delta slope region) to 1.5^o (delta fan region) as shown in Fig. 6-1. A typical model simulation result in relation to channel bed slope is shown in Fig. 6-16. In the calculation, θ is gradually changed from 17^o to 1.5^o over a distance of about 300 m. The current in this specific case can maintain a supercritical state only about 100 m after it has reached the delta fan region when initial conditions for accelerating flow are imposed. Then a hydraulic jump may occur as indicated by R and H in Fig. 6-16. According to Normark and Dickson [1976], a 5 inch thick delta layer spread over a wide area has formed as the result of a taconite tailings discharge over many years. There is also evidence that accelerating-erosive currents formed over the delta slope under appropriate initial conditions and that they transported

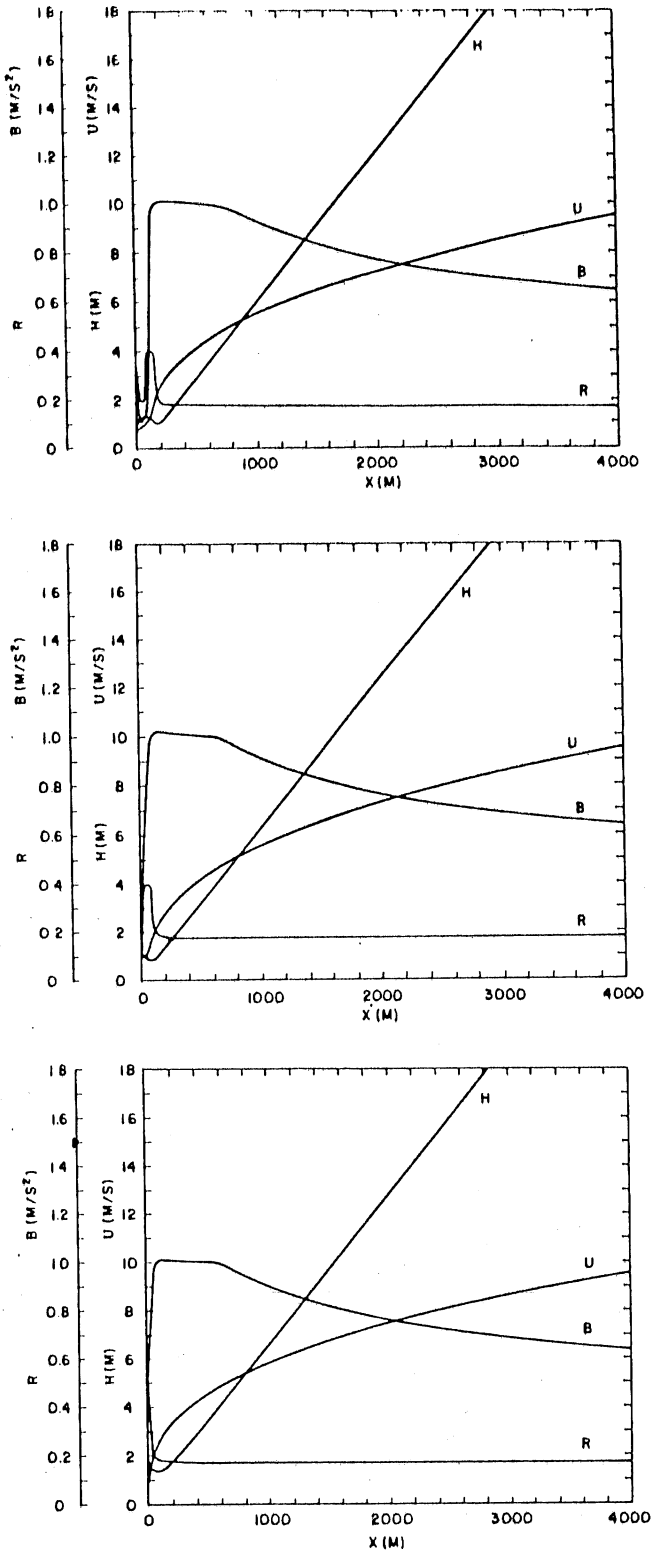

Fig. 6-11 Examples of accelerating-erosive turbidity currents in Scripps Canyon in relation to initial conditions.

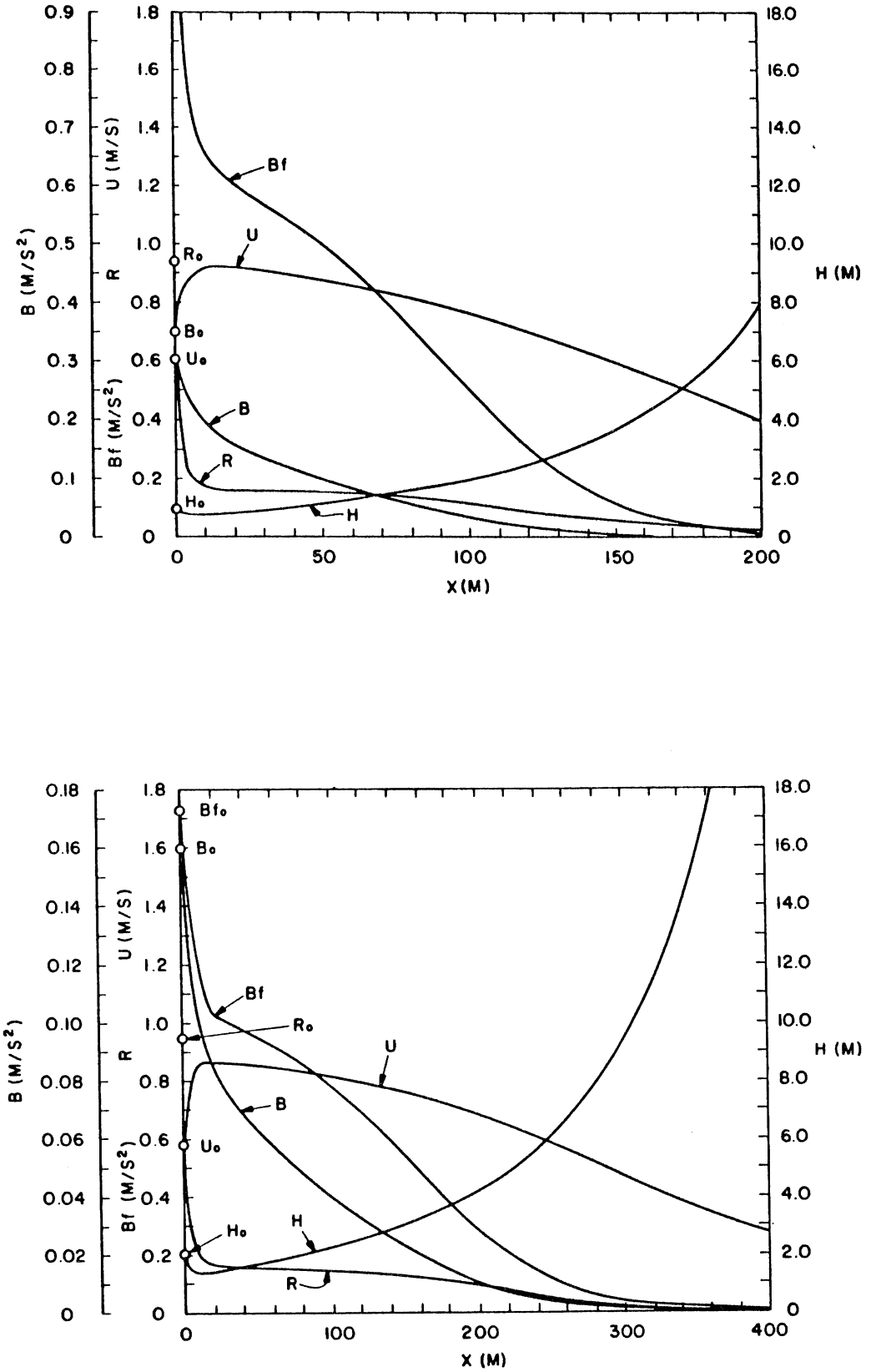

Fig. 6-12 Examples of decelerating-depositive turbidity currents in Scripps Canyon in relation to initial conditions.

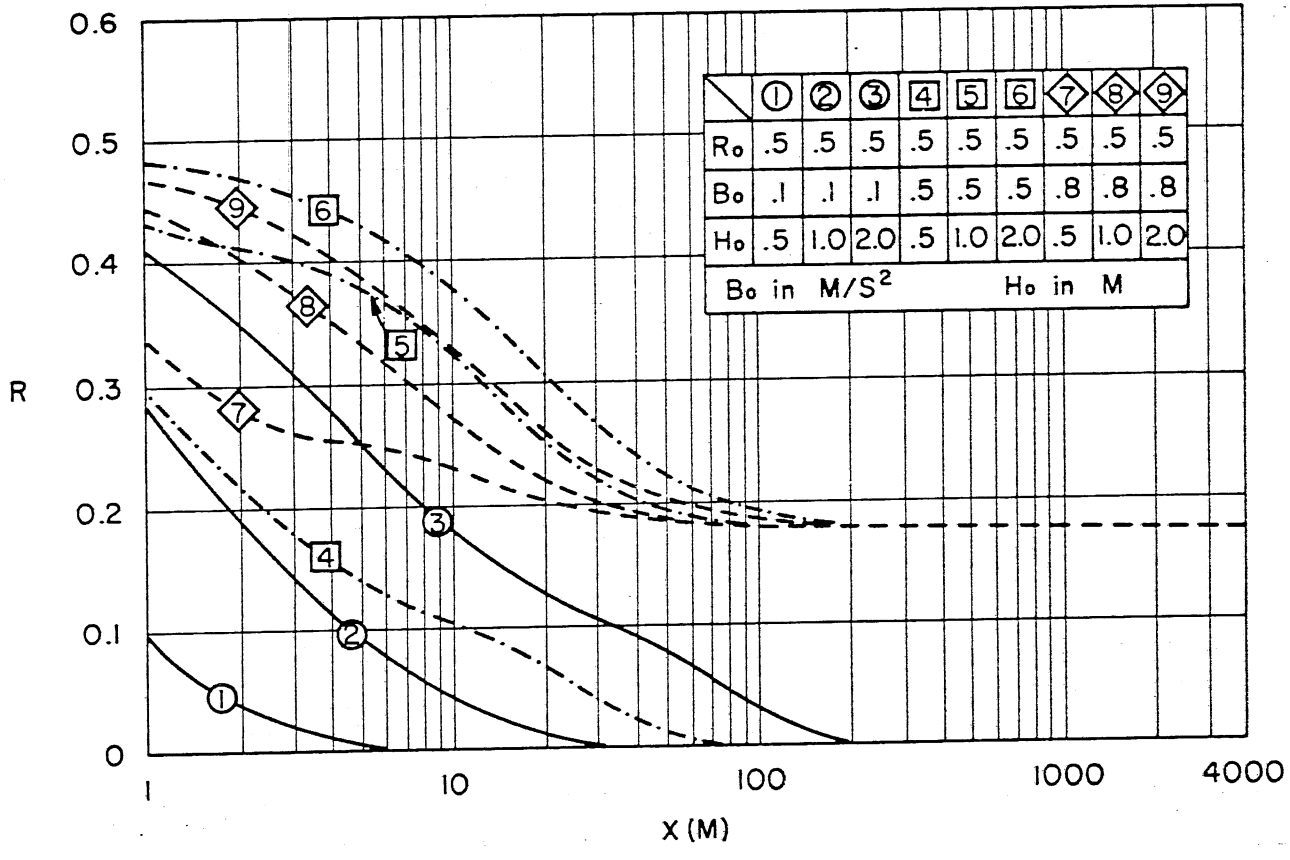

Fig. 6-13 Effect of initial conditions on Scripps Canyon turbidity currents.

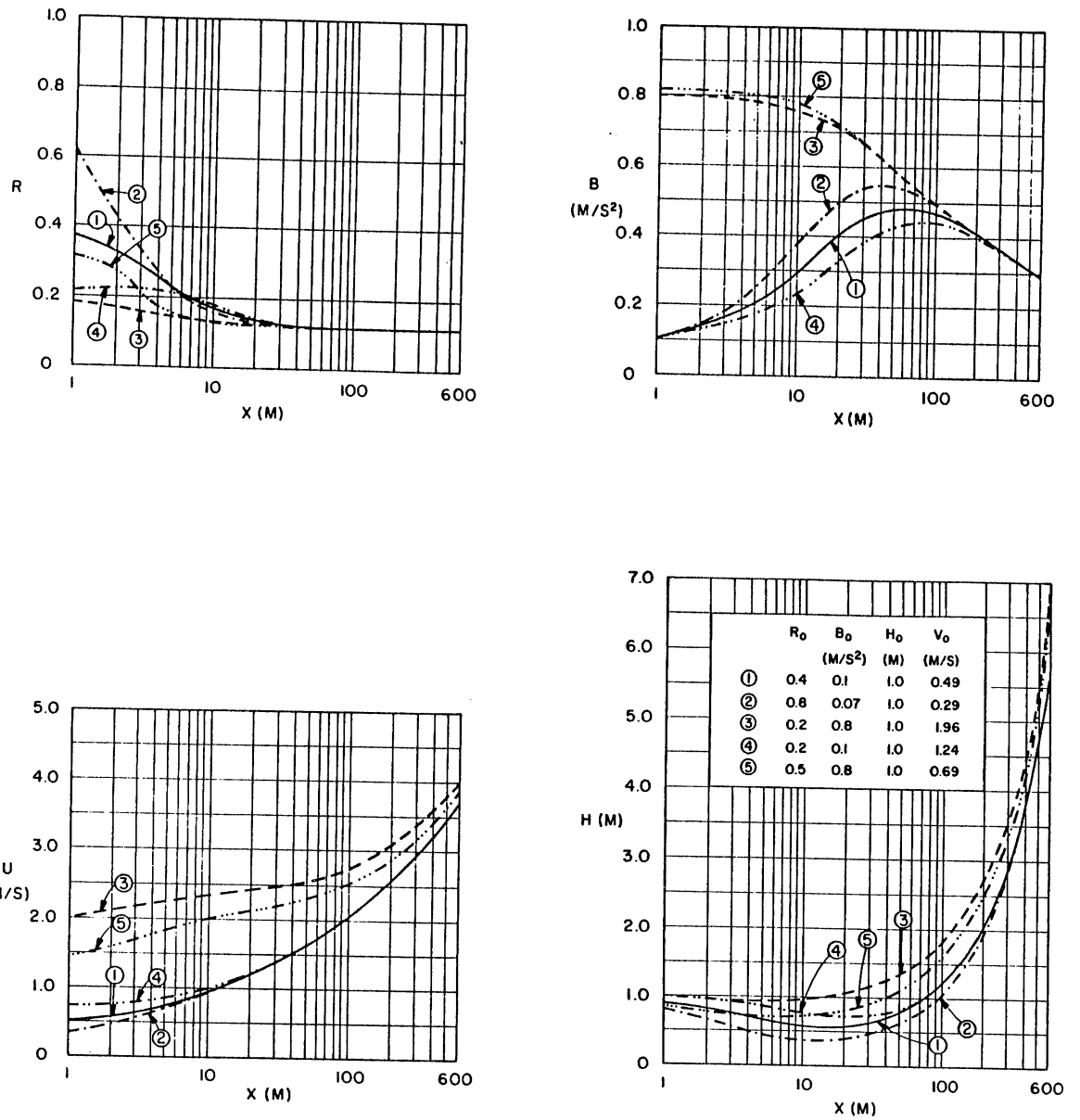

Fig. 6-14 Effect of initial conditions on Lake Superior turbidity currents (H_0= 1.0m).

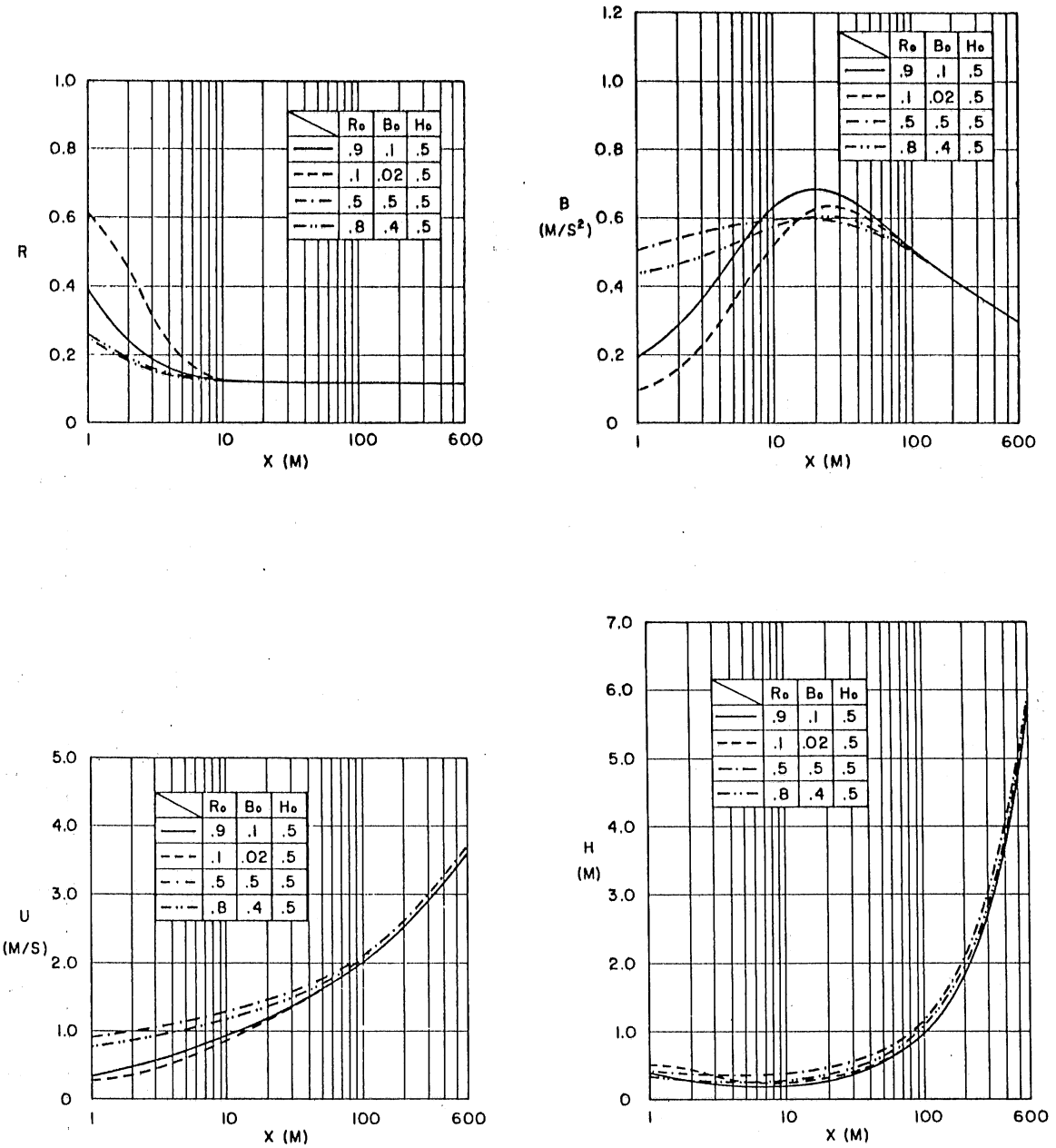

Fig. 6-15 Effect of initial conditions on Lake Superior turbidity currents (H_o = 0.5m).

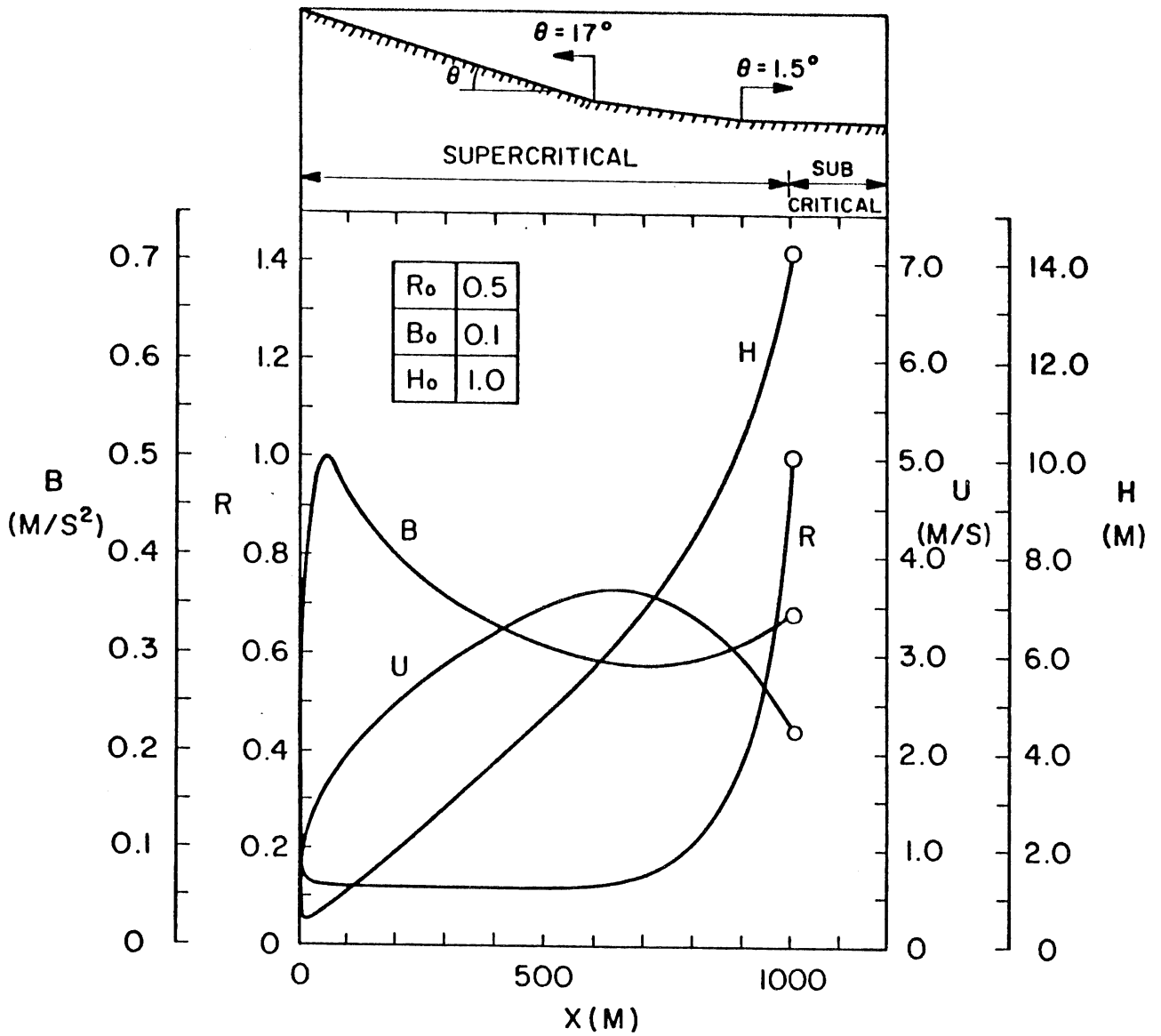

Fig. 6-16 Typical result of accelerating-erosive turbidity current model simulation for Lake Superior.

tailings into deeper parts of the lake over the delta fan, where sediments are deposited. This is a good example to demonstrate the mechanism of erosion, transportation, and deposition of suspended sediment by turbidity currents.

6.4 Effects of Shape Factors S_1 and S_2

Shape factors S_1 and S_2, which include the effects of the buoyancy force, are examined. Up to this point, all shape factors where set equal to unity. The case of Scripps Submarine Canyon is used for the simulation with alternative values of S_1 and S_2. The effects of S_1 and S_2 are illustrated in Fig. 6-17 and 6-18 for two values of C_{bo} (0.02 and 0.002) respectively.

According to Ellison and Turner [1959], S_1 and S_2 values vary within the ranges $S_1 = 0.2$ to 0.3, and $S_2 = 0.6$ to 0.9 for non-suspension gravity currents. They are assumed to be valid for erosive-depositive currents as well. Average values and combinations, namely $S_1 = 0.25$; $S_2 = 0.75$, and 0.2; 0.6, in addition to $S_1 = S_2 = 1.0$, are employed in Fig. 6-18. It must be noted that R = 1 represents the critical condition to determine whether a flow is super- or subcritical only if all shape factors are unity.

It can be seen in Figs. 6-17 and 6-18 that the combination of smaller S_1 and S_2 values with $C_{bo} = 0.02$ yield a closer agreement with the one measured velocity.

The roles of initial conditions combined with $S_1 = 0.2$ and $S_2 = 0.6$ are examined in Fig. 6-19. Shape factors S_1 and S_2 are indicators of express non-uniformity of buoyancy force. The buoyancy force profile

for a surface buoyant jet has been found to have a linear distribution (Chu and Vanvari, 1976; Tsubaki and Komatsu, 1979).

The difference in density profiles between surface buoyancy jets and underflows may be small provided that the velocity maximum point is close to the channel bed. Accordingly, the layer averaged value of S_2 is approximately equal to 0.75, which coincides with the mean value of Ellison and Turner's results. The combination of $S_1 = 0.2$ and $S_2 = 0.6$, therefore, may imply that the buoyancy force is larger near the bed; the buoyancy force of a turbidity current decreases more rapidly toward the edge of the upper boundary than that of a simple underflow.

6.5 Effect of Sediment Size (D_s)

The model assumes that the sediment is uniform or sufficiently uniform in grain size. The deposition and erosion mechanisms, however, are more complex when turbidity currents are made of a mixture of heterogeneous suspended particles and water. Examples of turbidity currents consisting of non-uniform suspended particles have been seen in major submarine canyons (Hydrographer, Hudson, Wilmington, and Norfolk) located along the continental margin off the northeastern United States (Keller and Shepard [1978]). Site of Hudson Canyon is shown in Fig. 6-20a as an example. Downcanyon maximum velocity components measured at 3 m above the bed are plotted against sediment median diameter in Fig. 6-20b, and data are tabulated in Table 6-1. For both Hydrographer Canyon and Hudson Canyon, two sets of data on downcanyon velocity and particle size are available. In Hudson submarine canyon, for example, the particle size decreasess from 0.243 mm at station depth 224 m, where

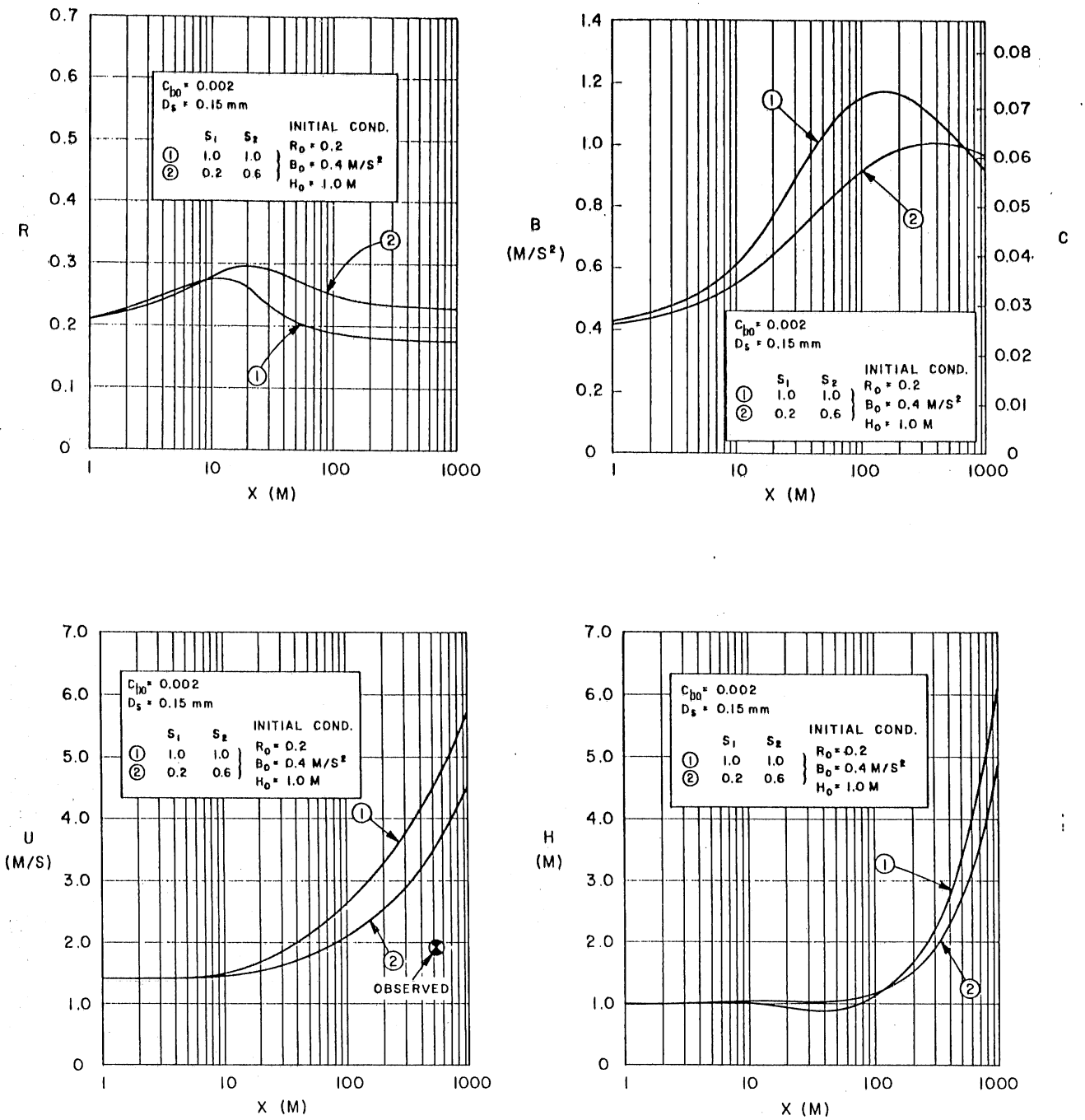

Fig. 6-17 Effect of shape factors S_1 and S_2 with C_{bo} = 0.002 on Scripps Canyon turbidity currents.

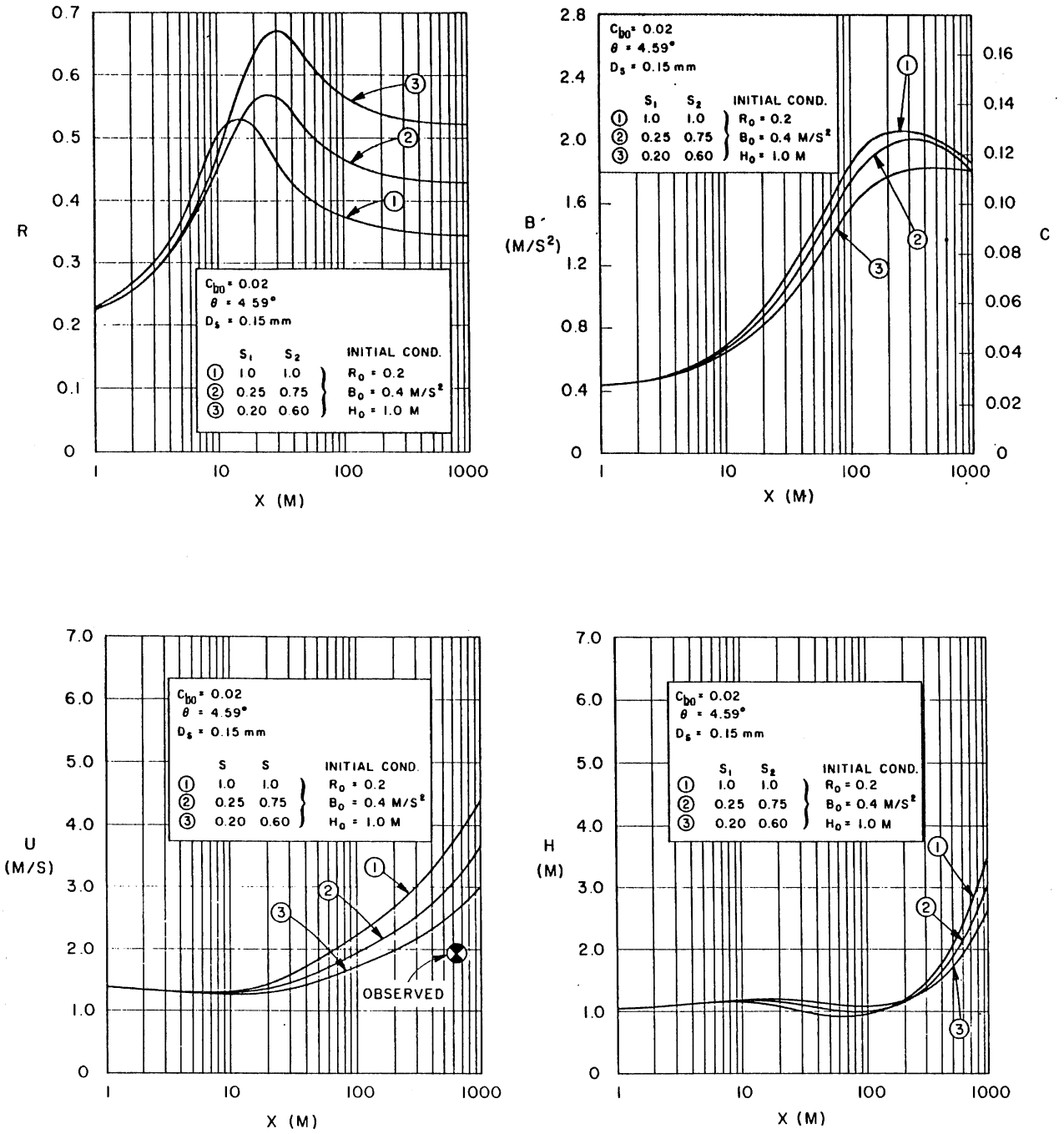

Fig. 6-18 Effect of shape factors S_1 and S_2 with C_{bo} = 0.02 on Scripps Canyon turbidity currents.

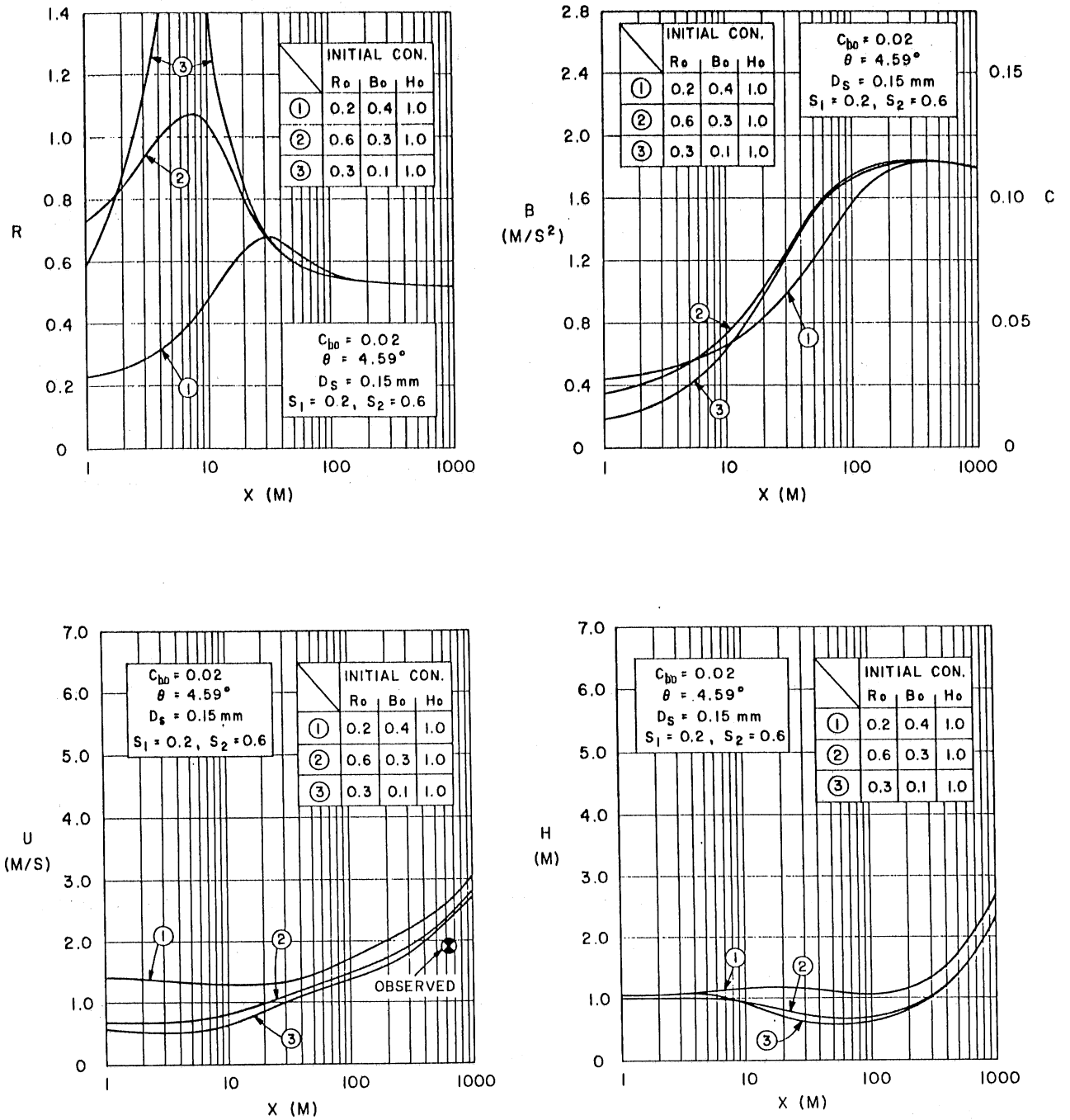

Fig. 6-19 Effect of initial conditons with $S_1 = 0.2$, $S_2 = 0.6$, and $C_{bo} = 0.02$ on Scripps Canyon turbidity currents.

maximum measured velocity is 33 cm/s, to 0.005 mm at 1,222 m, where velocity is 21 cm/s. The data indicates that the current velocity decreases in downstream direction as the grain size does.

The phenomenon is only possible in connection with entrainment and deposition of non-uniform sediments, which also explains the longitudinal sediment sorting or turbidity deposit sequence. However, it is presently impossible to quantify this sediment exchange mechanism of different sediment particle sizes between the flow and the bed. Because bed load transport and related phenomena such as sheltering and armoring effects in non-uniform flow condition are not fully understood even in open channel sediment transport. Experimental investigations are strongly desirable.

6.6 CONCLUSIONS

A model of the steady-state spatially varied turbidity current with erosion and deposition of sediment is applied to two acutal cases: a mine tailings discharge into Lake Superior near Silver Bay, Minnesota, and Scripps Submarine Canyon.

The model can qualitatively explain the origin of submarine canyons and the mechanics of underwater suspended sediment transport by simulating the growth and decay of the turbidity currents originating near the shore and controlled largely by erosion and deposition of sediment.

The behavoir of turbidity currents is found to vary depending on the the combination of initial conditions, size of sediment particle, and channel bed slope.

TABLE 6-1

Typical Measurements of Turbidity Currents made of Non-Uniform Sediment.

Name of Submarine Canyon	U_{max} cm/s	S.D. m	Material	D_{50}
Washington	20	600	sandy silt	0.21
Welmington	44	723	silty sand	0.044
Hudson	21	1222	clayey silt	0.004
	33	224	sand	0.243
Hydrographer	53	384	sand	0.190
	39	713	silty sand	0.044

S.D. = Station Depth

U_{max} = the maximum current velocity measured at 3 m above channel bed.

Velocity data shown above are down-canyon components. (source: Keller and Shepard, 1978)

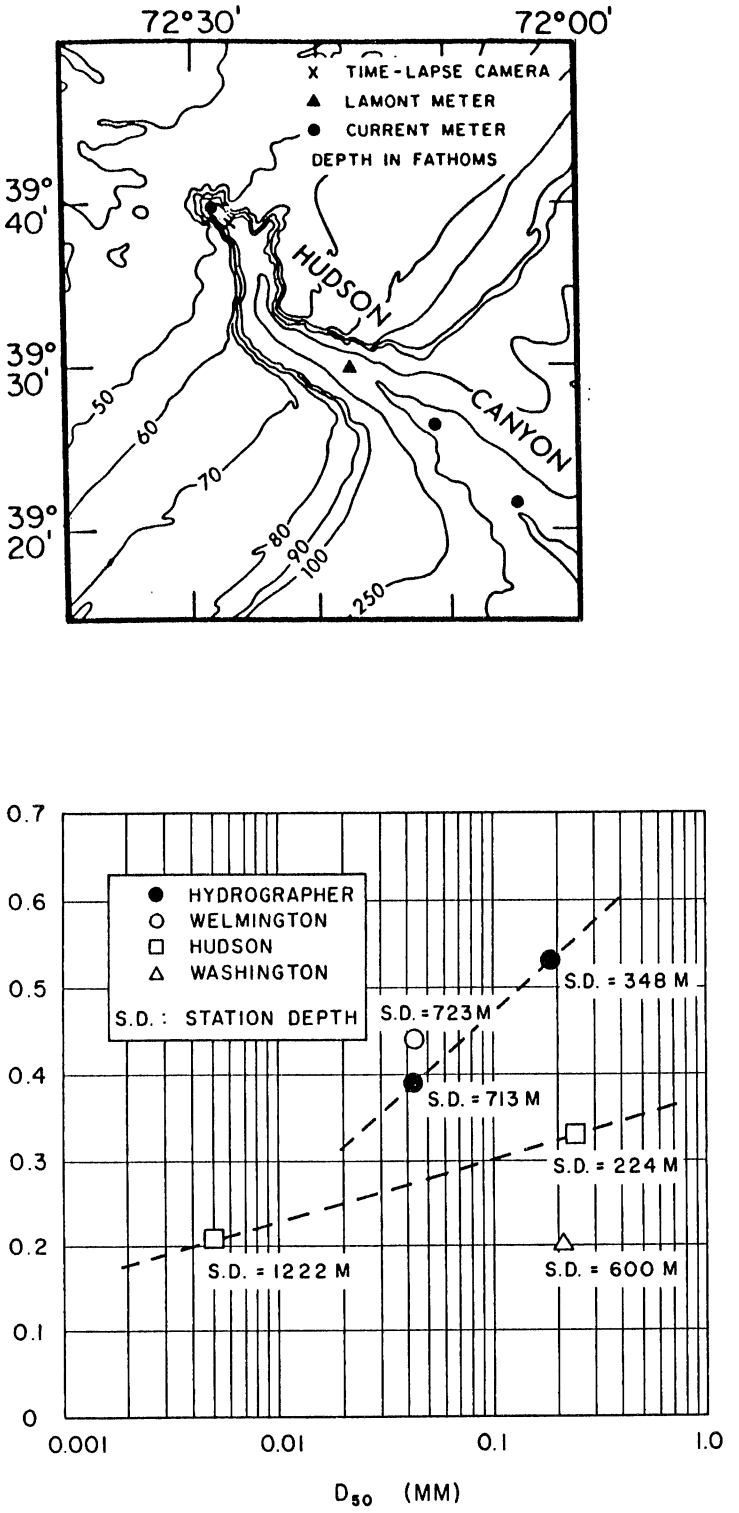

Fig. 6-20 U_{max} measured at 3 m above the channel bed vs grain size in major submarine canyons located along the continental margin off the northeastern United States. (Data source: Keller and Shepard, 1978.)

A classification can by made in terms of the rate of change in both current velocity and concentration. In erosive-depositional turbidity currents, the flows will either grow (accelerating-erosive type) or finally vanish (decelerating-depositional type).

The sensitivity of the model to model parameters for the distributions of velocity or buoyancy and for bed friction has been evaluated for the two site studies. Meaningful choices have been identified as $S_1 = 0.2$, $S_2 = 0.6$, and $C_{bo} = 0.02$.

The effect of initial conditions on the current growth or decay has also been studied. For accelerating-erosive currents, initial conditions appear to be of importance only over short distance.

7. FINAL COMMENTS AND GENERAL CONCLUSIONS

In this thesis, suspension gravity currents (turbidity currents) containing uniform material are investigated and analytically in two different channel geometries: sloping channels with constant width (Chap. 4) and sloping channels with diverging side walls (Chap. 5). The former is a special case of the latter. The model extends the non-suspension gravity current (density underflow) analysis by Ellison and Turner [1959].

Turbidity currents are erosive and depositive and therefore, play a significant role in aquatic environment. They contribute to the sedimentation problem in reservoirs, to redistribution of sediment in lakes, beach erosion along coastal regions and the formation of submarine canyons. These are only some examples associated with turbidity currents.

A sediment entrainment function (Chap. 4) is derived, utilizing available data for suspended sediment transport in surface (open channel) flow. It is applied to the model of subsurface turbidity currents. Simulations of turbidity currents at two sites (Lake Superior and Scripps Submarine Canyon) are also presented in order to demonstrate the qualitative validity of the model (Chap. 6).

Turbidity currents are caused by various mechanisms in nature. One of these, direct inflow of dense water into stagnant pooled clear water (so-called plunging flow) is investigated herein (Chap. 2).

The main findings are as follows:

1) The results of the plunging phenomenon analysis suggest that it is theoretically possible to predict a plunge depth (h_p) by imposing

downstream conditions obtained from gradually varied stratified flow analysis only when it occurs in a constant width channel or in the diverging channel with a steep slope.

In a channel of constant width the densimetric Froude number (F_p) at a plunge point is a function of channel friction coefficient (f_b), slope (S), and rate of initial mixing (γ) when the channel slope is mild. F_b is a function of γ on a steep slope. The rate of initial mixing cannot be determined theoretically, because it is essentially a turbulent mixing process. Experimental determination, however, is possible.

When a channel is expanding, channel divergence (δ) can add another complexity to plunging flow. In particular, δ can be of considerable significance if the channel aspect ratio (A_p) at the plunge line is small, but of less importance if δ is large. Densimetric Froude number and the rate of initial mixing vary, depending on where inflows plunge. The results from a constant width channel apply to a diverging channel only if A_p is large. Both F_p and γ can vary, dependent on channel geometry (S and δ). This is why experimental and field data are different among investigators.

2) A sediment entrainment function (E_s) is obtained empirically, using available flow. It is found that the sediment entrainment function is adequately described by two similarity parameters, suspension parameter (V_f/u_*) and particle Reynolds number (R_p). E_s posesses very steep slope against V_f/u_*. This implies that the resuspension mechanism is "explosive" once bed shear has reached critical value. This finding is

consistent with many other investigations. The significance of R_p has been mostly overlooked. In most previous investigations variations of R_p are usually within a small range. When bed material is constituted by different size of sediments, the parameter D_i/D_{50} is an additional similarity parameter.

3) With turbidity current model it is possible to estimate mean flow velocity (U), mean flow concentration (C), mean flow thickness (H), and the variation (η_b) of bed elevation due to aggradation and degradation caused by subaqueous suspended sediment transport, occurring in constant or slightly expanding channels.

The behavior of turbidity currents made of uniform material is dependent on (a) initial conditions (flow velocity (U_o), flow concentration (C_o), flow thickness (H_o), channel aspect ratio (A_o)), (b) properties of sediment (particle size (D_s), specific gravity of sediment (σ)), (c) property of water (kinematic viscosity (υ)), and (d) characteristics of channel (channel bed slope (S) and divergence angle (δ), friction factor at the bed (C_b) and at the wall (C_w)). The model, can predict at least qualitatively these unknowns. The model requires further elaboration in order to raise its capabilities to a fully quantitative level. Such refinement requires, among others, specification of shape factor S_1, S_2 etc., as a function of the flow itself. This is of particular importance when turbidity currents are depositing, which is more significant than eroding currents in many engineering applications. The uncertainty of the model mainly stems from lack of knowledge of velocity and concentration distributions, and

effects of the currents on bed forms. These are impossible to determine theoretically at present. Experimental investigations in both laboratory and field are necessary. In particular, it is most desirable to quantify the relationship between bed forms and the currents.

More results are presented in the end of each chapter.

Several worthwhile results were obtained in the course of this study. At the same time, the author has found more questions than answers for the problem investigated. For instance, the interaction between plunging process and sediment deposition, the mechanics of sediment exchange in an internal hydraulic jump, the interaction between the currents and the bed through bed load transport, bed forms in a non-uniform flow field and their relation to velocity and concentration profiles, and the sediment exchange and sorting mechanism for turbidity currents made of non-uniform sediments. These are only some of the questions. This study suggests future research of these problems and related topics.

LIST OF REFERENCES

Akiyama, J. and Fukushima, Y.
"Entrainment of Noncohesive Bed Sediment into Suspension," Proceedings of the Third International Sysmposium on River Sedimentation, (Wang, Shen, and Ding, ed.), University of Mississippi, pp. 804-813, 1986.

Akiyama, J. and Stefan, H.
"Theory of Plunging Flow into a Reservoir," Internal Memorandum no. IM-97, St. Anthony Falls Hydraulic Laboratory, University of Minnesota, December, 1981.

Akiyama, J. and Stefan, H
"Plunging Flow into a Reservoir: Theory," ASCE, Jour. Hydraulic Engineering, Vol. 110, No. HY4, April, 1984.

Akiyama, J. and Stefan, H.
"Turbidity Current with Erosion and Deposition," Journal of Hydraulic Engineering, ASCE, Vol. 111, No. HY12, December, 1985.

Akiayma, J. and Stefan, H.
"Prediction of Turbidity Currents in Reservoirs and Coastal Regions," Proceedings of the Third International Symposium on River Sedimentation, (Wang, Shen, and Ding, ed.), University of Mississippi, pp. 1295-1305, 1986.

Akiyama, J. and Stefan, H.
"Onset of Underflow in Slightly Diverging Channels," Journal of Hydraulic Engineering, ASCE, 1987, in Press.

Akiyama, J. and Stefan, H.
"Model of a Turbidity Current in a Diverging Channel," submitted to Journal of Water Resources Research, AGU, 1987.

Alavian, V.
"Behavior of Density Currents on an Incline," Journal of Hydraulic Engineering, ASCE, Vol. 112, No. HY1, January, pp. 27-42, 1986.

Apmann, R. P., and Rumer, R. R.
"Diffusion of Sediment in Developing Flow," Journal of Hydraulic Engineering, ASCE, Vol. 96, No. HY1, January, pp. 109-123, 1970.

Ashida, K. and Egashira, S.
"Hydraulic Characteristics of Thermocline in Reservoirs," Proceedings, 17th Congress of the IAHR, Vol. 2, 1977.

Ashida, K and Egashira, S.
"Basic Study on Turbidity Currents," Proceedings, Japan Society of Civil Engineering, 237, pp. 37-50, 1975, (in Japanese).

Bagnold, R. A.
"Auto-suspension of Transported Sediment; Turbidity Currents," Proceedings, Royal Society of London, Ser. A, 205, pp. 315-319, 1962.

Bata, G. and Knezevich, B.
"Some Observations of Density Currents in the Laboratory and in the Field," Proceedings of Minnesota International Hydraulic Convention, pp. 387-400, 1953.

Benjamin, T. B.
"Gravity Currents and Related Phenomena," Journal of Fluid Mechanics, Vol. 31, Part 2, pp. 209-248, 1968.

Bonnefille, R. and Goddet, J.
"Etude des Courants de Densite en Canal," Proceedings, 8th Congress IAHR, August, 1959.

Chu, F. H., Pilkey, W. D., Pilkey, O. H.
"An Analytical Study of Turbidity Current Steady Flow," Marine Geology, 33, pp. 205-220, 1979.

Chu, H. V. and Vanvari, M. R.
"Experimental Study of Turbulent Stratified Shearing Flow," Journal of Hydraulic Engineering, ASCE, Vol. HY6, June pp. 691-705, 1976.

Chu, H. V. and Baddour, E. R.
"Turbulent Gravity-Stratified Shear Flows," Journal of Fluid Mechanics, Vol. 138, pp. 353-378, 1984.

Colby, B. R. and Hembree, C. h.
"Computations of Total Sediment Discharge Niobrara River near Cody, Nebraska," Water Supply paper 1357, U.S. Geological Survey, Washington, D. C., 1955.

Coleman, N. I.
"A New Examination of Sediment Suspension in Open Channels," Journal of Hydrualic Research, IAHR, Vol. 7, No. 1, pp. 67-82, 1969.

Dietrich, E. W.
"The Setting Velocity of Natural-shaped Particle," Water Resources Research, Vol. 18, No. 6, pp. 1615-1626, December, 1982.

Dobbins, W. E.
"Effect of Turbulence on Sedimentation," Trans., ASCE, Vol. 109, Paper No. 2218, pp. 629-678, 1944.

Einstein, B. A.
"The Bed Load Function for Sediment Transportation in Open Channels," Technical Bulletin 1026, U.S. Department of Agriculture, Soil Conservation Service, Washington, D. C., 1950.

Einstein, B. A. and Chien, N.
"Effects of Heavy Sediment Concentration near the Bed on Velocity and Sediment Distribution," MRD Series No. 8, University of California, Institute of Engineering Research, and Corps of Engineering, Missouri River Div., Omaha, Nebraska, 1955.

Elder, R. A. and Wunderlich, W. O.
"Inflow Density Currents in TVA Reservoirs," Proceedings, International Symposium on Stratified Flows, Novosibrisk pp. 221-236, 1972.

Ellison, T. H. and Turner, J. S.
"Turbulent Entrainment in Stratified Flow," Journal of Fluid Mechanics, Vol. 6, pp. 423-448, 1959.

Engelund, F. and Fredsoe, J.
"A Sediment Transport Model for Straight Alluvial Channels," Nordic Hydrology 7, pp. 293-306, 1976.

Eskinazi, S. and Kruka, V.
"Mixing of a Turbulent Wall Jet into a Free-Stream," Journal of Engineering Mechanics Division, ASCE, Vol. 88, No. EM2, April, pp. 125-143, 1962.

Farrell, G. J. and Stefan, H. G.
"Buoyant Induced Plunging Flow into Reservoirs and Coastal Regions," Project Report No. 241, St. Anthony Falls Hydraulic Laboratory, University of Minnesota, July 1986.

Fietz, T. R. and Wood, I. R.
"Three Dimensional Density Current," Journal of Hydraulic Engineering, ASCE, Vol. 93, No. HY6, November, pp. 1-23, 1969.

Fisher, H. B., List, E. J., Koh, R. C., Imberger, J., and Brooks, N. H.
Mixing and Inland and Coastal Water, Academic Press, 1979.

Ford, D. F. and Johnson, M. C.
"Field Observations of Density Currents in Impoundments," Proceedings, Symposium on Surface Water Impoundments, Minneapolis, Minnesota, June, 1980, Publ. by ASCE, 1981.

Ford, D. F., Johnson, M. C., and Monismith, S. G.
"Density Inflows to DeGray Lake, Arkansas," Proceedings, Second International Symposium on Stratified Flows, IAHR, Trondheim, Norway, June, pp. 24-27, 1980.

Forthmann, E.
"Turbulent Jet Expansion," English Trans. N.A.C.A. TM-789, 1936.

Fukuoka, S., Fukushima, Y., and Nakamura, K.
"Study on the Plunge Depth Interface Form of Density Currents in a Two-Dimensional Reservoir," Proceedings of the Japan Society of Civil Engineers, 302, pp. 55-65, 1980. (in Japanese)

Fukushima, Y., Parker, G., and Pantin, H. M.
"Prediction of Ignition Turbidity Currents in Scripps Submarine Canyon," Marine Geology, Vol. 67, pp. 55081, 1985.

Garcia, M. H.
"Experimental Study of Turbidity Currents," M.S. thesis submitted to University of Minnesota, Minneapolis, Minnesota, September, 1985, 138 p.

Georgiev, B. V.
"Some Experimental Investigation on Turbulent Characteristics of Stratified Flows," Proceedings, International Symposium on Stratified Flows, Novosibirsk, pp. 507-514, 1972.

Glauert, M. B.
"The Wall Jet," Journal of Fluid Mechanics, Vol. 1, pp. 625-643, 1956.

Harper, W. L. and Waldrop, W. R.
"Numerical Hydrodynamics of Reservoir Stratification and Density Currents," Proceedings, Second International Symposium on Stratified Flows, IAHR, Trondheim, Norway, June, pp. 1011-1020, 1980.

Hauenstein, W. and Dracos, T.
"Investigation of Plunging Density Currents Generated by Inflows in Lakes," IAHR, Journal of Hydraulic Research, Vol. 22, No. 3, pp. 157-179, 1984.

Hebbert, B., Imberger, J., Loh, I., and Patterson, J.
"Collie River Underflow into the Wellington Reservoir," Journal of Hydraulic Engineering, ASCE, Vol. 105, HY5, May, pp. 533-545, 1979.

Heezen, B. C., Menzies, R. J., Schneider, E. D., Erwing, W. M. and Granelli, N. C. L.
"Congo Submarine Canyon," American Association Petrol. Geol. Bulletin, 48(7), 1126-1127, 1130-1143, 1148-1149, 1964.

Heezen, B. C. and Ewing, M
"Orleansville Earthquake and Turbidity Currents," Bulletin of the American Association Petrol. Geol., 39, 2505-2514, 1955.

Heezen, B. C. and Ewing, M.
"Turbidity Currents and Submarine Slumps and Grand Banks Earthquake," American Journal of Science, 250, 849-873, 1952.

Hinze, J. O.
Turbulence, McGRAW-HILL, 2nd Edition, 1975.

Hinze, J. O.
"On the Hydrodynamics of Turbidity Currents," Geol. Miinbouw, Vol. 39e, pp. 18-25, 1960.

Hjemfelt, A. T. and Lenau, C. W.
"Nonequilibrium Transport of Suspended Sediment," Journal of Hydraulic Engineering, ASCE, Vol. 96, No. HY7, July, pp. 1567-1580, 1970.

Howard, C. S.
"Density Currents in Lake Mead," Proceedings, Minnesota International Hydraulic Covention, pp. 355-368, 1953.

Ikeda, S. and Asaeda, T.
"Sediment Suspension with Ripple Bed," Journal of the Hydraulic Engineering, ASCE, Vol. 109, HY8, pp. 409-423, 1983.

Ippen, A. T. and Harleman, D. R. F.
"Steady-State Characteristics of Subsurface Flow," National Bureau of Standards (U.S.) Circular 521, pp. 79-93, 1952.

Irwin, H. P.
"Meaurements in a Self-Preserving Plane Wall Jet in a Positive Pressure Gradient," Journal of Fluids Mechanics, Vol. 61, Part 1, pp. 33-63, 1973.

Ishibashi, T., Akimoto, T., Shirasuna, T., Ishikawa, H., Saito, S., and Mayanaga, Y.
"Field Survey on the Flow and Heat Balance in a Stratified Reservoir," Proceedings of the 21st Japanese Conference on Hydraulics, pp. 1-8, 1977. (in Japanese) as quoted in Kan and Tamai [1981].

Itakura, T. and Kishi, T.
"Study on the Turbidity Density Current in a Reservoir," 16 Symposium on Science of Natural Disaster, pp. 233-234, 1979, (in Japanese) as quoted in Kan and Tamai [1981].

Itakura, T. and Kishi, T.
"Open Channel Flow with Suspended Sediments," Journal of Hydraulic Engineering, ASCE, Vol. 106, No. HY8, pp. 1345-1352, 1980.

Inman, D. L., Nordstrom, C. E., and Flick, R. E.
"Currents in Submarine Canyons: an Air-Sea-Land Interaction," Annual Rev. of Fluid Mechanics, pp. 275-310, 1976.

Jain, S. C.
"Plunging Phenomena in Reservoirs," Proceedings of Symposium on Surface Water Impoundaments, Minneapolis, Minnesota, June, 1980, published by ASCE, 1981.

Johnson, T. R.
Unpublished data for negatively buoyant flow in a diverging channel, 1986.

Kan, K. and Tamai, N.
"On the Plunging Point and Initial Mixing of the Inflow into Reservoirs," Proceedings of the 25th Japanese Conference on Hydraulics, pp. 631-636, 1981. (in Japanese).

Kato, H. and Phillips, O. M.
"On the Penetration of a Turbulent Layer into a Stratified Fluid," Journal of Fluid Mechanics, Vol. 37, pp. 643-655, 1969.

Keller, G. H. and Shepard, F. P.
"Currents and Sedimentary Process in Submarine Canyons off the Northeast United States," Cp. 2, pp. 15-32, Sedimentation in Submarine Canyons, Fans, and Trenches, ed. by Stanley, D. J. and Kelling, G. Dowden, Hutchinson & Ross, Inc. 1978.

Krause, D. C., White, W. C., Piper, D. W., and Heezen, B. C.
"Turbidity Currents and Cable Breaks in the Western New Britain Trench," Geological Society of American Bulletin, Vol. 81, pp. 2153-2160, July 1970.

Komer, P. D.
"The Channelized Flow Turbidity Currents with Application to Monterey Deep-Sea Fan Channel," Journal of Geophysical Research, Vol. 74, No. 18, pp. 4544-4558, 1969.

Komura, S.
"Discussion of Sediment Transportation Mechanics: Introduction and Properties of Sediment," Journal of Hydraulic Engineering, ASCE, Vol. 89, No. HY1, January, pp. 263-266, 1963

Lambert, A. M., Kelts, K. R., and Marshall, N. R.
"Measurements of Density Underflows in Walensee, Switzerland," Sedimentology, Vol. 23, pp. 87-105, 1976.

Lane, E. W. and Kalinske, A. A.
"Engineering Calculation of Suspended Sediment," Transaction, A.G.U., No. 22, pp. 603-607, 1941

Laursen, E. M.
"The Total Sediment Load of Stream," Proceedings, ASCE, Vol. 84, No. HY1, January, 1958.

Lin, P., Huan, J., and Li, X.
"Unsteady Transport of Suspended Load at Small Concentrations," Journal of Hydraulic Engineering, ASCE, Vol. 109, No. HY1, January, pp. 86-98, 1983

Lofquist, K.
"Flow and Stress Near an Interface between Stratified Liquids," Physics of Fluids, 3, pp. 158-175, 1960.

Lutni, S.
Some New Aspects of Two-Dimensional Turbidity Currents," Sedimentology, Vol. 28, pp. 97-105, 1980.

McTigue, D. F.
"Mixture Theory for Suspended Sediment Transport," Journal of Hydraulic Engineering, ASCE, Vol. 107, No. HY6, June 1981.

Mai, C. C.
"Non-uniform Diffusion of Suspended Sediment, " Journal of Hydrualic Engineering, ASCE, Vol. 95, No. HY1, January, pp. 581-584, 1969.

Middleton, G. V.
"Experiments in Density and Turbidity Currents II. Uniform Flow of Density Currents," Canadian Journal of Earth Sciences, Vol. 3, pp. 627-637, 1966.

Morton, B. R., Taylor, G., and Turner, J. S.
"Turbulent Gravitational Convection from Maintained and Instantaneous Sources," Proceedings of Royal Society, A234, pp. 1-23, 1956.

Nordin, C. F. and Dempster, G. R.
"Vertical Distribution of Velocity and Suspended Sediment Middle Rio Grande New Mexico," Professional paper 462-B, U.S.G.S., Washington, D. C., 1963.

Normark, R. W. and Dickson, H. F.
"Sublacustrine Fan Morphology in Lake Superior," The American Association of Petroleum Geologist Bulletin, Vol. 60, No. 7, July, 1976.

Onish, Y., Jain, S. C., and Kennedy, J. F.
"Effects of Meandering in Alluvial Streams," Journal of Hydraulic Engineering, ASCE, Vol. 102, No. HY7, July, pp. 899-917, 1976.

Pantin, H. M.
"Interaction between Velocity and Effective Density in Turbidity Flow: Phase-Plane Analysis, with Criteria for Autosuspension," Marine Geology, 31, pp. 59-99, 1979.

Parker, G. and Anderson, A. G.
"Basic Principles of River Hydraulics," Journal of Hydraulic Engineering, ASCE, Vol. 103, No. HY9, pp. 1077-1087, 1977.

Parker, G.
"Self-formed Straight Rivers with Equilibrium Banks and Mobile Bed, Part 1. The Sand-Silt River," Journal of Fluid Mechanics, Vol. 89, pp. 109-125, 1978.

Parker, G.
"Conditions for the Ignition of Catastrophically Erosive Turbidity Currents," Marine Geology, Vol. 89, pp. 109-125, 1978.

Partheniades, E.
"Erosion and Deposition of Cohesive Soils," Journal of Hydraulic Engineering, ASCE, Vol. 91, No. HY1, January, pp. , 1965.

Patel, R. P. and Newman, B. G.
"Self-Preserving Two-Dimensional Jets and Wall Jets in a Moving Stream," McGill University Report AE. 5, 1961.

Rajaratnam, N.
Turbulent Jets, ELSEVIER, 1976.

Rajaratnam, N.
"Plane Turbulent Wall Jets on Rough Boundaries," Tech. Rep. Dept. of Civil Engineering, University of Alberta, Edmonton, 1965.

van Rijn, L. C.
"Sediment Transport, Part II: Suspended Load Transport," Journal of Hydraulic Engineering, ASCE, Vol. 110, No. HY11, November, pp. 1613-1641, 1984.

Rouse, H.
"Experiments on the Mechanics of Sediment Suspension," 5th International Congress of Applied Mechanics (Den Hartog and Peters, ed.) John Wiley and Sons, New York, 1938.

Samaga, B. R., Ranga Raju, K. G., and Garde, R. J.
Concentration Distribution of Sediment Mixtures in Open-Channel Flow," Journal of Hydraulic Research, Vol. 23, No. 5, pp. 467-483, 1985.

Savage, S. B. and Brimberg, J.
"Analysis of Plunging Phenomena in Water Resources, " IAHR, Journal of Hydraulic Research, Vol. 13, No. 2, pp. 187-204, 1975.

Schlichting, H.
Boundary Layer Theory, 7th Edition, McGRAW-HILL, 1979

Sheng, Y. P. and Lick, W.
"The Transport and Resuspension of Sediments in a Shallow Lake," Water Resources Research, Vol. 84, No. C4, pp. 1809-1826, 1979.

Schwarz, W. H. and Cosart, W. P.
"Two Dimensional Turbulent Wall Jet," Journal of Fluid Mechanics, Vol. 10, 1961.

Singh, B. and Shah, C. R.
"Plunging Phenomenon of Density Currents in Reservoirs," LaHouille Blanche, Vol. 26, No. 1, pp. 59-64, 1971.

Stefan, H.
"High Concentration Turbidity Currents in Reservoirs," Proceedings, 15th International Congress of IAHR, Istanbul, 1973.

Stefan, H. and Hayakawa, N.
"Mixing Induced by an Internal Hydraulic Jump," Water Resources Bulletin, American Water Resources Association, Vol, 8, No. 3, pp. 531-545, 1972.

Straub, L. G., Anderson, A. G., and Flammer, G. H.
"Experiments on the Influence of Temperature on Sediment Load," MRD Sediment Series No. 10, St. Anthony Falls Hydraulic Laboratory, Minneapolis, Minnesota, 1958.

Tesaker, E.
"Uniform Turbidity Current Experiments," Ph.D thesis submitted to the Technical University of Norway, Trondheim, 1969.

Tsubaki, T. and Komatsu, T.
"Flow Properties and Turbulent Entrainment of Stratified Inclined Plume," Proceedings, 23rd National Hydraulic Conference, Japan Society of Civil Engineering, pp. 415-422, 1979. (in Japanese).

Tsubaki, T. and Komatsu, T.
"Flow Properties and Turbulent Entrainment of Two-Dimensional Stratified Surface Jet," Proceedings of the Japan Society of Civil Engineering, No. 273, pp. 69-81, 1978.

Turner, J. S.
Buoyancy Effects in Fluids, Cambridge University Press, England, 1973.

Vanoni, V. A.
"Some Experiments on the Transportation of Suspended Load," Trans., American Geophysical Union, Vol. 22, pp. 608-628, 1941.

Vanoni, V. A. and Nomicos, G. N.
"Resistance Properties of Sediment Laden Stream," Trans., ASCE, Vol. 125, Paper No. 3055, pp. 1140-1175, 1960.

Velikanov, M. A.
"Principle of the Gravitational theory of the Movement of Sediments," Acad. of Sci. Bull, USSR, Geophys. Series, No. 4, pp. 349-359, 1954.

Verhoff, A.
"The Two-Dimensional Turbulent Wall Jet with and without an External Stream," Rep. 626, Princeton University, 1963.

Wilkinson, D. L.
"Dynamics of Contained Oil Slicks," Journal of Hydraulic Engineering, ASCE, Vol. 98, No. HY6, June, pp. 1013-1030, 1972.

Wilkinson, D. L. and Wood, I. R.
A Rapidly Varied Flow Phenomenon in a Two Layer Flow," Journal of Fluid Mechanics, Vol. 47, pp. 241-256, 1971.

Willis, J. C.
"Suspended Load from Error Function Models," Journal of Hydraulic Engineering, ASCE, Vol. 105, No. HY7, July, 1979.

Willis, J. C., Coleman, N. L., and Ellis, W. M.
"Laboratory Study of Transport of Fine Sand," Journal of Hydraulic Engineering, Vol. 98, No. HY3, pp. ,1972.

Wunderlich, W. O. and Elder, R. A.
"Mechanics of Flow Through Man-Made Lakes," Man-Made Lakes: Their Problems and Environmental Effects, W. C. Ackermann, G. F. White, and E. B. Worthington, eds., American Geophysical Union, Washington, D. C., 1973.

Yalin, M. S.
Mechanics of Sediment Transport, 2nd Edition, PERGAMAN PRESS, 1977.

Yalin, M. S. and Krishinappan, B. G.
"Stochastic Aspects of Saltation Paths of Cohesiveless Sediment," Proceedings, 3rd International Symposium on Stochastic Hydraulics, Tokyo, Japan, pp. 325-336, 1980.

APPENDIX I. DATA FOR PLUNGE DEPTH (2-D)

Singh & Shah [1971]
S = 1/47 ~ 1/179

$(q^2/g')^{1/3}$ (cm)	h_f (cm)	$(q^2/g')^{1/3}$ (cm)	h_p (cm)
16.0	22.0	4.8	9.0
14.6	22.5	4.5	8.3
13.4	19.5	4.7	6.8
12.2	19.6	3.3	7.9
12.3	16.5	2.2	4.6
11.1	17.2	2.3	4.6
10.9	17.6	2.2	4.7
10.9	15.3	2.5	4.6
9.8	13.1	2.5	5.5
9.3	13.4	2.7	6.5
8.8	12.5	3.3	6.4
7.2	13.9	2.4	1.3
6.8	13.2	2.3	2.3
8.9	11.9	2.4	3.4
8.0	11.0	2.3	1.2
5.8	13.0	2.2	2.2
6.5	12.4	2.2	2.6
7.9	11.3	2.1	3.2
7.6	11.6	1.8	1.0
7.7	10.8	1.8	1.3
6.7	11.2	1.8	1.4
7.3	10.2	1.8	1.7
7.2	10.4	1.7	2.7
7.0	10.3	1.6	2.9
6.1	10.2	1.5	2.4
5.4	9.5	1.3	2.6
5.1	9.5	1.6	2.1
4.2	9.8	1.6	1.9
4.4	9.4	1.3	1.7
5.2	8.9	1.5	1.5
5.1	7.8	1.4	1.0

Fukuoka et al [1980]

S = 1/10

$(q^2/g')^{1/3}$ (cm)	h_p (cm)
2.3	4.1
4.78	6.8
7.08	9.1
4.24	6.3
6.36	8.6
5.07	6.2
4.30	6.3

S = 1/60

2.26	4.3
4.86	6.5
7.21	10.7
3.66	5.2
5.37	7.6
1.47	2.3
2.25	3.2

Farrell and Stefan [1986]

S = 1/21

$(q^2/g')^{1/3}$ (cm)	h_p (cm)
16.15	20.73
16.15	20.73
16.15	20.73
13.11	16.15
18.29	24.08
18.59	24.69
7.92	10.36

Hebbert et al [1979]

S = 1/1000

$(q^2/g')^{1/3}$ (m)	h_p (m)
1.68	5.60
3.50	12.00
3.38	11.60
6.16	21.00
6.00	20.20
4.80	16.20

Ford and Johnson [1981]

S = 1/1200

$(q^2/g')^{1/3}$ (cm)	h_p (m)
1.05	1.50
3.61	6.10
3.38	6.00
3.14	8.00
3.84	7.10
0.815	1.800
0.408	1.700

APPENDIX B - DATA FOR SEDIMENT ENTRAINMENT FUNCTION

(i) Laboratory Data

Straub, Anderson, and Flammer (1958)

[Q = 14.16 l/s]
[η_a = 0.05]

Run No.	H (cm)	R (cm)	S_e	u_* (cms)	$\bar{U}$ (cm/s)	c_a (g/l)	D_{50} (mm)	V_f (m/s)	T (^oF)	ν (cm^2/s)	c_a	V_f/U_*
1	7.47	5.67	0.00235	3.61	62.2	1.92	0.163	1.60	86	0.0088	0.00072	0.443
2	7.25	5.52	0.00256	3.72	64.0	4.73	0.163	1.50	75	0.0099	0.00178	0.403
3	7.07	5.39	0.00282	3.86	65.5	5.60	0.163	1.30	63	0.0117	0.00211	0.336
4	7.04	5.49	0.00324	4.18	65.8	7.13	0.163	1.20	52	0.0137	0.00269	0.287
5	6.86	5.24	0.00326	4.09	67.7	10.18	0.163	1.04	42.5	0.0160	0.00384	0.254
6	6.80	5.27	0.00362	4.32	68.3	10.53	0.163	0.94	35	0.0182	0.00397	0.217

$V_f D/\nu$	$\frac{U_*}{(\gamma_s-1)gD}$	R_p	$(\frac{V_f}{U_*})R_p^{-0.5}$
2.96	0.494	10.6	0.150
2.47	0.525	9.07	0.146
1.81	0.565	7.80	0.131
1.42	0.663	6.92	0.118
1.06	0.635	6.30	0.090
0.84	0.708	5.89	0.096

Vanoni and Nomicos (1959)

Run #	Q (l/s)	H (cm)	R (cm)	S	u_* (cm/s)	$\bar{U}$ (cm/s)	D_{50} (mm)	V_f (cm/s)	η_a	c_a (g/l)	c_a (Vol. con.)	V_f/u_*	ν (at 25°)	$\frac{V_f D_{50}}{\nu}$
1	8.67	8.66	5.24	0.00250	3.60	37.49	0.105	0.945	0.153	15.0	0.0057	0.263	0.00898	1.10
3	12.26	7.44	4.79	0.00200	3.08	61.57	0.105	0.945	0.050	25.0	0.0094	0.307	0.00898	1.10
5	14.41	7.83	4.94	0.00206	3.17	68.88	0.105	0.945	0.055	25.0	0.0094	0.298	0.00898	1.10
7	14.41	7.77	4.91	0.00258	3.54	69.49	0.161	1.890	0.077	6.8	0.0026	0.534	0.00898	3.29

$\frac{u_*^2}{(\gamma s-1)gD_{50}}$	R_p	$(\frac{V_f}{U_*})Rp^{-0.50}$
0.763	.254	.128
0.559	.297	.149
0.592	.287	.145
0.738	.344	.193

Einstein & Chien (1955)

Run no.	Q (l/s)	H' (cm)	R (cm)	S_e ($x10^{-3}$)	u_* (cm/s)	V (cm/s)	η_a	c_a (g/l)	c_{a*} (g/l)	D_s (mm)	V_f (cm/s)
Coarse Sand											
S-1	78.72	13.75	9.57	13.9	11.42	187				1.300	14.9
	79.29	13.81	9.60	14.1	11.52	187	0.0397	58.0	48		
S-2	74.76	11.95	8.69	19.4	12.85	204				1.300	14.9
	74.47	11.95	8.69	19.3	12.82	204	0.0536	121.0	130		
S-3	74.19	11.61	8.60	20.9	13.27	208				1.300	14.9
	74.47	11.64	8.56	20.9	13.24	208	0.0550	150.5	170		
S-4	73.91	11.52	8.75	23.6	14.23	210				1.300	14.9
	74.19	11.52	8.81	23.7	14.30	210	0.0646	197.5	230		
S-5	74.19	11.09	8.44	25.5	14.52	218				1.300	14.9
	73.9	10.85	8.23	25.8	14.43	223	0.0660	328.0	400		
Medium Sand											
S-6	82.97	14.33	9.97	14.3	11.82	189				0.940	12.5
	82.93	14.23	9.97	14.3	11.82	190	0.0447	28.0	25		
S-7	83.25	14.33	9.91	14.3	11.78	189				0.940	12.5
	82.40	14.14	9.72	14.2	11.63	190	0.0388	87.3	50		
S-8	80.70	13.87	9.66	14.3	11.64	190				0.940	12.5
	81.27	13.87	9.45	14.0	11.39	191	0.0317	111.5	68		
S-9	81.55	13.62	9.48	15.0	11.80	195				0.940	12.5
	80.14	13.41	9.39	15.3	11.87	194	0.0363	173.0	130		
S-10	80.70	13.17	9.48	17.3	12.68	200				0.940	12.5
	79.57	12.83	9.24	17.3	12.52	202	0.0403	262.5	180		
Fine Sand											
S-11	74.44	13.26	8.72	13.1	10.58	193				0.274	4.11
	74.44	13.32	8.81	13.1	10.63	192	0.0286	31.4	20		
S-12	78.15	13.19	8.44	12.2	10.05	193				0.274	4.11
	78.15	13.19	8.44	12.4	10.13	193	0.0300	204.6	130		
S-13	77.87	13.41	8.81	12.6	10.43	189				0.274	4.11
	77.31	13.32	8.90	12.8	10.57	189	0.0321	352.0	230		
S-14	77.31	12.31	8.67	17.4	12.16	205				0.274	4.11
	77.31	12.41	8.72	17.0	12.05	203	0.0331	386.0	300		
S-15	77.31	12.44	8.75	16.9	12.04	202				0.274	4.11
	77.31	12.41	8.69	16.7	11.93	203	0.0344	625.0	520		
S-16	75.04	11.89	8.50	18.6	12.45	206				0.274	4.11
	75.04	11.92	8.56	18.7	12.52	205	0.0372	621.0	530		

where:

c_{a*} = c_a at η_a = 0.05

R = Hy. Radius

S_e = energy slope

Omishi, Jain, and Kennedy (1976)

(Straight Channel)
D_{50} = .25 mm

Run No.	H (ft)	U (ft/s)	Sx10^4	$\bar{C}$ (g/l)	T (^oC)	V_f (ft/s)	u_* (ft/s)	V_f/u_*	γ	c_a	R_p	$(\frac{Vf}{u_*})R_p^{-0.5}$	Bed Form
1	.335	1.21	15.4	.326	28.4	.109	.126	.865	35.23	.0001	9.93	.274	D
2	.331	1.625	19.35	3.614	20.0	.099	.139	.712	26.84	.0010	7.38	.262	D
3	.316	1.92	16.5	5.161	21.8	.103	.124	.831	33.30	.0015	8.20	.290	T
4	.353	1.32	16.3	.948	25.5	.107	.133	.805	31.85	.0003	9.24	.265	D
5	.329	1.41	18.4	2.355	21.0	.102	.136	.750	28.86	.0007	7.97	.266	D
6	.267	1.33	25.4	1.508	21.0	.102	.164	.708	26.64	.0004	7.97	.251	D
7	.246	1.66	25.6	2.541	21.0	.102	.160	.729	27.76	.0008	7.97	.258	D
8	.253	1.26	26.7	1.523	21.0	.102	.145	.703	26.37	.0004	7.97	.249	D
9	.248	1.145	25.6	1.368	24.0	.105	.141	.745	28.59	.0004	8.79	.251	D
10	.402	1.56	14.65	1.974	24.0	.105	.133	.789	30.97	.0006	8.79	.266	D
11	.437	1.35	12.2	.474	26.0	.107	.126	.849	36.32	.0001	9.24	.279	D
12	.417	1.11	10.9	.319	25.0	.106	.117	.906	37.60	.0009	9.05	.301	D
13	.444	1.73	15.6	3.342	25.0	.106	.144	.736	28.11	.0009	9.05	.244	D

D: Dune
T: Transition

Einstein and Chien (1955)

Run No.	c_a Vol. Conc.	V_f/u_*	T ^oF	T ^oC	ν (m^2/s)	$\frac{u_*^2}{(\sigma - 1)gd}$	R_p	$(\frac{V_f}{u_*})R_p^{-0.50}$
S-1	0.0181	1.29	72.0	22.2	0.00961	0.631	196	0.114
S-2	0.0491	1.16	63.0	17.2	0.0107	0.782	175	0.108
S-3	0.0642	1.13	67.0	19.4	0.0102	0.834	184	0.103
S-4	0.0867	1.04	73.0	22.7	0.00950	0.973	199	0.091
S-5	0.151	1.03	65.0	18.3	0.0105	0.991	180	0.094
S-6	0.00943	1.06	79.0	26.1	0.00873	0.919	132	0.112
S-7	0.0189	1.07	68.0	20.0	0.0101	0.840	115	0.121
S-8	0.0257	1.09	68.5	20.3	0.0100	0.853	116	0.122
S-9	0.0491	1.05	74.0	23.3	0.00936	0.927	124	0.114
S-10	0.0679	0.998	79.0	26.1	0.00873	1.03	133	0.109
S-11	0.00755	0.387	70.5	21.4	0.00979	2.57	18.6	0.101
S-12	0.0491	0.405	71.0	21.7	0.00972	2.34	18.8	0.106
S-13	0.0868	0.389	71.0	21.7	0.00972	2.57	18.8	0.101
S-14	0.113	0.341	69.0	20.5	0.00999	3.30	18.3	0.089
S-15	0.196	0.344	66.0	18.9	0.00103	3.24	17.6	0.090
S-16	0.200	0.328	64.0	17.8	0.00106	3.57	17.2	0.086

Wills and Kennedy (1977)

[D_{50} = 0.54 mm]
[V_f = 0.28 ft/s]

Run No.	Q (cfs)	H (ft)	S_e ($\times 10^3$)	u_* (fps)	$\bar{C}$ (ppm)	T (^oF)	V_f/U_*	R_p	γ	Ca	$(\frac{V_f}{u_*})R_p^{-0.5}$
1	0.61	0.37	1.62	0.138	540	61.5	2.03	42.2	119.03	0.018	0.633
2	0.69	0.36	2.84	0.182	1300	64.0	1.54	43.5	79.87	0.029	0.233
3	0.83	0.35	3.09	0.186	1970	68.0	1.51	45.6	77.43	0.044	0.223
4	1.00	0.35	4.43	0.224	3010	65.0	1.25	44.0	59.36	0.50	0.188
5	1.10	0.34	5.77	0.251	3880	64.5	1.12	43.7	50.51	0.056	0.169
6	1.26	0.36	7.13	0.289	4330	70.0	0.97	46.8	41.34	0.051	0.142
7	1.43	0.33	8.00	0.290	↓	77.0	0.97	51.3	41.16	↓	0.135
8	1.67	0.36	7.92	0.302	6670	80.0	0.93	53.5	38.84	0.074	0.127
9	1.64	0.38	8.58	0.322	5690	78.5	0.87	52.4	35.52	0.057	0.120
10	1.20	0.35	7.99	0.300	4590	78.0	0.93	52.0	39.19	0.051	0.129
11	0.90	0.35	5.11	0.239	2620	78.0	1.17	52.0	54.15	0.041	0.163
12	0.68	0.39	2.92	0.191	910	77.0	1.47	51.3	74.56	0.020	0.205
13	0.76	0.48	1.40	0.148	510	78.0	1.89	52.0	107.61	0.016	0.262
14	1.01	0.42	3.47	0.217	1180	78.0	1.29	52.0	62.09	0.021	0.179
15	1.34	↓	↓	↓	2610	78.0	↓	52.0	↓	↓	↓
16	1.70	0.41	6.18	0.284	5370	78.0	0.99	52.0	31.86	0.049	0.137
17	1.30	0.44	4.24	0.244	3160	78.0	1.15	52.0	52.58	0.047	0.160
18	1.34	0.40	5.74	0.272	6050	90.0	1.03	62.5	45.01	0.077	0.130
19	1.27	0.47	4.37	0.257	2600	100.0	1.09	75.3	48.78	0.036	0.125
20	1.26	0.40	5.59	0.269	4980	100.0	1.04	75.3	45.76	0.065	0.120
21	0.98	0.45	3.39	0.221	1730	98.0	1.27	72.3	60.52	0.030	0.149
22	0.73	0.46	1.45	0.147	630	100.0	1.91	75.3	108.68	0.020	0.220
23	0.62	0.49	0.864	0.117	320	100.0	2.39	75.3	151.10	0.014	0.275
24	0.63	0.48	0.831	0.114	20	65.0	2.46	43.5	156.89	0.0008	0.372
25	0.85	0.47	1.85	0.165	640	64.5	1.70	43.5	92.24	0.017	0.258
26	1.26	0.42	4.24	0.241	2880	66.0	1.16	44.5	53.49	0.044	0.174
27	1.62	0.49	6.04	0.282	5470	64.5	0.99	43.5	42.80	0.067	0.149
28	1.25	0.45	3.78	0.234	2120	52.0	1.20	38.1	55.80	0.034	0.194
29	0.97	0.45	2.50	0.191	1080	51.0	1.47	37.3	74.56	0.023	0.240
30	0.71	0.49	1.17	0.135	170	52.0	2.07	38.1	122.87	0.0006	0.336
31	0.58	0.45	1.15	0.129	20	53.0	2.17	38.5	131.25	0.0008	0.350
32	0.84	0.44	1.86	0.161	560	70.0	1.74	46.8	95.30	0.015	0.254
33	1.11	0.42	4.05	0.234	1660	72.0	1.20	48.0	55.80	0.026	0.172
34	1.43	0.40	5.97	0.278	4010	71.0	1.00	47.4	43.29	0.050	0.145

Brooks (1952)

Run No.	Q (cfs)	H (ft)	S	U_* (ft/s)	T (^oC)	ν (x10^5)	V_f (ft/s)	V_f/U_*	R_p	γ	$\bar{C}$ (g/l)	C_a	$(\frac{V_f}{U_*})Rp^{-0.5}$	B.C.
SAND BED (D = 0.16mm)														
2	0.54	0.284	0.0018	0.100	17	1.15	0.051	0.51	2.32	17.01			0.335	S
3	0.435	0.243	0.0025	0.112	22	1.03	0.056	0.50	2.85	16.56	1.95	0.00938	0.296	S
4	0.43	0.236	0.0024	0.108	12.5	1.30	0.046	0.43	1.86	13.55	2.45	0.00930	0.315	S
5	0.28	0.180	0.0031	0.115	26	0.94	0.061	0.53	3.41	17.91	1.90	0.00960	0.287	M
6	0.345	0.195	0.0024	0.103	21	1.05	0.056	0.54	2.80	18.37	2.45	0.01280	0.323	S
7	0.435	0.243	0.0021	0.103	31.5	0.84	0.064	0.62	4.00	22.18	2.15	0.01350	0.310	S
8	0.375	0.24	0.0023	0.110	27.5	0.91	0.062	0.56	3.58	19.30	1.50	0.0082	0.296	M
9	0.285	0.245	0.0026	0.115	27.5	0.91	0.062	0.54	3.58	18.37	1.10	0.0057	0.286	D
10	0.200	0.25	0.0020	0.100	24	0.98	0.058	0.58	3.11	20.24	0.20	0.0011	0.329	D
11	0.205	0.155	0.0033	0.110	26	0.94	0.061	0.55	3.41	18.83	2.70	0.0144	0.298	M
12d	0.370	0.30	0.0022	0.111	26	0.94	0.061	0.55	3.41	18.83	0.72	0.00383	0.298	D
13	0.215	0.197	0.0035	0.124	26.5	0.93	0.061	0.49	3.44	16.12	1.20	0.00598	0.264	D
SAND BED (D = 0.10mm)														
21	0.435	0.236	0.00225	0.106	25.0	0.96	0.027	0.27	0.922	7.52	4.85	0.01040	0.293	S
21a	0.435	0.236	0.0022	0.104	25.0	0.96	0.027	0.26	0.922	7.19	4.90	0.100	0.271	S
23	0.325	0.189	0.00245	0.102	25.0	0.96	0.027	0.26	0.922	7.19	5.10	0.0104	0.271	S
24e	0.265	0.226	0.0028	0.116	25.0	0.96	0.027	0.23	0.922	6.23	4.00	0.0071	0.240	D
24e	0.265	0.179	″	″	25.0	0.96	0.027	″	0.922	″	7.00	″	″	LP
25	0.20	0.187	0.0033	0.118	25.0	0.96	0.027	0.23	0.922	6.23	5.30	0.0094	0.240	D
26	0.20	0.279	0.0013	0.084	25.0	0.96	0.027	0.32	0.922	9.27	0.19	0.0005	0.333	D
27	0.20	0.231	0.00235	0.107	25.0	0.96	0.027	0.25	0.922	6.87	1.35	0.0026	0.260	D
28	0.33	0.284	0.0024	0.116	25.0	0.96	0.027	0.23	0.922	6.23	3.60	0.0064	0.240	D
29	0.52	0.280	0.00185	0.101	25.2	0.96	0.027	0.27	0.922	7.52	3.45	0.0074	0.293	S
30	0.265	0.281	0.00215	0.108	25.0	0.96	0.027	0.25	0.922	6.87	1.75	0.0034	0.260	D

Ismail (1951)

Run No.	U (cm/s	i	$\bar{C}$ (g/l)	T (^{o}C)	υ (cm^2/s)	V_f (cm/s)	H (cm)	u_* (cm/s)	c_a (g/l)	η_a	c_{a*} (vol. c)
73	51.5	0.00277	2.39	21.0	0.0111	0.814	4.15	2.926	85	0.0345	0.0242
74	71.9	0.00415	7.23	25.0	0.0102	0.878	3.505	3.383	150	0.0625	0.0547
75	90.2	0.00591	12.57	21.6	0.0111	0.847	3.414	3.840	83	0.0625	0.0472
76	108.2	0.00827	12.65	24.5	0.0103	0.867	3.200	4.420	110	0.0345	0.0377
77	127.4	0.0115	12.28	26.2	0.0100	0.896	3.475	5.365	90	0.0345	0,0309
78	149.7	0.01487	12.38	25.4	0.0101	0.883	3.656	6.431	75	0.0345	0.0253

V_f/u_*	$\bar{C}$	$\frac{U_*^2}{(\gamma_s-1)gd}$	R_p	Bed cond.
0.278	2.39	0.531	4.07	Dune
0.259	7.23	0.707	4.48	Dune
0.206	12.57	0.912	4.13	Dune
0.196	12.65	1.21	4.23	Dune
0.167	12.28	1.78	4.62	Dune
0.137	12.38	2.56	4.52	Dune

where i = Hy. Gradient

Vanoni (1941)

Run no.	Q (l/s)	H (cm)	S_e	u_* (cm/s)	V (cm/s)	c_a (g/l)	T (^{o}C)	D_s (mm)	V_f (cm/s)	$\bar{C}_m$ (g/l)	γ	c_a (vol.c)
14	154.2	16.40	0.0025	6.34	111.3	9.09	24.0	0.160	1.80	1.33	6.83	0.00343
15	"	8.35	0.0025	4.51	"	5.25	21.0	0.16	1.76	0.59	8.90	0.00198
16	"	16.37	0.00125	4.48	"	3.02	21.5	0.16	1.76	0.59	5.12	0.00140
17	"	8.20	0.00125	3.17	"	0.995	19.3	0.16	1.73	0.48	6.29	0.000375
18	91.3	14.08	0.00125	4.15	76.8	4.89	20.0	0.10	0.84	1.18	4.14	0.00185
19	"	7.19	0.00125	2.97	"	1.44	20.3	0.100	0.84	0.17	8.47	0.00054
20	119.6	14.08	0.0025	5.88	100.58	4.27	22.0	0.100	0.87	"	"	0.00161
21	41.7	7.13	0.0025	4.15	69.19	3.42	19.7	0.100	0.84	"	"	0.00129
22	"	8.99	0.0025	4.69	"	6.75	17.8	0.133	1.24	"	"	0.00255

V_f/u_*	υ (cm^2/υ)	T_*	R_p	$(\frac{V_f}{u_*})R_p^{-0.26}$
0.284	0.00920	1.55	8.84	0.104
0.390	0.00988	0.786	8.24	0.148
0.393	0.00976	0.776	8.34	0.148
0.545	0.00103	0.388	7.93	0.210
0.202	0.0101	1.07	3.98	0.107
0.283	0.0100	0.546	4.00	0.150
0.147	0.00965	2.14	4.17	0.076
0.202	0.0102	1.07	3.69	0.107
0.264	0.0106	1.02	5.82	0.117

where T = temperature

Willis, Coleman and Ellis (1972)

Plane Bed (D = 0.1mm , V_f 0.027 ft/s)

Run No.	g (cfsf)	H (ft)	S (x 10^3)	u_* (ft/s)	V_f/u_*	R_p	r	$\bar{c}$	c_a (x10^2)		$(\frac{V_f}{u_*})R_p^{-0.5}$
1	3.00	0.84	1.48	0.200	0.135	1.05	3.58	0.370	0.38		0.132
2	3.00	0.99	0.923	0.172	0.157	1.06	4.14	0.195	0.23		0.154
4	3.00	1.00	0.692	0.149	0.181	0.999	4.78	0.219	0.30		0.181
5	1.76	0.64	1.020	0.145	0.186	0.999	4.92	0.283	0.38		0.186
14	2.50	0.93	0.654	0.140	0.193	0.863	5.12	0.171	0.23		0.208
15	2.75	0.94	0.692	0.144	0.188	0.898	4.98	0.202	0.30		0.200
16	3.25	0.95	0.885	0.165	0.164	0.891	4.32	0.339	0.45		0.174
17	3.50	0.95	1.150	0.188	0.144	0.875	3.80	0.500	0.53		0.154
18	3.75	0.92	1.870	0.235	0.115	0.929	3.11	0.678	0.60		1.120
19	4.00	0.91	1.100	0.180	0.150	0.943	3.96	0.837	0.98		0.155
20	4.00	1.00	1.190	0.196	0.138	0.868	3.65	0.547	0.60		0.148
21	3.75	1.00	0.827	0.163	0.166	0.935	4.37	0.397	0.53		0.171
22	3.50	1.04	0.712	0.154	0.175	0.916	4.62	0.292	0.38		0.182
23	3.25	1.01	0.442	0.120	0.225	0.904	6.08	0.225	0.38		0.236
24	3.00	1.01	0.462	0.123	0.220	0.936	5.92	0.160	0.30		0.227
25	2.75	1.00	0.538	0.132	0.205	0.943	5.47	0.129	0.23		0.211
36	2.50	0.89	0.673	0.139	0.194	0.929	5.15	0.170	0.23		0.201
37	2.75	0.90	0.788	0.151	0.179	0.949	4.73	0.309	0.45		0.227
38	3.00	0.90	0.808	0.153	0.176	0.910	4.65	0.371	0.53		0.185
39	3.25	0.89	0.981	0.168	0.161	0.880	4.24	0.489	0.60		0.172
40	3.50	0.90	1.130	0.181	0.149	0.892	3.93	0.589	0.68		0.158
41	3.75	0.89	1.980	0.238	0.113	0.898	3.07	0.659	0.60		0.120
42	4.00	0.88	1.290	0.191	0.141	0.835	3.73	1.130	1.20		0.154
44	4.24	0.95	1.500	0.214	0.126	0.585	3.37	1.170	1.13		0.136
45	4.23	0.82	1.380	0.191	0.141	0.874	3.73	1.940	2.03		0.151
46	3.73	0.78	1.210	0.174	0.155	0.904	4.09	1.410	1.65		0.163
47	3.50	0.79	1.400	0.189	0.143	0.772	3.78	1.340	1.43		0.163
48	3.24	0.80	1.130	0.171	0.158	0.852	4.16	0.810	0.98		0.171
49	2.99	0.81	1.080	0.168	0.161	0.846	4.24	0.635	0.75		0.175
50	2.75	0.80	1.120	0.170	0.159	0.857	4.19	0.466	0.53		0.172
51	2.50	0.80	0.807	0.144	0.188	0.841	4.98	0.323	0.45		0.205
52	2.25	0.78	0.538	0.116	0.233	0.846	6.32	0.236	0.45		0.254
62	2.25	0.79	0.826	0.145	0.186	0.929	4.92	0.234	0.30		0.193
63	2.50	0.76	0.846	0.144	0.188	0.949	4.98	0.314	0.45		0.194
65	2.75	0.77	1.100	0.165	0.164	0.923	4.32	0.415	0.53		0.171
66	3.00	0.76	1.290	0.178	0.152	0.985	4.01	0.583	0.68		0.154
71	1.75	0.62	✓	✓	✓	0.868	✓	0.350	✓		✓
72	1.50	0.58	0.827	0.124	0.218	0.892	5.86	0.228	0.38		0.231
78	1.12	0.45	1.270	0.136	0.200	0.898	5.33	0.316	0.45		0.212
83	0.88	0.39	1.330	0.129	0.209	0.892	5.59	0.345	0.53		0.221
86	1.50	0.53	1.080	0.136	0.199	0.835	5.30	0.328	0.53		0.217
90	1.87	0.62	1.060	0.145	0.186	0.857	4.92	0.345	0.45		0.200
102	2.25	0.69	0.808	0.134	0.201	0.863	5.33	0.348	0.53		0.217
103	2.50	0.69	0.981	0.148	0.182	0.868	4.81	0.489	0.68		0.195

Willis, Coleman and Ellis (1972)

Dune Bed (D_s = 0.01mm, V_f = 0.027 ft/s)

Run No.	q (cfs/f)	H (ft)	S (x10³)	u_* (ft/s)	V_f/u_*	R_p	r	$\bar{C}$	c_a (x10³)	$(\frac{V_f}{u_*})R_p^{-0.5}$
6	1.06	0.70	√	√	√	0.943	√	0.1610	√	√
7	1.98	1.13	√	√	√	0.986	√	0.0978	√	√
8	2.34	1.16	√	√	√	0.999	√	0.1300	√	√
9	1.74	0.90	0.962	0.167	0.162	0.847	4.268	0.2100	0.26	0.177
10	1.74	1.10	0.519	0.136	0.199	0.825	5.297	0.0582	0.09	0.219
11	1.50	1.10	0.442	0.125	0.216	0.857	5.802	0.0198	0.03	0.233
12	2.00	1.05	0.654	0.149	0.181	0.880	4.784	0.1260	0.17	0.194
13	2.25	1.00	0.500	0.127	0.213	0.857	5.711	0.1740	0.28	0.230
26	2.50	1.05	0.481	0.128	0.211	0.916	5.651	0.1360	0.22	0.219
27	2.25	1.20	0.519	0.142	0.190	0.957	5.038	0.0912	0.13	0.194
28	2.01	1.23	0.538	0.146	0.185	0.964	4.896	0.0577	0.08	0.189
29	1.71	1.24	0.346	0.118	0.229	0.986	6.200	0.0159	0.03	0.231
30	1.25	1.00	0.308	0.100	0.270	0.956	7.524	0.0087	0.02	0.275
31	1.50	1.04	0.462	0.124	0.218	0.956	5.862	0.0293	0.05	0.222
32	1.71	1.03	0.635	0.145	0.186	0.923	4.925	0.0737	0.10	0.193
33	1.75	1.03	0.615	0.143	0.189	0.936	5.010	0.0784	0.11	0.195
34	2.00	0.98	0.769	0.156	0.173	0.892	4.564	0.1430	0.19	0.183
35	2.24	0.86	0.750	0.144	0.188	0.916	4.981	0.1630	0.23	0.196
53	2.00	0.78	0.538	0.116	0.233	0.830	6.325	0.2720	0.49	0.256
54	1.50	0.94	0.730	0.149	0.181	0.852	4.784	0.0829	0.11	0.195
55	1.76	0.94	0.884	0.164	0.165	0.857	4.348	0.1750	0.22	0.178
56	2.00	0.81	0.788	0.143	0.189	0.807	5.010	0.2060	0.29	0.210
57	1.25	0.95	0.712	0.148	0.182	0.830	4.812	0.0213	0.03	0.200

Willis, Coleman, and Ellis (1972)

Anti-Dune Bed (D_s = 0.1mm , V_f = 0.027 ft/s)

Run No.	q (cfsf)	H (ft)	S (x10³)	u_* (ft/s)	V_f/u_*	R_p	γ	$\bar{C}$	c_a (x10²)	$(\frac{V_f}{U_*})Rp^{-0.5}$
3	3.00	0.69	1.44	0.179	0.151	1.050	3.98	1.404	1.58	0.148
43	3.95	0.80	1.67	0.207	0.130	0.904	3.46	1.88	1.82	0.137
67	3.26	0.78	√	√	√	0.857	√	1.10	√	√
68	3.50	0.74	√	√	√	0.880	√	1.63	√	√
69	4.00	0.72	√	√	√	0.943	√	3.49	√	√
70	4.25	0.70	√	√	√	0.857	√	5.26	√	√
79	1.25	0.42	1.02	0.117	0.231	0.898	6.26	0.438	0.77	0.245
80	1.50	0.43	1.76	0.156	0.173	0.916	4.56	1.10	1.42	0.182
81	1.12	0.34	1.75	0.138	0.196	0.929	5.21	1.06	1.56	0.204
82	1.00	0.36	1.42	0.128	0.211	0.910	5.65	0.581	0.93	0.228
87	1.62	0.52	1.12	0.137	0.197	0.835	5.24	0.446	0.66	0.207
88	1.75	0.49	1.12	0.133	0.203	0.846	5.41	0.685	1.05	0.221
89	1.87	0.50	1.12	0.134	0.201	0.846	5.36	0.913	1.39	0.219
91	2.00	0.60	1.10	1.146	0.185	0.857	4.90	0.466	0.65	0.200
92	2.12	0.61	1.19	0.153	0.176	0.857	4.65	0.559	0.74	0.190
93	2.25	0.60	1.54	0.172	0.157	0.874	4.14	0.786	0.92	0.168
94	2.38	0.58	1.23	0.152	0.178	0.846	4.70	1.01	1.34	0.194
95	2.50	0.59	1.44	0.165	0.164	0.846	4.32	1.36	1.66	0.179
96	2.75	0.69	1.81	0.201	0.134	0.868	3.56	1.00	1.00	0.145
104	2.75	0.67	1.21	0.162	0.167	0.874	4.40	0.808	1.00	0.179
105	3.00	0.70	2.04	0.214	0.126	0.898	3.37	1.248	1.19	0.182

MIDDLE RIO GRANDE (Nordin and Dempster [1963])

Sediment Size Distribution

Bernallilo	0.0625 > D	0.77%	0.77%
	0.0625 < D < 0.125	5.45%	4.68%
	0.125 < D < 0.25	35.12%	29.68%
	0.25 < D < 0.5	83.51%	48.39%
	0.5 < D < 1.0	95.59%	12.08
	1.0 < D	100.00%	4.41%
Socorro	0.0625 > D	4.18%	4.18%
	0.0625 < D < 0.125	17.03%	12.85%
	0.125 < D < 0.25	74.36%	57.33%
	0.25 < D < 0.5	96.11%	21.75%
	0.5 < D < 1.0	97.79%	1.68%
	1.0 < D	100.00%	2.21%
Bernardo	0.0625 > D	67.9%	67.9%
	0.0625 < d < 0.125	76.3%	8.4%
	0.125 < d < 0.025	90.1%	13.8%
	0.25 < d < 0.5	99.2%	9.1%
	0.5 < d < 0.1	100.0%	0.8%

MIDDLE RIO GRANDE (Nordin and Dempster [1963])

Reach	Date	Section	D_{16}	D_{50}	D_{84}	$M = \frac{\overline{d_{84}}}{\sqrt{d_{16}}}$
Bernallio	6/02/53	A-2	0.18	0.32	0.48	1.63
	6/04/53	A-2	0.17	0.33	0.73	2.07
		A	0.16	0.30	0.46	1.70
		C	0.24	0.42	0.91	1.95
		E	0.15	0.26	0.42	1.67
	4/13/54	B	0.13	0.26	0.42	1.80
		C	0.15	0.37	0.46	1.75
		D	0.15	0.29	0.49	1.81
		E	0.16	0.31	0.59	1.92
	5/19/54	B	0.16	0.31	0.53	1.82
		C	0.17	0.27	0.66	1.97
		D	0.17	0.31	0.57	1.83
		E	0.16	0.30	0.45	1.68
Socorro	4/16/54	A-1	0.11	0.17	0.70	2.52
		A-2	0.10	0.17	0.23	1.52
		B	0.09	0.16	0.24	1.63
		B-1	0.13	0.21	0.38	1.71
	5/21/54	A-1	0.13	0.19	0.32	1.57
		A-2	0.10	0.16	0.30	1.73
		B	0.081	0.15	0.23	1.69
		B-1	0.13	0.19	0.31	1.54
	8/17/54	A-1	0.13	0.24	0.42	1.80
		A-2	0.14	0.25	0.42	1.73
Bernardo	7/10/61	✓	0.0033	0.048	0.19	7.95
	8/18/61	✓	✓	✓	✓	✓
	8/19/61	✓	✓	✓	✓	✓
Niobrara River	3/03/50	✓	0.16	0.295	0.85	2.30
	4/27/51	✓	0.17	0.31	0.49	1.70
	6/19/52	✓	0.165	0.28	0.45	1.65

MIDDLE RIO GRANDE DATA (Nordin and Dempster [1963])

Reach	Date	Sec.	Q (m^3/s)	B(Width) (m)	$\bar{D}$ (m)	$\bar{V}$ (m/s)	$\bar{T}$ (^oT)	S	u_*
Bernallio	6/ 2/53	A-2	60.88	82.3	0.780	0.948	21.7	0.000826	0.0796
	6/ 4/53	A-2	59.18	82.3	0.756	0.951	16.7	0.000826	0.0783
		A	55.78	121.0	0.515	0.896	18.9	0.000826	0.0646
		C	58.62	114.6	0.719	0.710	21.7	0.000826	0.0762
		E	50.40	81.7	0.753	0.820	21.1	0.000826	0.0780
	4/13/54	B	33.98	131.7	0.433	0.597	16.7	0.000824	0.0607
		C	32.84	112.8	0.442	0.661	17.2	0.000824	0.0616
		D	32.84	121.6	0.466	0.576	17.2	0.000824	0.0628
		E	33.98	80.8	0.604	0.701	16.7	0.000826	0.0713
	5/19/54	B	41.06	132.3	0.405	0.765	20.0	0.000864	0.0585
		C	40.49	116.7	0.597	0.579	27.8	0.000864	0.0710
		D	39.93	122.2	0.457	0.716	27.8	0.000864	0.0622
		E	40.49	81.1	0.594	0.838	21.1	0.000864	0.0710
Socorro	4/16/54	A-1	19.74	53.3	0.466	0.792	12.8	0.000758	0.0543
		A-2	19.74	73.5	0.305	0.884	14.4	0.000758	0.0476
		B	19.74	136.2	0.201	0.719	20.6	0.000980	0.0438
		B-1	19.74	61.6	0.439	0.732	22.2	0.000980	0.0649
	5/21/54	A-1	25.23	67.7	0.354	1.052	20.6	0.000844	0.0539
		A-2	25.49	71.0	0.365	0.978	19.4	0.000844	0.0552
		B	24.75	99.7	0.326	0.762	22.8	0.001000	0.0567
		B-1	23.79	112.2	0.277	0.765	23.9	0.001000	0.0521
	8/17/54	A-1	101.94	78.6	0.701	1.850	22.2	0.000855	0.0768
		A-2	100.52	71.3	0.725	1.942	24.4	0.000855	0.0780
Bernardo	7/10/61		11.41	25.0	0.521	0.878	22.2	0.000385	0.0430
	8/18/61		18.00	27.4	0.634	1.036	23.9	0.000490	0.0552
	8/19/61		67.39	36.3	1.360	1.359	23.3	0.000240	0.0567

MIDDLE RIO GRANDE DATA (Nordin and Dempster [1963])

D_1 = 0.0625 ~ 0.125mm, D_g = 0.0883mm, V_f = 0.65 cm/s

Reach	Date	Sec.	$c_{0.05}$ (ppm)	$c_{0.05}$ (Vol. C)	$\frac{c_{0.05}}{c_b}$	V_f/u_*	$\frac{U_*^2}{(\sigma-1)gD}$	R_{pi}	$\frac{Di}{D_{50}}$	$(\frac{V_f}{u_*})(\frac{Di}{D_{50}})^{-1.4}$
Bernallio	6/02/53	A-2	865	0.000326	0.00959	0.817	4.44	0.57	0.276	0.495
	6/04/53	A-2	565	0.000213	0.00666	0.0830	4.29	0.57	0.276	0.495
		A	760	0.000287	0.00574	0.101	2.92	0.57	0.294	0.561
		C	428	0.000162	0.0108	0.0853	4.07	0.58	0.210	0.758
		E	366	0.000138	0.00354	0.0833	4.26	0.57	0.340	0.386
	4/13/54	B	1010	0.000381	0.00320	0.107	2.58	0.57	0.340	0.484
		C	520	0.000196	0.00377	0.106	2.65	0.57	0.240	0.782
		D	730	0.000275	0.00437	0.104	2.76	0.57	0.304	0.551
		E	630	0.000237	0.00484	0.912	3.56	0.57	0.285	0.529
	5/19/54	B	625	0.000236	0.00513	0.111	2.40	0.57	0.285	0.643
		C	750	0.000283	0.00786	0.0915	3.53	0.57	0.327	0.438
		D	462	0.000174	0.00561	0.105	2.71	0.57	0.285	0.609
		E	715	0.000270	0.00643	0.915	3.53	0.57	0.294	
Socorro	4/16/54	A-1	1620	0.000611	0.00466	0.120	2.07	0.57	0.519	0.300
		A-2	1860	0.000702	0.00447	0.137	1.59	0.57	0.519	0.343
		B	1630	0.000615	0.00312	0.148	1.34	0.57	0.551	0.341
		B-1	1520	0.000574	0.00692	0.100	2.95	0.57	0.420	0.337
	5/21/54	A-1	2960	0.00117	0.00873	0.121	2.03	0.57	0.465	0.353
		A-2	5200	0.00196	0.0117	0.118	2.13	0.57	0.552	0.271
		B	1350	0.000509	0.00251	0.115	2.25	0.57	0.589	0.242
		B-1	2640	0.000996	0.0111	0.125	1.90	0.57	0.465	0.365
	8/17/54	A-1	13400	0.00506	0.0693	0.0846	4.13	0.57	0.367	0.345
		A-2	22300	0.00841	0.165	0.0833	4.26	0.57	0.353	0.357
Bernardo	7/10/61	✓	600	0.000226	0.00129	0.151	1.29	0.57	1.84	0.0643
	8/18/61	✓	460	0.000174	0.00446	0.118	2.13	0.57	✓	✓
	8/19/61	✓	2000	0.000755	0.115	0.115	2.25	✓	✓	✓

MIDDLE RIO GRANDE DATA (Nordin and Dempster [1963])

D = 0.125 ~0.25mm, D_g = 0.177mm, V_f = 2.03 cm/s

Reach	Date	Sec.	$c_{0.05}$ (ppm)	$c_{0.05}$ (Vol. C)	$\frac{c_{0.05}}{c_b}$	V_f/u_*	$\frac{u_*^2}{(\sigma-1)gD}$	Rp_1	$\frac{Di}{D_{50}}$	$(\frac{V_f}{u_*})(\frac{Di}{D_{50}})^{-1.4}$
Bernallio	6/02/53	A-2	868	0.000328	0.00138	0.255	2.21	3.59	0.553	0.584
	6/04/53	A-2	540	0.000204	0.000671	0.259	2.14	3.59	0.536	0.620
		A	1050	0.000396	0.00147	0.314	1.46	3.59	0.590	0.657
		C	512	0.000193	0.00128	0.266	2.03	3.59	0.421	0.893
		E	695	0.000262	0.000668	0.260	2.12	3.59	0.681	0.445
	4/13/54	B	1420	0.000536	0.00161	0.334	1.29	3.59	0.681	0.572
		C	792	0.000299	0.000810	0.330	1.33	3.59	0.473	0.941
		D	1009	0.000381	0.00117	0.323	1.38	3.59	0.610	0.645
		E	1012	0.000382	0.00129	0.285	1.78	3.59	0.571	0.625
	5/19/54	B	895	0.000338	0.00116	0.347	1.20	3.59	0.571	0.760
		C	910	0.000343	0.00130	0.286	1.76	3.59	0.656	0.516
		D	380	0.000143	0.000464	0.326	1.35	3.59	0.571	0.714
		E	1011	0.000381	0.00120	0.285	1.76	3.59	0.590	0.596
Socorro	4/16/54	A-1	2250	0.000849	0.00165	0.373	1.03	3.59	1.04	0.353
		A-2	2560	0.000966	0.00143	0.426	0.792	3.59	1.04	0.403
		B	940	0.000354	0.000584	0.463	0.670	3.59	1.11	0.400
		B-1	1076	0.000406	0.000710	0.313	1.47	3.59	0.842	0.398
	5/21/54	A-1	4100	0.00155	0.00259	0.377	1.01	3.59	0.932	0.416
		A-2	7300	0.00275	0.00413	0.368	1.06	3.59	1.11	0.318
		B	980	0.000370	0.000609	0.358	1.12	3.59	1.18	0.284
		B-1	5600	0.00211	0.00311	0.390	0.948	3.59	0.932	0.430
	8/17/54	A-1	22000	0.00830	0.0203	0.264	2.06	3.59	0.738	0.404
		A-2	55000	0.0208	0.0512	0.260	2.13	3.59	0.708	0.422
Bernardo	7/10/61	✓	980	0.000370	0.00172	0.472	0.646	✓	✓	✓
	8/18/61	✓	430	0.000162	0.00197	0.368	1.06	✓	✓	✓
	8/19/61	✓	1050	0.000623	0.00328	0.358	1.12	✓	✓	✓

MIDDLE RIO GRANDE DATA (Nording and Dempster [1963])

D_i = 0.25 ~0.5mm D_g = 0.354mm V_f = 5.21 cm/s

Reach	Date	Sec.	$c_{0.05}$ (ppm)	$c_{0.05}$ (Vol. C)	$\frac{c_{0.05}}{c_b}$	V_f/u_*	$\frac{u_*^2}{(\sigma - 1)gD}$	Rp_i	$\frac{Di}{D_{50}}$	$(\frac{V_f}{u_*})(\frac{Di}{D_{50}})^{-1.4}$
Bernallio	6/02/53	A-2	286	0.000108	0.000184	0.654	1.11	18.4	1.11	0.565
	6/04/53	A-2	65	0.0000245	0.0000609	0.665	1.07	18.4	1.07	0.605
		A	152	0.0000574	0.000102	0.807	0.729	18.4	1.18	0.640
		C	177	0.0000668	0.000163	0.683	1.01	18.4	0.843	0.867
		E	60	0.0000226	0.0000442	0.668	1.06	18.4	1.36	0.434
	4/13/54	B	216	0.0000815	0.000161	0.858	0.644	18.4	0.843	1.09
		C	53	0.0000200	0.0000422	0.846	0.663	18.4	0.956	0.901
		D	340	0.000128	0.000286	0.829	0.689	18.4	1.22	0.627
		E	490	0.000185	0.000411	0.730	0.888	18.4	1.14	0.608
	5/19/54	B	326	0.000123	0.000258	0.891	0.598	18.4	1.14	0.742
		C	310	0.000117	0.000256	0.734	0.881	18.4	1.31	0.503
		D	55	0.0000208	0.0000442	0.838	0.676	18.4	1.14	0.698
		E	327	0.000123	0.000231	0.734	0.881	18.4	1.18	0.582
Socorro	4/16/54	A-1	√	√	√	0.959	√	√	√	√
		A-2	√	√	√	1.09	√	√	√	√
		B	√	√	√	1.19	√	√	√	√
		B-1	194	0.0000732	0.000268	0.803	0.736		1.68	0.388
	5/21/54	A-1	√	√	√	0.967	√	√	√	√
		A-2	√	√	√	0.944	√	√	√	√
		B	√	√	√	0.919	√	√	√	√
		B-1	√	√	√	1.00	√	√	√	√
	8/17/54	A-1	7000	0.00264	0.00644	0.678	1.03		1.48	0.390
		A-2	11500	0.00434	0.00879	0.667	1.06		1.42	0.408

Date	Sta.	Q	Total Depth	(H-y)/y	0.0625 - 0.125	0.125 - 0.25	0.25 - 0.5	Total
03/03/50	97	392	1.5	0.5	223	209	21.6	720
				2	318	435	63.6	1060
	109	392	1.7	0.416	358	437	22.4	1120
				1.125	508	875	53	1750
				2.400	617	1490	128	2570
	120	392	1.8	0.385	357	347	41	1020
				1.25	378	517	63	1260
				2.60	463	907	167	1850
	129	392-398	2.2	0.294	277	178	14	710
				0.833	310	258	17	860
				1.75	354	354	30	1010
				3.40	384	508	62	1240
	141	398	2.4	0.263	228	114	6	600
				0.600	261	147	7	670
				1.40	332	216	8	830
				1.40	356	416	10	1040
04/27/51	14	440	2.4	0.263	157	51	8	393
				1.000	196	76	0	478
				3.800	248	159	13	636
	25	440	2.5	0.25	244	150	6	626
				0.923	320	252	59	843
				4.00	515	811	356	1980
	41	435	2.1	0.313	321	312	17	868
				0.909	449	639	41	1360
	46	405	1.9	0.357	379	262	27	903
				1.11	540	599	44	1460
				2.80	392	2703	523	4360
	59	405	1.7	0.416	216	130	5	540
				1.13	299	177	0	680
				2.40	408	584	82	1360
06/19/52	12	226	2.1	0.313	106	106	13	313
				1.100	157	186	24	477
				6.00	171	235	52	573
	22	230	2.2	0.294	55	53	14	196
				1.00	76	144	72	380
				6.33	81	188	94	448
	32	215	1.8	0.278	80	105	20	285
				1.00	90	197	37	410
				5.00	87	461	127	795
	45	226	2.0	0.333	81	149	34	338
				1.00	198	1726	821	2830
				3.00	195	1062	425	1770

NIOBRARA RIVER (Colby and Hembree [1955])

							Composition of bed material Percent finer than indicated size					
Date	Q	W	$\bar{D}$	$\bar{U}$	T	Slope	0.062	0.125	0.250	0.500	1.00	2.00
03/03/50	401	70	1.6	3.57	41	0.00170	✓	4	42	76	86	92
04/27/51	455	71	1.73	3.70	58	0.00168	0	2	34	86	96	99
06/19/52	234	70	1.56	2.15	62	0.00125	0	1	41	91	99	100

NIOBARA RIVER (Colby and Hembree [1955])

D_i = 0.0625 - 0.125, D_g = 0.0883mm, V_f = 0.65 cm/s

Date	Sta.	$c_{0.05}$ (ppm)	u_*	$c_{0.05}$ (Vol. C)	$\frac{c_{0.05}}{p_i}$	V_f/u_*	$\frac{u_*^2}{(\sigma-1)gD}$	R_{pi}
3/03/50	97	540	8.72	0.000204	0.0051	0.0745	5.33	0.0893
	109	1180	9.29	0.000445	0.0111	0.0699	6.04	0.0838
	120	668	9.56	0.000252	0.0063	0.0680	6.40	0.815
	129	482	10.6	0.000182	0.0046	0.0613	7.87	0.0735
	141	465	11.0	0.000175	0.0044	0.0590	8.47	0.0707
4/27/51	14	320	11.0	0.000121	0.0061	0.0590	8.47	0.0731
	25	840	11.2	0.000317	0.0159	0.581	8.79	0.720
	41	1170	10.3	0.000442	0.0221	0.0631	7.43	0.0781
	46	1270	9.7	0.000479	0.0240	0.0670	6.59	0.0830
	59	860	9.2	0.000324	0.0162	0.0707	5.93	0.875
6/19/52	12	220	8.9	0.0000830	0.0083	0.073	5.55	0.846
	22	104	9.1	0.0000392	0.0039	0.071	5.80	0.823
	32	125	8.2	0.0000472	0.0047	0.79	4.71	0.916
	45	390	8.6	0.0000147	0.0014	0.076	5.18	0.0881

NIOBARA RIVER (Colby and Hembree [1955])

D_i = 0.125 - 0.25mm, D_g = 0.177mm, V_f = 2.03 cm/s

Date	Sta.	$c_{0.05}$ (ppm)	u_* (cm/s)	$c_{0.05}$ (vol. c)	$c_{0.05}/P_i$	V_f/u_*	$\frac{u_*^2}{(\sigma-1)gD}$	R_{pi}
03/03/50	97	1450	8.72	0.000547	0.00144	0.233	2.65	0.106
	109	6400	9.29	0.00241	0.00634	0.219	3.02	0.992
	120	2500	9.56	0.000943	0.00248	0.212	3.19	0.0960
	129	1130	10.6	0.000426	0.00112	0.192	3.93	0.0870
	141	1050	11.0	0.000396	0.00104	0.185	4.23	0.0838
04/27/51	14	340	11.0	0.000128	0.00040	0.185	4.23	0.0865
	25	1660	11.2	0.000626	0.00196	0.181	4.38	0.0847
	41	4750	10.3	0.00179	0.00559	0.197	3.71	0.0922
	46	4600	9.7	0.00173	0.00541	0.209	3.29	0.0978
	59	1330	9.2	0.000502	0.00157	0.221	2.96	0.103
06/19/52	12	340	8.9	0.000128	0.00032	0.228	2.77	0.0998
	22	320	9.1	0.000121	0.00030	0.223	2.89	0.0479
	32	890	8.2	0.000336	0.00084	0.248	2.35	0.109
	45	2300	8.6	0.000868	0.00217	0.236	2.58	0.103

NIOBARA RIVER (Colby and Hembree [1955])

D_i = 0.25 - 0.5mm, D_g = 0.354mm, V_f = 5.21 cm/s (5)

Date	Sta.	$c_{0.05}$ (ppm)	u_* (cm/s)	$c_{0.05}$ (Vol. C)	$c_{0.05}/p_i$	V_f/u_*	$\frac{u_*^2}{(\sigma-1)gD}$	R_{pi}
05/03/50	97	270	8.72	0.000102	0.00030	0.597	1.33	0.099
	109	1340	9.29	0.000506	0.00149	0.561	1.51	0.043
	120	860	9.56	0.000325	0.00096	0.545	1.60	0.090
	129	270	10.6	0.000102	0.0003	0.492	1.96	0.082
	141	↓	11.0	↓	↓	↓	↓	↓
04/27/51	14	↓	11.0	↓	↓	↓	↓	↓
	25	2400	11.2	0.000906	0.00174	0.465	2.19	0.077
	41	510	10.3	0.000192	0.000377	0.506	1.85	0.084
	46	↓	9,7	↓	↓	↓	↓	↓
	59	↓	9.2	↓	↓	↓	↓	↓
06/19/52	12	85	8.9	0.0000321	0.0000642	0.585	1.38	0.097
	22	176	9.1	0.0000664	0.000133	0.572	1.45	0.095
	32	264	8.2	0.0000996	0.000199	0.635	1.17	0.105
	45	↓	8.6	↓	↓	↓	↓	↓